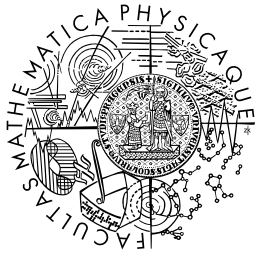

FACULTY
OF MATHEMATICS
AND PHYSICS
Charles University

DOCTORAL THESIS

Jiří Veselý

Exact Spacetimes and Their Physical Properties

Institute of Theoretical Physics

Supervisor of the doctoral thesis:	doc. RNDr. Martin Žofka, Ph.D.
Study programme:	Physics
Study branch:	Theoretical Physics, Astronomy and Astrophysics

Prague 2022

I declare that I carried out this doctoral thesis independently, and only with the cited sources, literature and other professional sources.

I understand that my work relates to the rights and obligations under the Act No. 121/2000 Sb., the Copyright Act, as amended, in particular the fact that the Charles University has the right to conclude a license agreement on the use of this work as a school work pursuant to Section 60 subsection 1 of the Copyright Act.

Prague, 08/20/2022 Jiří Veselý

As I think about my studies at Charles University, many people who deserve my thanks come to my mind—my teachers, classmates, friends. As I do not think it is possible to name everyone without omitting someone, I shall keep this dedication short.

First and foremost, I would like to thank my supervisor Martin Žofka for his guidance and for enduring my incessant questions and nitpicking over the course of the last eight years.

Next, it has been a pleasure to study alongside Jan Dvořák, Jakub Káninský, and Michal Karamazov. It has often been a relief to know that I did not have to suffer through the hardships of higher education alone, as I have suffered alongside people I could count on.

Last but not least, words cannot express my gratitude to my parents for their everlasting support, without which finishing my studies would certainly prove much more difficult.

To all those I named and to all those I did not: Thank you.

Title: Exact Spacetimes and Their Physical Properties

Author: Jiří Veselý

Institute: Institute of Theoretical Physics

Supervisor: doc. RNDr. Martin Žofka, Ph.D., Institute of Theoretical Physics

Abstract: Motivated by our desire to find generalizations of the Bonnor–Melvin spacetime, the thesis investigates seven static, cylindrically-symmetric and electrovacuum exact solutions to the Einstein–Maxwell equations. They contain a magnetic field and six of them also include the cosmological constant. After discussing some of the methods we use during our investigation, we present the basic properties of the spacetimes, and for each of them we also study charged test particle motion and their admissible shell sources composed of particle streams. We also perform numerical computations to determine whether the equations admit more general solutions than the exact ones we derived.

Keywords: general relativity exact spacetimes algebraic classification spacetime topology causal structure horizons singularities asymptotic properties

Contents

Introduction

Since Albert Einstein's discovery of the general theory of relativity in 1915, considerable research has been devoted to the topic of exact spacetimes, i.e., non-approximate (as opposed to numerical) solutions to the Einstein field equations governing the relationship between the curvature of a spacetime and its matter and energy content. When an electromagnetic field is involved, one must simultaneously also solve the Maxwell equations adjusted to be covariant in the general-relativistic framework, which relate the field and its sources. The Einstein–Maxwell equations are, however, notoriously difficult to solve in more general settings. Indeed, Einstein himself is said to have been surprised that the first non-trivial solution—the black hole spacetime of Karl Schwarzschild—was found a mere month after the publication of the theory, even though it was not interpreted as describing a black hole until decades later. The key ingredient to Schwarzschild's discovery was the assumption of spherical symmetry. In subsequent years, other exact solutions were found by taking advantage of a particular symmetry. Among them is the 1919's solution of Tullio Levi–Civita, which represents the most general vacuum, static and cylindrically-symmetric metric without the cosmological constant. Despite the fact that this solution is over a hundred years old now, cylindrical spacetimes still remain popular, with a thorough review by Bronnikov et al. [2020] published recently. While not very realistic, as cylindrically-symmetric systems must extend infinitely along the axis, this symmetry can be a good approximation of certain situations. For instance, collapsing rotating objects can produce spindle-like structures as noted in, e.g., Yoo et al. [2017] and East [2019], and these structures may be considered to be approximately cylindrically symmetric in their vicinity. Moreover, according to Bronnikov et al. [2020] the study of cosmic strings and superstrings as discussed in, e.g., Copeland and Kibble [2010] also increased academic interest in this particular symmetry in recent years. In this thesis, we too shall consider spacetimes that admit cylindrical symmetry.

While all exact solutions are interesting in their own right, it is always welcome if they can be assumed to approximately model a realistic and observable astrophysical phenomenon. It was lucky in this respect that Schwarzschild's assumption of spherical symmetry lead to a model of a static black hole immersed in vacuum. An even more realistic spacetime time is the one discovered by Roy Kerr in 1963, which represents a rotating black hole. In a matter of a few years after their respective discovery, both black-hole models were generalized to include electric charge; the non-rotating Reissner–Nordström and rotating Kerr–Newman spacetimes were born. However, as our daily life shows, macroscopic objects tend to be electrically neutral, and there is hardly anything more macroscopic than astrophysical black holes. Magnetic fields, on the other hand, appear more relevant on cosmological scales from both theoretical and observational points of view, as supported by papers such as Neronov and Vovk [2010], Tavecchio et al. [2010], Durrer and Neronov [2013], and Kunze [2013]. The large-scale magnetic fields may be of primordial origin as noted by Subramanian [2016] and they might have played a critical role in the early universe according to Jedamzik and Pogosian [2020]. Works such as Pétri [2017] and Carrasco et al. [2018] note that magnetic

fields often occur in strong gravitational fields like those in the vicinity of compact massive objects, so they merit investigation within the framework of general relativity. A particular well-known exact spacetime modeling a magnetic field that happens to be cylindrically symmetric is the Bonnor–Melvin solution, also known as the Melvin universe. It was discovered separately by William Bowen Bonnor [1954] and Mael Avrami Melvin [1964], and is the main inspiration for this work. In recent years, there has been increased interest in the solution: There are many papers studying black holes immersed in the Bonnor–Melvin background, such as Radu [2002], Brito et al. [2014], Booth et al. [2015], and Astorino et al. [2016]; (anti-)photon surfaces were studied in Gibbons and Warnick [2016]; the solution was used to generate cosmological models in Kastor and Traschen [2015]; its analogues have been discussed in $d \geq 3$ dimensions in Tahamtan and Halilsoy [2013], in theories of non-linear electrodynamics in Gibbons and Herdeiro [2001], in Born–Infeld gravity in Bambi et al. [2015], and in string theory in Tseytlin [1995]; and so on. Note that other cylindrical spacetimes with a magnetic field were studied in, e.g., Richterek et al. [2000], and also form a part of the review paper Bronnikov et al. [2020].

Apart from cylindrical symmetry and magnetic fields, there is one more key element to the spacetimes we are going to study that was missing in the above-mentioned solutions: the cosmological constant. It was first introduced by Einstein to his field equations in 1917 to make sure that they admitted a static model of the universe, compliant with the sentiment of the period that on large scales the universe was static. When this notion was later dismissed, Einstein disowned the constant and, as legend has it, called it his 'biggest blunder'. Nonetheless, the turn of the millennium brought a renewed interest in the constant, as observations of supernovae redshifts published in papers such as Riess et al. [1998] and Perlmutter et al. [1999] provided evidence that the expansion of the universe accelerates. This research, which lead to the 2011 Nobel Prize in Physics being awarded to Saul Perlmutter, Brian P. Schmidt, and Adam G. Riess, attributed the acceleration to the very cosmological term in the Einstein equations. As noted in Carroll [2001], the effects of the cosmological constant are sometimes dubbed 'dark energy', but they are not necessarily synonymous, because other, perhaps less appealing explanations for the dark energy driving the expansion of the universe have been proposed. Corroborating the previous research, the results of the Planck spacecraft's mission, which were published in Aghanim et al. [2020], also shown that the dark energy, although very low in density, forms the majority of the mass-energy content of the universe due to the energy's homogeneity everywhere across space. It is, therefore, logical to consider the cosmological term in the Einstein equations and study exact spacetimes that admit the constant. The above-mentioned black-hole solutions have already been generalized to the case of a non-zero cosmological constant, long before the revolutionary observations were made, in fact. Instead, we set out to derive generalizations of the Bonnor–Melvin spacetime, leading to our analysis of several electrovacuum, cylindrically-symmetric spacetimes with a magnetic field and a non-zero cosmological constant. To have a full discussion from the mathematical point of view, we consider either sign of the constant in spite of the fact that the observations suggest that it is positive.

This thesis is divided into three main parts. The purpose of the first part is

to lay the foundation for our original results presented in the subsequent chapters. We first tackle the concept of cylindrical symmetry and then we move on to introduce the chief methods we use to investigate the examined spacetimes. Namely, we focus on charged test particle motion and also on finding shell sources with reasonable properties using Israel's cut-and-paste method. Furthermore, the spacetimes that feature more intricate causal structure also merit their conformal diagrams to be drawn. The emphasis in the opening part of the thesis is, therefore, on an explanation of our approach to each of these notions. We finish this part by briefly reminding the reader of some of the previously discovered and well-known cylindrical spacetimes relevant to our current work.

The second part of the thesis is the principal and, by far, also the longest one. Here, we discuss the properties of the examined static and cylindrically-symmetric spacetimes themselves, featuring a magnetic field and—barring one exception—the cosmological constant. We first derive the spacetimes using the Einstein–Maxwell equations, while discussing some additional symmetries allowing us to solve the equations analytically. We then focus on each of the seven spacetimes in turn, applying the methods outlined in the first part. Not only do we investigate particle motion and find shell sources connecting our spacetimes to the previously known solutions mentioned in the opening part whenever possible, but we also discuss some additional properties and try to gain more insights regarding the physics of the spacetimes.

The last part contains further information that is not particular to any single exact spacetime discussed in the preceding chapters. We first unify and expand our findings about shell sources by considering shells on the interface of each possible pair of the studied spacetimes. We also discuss whether the properties of the shells are similar to those examined in the literature. Next, we shed the additional symmetries that were needed to derive our exact spacetimes and we solve the Einstein–Maxwell equations numerically. We thus assemble a catalog of general solutions with unique physical properties. Finally, we delve into the equations for the general solutions analytically to see if they have the so-called Painlevé property, which could prove to be instrumental in trying to find the exact solutions.

Last but not least, in the appendix closing the thesis we discuss a relaxed variant of cylindrical symmetry that requires only the spatial part of the metric to be cylindrical, while the temporal part can be arbitrary as long as the spacetime remains static. We derive a magnetic spacetime and see that it is locally the same as one of the previous solutions examined in this work.

In fact, although we have answered many of our original questions that aroused our curiosity at the onset of the thesis, our investigation opened many more new and fascinating issues to focus on in our future work.

Notation and tensor & unit formalism

In this work, we shall use boldface when referring to tensors other then the basis tensors or scalar quantities. When it is convenient, we use the standard index notation to describe tensors, with upper indices being contravariant and lower indices covariant. Using the Einstein summation convention for, e.g., a covector, we can write $\mathbf{a} = a_\mu \, \mathrm{d}x^\mu$, with Greek indices representing an arbitrary coordinate.

As it represents the same tensor quantity, raising and lowering of indices shall not be differentiated when using the boldface notation. Basis vectors are denoted ∂_{x^μ}.

Before we start working with specific spacetimes, we shall derive and explain some general formulae, which shall be valid for every spacetime considered in this work. In these formulae we shall use the usual notation for cylindrical coordinates (t, r, z, ϕ), where t is the time coordinate, r is the radial coordinate and it is the only coordinate that a static cylindrical metric can be a function of, and ϕ is cyclic. In particular spacetimes, the coordinates may be denoted somewhat differently.

Unless stated otherwise, primes represent derivatives with respect to the radial coordinate, $f'(r) = \frac{\mathrm{d}}{\mathrm{d}r} f(r)$, with $\frac{\mathrm{d}}{\mathrm{d}r}$ being the total derivative with respect to the variable r. Partial derivatives shall be denoted using a comma $a_{\mu,\nu}$ and covariant derivatives using a semicolon $a_{\mu;\nu}$, while covariant absolute derivatives with respect to a variable r are denoted $\frac{\mathrm{D}}{\mathrm{d}r}$.

We adopt the sign convention of the legendary 'MTW' textbook Misner et al. [1973]. The signature of the metric tensor considered in this work is $(-+++)$, which means that time-like vectors have negative magnitude. For a metric with the components $g_{\mu\nu}$ in a given coordinate system, the Christoffel symbols

$$\Gamma^{\alpha}{}_{\mu\nu} \equiv g^{\alpha\beta}\,\Gamma_{\beta\mu\nu} \equiv \frac{1}{2}\,g^{\alpha\beta}\left(g_{\beta\mu,\nu} + g_{\nu\beta,\mu} - g_{\mu\nu,\beta}\right)$$

provide us with the means to express the Riemann tensor in the coordinate basis,

$$R^{\alpha}{}_{\beta\gamma\delta} = \Gamma^{\alpha}{}_{\beta\delta,\gamma} - \Gamma^{\alpha}{}_{\beta\gamma,\delta} + \Gamma^{\alpha}{}_{\mu\gamma}\Gamma^{\mu}{}_{\beta\delta} - \Gamma^{\alpha}{}_{\mu\delta}\Gamma^{\mu}{}_{\beta\gamma}\,.$$

We fix the sign of the Ricci tensor by considering the contraction

$$R_{\mu\nu} \equiv R^{\alpha}{}_{\mu\alpha\nu}\,.$$

With the Ricci scalar curvature $R \equiv R^{\mu}{}_{\mu}$, the Einstein tensor takes the form

$$G_{\mu\nu} \equiv R_{\mu\nu} - \frac{1}{2} R\, g_{\mu\nu}\,.$$

Using the geometrized unit system, the speed of light and the gravitational constant are set equal to unity throughout this thesis. The values of physical quantities shall be expressed using an arbitrary unit of length denoted u.

1. Preliminaries

1.1 What is cylindrical symmetry?

The aim of this thesis is to analyze spacetimes with cylindrical symmetry. However, while cylindrical symmetry tends to be easy to define and understand in classical physics, as one can rely on the coordinates to have a graspable meaning there, the nature of general relativity requires us to transcend beyond the limitations of the coordinate system and define symmetries covariantly. Indeed, according to Bronnikov et al. [2020] there exists some confusion regarding the definition of cylindrical symmetry in the literature.

In our work, we shall employ an intuitive approach to the desired symmetry. Analogously to, e.g., Linet [1986], as an ansatz we consider the cylindrically-symmetric, static metric

$$\mathrm{d}s^2 = -\exp A(r)\,\mathrm{d}t^2 + \mathrm{d}r^2 + \exp B(r)\,\mathrm{d}z^2 + \exp C(r)\,\mathrm{d}\phi^2 \tag{1.1}$$

with at least three orthogonal Killing vector fields[1] ∂_t, ∂_z, and ∂_ϕ. The first of them, ∂_t, is timelike and it brings about the stationarity of the spacetime. Coupled with the fact that the vector field is orthogonal to surfaces of constant coordinate time t, this means that the metric is also static. The last two Killing vector fields are spacelike, and we assume that ∂_ϕ has closed orbits, therefore ϕ is the bounded angular coordinate. In order to avoid laborious work with dimensions, we consider the metric functions to be dimensionless, which means that at this point, every coordinate has the dimension of length, somewhat unintuitively also including ϕ. However, the coordinates tend to undergo some transformations during the course of the work, so the dimensions may vary in the final product. The angular coordinate in particular is always rescaled in the end so that it is dimensionless and the hypersurfaces at $\phi = 0$ and $\phi = 2\pi$ are identified. Note, however, that the ansatz treats the z and ϕ coordinates the same way, so at this point the interpretation of the coordinates is completely arbitrary. While we shall mostly respect the cylindrical interpretation throughout this thesis, some spacetimes are perhaps more suited for, e.g., the toroidal interpretation (with the z coordinate also periodic) or the planar interpretation (with ϕ unbounded). We shall discuss these cases as we come across them.

The absence of the off-diagonal elements in the spatial part of the metric makes the system invariant under reflections in any plane containing the axis as well as in planes perpendicular to it. The resulting symmetry of the studied spacetimes is then called 'whole-cylinder symmetry' in works such as Thorne [1965], Melvin [1965], and Carot et al. [1999].

An important ingredient to both cylindrical and its parent axial symmetry is the axis, which can be found wherever the norm of the Killing vector ∂_ϕ vanishes (i.e., $g_{\phi\phi} \to 0$ in our coordinates). While it is natural to expect a cylindrically-symmetric spacetime to have a single axis, we do not insist on it. In fact, we shall encounter also spacetimes with no axes or with two of them. Note that

[1] There may be more Killing vector fields than three, depending on the particularities of the metric functions in a given spacetime.

the extrinsic curvature scalar K, which is the trace of $\mathbf{K}$ (1.41) as defined and discussed in Sec. 1.2.2, can be expected to diverge to positive infinity in the limit as the radial coordinate approaches that of the axis, because it gives the divergence of the normal field to the cylindrical hypersurfaces we consider. Also note that Carot [2000] states that the Petrov algebraic type of the Weyl tensor at points on an axis in axial spacetimes can only be D or O. Our spacetimes do not violate this theorem.

The studied spacetimes that are bereft of an axis can be separated into three categories:

- In the spacetimes with a radial magnetic field of Sec. 2.4 and Sec. 2.6, the axes are singular and thus not a part of the manifold. Nonetheless, papers such as Barnes [2000] and Bronnikov et al. [2020] admit that even physically-realistic cylindrical spacetimes may contain singular axes.

- The azimuthal inhomogeneous spacetime of Sec. 2.8 has the monotonically increasing $g_{\phi\phi} = r^2$, but what would be the axis at $r = 0$ lies outside of the allowed interval of r. However, we do not consider this to be an issue with respect to the question of cylindrical symmetry, as similar situations can arise from the application of Israel's cut-and-paste formalism (which we shall introduce in Sec. 1.2.2 and use throughout the thesis) by, e.g., connecting two instances of the asymptotic region of a cylindrical spacetime through a thin shell. We view the resulting spacetime to be just as cylindrical as the original one, but the part containing the axis would be left out. Similar arguments can be found in, e.g., Carot et al. [1999] and Barnes [2000]. Having said that, in the end we suggest that this particular metric may be better understood as having toroidal symmetry anyway.

- On the other hand, our radial and azimuthal homogeneous solutions of Sec. 2.5 and 2.7, respectively, have $g_{\phi\phi} = \text{const.}$, which seems more questionable. Again, this suggests that it may be reasonable to view these spacetimes as having a different kind of symmetry. Indeed, Bronnikov et al. [2020] even goes as far as to say that the existence of an axis is essential in cylindrical spacetimes. However, we choose to keep considering ϕ as a 2π-periodic coordinate in these cases to match the theme of the thesis. We discuss alternative interpretations in the corresponding sections. Both spacetimes contain a cylinder that is invariant with respect to a reflection of the radial coordinate under which the metric is invariant. This cylinder can perhaps be viewed as the closest substitute for an axis, but we refrain from calling it so.

In more technical terms, the Killing vectors ∂_z and ∂_ϕ commute, $[\partial_z, \partial_\phi] = 0$, and they generate the Abelian group G_2. As required by, e.g., Carot et al. [1999], the orbits of the group are locally spacelike cylinders denoted S_2. The paper then states that a spacetime is cylindrically symmetric if and only if it admits a G_2 on S_2 group of isometries that contains an axial symmetry. The axial symmetry is generated by the spacelike Killing field ∂_ϕ, but Carot et al. [1999] notably also requires its set of fixed points to be non-empty, which disqualifies especially the

two spacetimes with $g_{\phi\phi}$ constant[2]. Indeed, Carot et al. [1999] and Bronnikov et al. [2020] define the axis as the set of fixed points under the action of the G_2 group. Now, let us extend the group to also include the timelike Killing field ∂_t to obtain G_3 acting on timelike orbits T_3. Spacetimes with such a group are stationary, but they are not static unless they admit a timelike Killing field that is integrable. To see that our ansatz leads to static spacetimes, we first note that in our case G_3 is Abelian as well, as ∂_t commutes with the other fields too. The Killing vectors are hypersurface orthogonal, as all of them satisfy the relation $\xi_{[\alpha;\beta}\xi_{\gamma]} = 0$ (or $\mathrm{d}\boldsymbol{\xi}\wedge\boldsymbol{\xi} = 0$), where $\boldsymbol{\xi}$ represents any of the three Killing vector fields. Therefore, all 2D subgroups are orthogonally transitive, as every pair of vectors also satisfies the weaker condition $\xi_{[\alpha;\beta}\xi_{\gamma}\eta_{\delta]} = 0$ (or $\mathrm{d}\boldsymbol{\xi}\wedge\boldsymbol{\xi}\wedge\boldsymbol{\eta} = 0$) as defined in Stephani et al. [2009], where $\boldsymbol{\eta}$ is the other Killing field of the pair. According to Carot et al. [1999], $[\partial_z, \partial_t] = 0$ with the orthogonal transitivity of the original G_2 on S_2 imply staticity. As ansatz (1.1) fulfills both conditions, our spacetimes pass this more technical criterion and are indeed static and cylindrically symmetric as long as their $g_{\phi\phi}$ is not constant.

Note that in the Appendix, we limit the cylindrical symmetry to the spatial part of the spacetime (by requiring the spatial part of the metric to match that of the Minkowski spacetime written in cylindrical coordinates, see Sec. 1.3.1), but we permit g_{tt} to be the function of any of the three spatial coordinates.

1.1.1 Regularity of axes

Due to their symmetries, each of the studied spacetimes has the Killing vector $\boldsymbol{\eta} = \partial_\phi$, which has closed orbits and generates translations in the azimuthal direction, with the dimensionless ϕ coordinate taking on values from the interval $[0, 2\pi)$. Recall that we may need to rescale the coordinate to comply with the previous assumption. Some of the solutions may have one or two axes of symmetry where the norm of the Killing vector $\eta^2 = g_{\mu\nu}\eta^\mu\eta^\nu$ vanishes. In that case the coordinate ϕ is degenerate there, which complicates the analysis of the spacetime at the axis. It is then harder to determine whether the axis is regular or not. Publications such as Mars and Senovilla [1993], Wilson and Clarke [1996], Carot et al. [1999], Carot [2000], Stephani et al. [2009], and Bronnikov et al. [2020], mention this issue. Non-regular axes tend to suffer from a deficit angle, a conical singularity typically related to a distributional matter content along the axis.

For an axis located at the radial coordinate $r = r_a$, the condition for the so-called elementary flatness is

$$\lim_{r\to r_a} \frac{g^{\mu\nu}\left(\eta^2\right)_{,\mu}\left(\eta^2\right)_{,\nu}}{4\eta^2} = 1\,. \tag{1.2}$$

If this regularity condition holds, the 2π-periodicity of the axial coordinate is ensured near the axis. In the first approximation, the length of a circular orbit around an axis is then 2π times the distance to the axis, as one would expect in a flat spacetime.

[2]While the spacetimes of the first two bullet points above also technically do not contain the axis as it would be located at a non-accessible value of the radial coordinate, Carot et al. [1999] is more accepting of such cases.

More precisely, it is possible to relate the condition (1.2) to the derivative of the proper circumference of circles around the axis

$$\mathcal{C} = \int_0^{2\pi} \sqrt{g_{\phi\phi}}\, \mathrm{d}\phi \tag{1.3}$$

with respect to their proper radius r_p. In the ansatz (1.1) the proper radius is given by the difference of the radial coordinate of the circle and the axis and so we have $\mathrm{d}r_p = \mathrm{d}r$ with r being the circle's coordinate radius. However, our derivation of the final metric tensors for the exact solutions we examine in the next part of the thesis may include transformations of the radial coordinate, so the r coordinate appearing in the metric may not correspond to proper distance. In that case, we have $\mathrm{d}r_p = \sqrt{g_{rr}}\mathrm{d}r$, assuming that the axis is located at a lower value of the radial coordinate than the circle. Therefore, the sought derivative is

$$\frac{\mathrm{d}\mathcal{C}}{\mathrm{d}r_p} = \frac{1}{\sqrt{g_{rr}}} \frac{\mathrm{d}\mathcal{C}}{\mathrm{d}r}\,. \tag{1.4}$$

Now, we can take advantage of the fact that we shall be dealing exclusively with diagonal metric tensors[3], which do not depend on the ϕ coordinate. We then have $\mathcal{C} = 2\pi\sqrt{g_{\phi\phi}}$ and $\mathrm{d}\mathcal{C}/\mathrm{d}r = \pi g_{\phi\phi,r}/\sqrt{g_{\phi\phi}}$. Seeing that $\eta^2 = g_{\phi\phi}$, we can replace the derivatives of η^2 in (1.2) with the derivatives of $\mathcal{C}$, leading to the expected result $\mathrm{d}\mathcal{C}/\mathrm{d}r_p \to 2\pi$ as we approach the axis.

1.2 Technicalities

In order to streamline the whole process, we shall now present methods and formulae used in the subsequent chapters to gain more insights into the derived spacetimes. For the sake of brevity, most of these details were left out of the published papers, a necessary evil we shall attempt to remedy here. The solutions themselves are derived later, in Sec. 2.1.

Not every procedure we use to examine the spacetimes, however, merits a discussion here. We shall talk chiefly about methods of investigating particle motion and shell sources, as these form a considerable part of the work and we deem it necessary to point out the specifics of dealing with our spacetimes, so that when we present the spacetimes themselves, we can focus on the results and not on how we arrived to them. We also summarize the transformations leading to the conformal diagrams we draw for some of the spacetimes. On the other hand, what we shall not discuss are 'cookbook-like' algorithms we use without any modifications of our own. Such algorithms are, e.g., the one for determining the Petrov algebraic classification of the solution's Weyl tensor (adopted from chapter 2 of Griffiths and Podolský [2009]) or the one for determining optical scalars for null geodesic congruences (adopted from chapter 2.4 of Poisson [2004]).

1.2.1 Electrogeodesics

One way to study a spacetime is through test particle motion. We shall use the Lagrangian formalism to examine motion of both uncharged and charged test

[3]Non-diagonal metric tensors appear as a stepping stone when drawing conformal diagrams as explained in Sec. 1.2.3, but they are not used to obtain any other information about the spacetimes.

particles, yielding geodesics and electrogeodesics, respectively. Here we follow our previous work Veselý and Žofka [2018] and Veselý and Žofka [2019a] dealing with the Kerr–Newman–(anti-)de Sitter solution. Our aim is not to provide a complete analytical solution of the full equations of motion, we rather place our focus on a few select interesting cases.

In the Lagrangian formalism, test particle motion can be described using the scalar Lagrangian function $\mathcal{L}$. For uncharged particles, we consider the Lagrangian density

$$\mathcal{L}(x^\alpha, \dot{x}^\alpha) = \frac{1}{2} g_{\mu\nu} \dot{x}^\mu \dot{x}^\nu, \tag{1.5}$$

where $\dot{x}^\mu$ is the derivative of the particle's position x^μ with respect to a variable used to parametrize motion, such as the proper time τ for massive particles. Considering only affine parametrization, the particle's four-velocity $\dot{x}^\mu$ satisfies the normalization equation

$$g_{\mu\nu} \dot{x}^\mu \dot{x}^\nu = \delta \,, \tag{1.6}$$

where $\delta = -1$ for massive particles and $\delta = 0$ for massless photons.

While one could generally study the equations of motion derived from the Lagrangian directly, such a process can prove to be rather cumbersome. Instead, we shall utilize an effective potential $V(r)$ describing motion in the radial direction with respect to the particle's radial position independent of the affine parameter. The potential can be derived by expressing $\dot{r}$ from the normalization equation and replacing the other components of the four-velocity with the corresponding constants of motion. Because we are going to work exclusively with cylindrical spacetimes, the metric will always be a function of the radial coordinate only, $g_{\mu\nu}(r)$, and, by extension, it will also be the only coordinate appearing in $\mathcal{L}$. Therefore, there are three constants of motion corresponding to the three cyclic coordinates,

$$-E = \frac{\partial \mathcal{L}}{\partial \dot{t}} = g_{tt} \dot{t} \,, \tag{1.7}$$

$$Z = \frac{\partial \mathcal{L}}{\partial \dot{z}} = g_{zz} \dot{z} \,, \tag{1.8}$$

$$L = \frac{\partial \mathcal{L}}{\partial \dot{\phi}} = g_{\phi\phi} \dot{\phi} \,, \tag{1.9}$$

where we also made use of the fact that our solutions will always have a diagonal metric. We require E to be positive so that the particle moves forward in coordinate time. After plugging the constants into (1.6), we obtain the effective potential

$$V(r) = \frac{1}{2 g_{rr}} \left[-\delta + \frac{E^2}{g_{tt}} + \frac{Z^2}{g_{zz}} + \frac{L^2}{g_{\phi\phi}} \right] \tag{1.10}$$

satisfying

$$\frac{1}{2} \dot{r}^2 = -V(r) \,. \tag{1.11}$$

A particle can move in the area with $V(r) \leq 0$ and its turning points in the radial direction fulfill $V(r) = 0$.

Furthermore, the potential can be separated[4] by considering

$$V(r) = \frac{1}{2g_{tt}g_{rr}}\left(E^2 - W^2(r)\right) \tag{1.12}$$

with

$$W^2(r) = g_{tt}\left[\delta - \frac{Z^2}{g_{zz}} - \frac{L^2}{g_{\phi\phi}}\right] \tag{1.13}$$

A particle can move in the area satisfying $W^2(r) \leq E^2$ and its turning points in the radial direction fulfill $W^2(r) = E^2$. The advantage in using W^2 over V is that when plotting the potentials, it is much easier to infer the behavior of various particles with different values of E (but the same L and Z) from the chart of W^2.

When it comes to charged test particles, the situation gets somewhat more complicated. The Lagrangian density gains an additional term corresponding to the electromagnetic interaction,

$$\mathcal{L}(x^\alpha, \dot{x}^\alpha) = \frac{1}{2}g_{\mu\nu}\dot{x}^\mu\dot{x}^\nu + \kappa\dot{x}^\mu A_\mu\,, \tag{1.14}$$

where κ is the particle's charge-to-mass ratio and $\mathbf{A}$ is the electromagnetic four-potential. For axial and azimuthal fields, we can repeat the procedure for uncharged particles, because $\mathbf{A}$ can be taken as a function of the radial coordinate only. The studied axial fields are of the form $\mathbf{F} = F_{r\phi}(r)\,\mathrm{d}r \wedge \mathrm{d}\phi$, so a convenient choice of the electromagnetic potential satisfying $\mathrm{d}\mathbf{A} = \mathbf{F}$ is

$$\mathbf{A} = \left(\int F_{r\phi}(r)\,\mathrm{d}r\right)\mathrm{d}\phi \tag{1.15}$$

which means that E and Z stay the same as in the uncharged case, but

$$L = \frac{\partial\mathcal{L}}{\partial\dot{\phi}} = g_{\phi\phi}\dot{\phi} + \kappa A_\phi\,, \tag{1.16}$$

from which we express $\dot{\phi}$ to plug in the normalization equation (1.6), equivalent to taking $L \to L - \kappa A_\phi$ in the uncharged potential (1.10). Similarly, for azimuthal fields we have $\mathbf{F} = F_{rz}(r)\,\mathrm{d}r \wedge \mathrm{d}z$, so

$$\mathbf{A} = \left(\int F_{rz}(r)\,\mathrm{d}r\right)\mathrm{d}z \tag{1.17}$$

and the one changed constant of motion is

$$Z = \frac{\partial\mathcal{L}}{\partial\dot{z}} = g_{zz}\dot{z} + \kappa A_z\,, \tag{1.18}$$

leading to the change $Z \to Z - \kappa A_z$ in (1.10). Finally, for radial fields we always have $\mathbf{F} = F_{z\phi}\,\mathrm{d}z \wedge \mathrm{d}\phi$ with $F_{z\phi} = \text{const.}$ for our spacetimes. Unfortunately, a potential satisfying $\mathrm{d}\mathbf{A} = \mathbf{F}$ must necessarily depend on z and/or ϕ. Choosing

$$\mathbf{A} = F_{z\phi}\,z\,\mathrm{d}\phi \tag{1.19}$$

[4]We choose to separate the constant of motion E from the effective potential, because then the separated potential resembles the potentials that one may encounter in classical physics. It is, however, only a matter of convention, as we could equivalently choose to separate any other of the constants.

to avoid having to deal with the periodicity of ϕ, this means that z is not a cyclic coordinate in the Lagrangian anymore, and we, therefore, lose the constant of motion Z. This means we cannot use the effective potential V.

Not all hope is lost for the spacetimes with a radial magnetic field, however, as an alternative approach that may be worthwhile to pursue is to analyze the Hamilton–Jacobi equation, which has been used to provide interesting results for black-hole spacetimes in, e.g., Hackmann et al. [2010a,b] and Hackmann and Xu [2013]. The equation reads

$$\mathcal{H}\left(x^\alpha, \frac{\partial S}{\partial x^\alpha}\right) + \frac{\partial S}{\partial \lambda} = 0\,, \tag{1.20}$$

where S is a scalar function describing the action of the system, λ is the variable used to parametrize motion, and $\mathcal{H}$ is the Hamiltonian function, which for the Lagrangian (1.14) becomes

$$\mathcal{H}(x^\alpha, p_\alpha) = \frac{1}{2} g^{\mu\nu} \left(p_\mu - \kappa A_\mu\right)\left(p_\nu - \kappa A_\nu\right). \tag{1.21}$$

Note that the generalized four-momenta

$$p_\alpha = \frac{\partial \mathcal{L}}{\partial \dot{x}^\alpha} = g_{\alpha\mu}\dot{x}^\mu + \kappa A_\alpha \tag{1.22}$$

are considered to be the derivatives of S in the Hamilton–Jacobi equation. The elements of p_α are the constants of motion if the particular x^α is a cyclic coordinate.

As for the action, for the systems with three cyclic coordinates we have

$$S = -\frac{1}{2}\delta\lambda - Et + L\phi + Zz + R(r)\,. \tag{1.23}$$

It is possible to express the derivative of the only unknown function $R(r)$ from (1.20), but there is no point in doing so as it is equivalent to the effective potential V through (1.22) and (1.11): $R'(r) = p_r = g_{rr}\dot{r} = \pm g_{rr}\sqrt{-2V}$. On the other hand, for charged particle motion in the spacetimes with a radial magnetic field, we are one constant of motion short to use the effective potential V, but if we assume separability of the action, we can use (1.20) with

$$S = -\frac{1}{2}\delta\lambda - Et + L\phi + Z(z) + R(r)\,, \tag{1.24}$$

where $Z(z)$ is now also an unknown function. In the fortuitous case when the Hamilton–Jacobi equation itself is separable, i.e., it is possible to rewrite it as $f(r) = g(z)$, both sides are then equal to the so-called Carter constant K, which simplifies the analysis of the problem by replacing the lost constant of motion Z. Using the constant, we can express $R'(r)$ from $f(r) = K$ and similarly $Z'(z)$ from $g(z) = K$ to introduce two new effective potentials

$$V_r(r) = -\frac{1}{2}\left(\frac{R'(r)}{g_{rr}(r)}\right)^2, \tag{1.25}$$

$$V_z(r,z) = -\frac{1}{2}\left(\frac{Z'(z)}{g_{zz}(r)}\right)^2, \tag{1.26}$$

satisfying

$$\frac{1}{2}\dot{r}^2 = -V_r(r)\,, \tag{1.27}$$

$$\frac{1}{2}\dot{z}^2 = -V_z(r,z)\,, \tag{1.28}$$

so that we have analogous relations to those above instead of having to work in the phase space. Because (1.27) has the same form as (1.11), the new potential for radial motion can be analyzed in the same way as the previously-discussed effective potential V. However, unless g_{zz} is constant, V_z is a function of two coordinates, which needs to be taken into account when examining motion along the z direction using (1.28).

In the course of this work we shall encounter a spacetime where the Hamilton–Jacobi equation with particle charge included is not separable (namely the non-cosmological spacetime with a radial magnetic field of Sec. 2.4), which renders the method of the effective potentials sadly unusable for charged test particle motion. On a more positive note, according to, e.g., Gutzwiller [1990], Lichtenberg and Lieberman [1992], and Schuster and Just [2005], this particular system does not retain enough constants of motion to be integrable and we may therefore be able to observe deterministic chaos in the solutions to the equations of motion. Indeed, by numerically integrating the full equations of motion

$$\frac{\mathrm{D}\dot{x}^\mu}{\mathrm{d}\tau} \equiv \ddot{x}^\mu + \Gamma^\mu{}_{\alpha\beta}\dot{x}^\alpha\dot{x}^\beta = \kappa F^\mu{}_\alpha\,\dot{x}^\alpha, \tag{1.29}$$

where $\Gamma^\mu{}_{\alpha\beta}$ are the Christoffel symbols of the second kind, we have found indications of chaotic motion for charged test particles in the above-mentioned solution, as we briefly discuss in the corresponding chapter.

Our goals

There are two problems we are mainly interested in. First, we want to determine whether test particles can reach interesting locations such as the axis, singularities, horizons and the radial infinity (wherever applicable), which can be done by computing the limits of the potentials. Second is the question of the existence and stability of stationary circular orbits in the planes of $z = \text{const.}$, which are perpendicular to the spacetime's axis or axes of symmetry, provided the spacetime contains any axes. The radii of stationary orbits r_0 must satisfy $V(r_0) = 0 = V'(r_0)$, or, equivalently, $W^2(r_0) = E^2$ with $(W^2)'(r_0) = 0$. From these relations we usually express E^2 and L^2 and determine the allowed range of r_0 by requiring both of them to be positive, so that the constants themselves are not imaginary. The stability of the orbits is given by the sign of the second derivative of the potentials (at r_0 the sign of the second derivative is the same for both V and W^2), with stable orbits lying in the minima of the potentials and unstable in the maxima. As we consider planar orbits, we set $\dot{z} = 0$, which fixes the value of Z (to zero for uncharged particles).

The endpoints of the allowed range of r_0 for uncharged massive particles are suspected of being photon orbit radii. To verify or disprove this by finding the photon orbits, we must proceed differently from the massive case, as solving $V(r_0) = 0 = V'(r_0)$ or their equivalent for E and L while considering $\delta = 0$

necessarily leads to the unphysical solution $E = 0 = L$, implying a motionless photon. Instead, we replace $\dot{\phi}$ with

$$\Omega = \frac{\mathrm{d}\phi}{\mathrm{d}t} = \frac{\dot{\phi}}{\dot{t}} \tag{1.30}$$

in both the photon normalization equation (1.6), $g_{\mu\nu}\dot{x}^\mu\dot{x}^\nu = 0$, and the stationary (i.e., $\ddot{x}^\mu = 0$) photon (i.e., $\kappa = 0$) remnant of (1.29), $\Gamma^\mu{}_{\alpha\beta}\dot{x}^\alpha\dot{x}^\beta = 0$, while setting $\dot{r} = 0 = \dot{z}$ in both. Due to peculiarities of our spacetimes, $\dot{t}$ can be eliminated from either equation, thus dismissing the unphysical solution with $E = 0$. Therefore, we solve the equations for Ω and, more importantly, the photon orbit radii r_0, which take only discrete values for photons.

The Killing constants

While the previous approach is sufficient for us to establish effective potentials for charged radial motion if the spacetime admits it, note that a more complete set of constants of motion can be procured by taking advantage of all the spacetime's symmetries as described by the Killing vector fields denoted $\boldsymbol{\xi}$, which satisfy the relation

$$\xi_{\alpha;\beta} + \xi_{\beta;\alpha} = 0\,, \tag{1.31}$$

equivalent to saying that the Lie derivative of metric with respect to $\boldsymbol{\xi}$ vanishes, $\pounds_{\boldsymbol{\xi}}\mathbf{g} = 0$. To find out what the conserved quantity is, we must come up with an expression the time derivative of which vanishes. As conserved quantities in classical physics tend to be connected to the symmetries of a given system, a reasonable relativistic candidate could be the scalar product of a Killing vector and the four-velocity of the particle, $\xi_\alpha\dot{x}^\alpha$. Its time derivative is

$$\frac{\mathrm{d}}{\mathrm{d}\tau}(\xi_\alpha\dot{x}^\alpha) = \frac{\mathrm{D}}{\mathrm{d}\tau}(\xi_\alpha\dot{x}^\alpha) = \xi_{\alpha;\beta}\dot{x}^\alpha\dot{x}^\beta + \xi_\alpha\frac{\mathrm{D}\dot{x}^\alpha}{\mathrm{d}\tau}\,. \tag{1.32}$$

The first term vanishes due to the antisymmetry of $\xi_{\alpha;\beta}$, and we can insert the right-hand side of the equations of motion (1.29) into the second term to obtain

$$\frac{\mathrm{d}}{\mathrm{d}\tau}(\xi_\alpha\dot{x}^\alpha) = \kappa\xi^\alpha F_{\alpha\beta}\dot{x}^\beta. \tag{1.33}$$

Therefore, for uncharged particles with $\kappa = 0$ we obtain as many constants of motion $\xi_\alpha\dot{x}^\alpha$ as there are Killing vector fields in the given spacetime. Only a subset of these constants, which (for a general $\dot{x}^\beta$) correspond to the Killing vectors that satisfy $\xi^\alpha F_{\alpha\beta} = 0$, is valid for charged particles as well. An alternative derivation of this result can be found in, e.g., Sommers [1973]. Take note that since the time derivative does not contain κ, the subset of constants that are applicable for charged particles does not actually distinguish between charged and uncharged particles at all. Therefore, we cannot reproduce constants such as (1.16) or (1.18) in this way.

Another reasonable candidate is the scalar product of a Killing vector and the generalized four-momentum given by (1.22). We can start by adding

$$\frac{\mathrm{d}}{\mathrm{d}\tau}(\kappa\xi_\alpha A^\alpha) = \frac{\mathrm{D}}{\mathrm{d}\tau}(\kappa\xi_\alpha A^\alpha) = \kappa\dot{x}^\beta\left(\xi_{\alpha;\beta}A^\alpha + \xi^\alpha A_{\alpha;\beta}\right) \tag{1.34}$$

to (1.33). After considering $F_{\alpha\beta} = A_{\beta;\alpha} - A_{\alpha;\beta}$ and using the antisymmetry of $\xi_{\alpha;\beta}$ once more, we obtain

$$\frac{\mathrm{d}}{\mathrm{d}\tau}\left(p_\alpha\,\xi^\alpha\right) = \kappa\dot{x}_\beta\left(\xi^\alpha A^\beta{}_{;\alpha} - A^\alpha\xi^\beta{}_{;\alpha}\right) = \kappa\dot{x}_\beta\pounds_{\boldsymbol{\xi}}A^\beta, \tag{1.35}$$

which means that for charged particles, $p_\alpha\,\xi^\alpha$ is a constant of motion if the Lie derivative $\pounds_{\boldsymbol{\xi}}\mathbf{A}$ vanishes. For uncharged particles, p_α becomes $\dot{x}_\alpha$ and both sets of constants are the same.

Both results seem to suggest that constants of motion for charged particles are connected to those Killing vector fields that correspond not only to symmetries of the metric but also to symmetries of the quantities that govern the electromagnetic field.

The results can be generalized for Killing tensors of higher rank, which are totally symmetric but their covariant derivative is totally antisymmetric, i.e., $k_{\alpha\ldots} = k_{(\alpha\ldots)}$ and $k_{(\alpha\ldots;\mu)} = 0$, where the dots represent an arbitrary number of indices. Then, the constants of motion are scalar products of the tensor with as many instances of the four-velocity as the rank of the tensor permits, but a further condition must again be satisfied if the constant is to be valid for charged particles as well. To demonstrate on a second-rank Killing tensor, we have

$$\frac{\mathrm{d}}{\mathrm{d}\tau}\left(k_{\alpha\beta}\dot{x}^\alpha\dot{x}^\beta\right) = \frac{\mathrm{D}}{\mathrm{d}\tau}\left(k_{\alpha\beta}\dot{x}^\alpha\dot{x}^\beta\right) = k_{\alpha\beta;\gamma}\dot{x}^\alpha\dot{x}^\beta\dot{x}^\gamma + 2k_{\alpha\beta}\frac{\mathrm{D}\dot{x}^\alpha}{\mathrm{d}\tau}\dot{x}^\beta = 2\kappa k_{\alpha\beta}F^\alpha{}_\gamma\,\dot{x}^\gamma\dot{x}^\beta\,. \tag{1.36}$$

Like in (1.32), the first term vanished due to the antisymmetry of $k_{\alpha\beta;\gamma}$. For the right-hand side to vanish for any $\dot{x}^\alpha$, we must either consider uncharged particles with $\kappa = 0$, or the Killing tensor must fulfill $k_{\alpha(\beta}F^\alpha{}_{\gamma)} = 0$. It is clear to see that the latter condition becomes $k_{\alpha(\ldots}F^\alpha{}_{\mu)} = 0$ for Killing tensors of higher rank, a result known in Sommers [1973] as well.

Note, however, that some of the constants of motion constructed from the Killing tensors may be powers or products of the constants that can be obtained from the Killing vectors, or, more generally, from the Killing tensors of lower ranks. To demonstrate that for a Killing tensor of rank two, let us consider two (not necessarily different) Killing vectors $\boldsymbol{\xi}$ and $\boldsymbol{\zeta}$. If we take $k_{\alpha\beta} = \xi_{(\alpha}\zeta_{\beta)}$, the symmetrized covariant derivative vanishes and this $\mathbf{k}$ indeed is a Killing tensor. Due to the symmetry of $\dot{x}^\alpha\dot{x}^\beta$, the corresponding constant is $k_{\alpha\beta}\dot{x}^\alpha\dot{x}^\beta = \xi_\alpha\dot{x}^\alpha\,\zeta_\beta\dot{x}^\beta$, clearly a product of the constants given by the two Killing vectors separately. If both of the constants are valid for charged particles, their product also is. Denoting n the number of Killing vectors ($n \geq 3$ for our spacetimes), in this way we get $\binom{n+1}{2}$ second-rank constants that bear no additional information and can be discarded.

Furthermore, also note that one of the Killing tensors of rank two is the metric itself, because it is symmetric and its covariant derivative vanishes even without the symmetrization. The corresponding constant of motion is the normalization of the four-velocity (1.6). Unsurprisingly, the normalization is valid for both uncharged and charged particles, as $g_{\alpha(\beta}\,F^\alpha{}_{\gamma)} = F_{(\beta\gamma)} = 0$ due to the antisymmetry of $\mathbf{F}$.

While we tend to draw more interesting implications for particle motion from the effective potentials above, these new constants of motion may provide further insight in specific cases, which shall be discussed accordingly. We shall limit

ourselves to the constants related to Killing tensors of rank at most two to keep the constants at most quadratic in the elements of the four-velocity. As it turns out, unfortunately, in the studied spacetimes the second-rank Killing tensors do not produce any constants of motion that are not determined completely by the constants obtained from the Killing vectors and the normalization of the four-velocity.

Even though the constants we derived in this section are mentioned in papers such as Frolov and Krtouš [2011], their usefulness can be limited by the number of independent Killing vector fields in a given spacetime and by the difficulty of computing higher-rank Killing tensor fields. For example, according to Visser [2009] the Kerr solution only has two Killing vectors corresponding to the two translational symmetries. These are covered by the cyclic coordinates in the Lagrangian, which is probably the reason why this extended method of obtaining constants of motion is not mentioned in papers dealing with related spacetimes such as Hackmann et al. [2010a,b] and Hackmann and Xu [2013]. Fortunately for us, some of our spacetimes have as much as six independent Killing vector fields, which means that we do get new information from the procedure described here.

As hinted above, the constant $\partial\mathcal{L}/\partial\dot{x}^Z$ corresponding to a cyclic coordinate x^Z of the Lagrangian $\mathcal{L}$ also corresponds to a certain Killing vector. To see this, we can use the pristine form of the equations of motion, i.e., the Euler–Lagrange equations,

$$\frac{\mathrm{d}}{\mathrm{d}\tau}\left(\frac{\partial\mathcal{L}}{\partial\dot{x}^\alpha}\right) - \mathcal{L}_{,\alpha} = 0\,. \tag{1.37}$$

Recalling that $\partial\mathcal{L}/\partial\dot{x}^\alpha = p_\alpha$, the dot product with a vector field $\boldsymbol{\xi}$ gives

$$\xi^\alpha\mathcal{L}_{,\alpha} = \xi^\alpha\frac{\mathrm{d}}{\mathrm{d}\tau}\,p_\alpha = \frac{\mathrm{d}}{\mathrm{d}\tau}(p_\alpha\xi^\alpha) - p_\alpha\frac{\mathrm{d}}{\mathrm{d}\tau}\,\xi^\alpha. \tag{1.38}$$

Now, the cyclic coordinate fulfills

$$\mathcal{L}_{,Z} = \frac{1}{2}g_{\mu\nu,Z}\dot{x}^\mu\dot{x}^\nu + \kappa A_{\mu,Z}\dot{x}^\mu = 0\,. \tag{1.39}$$

As the first term is quadratic in $\dot{x}^\mu$ and the second is not, both partial derivatives must vanish if $\kappa \neq 0$. The unavoidable first condition, $g_{\mu\nu,Z} = 0$, means that the metric supports a translational symmetry in x^Z, which is in the given coordinates represented by the constant Killing vector field $\boldsymbol{\xi} = \partial_{xz}$ satisfying $\xi^\alpha\mathcal{L}_{,\alpha} = \mathcal{L}_{,Z} = 0$ and $\mathrm{d}\boldsymbol{\xi}/\mathrm{d}\tau = 0$. Note that both expressions are covariant despite containing generally non-covariant derivatives[5]. Therefore, inserting this $\boldsymbol{\xi}$ into (1.38), we get the anticipated constant

$$0 = \frac{\mathrm{d}}{\mathrm{d}\tau}(p_\alpha\xi^\alpha) = \frac{\mathrm{d}}{\mathrm{d}\tau}\,p_Z = \frac{\mathrm{d}}{\mathrm{d}\tau}\left(\frac{\partial\mathcal{L}}{\partial\dot{x}^Z}\right), \tag{1.40}$$

which is manifestly of the form $p_\alpha\xi^\alpha$ in accordance with the previous results. For charged particles, the electromagnetic field must also fulfill $A_{\mu,Z} = 0$, so that

[5]The Lagrangian $\mathcal{L}$ is a scalar quantity, so its partial derivative is a vector and $\xi^\alpha\mathcal{L}_{,\alpha}$ is a scalar. Looking at (1.38), the left-hand side is a scalar and the first term on the right-hand side is similarly also a scalar, being a derivative of manifestly scalar $p_\alpha\xi^\alpha$. This means that $p_\alpha\,\mathrm{d}\xi^\alpha/\mathrm{d}\tau$ must also be a scalar quantity. As the four-momentum p_α is a covector, $\mathrm{d}\xi^\alpha/\mathrm{d}\tau$ is a vector.

the second term in $\mathcal{L}_{,Z}$ (1.39) vanishes as well. Since $\boldsymbol{\xi}$ is a basis vector, this additional condition is actually equivalent to $\pounds_{\boldsymbol{\xi}}\mathbf{A} = 0$, which is consistent with the analysis performed above. To sum up, while all cyclic coordinates correspond to translational symmetries of the metric, their Killing vectors must also reflect a symmetry of the electromagnetic field if the constants are to be valid for charged particles as well—both the gravitational and electromagnetic fields need to share the same symmetry.

1.2.2 Shell sources

A shell source is an infinitely thin shell that is located on the interface of two spacetimes, one of which is a studied spacetime that is understood as being generated by the shell. The spacetime at the other side of the shell is preferably an understood and realistic solution that is already known in the literature. While we do not aim to convince the reader that infinite cylindrical spacetimes are to any degree realistic, having an at least somewhat-realistic shell-source model can be an indication of situations where the spacetime can prove to be a useful approximation. Moreover, by examining the properties of the shell, one may hope to learn something about the properties of the investigated spacetime's metric in turn.

In order to find admissible shell sources, we employ the Israel junction conditions, first introduced in Israel [1966] and expanded for charged shells in Kuchař [1968]. They are used for connecting two parts of generally distinct spacetimes along a matching hypersurface. The fulfillment of the Einstein–Maxwell equations at the hypersurface is guaranteed by the induced energy-stress tensor $\mathbf{S}$ and induced current $\mathbf{s}$ appearing there, giving the shell the properties we are interested in.

The induced quantities and the shell's geometry

Let us here summarize the details of computation of the two induced tensors. Denoting ξ^i the coordinates on the hypersurface Σ and $x^\alpha_\pm$ in the two neighboring spacetimes, a convenient set of tangent vectors to Σ is $e^\alpha_{i\pm} = \partial x^\alpha_\pm/\partial\xi^i$. The normal fields $n^\alpha_\pm$ in the two spacetimes are oriented in such a way that they point in the same direction after crossing Σ. We normalize both sets of the four vectors in each spacetime to unity. The extrinsic curvature tensor K_{ij} associated with the embedding of Σ in a given spacetime is

$$K_{ij} = n_{\alpha;\beta} e^\alpha_i e^\beta_j \,. \tag{1.41}$$

Denoting $K^\pm_{ij}$ the curvature tensors associated with the two respective spacetimes and $[K_{ij}] = K^+_{ij} - K^-_{ij}$, we obtain the induced stress-energy tensor

$$S_{ij} = \frac{1}{8\pi}\left([K]h_{ij} - [K_{ij}]\right), \tag{1.42}$$

where we used the induced metric tensor on the hypersurface h_{ij} to contract $[K] = [K_{ij}]h^{ij}$.

As we are using Israel's formalism to find a shell source for our spacetimes, we first choose a suitable hypersurface in the investigated spacetimes splitting them

in two. We use cylindrical hypersurfaces and, omitting the $\pm$ signs distinguishing the two spacetimes being connected, we always consider the tetrad

$$\begin{aligned} \mathbf{e_T} &= \frac{1}{\sqrt{-g_{tt}}}\,\partial_t\,, \quad & \mathbf{e_Z} &= \frac{1}{\sqrt{g_{zz}}}\,\partial_z\,, \\ \mathbf{e_\Phi} &= \frac{1}{\sqrt{g_{\phi\phi}}}\,\partial_\phi\,, & \mathbf{n} &= \epsilon\,\frac{1}{\sqrt{g_{rr}}}\,\partial_r\,, \end{aligned} \tag{1.43}$$

where (T, Z, Φ) denote the coordinates on the cylindrical hypersurface with the usual interpretation as suggested by their names, and $\epsilon = \pm 1$ determines the orientation of the normal. The normal is to be directed from the minus spacetime to the plus spacetime, so, for example, the choice $\epsilon_- = \epsilon_+ = 1$ means that we preserve the part with lower radial coordinate from the minus spacetime, and the part with higher radial coordinate from the plus spacetime.

Next, we must make sure that the hypersurfaces in the two spacetimes being connected correspond to each other by fulfilling two conditions, a local one and a topological one. First, the induced metric on Σ is related to the full spacetime metric through $h_{ij} = g_{\mu\nu} e_i^\mu e_j^\nu$, and its computation must lead to the same result when viewed from both neighboring spacetimes. For us, the induced metric happens to be the three-dimensional Minkowski $h_{ij} = \mathrm{diag}(-1, 1, 1)$ for every considered spacetime[6], so this condition is always fulfilled. Second, the investigated spacetime has cylindrical symmetry, which means that at any given time the hypersurface will be a cylinder with axis corresponding to that of the two spacetimes. We must then make sure that the proper circumference of the hypersurface $\mathcal{C}$ (1.3) is the same when measured in both spacetimes[7], relating the respective coordinate radii.

The induced current on Σ is given by the difference of the projections of the electromagnetic tensors

$$F_{i\perp} = F_{\mu\nu} e_i^\mu n^\nu \tag{1.44}$$

on both sides of the hypersurface. The three-current is

$$s_i = \frac{1}{4\pi}[F_{i\perp}]\,. \tag{1.45}$$

We can then define the surface density of charge σ for a static observer on the hypersurface as a projection $\sigma = -s_i u^i$ of the induced current to a static observer's three-velocity u^i.

An interpretable shell

Not every connecting hypersurface that is permitted geometrically is also reasonable from a physical point of view, whatever the definition of 'reasonable' is.

[6] Take note that our computations yield the Minkowski spacetime seemingly expressed in Cartesian coordinates instead of cylindrical ones, where one would expect $h_{\Phi\Phi} = R^2$ with R denoting the radius of the shell. However, there is no radial coordinate R in the metric as the shells have a constant radius, so the two forms of the metric are connected through a simple rescaling of the angular coordinate, which does not introduce any off-diagonal elements.

[7] Like in Sec. 1.1.1 we assume in (1.3) that the angular coordinate is dimensionless with values $\phi \in [0, 2\pi)$, which we shall ensure by rescaling the coordinate in the examined spacetimes if necessary.

Some could argue that shell sources are necessarily unphysical because of their reduced dimensionality, which is a valid point that we are going to ignore here, arguing that the shell is the result of a limiting process starting from a shell of a finite thickness. Instead, let us have a look at the properties of the induced stress-energy tensor $\mathbf{S}$. There are various kinds of energy conditions that it may or may not satisfy (more on them in, e.g., Maeda and Martínez [2020]), but perhaps the most intuitive way of determining the shell's reasonableness is by comparing the computed $\mathbf{S}$ to an understood stress-energy tensor $\mathbf{S}^{(\mathrm{model})}$, such as the one for an incoherent dust,

$$\mathbf{S}^{(1)} = \mu\, \mathbf{u} \otimes \mathbf{u}\,, \tag{1.46}$$

where $\mathbf{u}$ is the relativistic three-velocity of the stream of dust particles on the hypersurface, and $\mu > 0$ is the density of the dust[8]. For the Minkowski metric and a general $\mathbf{u}$, we have

$$S^{(1)}_{ij} = \mu \begin{bmatrix} u_T^2 & u_T u_Z & u_T u_\Phi \\ u_T u_Z & u_Z^2 & u_Z u_\Phi \\ u_T u_\Phi & u_Z u_\Phi & u_\Phi^2 \end{bmatrix}. \tag{1.47}$$

In every single application of the formalism we have considered during our present work, the induced stress-energy tensor was diagonal[9]. Therefore, the off-diagonal elements of $S^{(\mathrm{model})}_{ij}$ must vanish, which for the dust model means that $u_Z = u_\Phi = 0$ and $u_T^2 = 1$ from the normalization of the relativistic velocity of massive particles, $u_i u^i = -1$. Therefore, in order to represent the incoherent dust of a single type of particles, a diagonal induced stress-energy tensor must have only one non-vanishing element, $S_{TT} > 0$. Unfortunately, we are not going to encounter such an agreeable $\mathbf{S}$ during our journey.

A very reasonable and much more useful model is the one used previously in Žofka and Langer [2005], where the authors consider an incoherent dust composed of four streams of particles. The three-velocities of the streams are chosen as follows:

$$\mathbf{u}_{(\mathbf{1})} = u_T\, \mathrm{d}T + u_Z\, \mathrm{d}Z + u_\Phi\, \mathrm{d}\Phi, \tag{1.48}$$
$$\mathbf{u}_{(\mathbf{2})} = u_T\, \mathrm{d}T - u_Z\, \mathrm{d}Z + u_\Phi\, \mathrm{d}\Phi, \tag{1.49}$$
$$\mathbf{u}_{(\mathbf{3})} = u_T\, \mathrm{d}T + u_Z\, \mathrm{d}Z - u_\Phi\, \mathrm{d}\Phi, \tag{1.50}$$
$$\mathbf{u}_{(\mathbf{4})} = u_T\, \mathrm{d}T - u_Z\, \mathrm{d}Z - u_\Phi\, \mathrm{d}\Phi. \tag{1.51}$$

The model stress-energy tensor is

$$\mathbf{S}^{(4)} = \mu \left(\mathbf{u}_{(\mathbf{1})} \otimes \mathbf{u}_{(\mathbf{1})} + \mathbf{u}_{(\mathbf{2})} \otimes \mathbf{u}_{(\mathbf{2})} + \mathbf{u}_{(\mathbf{3})} \otimes \mathbf{u}_{(\mathbf{3})} + \mathbf{u}_{(\mathbf{4})} \otimes \mathbf{u}_{(\mathbf{4})} \right), \tag{1.52}$$

where the choice of the same density μ for all four streams guarantees that the tensor is diagonal,

$$\mathbf{S}^{(4)} = 4\mu \left(u_T^2\, \mathrm{d}T^2 + u_Z^2\, \mathrm{d}Z^2 + u_\Phi^2\, \mathrm{d}\Phi^2 \right). \tag{1.53}$$

[8] We use μ instead of the perhaps more common ρ so that the quantity would not be confused with the radial coordinate, which is denoted ρ in some of the discussed spacetimes.

[9] Take note that as the intrinsic geometry of the hypersurface is flat, we need not distinguish between covariant and contravariant components when discussing diagonality.

From here, we can infer the conditions that a diagonal induced stress-energy tensor must fulfill so that the the shell source can be composed of four timelike streams of massive particles. First, S_{TT} must be positive and the remaining two diagonal elements must be non-negative. Second, the normalization of relativistic velocity for massive particles with $\delta = -1$ is equivalent to having

$$S_{TT} - S_{ZZ} - S_{\Phi\Phi} = -4\delta\mu = 4\mu > 0\,, \tag{1.54}$$

leaving us with four conditions in total. The last relation can be used to determine the model's μ from the induced stress-energy tensor, and the components of the three-velocity can then be obtained by comparing the elements of (1.53) to the induced tensor.

Note that the diagonal components of $\mathbf{S}$ have a clear physical interpretation: S_{TT} is the energy density on the shell and S_{ZZ} and $S_{\Phi\Phi}$ represent the pressure along the two respective directions. Due to our fortuitous choice of coordinates, these quantities are scalars, as they can be easily obtained by projections to the three-velocity of a static observer and to the two spacelike three-velocities aligned along Z and Φ, respectively. We could rename the energy density ρ and the pressures p_Z and p_Φ to use the usual symbols, but we shall not do that here in order to avoid confusing both us and the reader, as ρ is the radial coordinate in some of the discussed spacetimes and $\mathbf{p}$ can also represent the momentum of a particle. Nonetheless, even though $\mathbf{S}$ always comes with two indices in the following, let us keep in mind that the three components we encounter are always scalars.

While we do come across shells that satisfy our requirements in this work, note that the constructed shells do not fulfill the Einstein equations in 2+1 dimensions, as the induced flat metric would require the induced stress-energy tensor to vanish. However, the equations within the full four-dimensional spacetime are still valid as the shell is constructed in such a way that the junction conditions are satisfied.

As a side note, for a photon shell the expression (1.54) would be equal to zero, as photons have $\delta = 0$, and there would have to be necessarily at least one other non-zero diagonal element of $\mathbf{S}$ besides S_{TT}. However, because such a model can be viewed as an extreme version of a massive shell, considering only massive shells will suffice for our purposes due to continuity of the quantities involved. Moreover, photons do not carry electric charge, which means that the shells could not realistically contain any induced current.

Speaking of the currents, the four streams can model general induced currents when imbued with test electric charge,

$$\mathbf{s^{(4)}} = q_1\mathbf{u_{(1)}} + q_2\mathbf{u_{(2)}} + q_3\mathbf{u_{(3)}} + q_4\mathbf{u_{(4)}} \tag{1.55}$$

with components

$$\mathbf{s^{(4)}} = (q_1+q_2+q_3+q_4)\,u_T\,\mathrm{d}T + (q_1-q_2+q_3-q_4)\,u_Z\,\mathrm{d}Z + (q_1+q_2-q_3-q_4)\,u_\Phi\,\mathrm{d}\Phi\,. \tag{1.56}$$

As we deal with spacetimes with purely magnetic fields, there is no surface density of charge σ, equivalent to $s_T = 0$ for the diagonal induced metric, which would be impossible to be fulfilled by a single charged stream of particles as such a stream would be spacelike. However, as long as the sum of charges vanishes, a

superposition of four timelike streams can produce a spacelike total three-current. E.g., choosing $q \equiv q_1 = -q_2 = q_3 = -q_4$ results in the axial

$$\mathbf{s}^{(4)} = 4qu_Z \, \mathrm{d}Z \,. \tag{1.57}$$

Expressing u_Z from (1.53), we can compare a computed axial $\mathbf{s} = s_Z \, \mathrm{d}Z$ to the model to obtain an expression for particle charge q,

$$q = \frac{s_Z}{2}\sqrt{\frac{\mu}{S_{ZZ}}} = \frac{s_Z}{4}\sqrt{\frac{S_{TT} - S_{ZZ} - S_{\Phi\Phi}}{S_{ZZ}}} \,. \tag{1.58}$$

The choice $q \equiv q_1 = q_2 = -q_3 = -q_4$ similarly leads to

$$\mathbf{s}^{(4)} = 4qu_\Phi \, \mathrm{d}\Phi \tag{1.59}$$

and

$$q = \frac{s_\Phi}{2}\sqrt{\frac{\mu}{S_{\Phi\Phi}}} = \frac{s_\Phi}{4}\sqrt{\frac{S_{TT} - S_{ZZ} - S_{\Phi\Phi}}{S_{\Phi\Phi}}} \tag{1.60}$$

for azimuthal currents. Generally, we can consider

$$\begin{aligned}\mathbf{s}^{(4)} = \frac{1}{4}\left(\frac{s_Z}{u_Z} + \frac{s_\Phi}{u_\Phi}\right)\mathbf{u}_{(1)} + \frac{1}{4}\left(-\frac{s_Z}{u_Z} + \frac{s_\Phi}{u_\Phi}\right)\mathbf{u}_{(2)} \\ + \frac{1}{4}\left(\frac{s_Z}{u_Z} - \frac{s_\Phi}{u_\Phi}\right)\mathbf{u}_{(3)} + \frac{1}{4}\left(-\frac{s_Z}{u_Z} - \frac{s_\Phi}{u_\Phi}\right)\mathbf{u}_{(4)}\end{aligned} \tag{1.61}$$

to obtain the spacelike

$$\mathbf{s}^{(4)} = s_Z \, \mathrm{d}Z + s_\Phi \, \mathrm{d}\Phi \,, \tag{1.62}$$

where s_Z and s_Φ are determined by the induced three-current. This corresponds to the choice $q_4 = -q_1$ and $q_3 = -q_2$ in (1.55) with

$$\begin{aligned} q_1 &= \frac{\sqrt{\mu}}{2}\left(\frac{s_Z}{\sqrt{S_{ZZ}}} + \frac{s_\Phi}{\sqrt{S_{\Phi\Phi}}}\right), \\ q_2 &= \frac{\sqrt{\mu}}{2}\left(-\frac{s_Z}{\sqrt{S_{ZZ}}} + \frac{s_\Phi}{\sqrt{S_{\Phi\Phi}}}\right). \end{aligned} \tag{1.63}$$

Note that there may be intervals of the shell's radii where the induced-stress energy tensor $\mathbf{S}$ does not fulfill our requirements for the four-stream interpretation, but q may still be well defined.

If two particular parts of two spacetimes allow an interpretable shell on their interface, then the shell's radius is not fixed in most cases but can take any value from a specific interval. An endpoint of the interval can correspond to an endpoint of the interval of allowed radial coordinates within the spacetime due to an axis (singular or not) and it is also possible that the interval extends to radial infinity. Most often, however, there is nothing extraordinary about the extreme values of the allowed shell's radii from the viewpoint of the spacetime itself. What do the endpoints represent, then? Generally, we can distinguish two cases: Either one of the diagonal elements of $\mathbf{S}$ vanishes, or μ vanishes. In the former case, (1.53) implies that the corresponding element of the three-velocity of the streams vanishes, and beyond that point the three-velocity would need to be complex. On the other hand, the point where μ expressed from the relation

(1.54) vanishes corresponds to a photon shell as mentioned above. This can be seen after expressing the Lorentz factor from u_T,

$$\gamma = \sqrt{\frac{S_{TT}}{4\mu}}\,, \tag{1.64}$$

which clearly diverges in the limit of $\mu \to 0^+$ for a finite $S_{TT} > 0$.

It might seem natural to extend our shell-source model to the case of a perfect fluid, but it can be argued that a seemingly perfect fluid confined to a shell is not perfect anymore, as there cannot be any pressure along the normal to the hypersurface. This is not an issue for the incoherent dust, which is why we focus solely on dust shells.

Note that if a shell admits our desired dust interpretation, the induced stress-energy tensors actually comply with multiple energy conditions according to Maeda and Martínez [2020]. Denoting A either spatial coordinate and using our notation, for our 3D diagonal induced stress-energy tensor $\mathbf{S}$ the five energy conditions discussed in the paper read as follows:

- Null energy condition: $S_{TT} + S_{AA} \geq 0$.
- Weak energy condition: $S_{TT} + S_{AA} \geq 0$ and $S_{TT} \geq 0$.
- Strong energy condition: $S_{TT} + S_{AA} \geq 0$ and $S_{ZZ} + S_{\Phi\Phi} \geq 0$.
- Flux energy condition: $(S_{TT})^2 \geq (S_{AA})^2$.
- Dominant energy condition: $S_{TT} \geq |S_{AA}|$ and $S_{TT} \geq 0$.

The first three conditions are manifestly met by our dust shells, as the diagonal elements of $\mathbf{S}$ are non-negative. For the same reason, we can rewrite FEC and the first requirement in DEC as $S_{TT} - S_{AA} \geq 0$, which is fulfilled due to our relation (1.54), which implies both that $S_{TT} - S_{ZZ} > S_{\Phi\Phi} \geq 0$ and $S_{TT} - S_{\Phi\Phi} > S_{ZZ} \geq 0$. Therefore, the dust shells we aim to find fulfill each of the five standard energy conditions.

Lastly, note that there is another scalar quantity that can be used to describe the shell, its mass per unit proper length M_1, which is defined in publications such as Bičák and Žofka [2002], Žofka and Langer [2005], and Žofka and Bičák [2007] as

$$M_1 = \mathcal{C} S_{TT}\,. \tag{1.65}$$

Because the shell's circumference $\mathcal{C}$ given by (1.3) is by definition positive, we have $\operatorname{sgn}(M_1) = \operatorname{sgn}(S_{TT})$. While the scalar does not provide an additional constraint on the shells, a critical value of $M_1 = 1/4$ tends to appear in the literature as the maximum mass per unit length of shells located in spacetimes that are regular on both sides of the shell regardless of the matter content of the shell itself as long as the cosmological constant is not involved. This value has been known for quite some time, see, e.g., Raychaudhuri and Som [1962] and Langer [1969]. In the recent decades, this observation was made for shells connecting the (regular) asymptotic region of the Levi–Civita solution first to flat spacetime inside the shell by Bičák and Žofka [2002], and later to the Bonnor–Melvin spacetime by Žofka and Langer [2005]. The existence of an upper bound for M_1 for regular

spacetimes should come as no surprise, as the amount of matter in a given region has to be bounded for regular spacetimes that are free of horizons. Note that this result is reminiscent of the famous hoop conjecture, first proposed in Thorne [1972], which deals with compact matter and does not consider the presence of the cosmological constant, but our shells violate both assumptions. After adding a non-zero cosmological constant to the Levi–Civita solution, Žofka and Bičák [2007] find that further conditions must be fulfilled if $M_1 = 1/4$ is not to be exceeded for regular spacetimes. Singular composite spacetimes are not expected to fulfill any particular inequality with respect to $M_1 = 1/4$.

Our approach

We aim to use Israel's formalism to find admissible sources of (parts of) the seven spacetimes examined in this thesis. At the end of each of the seven corresponding sections, we first briefly discuss shells on the interface of two instances of the same spacetime, and then we try to find an interpretable shell leading to one of the better-known spacetimes listed in Sec. 1.3, ideally to the Minkowski spacetime of Sec. 1.3.1 as it is the simplest, and yet, perhaps paradoxically, the most realistic one. Finally, once all of our spacetimes have been properly introduced, in Sec. 3.1 we talk about their mutual connections.

While we would prefer to obtain analytical results, most shells are going to be examined purely numerically, using randomly-generated parameters in the two spacetimes on either side of the shell. This makes drawing graspable results binding the two sets of parameters together virtually impossible in most cases, which means we are unable to learn more about the meaning of the parameters of the two connected spacetimes. However, finding interpretable shells (especially those that cut out singularities if there are any in the given solution) even numerically still lends some credibility to the examined spacetime, as the shell can be seen as something of a wormhole leading to the examined solution from another spacetime that may be generally accepted as more realistic. Of course, we still have to ignore the fact the cylindrical symmetry is perhaps not very realistic in the first place...

Note that we do not insist on keeping the same value (or even the sign) of the cosmological constant on both sides of the connecting hypersurface. Therefore, the constant is considered to be constant in the two domains separated by the hypersurface, but there is a discontinuity on the shell itself. The shell then forms a so-called domain wall. In recent years, shells (even charged ones) serving as domain walls appear, for example, in the context of the AdS/CFT correspondence and holography with implications for cosmology in papers such as Alberghi et al. [1999], Freivogel et al. [2006a,b], Fu and Marolf [2019], de Alwis et al. [2020], and countless others, but they were considered in older papers as well, see, e.g., Coleman and De Luccia [1980] and Fischler et al. [1990].

For all interpretable shells we provide a summary of their corresponding curves of M_1 in Sec. 3.1. As we perform mainly numerical analysis, we are unable to draw analytical conclusions about the critical nature of the value of $M_1 = 1/4$, but we do check its uniqueness numerically and compare our results with the expectation that regular spacetimes should often have $M_1 \in (0, 1/4]$.

1.2.3 Penrose diagrams

Penrose conformal diagrams are a frequently-used way of depicting the global causal structure of a spacetime in which two spatial coordinates play somewhat less interesting role than the remaining one. Due to the cylindrical symmetry of the spacetimes studied in this work, we are interested in capturing the timelike and radial dimensions of spacetimes worthy of this endeavor. We are especially interested in the spacetimes with a radial magnetic field presented in Sec. 2.5 and 2.6, as they are the only solutions examined in this work with a non-trivial causal structure due to the presence of horizons.

The construction of the diagrams consists of employing such coordinate transformations that in timelike two-dimensional slices along the radial direction the areas radially bounded by the horizons, singularities, axes, and/or radial infinity can be described using finite coordinate intervals, which makes the subsequent rendering of the image straightforward. In our case, each point in these diagrams then represents a two-dimensional cylinder of the 'lost' coordinates z and ϕ located at a given coordinate in the slice.

Restricting ourselves to $z = 0 = \phi$, we begin with a metric of the form

$$\mathrm{d}s^2 = -f(r)\,\mathrm{d}t^2 + \frac{\mathrm{d}r^2}{f(r)}\,. \tag{1.66}$$

We introduce the so-called tortoise coordinate r^* as

$$\mathrm{d}r^* = \frac{\mathrm{d}r}{f(r)}\,, \tag{1.67}$$

which we will be generally able to integrate to express $r^*(r)$ using elementary functions, even though the same cannot be said for the inversion $r(r^*)$. After the transformation we have

$$\mathrm{d}s^2 = f(r(r^*))\left(-\mathrm{d}t^2 + \mathrm{d}r^{*2}\right). \tag{1.68}$$

If the spacetime contains any horizons, they are located at the radii where f vanishes. For practical purposes we shall consider each spacetime block bounded by the given horizons separately and arrange the blocks in the resulting diagram in the final step. While we always consider real f, the integral of $1/f$ can have an imaginary part if there is a horizon. Therefore, in each of the blocks we first select the imaginary part of the constant of integration in $r^*(r)$ to offset the imaginary part of the integral, effectively considering $r^* \to \Re(r^*)$. The real part of the constant is set the same for each spacetime block to maintain a sense of continuity, even though the function $r^*(r)$ actually diverges at the horizons for our spacetimes.

Next, on each block we introduce the analogy of the Eddington–Finkelstein coordinates,

$$u = \operatorname{sgn}(f)(t - r^*)\,, \tag{1.69}$$

$$v = \qquad +(t + r^*)\,, \tag{1.70}$$

leading to

$$\mathrm{d}s^2 = -\left|f(r(u,v))\right| \mathrm{d}u\,\mathrm{d}v\,. \tag{1.71}$$

The final transformation is to the so-called Penrose coordinates ψ a ξ,

$$\psi = \arctan v + \arctan u\,, \tag{1.72}$$

$$\xi = \arctan v - \arctan u\,. \tag{1.73}$$

The relation can be inverted

$$u = \tan \frac{1}{2}(\psi - \xi)\,, \tag{1.74}$$

$$v = \tan \frac{1}{2}(\psi + \xi)\,, \tag{1.75}$$

to obtain

$$\mathrm{d}u = \frac{1}{2}\frac{\mathrm{d}\psi - \mathrm{d}\xi}{\cos^2 \frac{1}{2}(\psi - \xi)}\,, \tag{1.76}$$

$$\mathrm{d}v = \frac{1}{2}\frac{\mathrm{d}\psi + \mathrm{d}\xi}{\cos^2 \frac{1}{2}(\psi + \xi)}\,, \tag{1.77}$$

leading to the metric

$$\mathrm{d}s^2 = \frac{|f(r(\psi,\xi))|}{(\cos\psi + \cos\xi)^2}\left(-\mathrm{d}\psi^2 + \mathrm{d}\xi^2\right) \tag{1.78}$$

conformally related to the two-dimensional flat metric, but with both coordinates bounded by $\pm\pi$ arctan u, where u is an arbitrary unit of length. This enables us to draw diagrams of finite size for each block. Note that another advantage of the diagrams is that radial photon geodesics travel at a 45-degree angle in the chart.

To sum up, the construction consists of going through the coordinate transformations $(t, r) \to (t, r^*) \to (u, v) \to (\psi, \xi)$. The last two coordinates are chosen in such a way that ψ is the temporal coordinate and ξ is the spatial one even in the dynamical areas of spacetimes with $f < 0$, where t and r exchange their physical interpretation. For each block we draw its boundaries and the lines of constant coordinates t and r, obtaining the usual diamond-shaped diagrams or their cropped variants, depending on the boundaries of the particular area of the spacetime. Finally, we shift ψ and ξ in the blocks so that they are arranged correctly with respect to the horizon positions to form a diagram encompassing all areas of the spacetime with unique physical properties. However, in some cases such a diagram may not represent a geodesically-complete spacetime and we have to stack copies of the diagram along the appropriate edges to achieve analytical maximality. This will be discussed on a per-diagram basis.

1.3 Better-known cylindrical spacetimes

In this section we provide a brief summary of select named spacetimes with cylindrical symmetry we shall refer to throughout the thesis. They are often assumed to be the limiting cases of the solutions we analyze and can be used in determining shell sources.

1.3.1 Minkowski

It is inconceivable that anyone who dabbles in Einstein's theories of relativity would not be intimately familiar with the flat Minkowski spacetime, the stage of the special theory. Calling this spacetime only a cylindrical one is somewhat of an understatement, because it is maximally symmetric. Having said that, for our purposes we shall use the cylindrical form of the metric,

$$\mathrm{d}s^2 = -\mathrm{d}t^2 + \mathrm{d}\rho^2 + \mathrm{d}z^2 + \rho^2\,\mathrm{d}\phi^2\,. \tag{1.79}$$

While we do not deem it necessary to write about this spacetime in length here, we shall present the main quantities pertaining to the use of Israel's formalism of Sec. 1.2.2. Considering a cylindrical hypersurface located at a given $\rho = \text{const.}$, its extrinsic curvature tensor (1.41) is simply

$$\mathbf{K} = \epsilon\rho^{-1}\,\mathrm{d}\Phi^2\,, \tag{1.80}$$

where ϵ determines the orientation of the normal as explained in Sec. 1.2.2. As the spacetime is a vacuum one, there is no electromagnetic field to project to the normal, so we have $\mathbf{F}_\perp = 0$. Lastly, the formula for the proper circumference (1.3) of the hypersurface is the Euclidean one,

$$\mathcal{C} = 2\pi\rho\,. \tag{1.81}$$

The proper circumference depends on the proper radius linearly, $\mathrm{d}\mathcal{C}/\mathrm{d}r_p = 2\pi$, as the ρ coordinate corresponds to proper distance, $\mathrm{d}r_p = \mathrm{d}\rho$.

1.3.2 Levi–Civita

A general cylindrically-symmetric and static vacuum exact solution without the cosmological constant is the Levi–Civita spacetime, discovered in Levi-Civita [1919] (republished in English in Levi-Civita [2011]) not long after the general theory of relativity itself was introduced, even though the spacetime's interpretation was not clear at the time. A possible form of the metric given by Richterek et al. [2000] and Griffiths and Podolský [2009] is

$$\mathrm{d}s^2 = -\rho^{4\sigma}\mathrm{d}t^2 + \rho^{4\sigma(2\sigma-1)}\left(\mathrm{d}\rho^2 + \mathrm{d}z^2\right) + C^2\rho^{2(1-2\sigma)}\mathrm{d}\phi^2 \tag{1.82}$$

with two parameters $C > 0$ and σ of any sign.

For sufficiently small positive values of σ, the spacetime can be interpreted as that of a uniform line source (which can be replaced by a regular region filled with matter) at the axis at $\rho = 0$ with σ representing the effective gravitational mass per unit proper length. The first papers dealing with this issue suggested the upper bound for this interpretation to be $\sigma = 1/4$, which was later extended to $\sigma = 1/2$ until finally Wang et al. [1997] found physically-reasonable cylindrical sources for the spacetime for $\sigma \in [0, 1]$. However, note that for $\sigma > 1/2$ we have $\lim_{\rho\to 0^+} g_{\phi\phi} = \infty$, so $\rho = 0$ represents the asymptotic region instead of the axis. The axis is then located at $\rho \to \infty$. The parameter C can give a deficit angle at the axis if $\sigma = 0$. It is not possible to regularize the axis for other values of σ, as the fraction in (1.2) is proportional to $\rho^{-8\sigma^2}$, so it cannot attain finite and non-zero values in the limit of either $\rho \to 0$ or $\rho \to \infty$.

The algebraic type of the spacetime depends on the value of σ. The spacetime is flat for $\sigma \in \{0, \frac{1}{2}, \infty\}$. For other values of σ, there is a curvature singularity at $\rho = 0$, regardless whether it represents the axis or the asymptotic region, as the Kretschmann scalar

$$R_{\alpha\beta\gamma\delta}R^{\alpha\beta\gamma\delta} = 64\sigma^2(4\sigma^2 - 2\sigma + 1)(2\sigma - 1)^2\rho^{-16\sigma^2+8\sigma-4} \tag{1.83}$$

diverges there. For $\sigma \in \{1/4, 1, -1/2\}$ the spacetime is of type D. The solution is otherwise algebraically general. For a general σ, the solution admits only three independent Killing vector fields, namely ∂_t, ∂_z, and ∂_ϕ, all three related to the translational symmetries of the metric.

The metric is not asymptotic to Minkowski space in cylindrical coordinates unless $\sigma = 0$. For $\sigma = 1$, the spacetime is the asymptotic form of the Bonnor–Melvin solution for large ρ.

Note that the spacetime is invariant under a transformation that switches the role of the z and ϕ coordinates if we also change $2\sigma \to 1/2\sigma$, which means that the parameter ranges $\sigma \in (0, 1/2]$ and $[1/2, \infty)$ are equivalent as long as the two coordinates are swapped.

In order to use this solution for determining shell sources, we need to compute the extrinsic curvature tensor (1.41),

$$\mathbf{K} = -\epsilon\,\rho^{-4\sigma^2+2\sigma-1}\left(2\sigma\ \mathrm{d}T^2 - 2\sigma(2\sigma-1)\ \mathrm{d}Z^2 + (2\sigma-1)\ \mathrm{d}\Phi^2\right), \tag{1.84}$$

and the proper circumference (1.3) of the shell,

$$\mathcal{C} = 2\pi C\rho^{1-2\sigma}. \tag{1.85}$$

Assuming we have the axis at $\rho = 0$ (requiring $\sigma < 1/2$), the derivative (1.4) of $\mathcal{C}$ with respect to the proper radius of the shell as measured from the axis $\mathrm{d}\mathcal{C}/\mathrm{d}r_p = 2\pi C(1-2\sigma)\rho^{-4\sigma^2}$ vanishes in the asymptotic region, so the circumference of circles with diverging proper radius does not depend on the coordinate radius itself. As the spacetime does not contain an electromagnetic field, we have $\mathbf{F}_\perp = 0$.

Note that the generalization of the Levi–Civita solution to include the cosmological constant was discovered independently by Linet [1986] and Tian [1986], and analyzed further in, e.g., da Silva et al. [2000], Žofka and Bičák [2007], and Griffiths and Podolský [2010].

1.3.3 The original Bonnor–Melvin solution

The Bonnor–Melvin spacetime, also known as the Melvin universe, is a cylindrical, electrovacuum, static solution of the Einstein–Maxwell equations without the cosmological term. It was originally discovered by Bonnor [1954] and later rediscovered by Melvin [1964]. Griffiths and Podolský [2009] present the metric

$$\mathrm{d}s^2 = \left(1 + \frac{1}{4}B^2\rho^2\right)^2\left(-\mathrm{d}t^2 + \mathrm{d}\rho^2 + \mathrm{d}z^2\right) + \left(1 + \frac{1}{4}B^2\rho^2\right)^{-2}\rho^2\,\mathrm{d}\phi^2 \tag{1.86}$$

with the coordinates $t, z \in \mathbb{R}$ and $\rho \in \mathbb{R}_0^+$ of the dimension of length, and dimensionless $\phi \in [0, 2\pi)$. There is an axis at $\rho = 0$. The only parameter B ensures

that there is a non-zero electromagnetic field. Due to the reasons stated in the introduction, we shall consider a purely magnetic field

$$\mathbf{F} = B\left(1+\frac{1}{4}B^2\rho^2\right)^{-2}\rho\,\mathrm{d}\rho\wedge\mathrm{d}\phi\,, \tag{1.87}$$

which is oriented along the z axis, but a duality rotation can be performed to obtain an electric component as well[10]. The magnitude of the field is highest at the axis and decreases monotonically to zero with increasing ρ,

$$F_{\mu\nu}F^{\mu\nu} = 2B^2\left(1+\frac{1}{4}B^2\rho^2\right)^{-4}. \tag{1.88}$$

The Kretschmann scalar is

$$R_{\alpha\beta\gamma\delta}R^{\alpha\beta\gamma\delta} = \frac{B^4\left(3B^4\rho^4-24B^2\rho^2+80\right)}{4\left(1+\frac{1}{4}B^2\rho^2\right)^8}\,. \tag{1.89}$$

The spacetime does not contain any curvature singularities and the axis is regular, condition (1.2) holds.

The solution is a type D spacetime except for the hypersurface $\rho = 2/|B|$ and in the limit $\rho\to\infty$, where it is type O. It belongs to the Kundt class of spacetimes[11]. It admits four Killing vector fields. Three of them, ∂_t, ∂_z, and ∂_ϕ, correspond to the three translational symmetries of the metric, while the last one, $z\partial_t + t\partial_z$, corresponds to boost in the t–z plane, along the axis. Therefore, the group of isometries of the Melvin universe is $ISO(1,1)\times E(1)$, where $ISO(d,1)$ is the Poincaré group of isometries of Minkowski spacetime of dimension $d+1$ and $E(d)$ is the d–dimensional Euclidean group.

Because of its cylindrical symmetry, the spacetime is not asymptotically flat. Along the radial direction it asymptotically approaches the Levi–Civita metric with $\sigma = 1$. Setting $B = 0$, we obtain the Minkowski spacetime in cylindrical coordinates.

As this solution is the forefather to the magnetic spacetimes examined in the following part of the thesis, we try to find a shell source for each of the spacetimes with this solution on the other side of the shell. In order to do that, we need to compute the relevant quantities. The extrinsic curvature tensor (1.41) is

$$\mathbf{K} = \epsilon\left(1+\frac{1}{4}B^2\rho^2\right)^{-2}\left(\frac{1}{2}B^2\rho\left(-\mathrm{d}T^2+\mathrm{d}Z^2\right)+\left(1-\frac{1}{4}B^2\rho^2\right)\rho^{-1}\,\mathrm{d}\Phi^2\right) \tag{1.90}$$

[10] A form of the metric containing both a magnetic and an electric component of the electromagnetic field is given in Kadlecová and Krtouš [2010] as

$$\mathrm{d}s^2 = \left(1+\frac{E^2+B^2}{4}\rho^2\right)^2(-\mathrm{d}t^2+\mathrm{d}\rho^2+\mathrm{d}z^2)+\left(1+\frac{E^2+B^2}{4}\rho^2\right)^{-2}\rho^2\,\mathrm{d}\phi^2$$

with

$$\mathbf{F} = E\,\mathrm{d}z\wedge\mathrm{d}t + B\left(1+\frac{E^2+B^2}{4}\rho^2\right)^{-2}\rho\,\mathrm{d}\rho\wedge\mathrm{d}\phi\,.$$

[11] According to Griffiths and Podolský [2009], a solution belongs to Kundt's class if it admits a null geodesic congruence with vanishing optical scalars: shear, expansion, and twist.

and the projection of the electromagnetic tensor (1.44) yields

$$\mathbf{F}_{\perp} = -\epsilon \left(1 + \frac{1}{4} B^2 \rho^2\right)^{-2} B \, \mathrm{d}\Phi \,. \tag{1.91}$$

The circumference (1.3) of the shells is

$$\mathcal{C} = \frac{2\pi\rho}{1 + \frac{1}{4} B^2 \rho^2} \,. \tag{1.92}$$

Its maximal value $2\pi/\left|B\right|$ is achieved for $\rho = 2/\left|B\right|$ and the function is monotonic on either side from the maximum with $\lim_{\rho\to 0^+} \mathcal{C} = \lim_{\rho\to\infty} \mathcal{C} = 0$, as illustrated in Fig. 1.1. Considering the proper radius of the shells r_p, the derivative (1.4),

$$\frac{\mathrm{d}\mathcal{C}}{\mathrm{d}r_p} = \frac{2\pi \left(1 - \frac{1}{4} B^2 \rho^2\right)}{\left(1 + \frac{1}{4} B^2 \rho^2\right)^3} \,, \tag{1.93}$$

yields the value of 2π at the axis as expected and vanishes for $\rho \to \infty$.

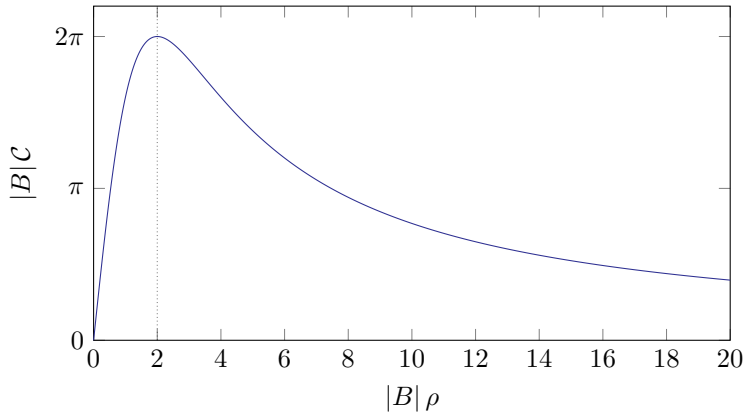

Figure 1.1: The circumference of shells at a given radial coordinate for the Bonnor–Melvin spacetime. The maximal value is achieved at $\left|B\right| \rho = 2$.

2. Magnetic spacetimes

2.1 Deriving the solutions

The magnetic spacetimes presented in this work have been found through direct manipulation of the Einstein–Maxwell equations, generally with a non-zero cosmological constant. Using the standard notation, the Einstein equations read

$$G_{\mu\nu} + \Lambda g_{\mu\nu} = 8\pi T_{\mu\nu}\,, \tag{2.1}$$

where

$$T_{\mu\nu} = \frac{1}{4\pi}\left(F_{\mu}{}^{\alpha}F_{\nu\alpha} - \frac{1}{4}g_{\mu\nu}F^{\alpha\beta}F_{\alpha\beta}\right) \tag{2.2}$$

is the stress-energy tensor of the electromagnetic field described by tensor $F_{\mu\nu}$ satisfying the Maxwell equations

$$F^{\mu\nu}{}_{;\nu} = 4\pi J^{\mu}, \tag{2.3}$$

$$\mathrm{d}\mathbf{F} = 0\,. \tag{2.4}$$

In correspondence with the original Bonnor–Melvin solution, sources of the magnetic field are taken to lie in spatial infinity or (whenever applicable) in singularities, so the four-current in (2.3) vanishes, $J^{\mu} = 0$.

Note that the electromagnetic stress-energy tensor satisfies $T^{\mu}{}_{\mu} = 0$. The trace of the Einstein equations (2.1) then implies that the Ricci scalar is $R = 4\Lambda$ for all electrovacuum spacetimes, including those studied throughout this work.

In the following, we shall use (1.1) as the ansatz for the sought cylindrically-symmetric and static metric tensors. As regards the magnetic field, the choice of the ansatz depends on its desired alignment. For the sake of completeness, we shall go through the equations for each alignment separately.

2.1.1 Axial magnetic field

Building on Žofka [2019], we first assumed the magnetic field to be of the form

$$\mathbf{F} = f(r)\,\mathrm{e}^{\frac{C(r)}{2}}\,\mathrm{d}r \wedge \mathrm{d}\phi\,, \tag{2.5}$$

corresponding to the original Bonnor–Melvin solution and manifestly satisfying one of Maxwell's equations, $\mathrm{d}\mathbf{F} = 0$. The quantity f (of the dimension 1/u with an arbitrary unit of length u) corresponds to one of the invariants of the electromagnetic field,

$$F_{\mu\nu}F^{\mu\nu} = 2f^2\,, \tag{2.6}$$

while the other invariant vanishes, $\star F_{\mu\nu}F^{\mu\nu} = 0$.

This $\mathbf{F}$ represents an axial magnetic field, i.e., a field aligned along the spacetime's axis. To see that more clearly, we can use Cartesian-like coordinates $x = r\cos\phi$ and $y = r\sin\phi$ and compare the obtained $\mathbf{F} = F_{r\phi}(r)/r\,\mathrm{d}x \wedge \mathrm{d}y$ with the electromagnetic tensor in the Minkowski spacetime, where $F_{xy} = B_z$.

After inserting the metric (1.1) and this **F** into the four non-trivial Einstein equations, we obtain a set of second-order non-linear ordinary differential equations for the four unknown quantities A, B, C, and f as functions of the radial coordinate r,

$$\begin{aligned} 2(B''+C'')+(B')^2+(C')^2+B'C'+4\Lambda+4f^2 &= 0\,, && (2.7)\\ 2(A''+C'')+(A')^2+(C')^2+A'C'+4\Lambda+4f^2 &= 0\,, && (2.8)\\ 2(A''+B'')+(A')^2+(B')^2+A'B'+4\Lambda-4f^2 &= 0\,, && (2.9)\\ A'B'+A'C'+B'C'+4\Lambda-4f^2 &= 0\,. && (2.10) \end{aligned}$$

The remaining Maxwell equation can be integrated to yield

$$f\mathrm{e}^{\frac{A+B}{2}} = \text{const.}, \tag{2.11}$$

which is, however, a consequence of the Einstein equations above:

The derivative of (2.10) yields

$$A''(B'+C')+B''(A'+C')+C''(A'+B')-8ff'=0\,. \tag{2.12}$$

Taking the other three Einstein equations, multiplying them with the first derivative of the respective absent metric function and summing them, we obtain

$$\begin{aligned} 2\Big[A''(B'+C')+B''(A'+C')+C''(A'+B')\Big]+4f^2(A'+B'-C')\\ +(A'+B'+C')\Big[A'B'+A'C'+B'C'+4\Lambda\Big]=0\,. \end{aligned} \tag{2.13}$$

Next, we substitute in the first square bracket from (2.12) and in the second one from (2.10) to get

$$16f\left[f'+\frac{1}{2}f(A+B)'\right]=0\,. \tag{2.14}$$

As we choose to disregard the solution with no magnetic field, we require

$$f'+\frac{1}{2}f(A+B)'=0\,, \tag{2.15}$$

the solution to which is (2.11), proving that the Maxwell equation is indeed not independent from the Einstein equations in this case.

To simplify the equations, it is possible to express the first derivatives of the metric functions A, B, and C as functions of f and its derivatives only. The first step is to add (2.9) and (2.10) to obtain

$$2(A'+B')'+(A'+B')^2+C'(A'+B')+8\Lambda-8f^2=0\,. \tag{2.16}$$

Now, first considering the case with a homogeneous magnetic field invariant, i.e., $f=\text{const.}$, equation (2.15) implies that $A+B$ is constant as well. The first three terms in the last equation vanish and we can immediately see that

$$f^2=\Lambda\,. \tag{2.17}$$

The relation (2.10) then simplifies to $A'B'=0$, so both of these functions must be constant. The Einstein equations reduce to

$$C''+\frac{1}{2}(C')^2+4\Lambda=0\,, \tag{2.18}$$

leading to

$$C(r) = 2\ln\sigma + 2\ln\sin\Big(\sqrt{2\Lambda}\,(r+R)\Big)\,, \tag{2.19}$$

where σ and R are constants of integration. After rescaling the coordinates, we obtain the metric

$$\mathrm{d}s^2 = -\mathrm{d}t^2 + \mathrm{d}r^2 + \mathrm{d}z^2 + \sigma^2\sin^2\Big(\sqrt{2\Lambda}\,r\Big)\,\mathrm{d}\phi^2 \tag{2.20}$$

with the magnetic field

$$\mathbf{F} = \sqrt{\Lambda}\sigma\sin\Big(\sqrt{2\Lambda}r\Big)\,\mathrm{d}r\wedge\mathrm{d}\phi \tag{2.21}$$

as discovered by Žofka [2019]. This solution is the topic of Sec. 2.2.

On the other hand, for a non-constant f we can use (2.15) to replace all three instances of $A'+B'$ in (2.16) with $-2f'/f$. It is then possible to express the first derivative of C as

$$C' = -2\frac{f''}{f'} + 4\frac{f'}{f} + 4\frac{f}{f'}\left(\Lambda - f^2\right). \tag{2.22}$$

The second derivative follows,

$$C'' = -2\frac{f'''}{f'} + 2\frac{f''}{(f')^2}\left(f'' - 2f(\Lambda - f^2)\right) + 4\frac{f''}{f} - 4\frac{(f')^2}{f^2} + 4\left(\Lambda - 3f^2\right). \tag{2.23}$$

Next, adding the first two Einstein equations (2.7), (2.8) and subtracting the last two (2.9), (2.10) from them, we obtain

$$A'B' = 2C'' + (C')^2 + 8f^2\,, \tag{2.24}$$

which for the homogeneous case reduces to (2.18). Together with (2.22) and (2.23), we can use this equation to express $A'B'$ as a function of f and its derivatives only. Further expressing $A'+B'$ from (2.15), we can rewrite equation (2.10) as a third-order non-linear ordinary differential equation for f as a function of r,

$$f'''f' - 2\,(f'')^2 + f''\left(6f\left(\Lambda - f^2\right) + \frac{(f')^2}{f}\right) + (f')^2\left(11f^2 - 9\Lambda\right) - 4f^2\left(\Lambda - f^2\right)^2 = 0\,. \tag{2.25}$$

Finally, we need to determine A and B. From (2.15) we know that

$$B' = -A' - \frac{2f'}{f}\,, \tag{2.26}$$

which we can insert into (2.10) to obtain a quadratic equation for A',

$$(A')^2 + \frac{2f'}{f}A' + \left[\frac{2f'}{f}C' - 4\left(\Lambda - f^2\right)\right] = 0\,. \tag{2.27}$$

Substituting for C' from (2.22), the solutions to the last two equations are

$$A' = -\frac{f'}{f} \pm \sqrt{4\frac{f''}{f} - 7\left(\frac{f'}{f}\right)^2 - 4\left(\Lambda - f^2\right)}\,, \tag{2.28}$$

$$B' = -\frac{f'}{f} \mp \sqrt{4\frac{f''}{f} - 7\left(\frac{f'}{f}\right)^2 - 4\left(\Lambda - f^2\right)}\,, \tag{2.29}$$

where the signs in front of the square roots must always be chosen to be opposite.

In order to obtain a general spacetime meeting our demands, we first need to solve (2.25), the differential equation for f. We then insert this f into (2.28), (2.29), and (2.22), and integrate these expressions, giving us the metric functions A, B, and C, respectively. However, in the general case such an endeavor appears to be necessarily limited to numerical computations only, which we shall perform and discuss later, in Sec. 3.2.

Nonetheless, there is still an exact spacetime to be discovered if we consider the special case of $A = B$, thus imposing boost symmetry in the z direction to the solution, which is also present in the original Bonnor–Melvin solution and coincidentally also appears in the homogeneous solution without our intervention. Einstein equations (2.7) and (2.8) now coincide and the three independent equations can be written as

$$2(A'' + C'') + (A')^2 + (C')^2 + A'C' + 4\Lambda + 4f^2 = 0\,, \tag{2.30}$$

$$4A'' + 3\,(A')^2 + 4\Lambda - 4f^2 = 0\,, \tag{2.31}$$

$$(A')^2 + 2A'C' + 4\Lambda - 4f^2 = 0\,. \tag{2.32}$$

The Maxwell equation (2.15) can be integrated to obtain

$$A = \ln \frac{\alpha}{f}\,, \tag{2.33}$$

where α is a constant of integration, hence

$$\exp A(r) = \exp B(r) = \frac{\alpha}{f(r)}\,. \tag{2.34}$$

The difference of the last two Einstein equations (2.31) and (2.32) yields

$$2A'' + (A')^2 - A'C' = 0\,, \tag{2.35}$$

which can easily be integrated to obtain

$$C = A + 2\ln\left(\sqrt{\beta}A'\right) = \ln\left(\frac{\alpha}{f}\right) + 2\ln\left(-\sqrt{\beta}\,\frac{f'}{f}\right), \tag{2.36}$$

where β is another constant of integration, leading to

$$\exp C(r) = \alpha\beta\,\frac{f'(r)^2}{f(r)^3}\,, \tag{2.37}$$

which means that axes are located wherever $f' = 0$ unless f also vanishes there. After inserting A and C into the remaining Einstein equations, we can see that they are not independent. (2.31) and (2.32) become

$$-4\frac{f''}{f} + 7\frac{(f')^2}{f^2} + 4\left(\Lambda - f^2\right) = 0\,, \tag{2.38}$$

while (2.30) yields

$$4\frac{f'''}{f'} - 22\frac{f''}{f} + 21\frac{(f')^2}{f^2} + 4\left(\Lambda + f^2\right) = 0\,, \tag{2.39}$$

which is, however, a consequence of the simpler previous equation, as expressing f''' from the derivative of (2.38),

$$-4\frac{f'''}{f} + 18\frac{f'f''}{f^2} - 14\frac{(f')^3}{f^3} - 8ff' = 0\,, \tag{2.40}$$

and inserting it into (2.39) yields again the original (2.38). As such, we are dealing with a single second-order differential equation for f,

$$4ff'' - 7\,(f')^2 - 4f^2\left(\Lambda - f^2\right) = 0\,. \tag{2.41}$$

This condition causes the square roots in the expressions (2.28) for A' and (2.29) for B' in the general solution to disappear, correctly yielding $A' = B'$. As the coordinate r does not explicitly appear in this equation, we may reduce its order by using f as the new independent coordinate with $v = f'$. We replace the second derivative of f with

$$f'' = (f')' = \frac{\mathrm{d}v}{\mathrm{d}r} = \frac{\mathrm{d}v}{\mathrm{d}f}\,f' = \frac{\mathrm{d}v}{\mathrm{d}f}\,v\,, \tag{2.42}$$

which means that the non-linear second-order equation (2.41) can be recast as a first-order equation

$$2v(f)\,\frac{\mathrm{d}v(f)}{\mathrm{d}f} - \frac{7}{2}\frac{v(f)^2}{f} = 2f\left(\Lambda - f^2\right), \tag{2.43}$$

which still remains non-linear. This, however, can be remedied via the substitution $w = v^2$, because then the first term on the left-hand side of the equation is simply the derivative $\mathrm{d}w/\mathrm{d}f$,

$$\frac{\mathrm{d}w(f)}{\mathrm{d}f} - \frac{7}{2}\frac{w(f)}{f} = 2f\left(\Lambda - f^2\right). \tag{2.44}$$

This equation can be solved by first considering only the homogeneous, left-hand-side part, which has the solution $w_0 = kf^{7/2}$, where k is an arbitrary constant of the dimension $\mathrm{u}^{-1/2}$ to guarantee the solution's dimension u^{-4}. We can use w_0 as an integration factor and divide the full equation by it to obtain

$$\frac{\mathrm{d}w(f)}{\mathrm{d}f}f^{-7/2} - \frac{7}{2}w(f)f^{-9/2} = \frac{\mathrm{d}}{\mathrm{d}f}\left(w(f)f^{-7/2}\right) = 2f^{-5/2}\left(\Lambda - f^2\right). \tag{2.45}$$

This equation can be solved by direct integration,

$$w(f)f^{-7/2} = \gamma - 4\sqrt{f} - \frac{4}{3}\Lambda f^{-3/2}\,. \tag{2.46}$$

As $w = v^2 = (f')^2$, we have

$$\frac{\mathrm{d}f}{\mathrm{d}r} = \pm\sqrt{\gamma f^{7/2} - 4f^4 - \frac{4}{3}\Lambda f^2}\,. \tag{2.47}$$

It does not appear possible to obtain a closed-form expression for $f(r)$. However, the metric functions $A = B$ (2.34) and C (2.37) do not depend explicitly on r,

they depend only on f and its first derivative. It is, therefore, convenient to consider the coordinate change $r \to f$ using (2.47), which replaces f' in (2.37) and appears in the transformed $g_{ff} = g_{rr}/(f')^2$. The metric produced in this way,

$$\mathrm{d}s^2 = \frac{1}{f}\left(-\mathrm{d}t^2 + \mathrm{d}z^2\right) + \frac{\mathrm{d}f^2}{\gamma f^{\frac{7}{2}} - 4f^4 - \frac{4}{3}\Lambda f^2} + \beta\frac{\gamma f^{\frac{7}{2}} - 4f^4 - \frac{4}{3}\Lambda f^2}{f^3}\mathrm{d}\phi^2\,, \quad (2.48)$$

with the corresponding magnetic field

$$\mathbf{F} = \sqrt{\frac{\beta}{f}}\,\mathrm{d}f \wedge \mathrm{d}\phi \quad (2.49)$$

were the topic of the paper Veselý and Žofka [2019b], and shall be examined in detail in Sec. 2.3.

Returning back to the general equation (2.25), it is possible to use the same substitution as above, $w = (f')^2$ viewed as a function of f, to reduce the order of the equation in hopes of finding a general solution more easily. The derivatives of f are thus[1]

$$f' = \sqrt{w}\,, \quad (2.50)$$

$$f'' = \frac{\mathrm{d}}{\mathrm{d}r}f' = \frac{1}{2}\frac{1}{\sqrt{w}}\frac{\mathrm{d}w}{\mathrm{d}r} = \frac{1}{2}\frac{1}{\sqrt{w}}\dot{w}f' = \frac{1}{2}\dot{w}\,, \quad (2.51)$$

$$f''' = \frac{\mathrm{d}}{\mathrm{d}r}f'' = \frac{1}{2}\frac{\mathrm{d}}{\mathrm{d}r}\dot{w} = \frac{1}{2}\ddot{w}f' = \frac{1}{2}\sqrt{w}\ddot{w}\,, \quad (2.52)$$

where a dot denotes differentiation with respect to f from now on in this section. After inserting the expressions into (2.25), we obtain

$$w\ddot{w} - \dot{w}^2 + \left[\frac{w}{f} - 6f\left(f^2 - \Lambda\right)\right]\dot{w} - 8\left(f^2 - \Lambda\right)^2 f^2 + 2w\left(11f^2 - 9\Lambda\right) = 0\,. \quad (2.53)$$

A general analytical solution of this equation (if there even is one in the first place) eludes us still.

The two spacetimes described above satisfy (2.25) with additional constraints. The homogeneous case requires $f' = 0$, whence we immediately have $f^2 = \Lambda$. For the boost-symmetric solution, we can express f'' from (2.41), compute f''' and insert both into (2.25) to see that it is fulfilled. However, the numerical computations in Sec. 3.2 suggest that there are other solutions with different properties than the two above.

For $\Lambda = 0$, one expects to be able to find the original Bonnor–Melvin spacetime among the solutions of equation (2.53), and indeed, we recover it for

$$w = \gamma f^{7/2} - 4f^4\,. \quad (2.54)$$

It may not be immediately obvious that this is the original solution, but by comparing this w with (2.47), it is obvious that it corresponds to the spacetime

[1] The sign of f' is not relevant, as it factors out in f'' and the other derivatives appear in (2.25) as $f'''f'$ and $(f')^2$ only, both necessarily positive.

described in Sec. 2.3 with $\Lambda = 0$. It will be shown in the corresponding section that after taking this limit, the spacetime can be transformed to one of the known forms of the Bonnor–Melvin metric. However, it turns out that there is another independent solution to be found,

$$w = 4\alpha f^3 - 4f^4, \tag{2.55}$$

which by virtue of (2.50) leads to

$$f = \frac{\alpha}{1 + \alpha^2 r^2}\,. \tag{2.56}$$

Using such f, however, results in a complex metric, as the argument of the square root in the expressions for A' (2.28) and B' (2.29) is negative,

$$4\,\frac{f''}{f} - 7\left(\frac{f'}{f}\right)^2 + 4f^2 = -\frac{4\alpha^2}{1 + \alpha^2 r^2}\,. \tag{2.57}$$

To remedy the issue, we can consider a purely imaginary α and factor the imaginary unit out, $\alpha \to \mathrm{i}\,\alpha$. Even though z now unusually replaces t in the role of the timelike coordinate, the resulting metric is real,

$$\begin{aligned}\mathrm{d}s^2 = {} & \left(1 - \alpha^2 r^2\right) \exp(2 \arcsin \alpha r)\, \mathrm{d}t^2 + \mathrm{d}r^2 \\ & - \left(1 - \alpha^2 r^2\right) \exp(-2 \arcsin \alpha r)\, \mathrm{d}z^2 + \frac{\mathrm{d}\phi^2}{1 - \alpha^2 r^2}\,,\end{aligned} \tag{2.58}$$

but the new f is not,

$$f = \frac{\mathrm{i}\,\alpha}{1 - \alpha^2 r^2}\,, \tag{2.59}$$

and it leads to an imaginary electromagnetic field tensor,

$$\mathbf{F} = \frac{\mathrm{i}\,\alpha}{\left(1 - \alpha^2 r^2\right)^{3/2}}\, \mathrm{d}r \wedge \mathrm{d}\phi\,. \tag{2.60}$$

The Wick rotation $\phi \to \mathrm{i}t$, $t \to \phi$, $z \to \mathrm{i}z$ makes $\mathbf{F}$ real again,

$$\mathbf{F} = \frac{\alpha}{\left(1 - \alpha^2 r^2\right)^{3/2}}\, \mathrm{d}t \wedge \mathrm{d}r\,, \tag{2.61}$$

and reestablishes t as the timelike coordinate,

$$\begin{aligned}\mathrm{d}s^2 = {} & -\frac{\mathrm{d}t^2}{1 - \alpha^2 r^2} + \mathrm{d}r^2 + \left(1 - \alpha^2 r^2\right) \\ & \times \left[\exp(-2 \arcsin \alpha r)\, \mathrm{d}z^2 + \exp(2 \arcsin \alpha r)\, \mathrm{d}\phi^2\right].\end{aligned} \tag{2.62}$$

Finally, as $\mathbf{F}$ now represents an electric field, we use a dual rotation to get the magnetic field

$$\mathbf{F} = \alpha\, \mathrm{d}z \wedge \mathrm{d}\phi\,. \tag{2.63}$$

Take note that while our original ansatz contained an axial magnetic field, we ended up with a radial one in this case. Even though it does not include the cosmological constant, thus deviating from the class of spacetimes we are mainly interested in, we covered this solution together with two others in our 'radial' paper Veselý and Žofka [2021]. It is the topic of Sec. 2.4.

2.1.2 Radial magnetic field

Inspired by the surprising twist described in the previous paragraph, we moved on to study spacetimes with a radial magnetic field by considering

$$\mathbf{F} = f(r)\,\mathrm{e}^{\frac{B(r)}{2}}\mathrm{e}^{\frac{C(r)}{2}}\,\mathrm{d}z \wedge \mathrm{d}\phi\,, \tag{2.64}$$

where f is again bound to the electromagnetic field invariant by (2.6), while the other invariant remains zero.

To see that we are dealing with a radial field, we again use Cartesian-like coordinates $x = r\cos\phi$ and $y = r\sin\phi$, which yields the slightly more complicated $\mathbf{F} = yF_{z\phi}(r)/r^2\,\mathrm{d}x \wedge \mathrm{d}z - xF_{z\phi}(r)/r^2\,\mathrm{d}y \wedge \mathrm{d}z$. By analogy with the Minkowski spacetime, we take $F_{xz} = -B_y$ and $F_{yz} = B_x$, which implies[2] $\vec{B} = -F_{z\phi}(r)/r\,\vec{e_r}$.

The new ansatz leads to two sign changes in the Einstein equations,

$$\begin{aligned}
2(B'' + C'') + (B')^2 + (C')^2 + B'C' + 4\Lambda + 4f^2 &= 0\,, &(2.65)\\
2(A'' + C'') + (A')^2 + (C')^2 + A'C' + 4\Lambda - 4f^2 &= 0\,, &(2.66)\\
2(A'' + B'') + (A')^2 + (B')^2 + A'B' + 4\Lambda - 4f^2 &= 0\,, &(2.67)\\
A'B' + A'C' + B'C' + 4\Lambda + 4f^2 &= 0\,. &(2.68)
\end{aligned}$$

The Maxwell equation (2.3) can be integrated to obtain

$$f\mathrm{e}^{\frac{B+C}{2}} = \text{const.}, \tag{2.69}$$

which also happens to be the exact requirement to fulfill the other Maxwell equation $\mathrm{d}\mathbf{F} = 0$, which is not satisfied trivially by the ansatz for $\mathbf{F}$ this time. The condition is not independent from the Einstein equations, as repeating exactly the same steps as in the axial case leads to the analogy of (2.15),

$$f' + \frac{1}{2}f(B + C)' = 0\,. \tag{2.70}$$

Once again our goal is to express the metric functions A, B, and C as functions of f and its derivatives. The procedure is completely analogous to the one described in the previous section. We begin by adding (2.65) and (2.68) to obtain

$$2(B' + C')' + (B' + C')^2 + A'(B' + C') + 8\Lambda + 8f^2 = 0\,. \tag{2.71}$$

Take note that the sign of the last term is different than in (2.16).

Dealing first with the case of $f = \text{const.}$, from (2.70) we see that $B + C$ is constant this time. It follows from the last equation that

$$f^2 = -\Lambda\,, \tag{2.72}$$

which means that Λ has to be negative, as opposed to the previous case. (2.68) reduces to $B'C' = 0$, meaning that B and C are both constant. We are left with one independent Einstein equation,

$$A'' + \frac{1}{2}(A')^2 + 4\Lambda = 0\,. \tag{2.73}$$

[2] In a similar argument in Veselý and Žofka [2021] we mistakenly consider the opposite sign of $\vec{B}$. The fact that $\vec{B}$ is radial, as we intended to prove, nonetheless holds.

The function

$$A(r) = 2\ln\left[\alpha\cosh\sqrt{-2\Lambda}\,(r-R)\right] \tag{2.74}$$

with the integration constants α and R solves this equation. A simple rescaling of the coordinates eliminates both constants and leads to

$$\mathrm{d}s^2 = -\cosh^2\left(\sqrt{-2\Lambda}\,r\right)\mathrm{d}t^2 + \mathrm{d}r^2 + \mathrm{d}z^2 + \sigma^2\mathrm{d}\phi^2 \tag{2.75}$$

with

$$\mathbf{F} = \sigma\sqrt{-\Lambda}\,\mathrm{d}z\wedge\mathrm{d}\phi \tag{2.76}$$

as published in Veselý and Žofka [2021] and discussed in Sec. 2.5.1. While in the paper we chose to represent the solution using this metric, a more general solution can be found,

$$\mathrm{d}s^2 = -\left(\mathrm{e}^{\sqrt{-2\Lambda}\,r} + a\,\mathrm{e}^{-\sqrt{-2\Lambda}\,r}\right)^2\mathrm{d}t^2 + \mathrm{d}r^2 + \mathrm{d}z^2 + \sigma^2\mathrm{d}\phi^2\,, \tag{2.77}$$

with the same expression for the magnetic field[3]. This metric is investigated in Sec. 2.5.2.

For the case of a non-constant f, the additional symmetry we are going to consider that will lead us to analytical results is $B = C$, imposing rotational symmetry in the z–ϕ plane (which we obtained in the homogeneous case automatically) upon the solution. The three independent Einstein equations are

$$2(A''+C'') + (A')^2 + (C')^2 + A'C' + 4\Lambda - 4f^2 = 0\,, \tag{2.78}$$

$$4C'' + 3\,(C')^2 + 4\Lambda + 4f^2 = 0\,, \tag{2.79}$$

$$(C')^2 + 2A'C' + 4\Lambda + 4f^2 = 0\,, \tag{2.80}$$

and the Maxwell equation yields

$$C = \ln\frac{\alpha}{f} \tag{2.81}$$

with a constant of integration α. Therefore, the two corresponding metric functions are

$$\exp B(r) = \exp C(r) = \frac{\alpha}{f(r)}\,, \tag{2.82}$$

which means that the electromagnetic field invariant (2.6) diverges at the axes. Taking the difference of the last two Einstein equations,

$$2C'' + (C')^2 - A'C' = 0\,, \tag{2.83}$$

leads to an analogy of (2.36),

$$A = C + 2\ln\left(\sqrt{\beta}C'\right) = \ln\left(\frac{\alpha}{f}\right) + 2\ln\left(-\sqrt{\beta}\,\frac{f'}{f}\right) \tag{2.84}$$

[3]Note that we can find a similar metric for the axial homogeneous spacetime of Sec. 2.2 as well, but the arguments of the exponential functions would be $\pm\mathrm{i}\sqrt{2\Lambda}\,r$. Since we do not aim to investigate complex spacetimes in this work, we are left with either a sine or a cosine in the metric. It does not matter which one we choose, as a shift in the radial coordinate can convert one into the other.

with a constant of integration β. The corresponding metric element is

$$\exp A(r) = \alpha\beta \frac{f'(r)^2}{f(r)^3}\,. \tag{2.85}$$

Take note that while after exchanging $A \leftrightarrow C$ the expressions for the metric elements (2.82) and (2.85) are the same as (2.34) and (2.37) in the axial case, their final form will differ due to the effect of the different signs of the terms with f' in the Einstein equations. Analogously to the axial case it can be shown that there is only one remaining independent Einstein equation,

$$4ff'' - 7\left(f'\right)^2 - 4f^2\left(\Lambda + f^2\right) = 0\,. \tag{2.86}$$

Using the substitution $w = (f')^2$ with the replacement rule for f'' (2.51), we get

$$\dot{w} - \frac{7}{2}\frac{w}{f} = 2f\left(\Lambda + f^2\right). \tag{2.87}$$

Like its axial counterpart, this equation can be integrated using the integration factor $f^{7/2}$, leading to the analogy of (2.47) with one different sign,

$$\frac{\mathrm{d}f}{\mathrm{d}r} = \pm\sqrt{\gamma f^{7/2} + 4f^4 - \frac{4}{3}\Lambda f^2}\,. \tag{2.88}$$

The coordinate change $r \to f$ allows us to obtain the spacetime

$$\mathrm{d}s^2 = -\frac{\gamma f^{\frac{7}{2}} + 4f^4 - \frac{4}{3}\Lambda f^2}{f^3}\mathrm{d}t^2 + \frac{\mathrm{d}f^2}{\gamma f^{\frac{7}{2}} + 4f^4 - \frac{4}{3}\Lambda f^2} + \frac{1}{f}\left(\mathrm{d}z^2 + \beta^2\mathrm{d}\phi^2\right) \tag{2.89}$$

with

$$\mathbf{F} = \beta\,\mathrm{d}z \wedge \mathrm{d}\phi\,, \tag{2.90}$$

originally presented in the same paper as the previous two radial solutions, Veselý and Žofka [2021], and discussed in Sec. 2.6 of this thesis.

Finally, for a non-constant f and $B \neq C$ we use (2.70) to replace all instances of $B' + C'$ in (2.71) with $-2f'/f$ to obtain

$$A' = -2\frac{f''}{f'} + 4\frac{f'}{f} + 4\frac{f}{f'}\left(\Lambda + f^2\right). \tag{2.91}$$

Adding (2.65) and (2.68) together and subtracting (2.66) and (2.67) from them, we get

$$B'C' = 2A'' + \left(A'\right)^2 - 8f^2, \tag{2.92}$$

where we can insert A' (2.91) and its derivative to express the right-hand side solely in terms of f and its derivatives. Inserting the above relations into (2.68), we obtain an equation for f similar to (2.25),

$$f'''f' - 2\left(f''\right)^2 + f''\left(6f\left(\Lambda + f^2\right) + \frac{\left(f'\right)^2}{f}\right) - \left(f'\right)^2\left(11f^2 + 9\Lambda\right) - 4f^2\left(\Lambda + f^2\right)^2 = 0\,, \tag{2.93}$$

which can be rewritten using our favorite substitution $w = (f')^2$ as

$$w\ddot{w} - \dot{w}^2 + \left[\frac{w}{f} + 6f\left(f^2+\Lambda\right)\right]\dot{w} - 8\left(f^2+\Lambda\right)^2 f^2 - 2w\left(11f^2+9\Lambda\right) = 0\,. \tag{2.94}$$

As before, we can use (2.70) to replace B' in (2.68) with

$$B' = -C' - \frac{2f'}{f}\,, \tag{2.95}$$

leading to an analogy of (2.27),

$$(C')^2 + \frac{2f'}{f}C' + \left[\frac{2f'}{f}A' - 4\left(\Lambda + f^2\right)\right] = 0\,. \tag{2.96}$$

As we know A' from (2.91), we can solve the last two equations to obtain two pairs of expressions for B' and C' in terms of f,

$$B' = -\frac{f'}{f} \pm \sqrt{4\frac{f''}{f} - 7\left(\frac{f'}{f}\right)^2 - 4\left(\Lambda + f^2\right)}\,, \tag{2.97}$$

$$C' = -\frac{f'}{f} \mp \sqrt{4\frac{f''}{f} - 7\left(\frac{f'}{f}\right)^2 - 4\left(\Lambda + f^2\right)}\,, \tag{2.98}$$

with opposite signs in front of the square roots.

The general strategy to obtain a spacetime satisfying our demands again consists of finding $f(r)$ by solving either (2.93) or the equivalent (2.94), inserting it into (2.91), (2.97), and (2.98), and integrating the resulting expressions to obtain A, B, and C, respectively. It should come as no surprise that this does not seem feasible to be performed analytically. Numerical experiments with this system too shall be performed in Sec. 3.2.

2.1.3 Azimuthal magnetic field

To obtain a spacetime with a magnetic field aligned with the ϕ direction, we consider

$$\mathbf{F} = f(r)\,\mathrm{e}^{\frac{B(r)}{2}}\,\mathrm{d}r \wedge \mathrm{d}z\,, \tag{2.99}$$

immediately satisfying $\mathrm{d}\mathbf{F} = 0$. As per the usual, the function f fulfills (2.6).

Again, the transformation to Cartesian-like coordinates defined as $x = r\cos\phi$ and $y = r\sin\phi$ enables us to see that this is an azimuthal field. In these coordinates, we have $\mathbf{F} = xF_{rz}(r)/r\,\mathrm{d}x\wedge\mathrm{d}z + yF_{rz}(r)/r\,\mathrm{d}y\wedge\mathrm{d}z$. The Minkowski-inspired relations $F_{xz} = -B_y$ and $F_{yz} = B_x$ then yield $\vec{B} = -F_{rz}(r)/r\,\vec{e_\phi}$.

Now, we could proceed along the lines of the previous two cases. However, there is a much simpler way of obtaining solutions with azimuthal magnetic fields analogous to the previous ones, because we can use the fact that the metric depends on neither ϕ nor z due to our choice of cylindrical symmetry. As far as the Einstein–Maxwell equations are concerned, it is possible to swap the functions B and C corresponding to the z and ϕ coordinates, respectively, without breaking

the validity of the entire set of equations, a trick not possible with the radial coordinate r. Therefore, the azimuthal solutions can be obtained by exchanging $g_{zz} \leftrightarrow g_{\phi\phi}$ in the metric and $F_{r\phi} \leftrightarrow F_{rz}$ in the magnetic field of a given axial solution. While seemingly trivial, such a change impacts the global structure of the spacetimes considerably, as what used to be an unbounded coordinate z is now to be understood as a bounded angular coordinate ϕ, and vice versa. The homogeneous solution with an azimuthal magnetic field is examined in Sec. 2.7 and the inhomogeneous one in Sec. 2.8.

As the azimuthal spacetimes have the same local properties as the corresponding axial ones, we shall put less emphasis on these spacetimes than on the rest. We focus mainly on the differences arising from the exchange $z \leftrightarrow \phi$, which affects, e.g., circular orbits and shell sources.

2.1.4 General magnetic field

The final logical step would be to consider a superposition of the previously-considered magnetic fields to dispose of their alignment along one of the prominent directions,

$$\mathbf{F} = f_z \, \mathrm{d}r \wedge \mathrm{d}\phi + f_r \, \mathrm{d}z \wedge \mathrm{d}\phi + f_\phi \, \mathrm{d}r \wedge \mathrm{d}z \, . \tag{2.100}$$

The left-hand side of the Einstein equations is unaffected by this change and remains diagonal. However, the stress-energy tensor on the right-hand side gains non-diagonal elements, which must be equal to zero in order for the equations to be fulfilled. The non-diagonal elements satisfy

$$T_{ij} \propto f_i f_j g^{kk}, \tag{2.101}$$

where $i \neq j \neq k \neq i$ are spatial indices. Therefore, the products of any two functions f_i must be equal to zero, which means that only one of them can be non-zero. As a result, the three cases studied above are the only possible configurations of the magnetic field permitted by our ansatz of cylindrical symmetry.

2.2 Bonnor–Melvin–Λ (Axial homogeneous spacetime)

The first of the presented magnetic spacetimes, forming the basis for our subsequent work, was derived and published in Žofka [2019]. The aim of the work was to dispose of the dependence of the electromagnetic invariant on the radial coordinate, thus ensuring the homogeneity of the magnetic field. This was made possible by including a positive cosmological constant, $\Lambda > 0$, preventing the collapse of the uniform magnetic field.

Two forms of the metric were presented in the paper. The first is

$$\mathrm{d}s^2 = -\mathrm{d}t^2 + \mathrm{d}r^2 + \mathrm{d}z^2 + \sigma^2 \sin^2\!\left(\sqrt{2\Lambda}\, r\right) \mathrm{d}\phi^2 \tag{2.102}$$

with

$$\mathbf{F} = \sqrt{\Lambda}\, \sigma \sin\!\left(\sqrt{2\Lambda}\, r\right) \mathrm{d}r \wedge \mathrm{d}\phi\,, \tag{2.103}$$

where the coordinates t, r, and z, along with the parameter σ, have the dimension of length, while ϕ is dimensionless. Depending on the value of σ, there may be a deficit angle at the axes. The condition (1.2) for elementary flatness fixes the value $\sigma^2 = 1/2\Lambda$, which is reflected in the rescaled variant

$$\mathrm{d}s^2 = -\mathrm{d}t^2 + \mathrm{d}z^2 + \frac{1}{2\Lambda}\left(\mathrm{d}r^2 + \sin^2 r\, \mathrm{d}\phi^2\right) \tag{2.104}$$

with the magnetic field[4]

$$\mathbf{F} = \frac{1}{2\sqrt{\Lambda}} \sin r\, \mathrm{d}r \wedge \mathrm{d}\phi\,, \tag{2.105}$$

where the coordinates t and z have the dimension of length, while r and ϕ are dimensionless. The second form of the metric, which we shall exclusively use from now on, clearly shows that the spacetime is locally a direct product of 2D Minkowski spacetime and a two sphere, which has a constant radius of $1/\sqrt{2\Lambda}$. This is typical for monopole compactifications of higher-dimensional solutions encountered in the string theory, see, e.g., Olasagasti and Vilenkin [2000] and Prasetyo and Ramadhan [2016]. Note that (70) of the latter paper is a variant of our (2.104). The magnetic field's invariant is indeed constant,

$$F_{\mu\nu}F^{\mu\nu} = 2\Lambda\,, \tag{2.106}$$

while the Kretschmann scalar is $16\Lambda^2$. There is no curvature singularity in the spacetime. The dual electromagnetic field to (2.105) is $\star\mathbf{F} = \sqrt{\Lambda}\, \mathrm{d}t \wedge \mathrm{d}z$, an electric field aligned along the axes[5].

The solution exhibits higher symmetry than the original Bonnor–Melvin solution, as it has two additional Killing vector fields, bringing the total number to

[4] There is a typo in equation (33) in Žofka [2019]. Also note that the sign of the magnetic field can be chosen arbitrarily.

[5] Žofka [2019] incorrectly states that the invariant $\star F_{\mu\nu}\star F^{\mu\nu}$ remains equal to 2Λ, but, in fact, its value is -2Λ. For dual fields, the invariant always has the opposite sign, $\star F_{\mu\nu}\star F^{\mu\nu} = -F_{\mu\nu}F^{\mu\nu}$. Furthermore, note that in order to keep the expressions simpler, we omit additional minus signs in $\star\mathbf{F}$ if they appear, as the signs of both $\mathbf{F}$ and $\star\mathbf{F}$ can be chosen arbitrarily for our solutions.

six. Apart from the three translational Killing vectors and the one corresponding to boost in the t–z plane, the two new vectors, $\sin\phi\ \partial_r + \cot r \cos\phi\ \partial_\phi$ and $\cos\phi\ \partial_r - \cot r \sin\phi\ \partial_\phi$ (in the rescaled coordinates), along with ∂_ϕ represent rotations on the two-sphere of constant coordinates t and z. This corresponds to the $ISO(1,1) \times SO(3)$ group of isometries.

The spacetime is type D. The metric (2.104) coincides with (7.19) in Griffiths and Podolský [2009] and, therefore, the solution is among those investigated in Plebański and Hacyan [1979]. The solution belongs to the Kundt class: The integral curves of the two principal null directions $\sqrt{2}(\partial_t \pm \partial_z)/2$ happen to be geodesics with vanishing optical scalars. The constant factor multiplying both vectors was chosen so that their scalar product is -1 as required by the algorithm in Poisson [2004].

The proper circumference (1.3) of circles centered around the axis at $r = 0$ is $\sqrt{2/\Lambda}\,\pi \sin r$, and it vanishes not only for vanishing radius, but somewhat similarly to the Bonnor–Melvin spacetime (where it vanished at the axis and in the asymptotic region) also for coordinate radius $r = \pi$ corresponding to proper radius $\pi/\sqrt{2\Lambda}$. Therefore, we may consider the solution to have a second axis there. In our analysis, we limit ourselves to the interval of r between these two axes, but the radial coordinate in the metric is periodic and one can choose another admissible interval without affecting the physics involved (bar the arbitrary sign of $\mathbf{F}$). As is usual wherever axial symmetry is involved, we do not extend the radial coordinate beyond any of the two axes, which lie in finite proper radial distance from each other in this spacetime.

The paper did not comment on the spacetime's limit for a vanishing cosmological constant, as it is not possible to perform the limit of $\Lambda \to 0^+$ in either metric in a straightforward manner. However, the transformation

$$\begin{aligned} x &= \sqrt{\frac{2}{\Lambda}}\,\tan\left(\frac{r}{2}\right)\cos\phi\,, \\ y &= \sqrt{\frac{2}{\Lambda}}\,\tan\left(\frac{r}{2}\right)\sin\phi\,, \end{aligned} \tag{2.107}$$

brings the metric (2.104) into the form

$$\mathrm{d}s^2 = -\mathrm{d}t^2 + \frac{\mathrm{d}x^2 + \mathrm{d}y^2}{\left(1 + \frac{\Lambda}{2}(x^2+y^2)\right)^2} + \mathrm{d}z^2 \tag{2.108}$$

with the magnetic field

$$\mathbf{F} = \frac{\sqrt{\Lambda}}{\left(1 + \frac{\Lambda}{2}(x^2+y^2)\right)^2}\,\mathrm{d}x \wedge \mathrm{d}y\,. \tag{2.109}$$

We thank Prof. Kjell Rosquist for pointing this transformation out. All coordinates have the dimension of length. This form of the metric becomes the Minkowski spacetime in the limit $\Lambda \to 0^+$.

Particle motion

In the original paper very little investigation of electrogeodesics was performed. We shall use the second form of the metric (2.104) with the corresponding magnetic field (2.105). For the Lagrangian density (1.14), two constants of motion

are trivial, $E = \dot{t}$ and $Z = \dot{z}$, but the last one is somewhat more complicated,

$$L = \frac{1}{2\Lambda}\left(\dot{\phi}\sin^2 r - \kappa\sqrt{\Lambda}\cos r\right). \tag{2.110}$$

The effective potential for radial motion is

$$V = \Lambda\left(-\delta - E^2 + Z^2 + \frac{2}{\sin^2 r}\left(\frac{\kappa}{2}\cos r + \sqrt{\Lambda}\,L\right)^2\right), \tag{2.111}$$

while its separated counterpart reads

$$W^2 = E^2 + \frac{V}{\Lambda} = -\delta + Z^2 + \frac{2}{\sin^2 r}\left(\frac{\kappa}{2}\cos r + \sqrt{\Lambda}\,L\right)^2. \tag{2.112}$$

Analysis of the potentials shows us that the only particles capable of reaching both axes necessarily fulfill $L = \kappa = 0$, i.e., they must be uncharged and exhibit no azimuthal motion, but they may be both massive particles and photons. For a non-zero L, an uncharged particle can never reach any of the two axes as the potential diverges there, and the particle will oscillate in the radial direction between them. While a similar fate befalls most charged particles as well, for certain special values of L,

$$L_\pm = \pm\frac{\kappa}{2\sqrt{\Lambda}}, \tag{2.113}$$

they may reach either the axis located at $r = 0$ (for L_-) or the one at $r = \pi$ (for L_+) but never both. For these two values of L, the potential is monotonous in the considered range $r \in [0, \pi]$,

$$V_\pm = \Lambda\left(-\delta - E^2 + Z^2 + \frac{\kappa^2}{2}\tan^{\mp 2}\frac{r}{2}\right), \tag{2.114}$$

so instead of oscillating between the two axes, these particles oscillate through one of them.

Concerning circular orbits in planes perpendicular to the axes, we set $Z = 0$ to have $\dot{z} = 0$ and look at the potential and its first derivative,

$$V\big|_{Z=0} = \Lambda\left(-\delta - E^2 + \frac{2}{\sin^2 r}\left(\frac{\kappa}{2}\cos r + \sqrt{\Lambda}\,L\right)^2\right), \tag{2.115}$$

$$V' = -\frac{\Lambda}{\sin^3 r}\left(2\sqrt{\Lambda}L + \kappa\cos r\right)\left(\kappa + 2\sqrt{\Lambda}L\cos r\right), \tag{2.116}$$

and see for which values of the parameters they both vanish. There is no need to consider $Z = 0$ in the derivative, as the term containing it vanishes anyway. Ideally, we would solve the equations for E and L to get an allowed range of orbit radii.

Starting with uncharged particles with $\kappa = 0$, this method yields only $L = 0$, which means no azimuthal motion, unless $r = \pi/2$, because midway between the two axes the derivative vanishes. For an uncharged particle to follow a circular orbit there, it must hold that $2\Lambda L^2 - E^2 - \delta = 0$, a condition valid for massive particles and photons alike. The condition also yields $\Omega^2 = (\mathrm{d}\phi/\mathrm{d}t)^2 = 2\Lambda$ for photons. The second derivative of V at $r = \pi/2$ is positive, $V''(\pi/2)|_{\kappa=0} = 4\Lambda^2 L^2$, which means the orbits are stable.

For charged particles, the addition of a non-zero κ enables particles to follow a circular orbit at any $r \neq \pi/2$ between the two axes as long as it has the correct constants of motion,

$$E^2 = \frac{1}{2}\left(-2\delta + \kappa^2 \tan^2 r\right), \tag{2.117}$$

$$L = -\frac{\kappa}{2\sqrt{\Lambda}} \frac{1}{\cos r}, \tag{2.118}$$

leading to $\dot{\phi} = -\kappa\sqrt{\Lambda}/\cos r$. The orbits are again stable, as the second derivative of V yields $\kappa^2\Lambda/\cos^2 r$ for the above L. For $r = \pi/2$, the term with κ in the potential vanishes, but the derivative does not vanish this time, $V'(\pi/2) = -2\Lambda^{3/2}\kappa L$. Therefore, to orbit at $r = \pi/2$ charged particles require $L = 0$. Even though generally (2.110) means that a vanishing L does not imply a vanishing $\dot{\phi}$ for a charged particle, $r = \pi/2$ is the only location when the implication holds and a charged particle cannot perform circular motion there, but it can stand still.

Actually, due to the symmetries of the spacetime, any massive particle not moving in any spatial direction in our coordinates at the initial time will remain still regardless of its charge or the absence thereof. Moreover, particles moving in the direction of the magnetic field do so with a constant four-velocity.

We can obtain more constants of motion using the Killing vectors through the procedure explained in Sec. 1.2.1. The boost vector yields the constant $z\dot{t} - t\dot{z}$ valid even for charged particles, which means we can express the dependence of z on coordinate time t as

$$z(t) = \frac{Z}{E}\, t + z_0\,. \tag{2.119}$$

The two rotational Killing vectors provide us with somewhat more exciting constants

$$\begin{aligned} A &= \sin(\phi)\,\dot{r} + \sin(r)\cos(r)\cos(\phi)\,\dot{\phi}\,, \\ B &= \cos(\phi)\,\dot{r} - \sin(r)\cos(r)\sin(\phi)\,\dot{\phi}\,, \end{aligned} \tag{2.120}$$

which are sadly valid only for uncharged particles, as these two particular Killing vector fields do not satisfy the additional conditions related to the symmetries of the electromagnetic field. Using the constant L (2.110) with $\kappa = 0$, we can replace $\dot{\phi} = 2\Lambda L/\sin^2 r$ in the two constants. In the general case when at least one of the constants is non-zero, we can then express r and $\dot{r}$ as functions of ϕ,

$$r(\phi) = \arctan\left(\frac{2\Lambda L}{A\cos\phi - B\sin\phi}\right) \mod \pi\,, \tag{2.121}$$

$$\dot{r}(\phi) = A\sin\phi + B\cos\phi\,, \tag{2.122}$$

where one has to consider modulo π in the first relation to obtain a continuous curve $r(\phi)$. Note that while these results are applicable only for uncharged particles (including photons), they do not depend on $\dot{z} = Z$, so any motion along the z axis is permitted. For an illustration comparing the theoretical curves of $r(\phi)$ and $\dot{r}(\phi)$ to a numerical computation see Fig. 2.1. As with analogous results for the remaining two homogeneous spacetimes shown in Fig. 2.14 and 2.23, the numerical and analytical results match very well despite being obtained by different means, which lends further credence to the numerical computations we use to check every analytical result.

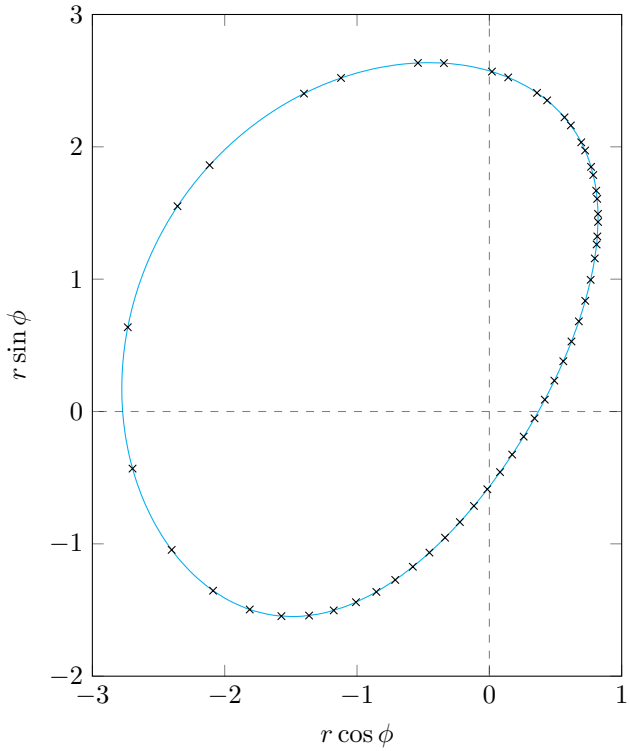

(a) The chart of $r(\phi)$ (2.121).

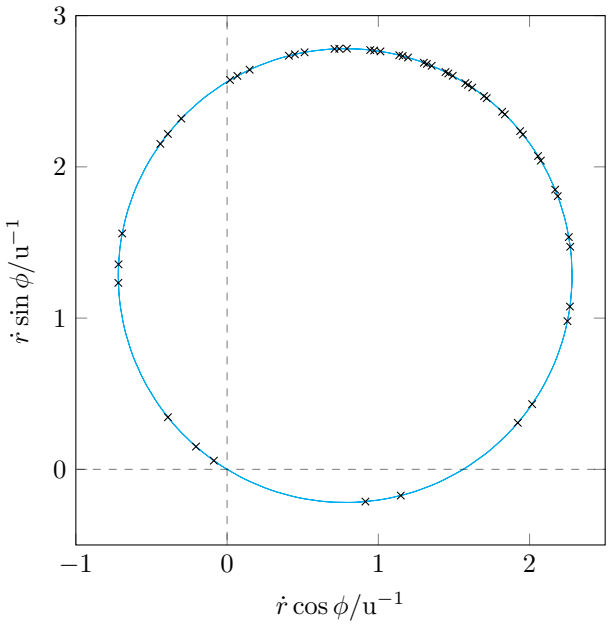

(b) The chart of $\dot{r}(\phi)$ (2.122).

Figure 2.1: The comparison of the cyan theoretical curves to the data points obtained by numerical integration of the equations of motion for a massive uncharged particle with the initial spatial coordinates $r = 1.5$, $\phi = 1$, and $z = 0$, and the initial spatial components of the four-velocity $\dot{r} = 3/\mathrm{u}$, $\dot{\phi} = 1/\mathrm{u}$, and $\dot{z} = 0.1$, in the spacetime with $\Lambda = 1\,\mathrm{u}^{-2}$. The relevant constants of motion are $L \approx 0.497\,\mathrm{u}$, $A \approx 2.56/\mathrm{u}$, and $B \approx 1.56/\mathrm{u}$. The equations of motion were integrated for the total proper time of 400 u, during which the particle went through the entire loop 201 times. Its position in the charts was marked every 8 u of proper time. The particle's motion along the z axis is irrelevant for the two charts.

Regarding the second-rank Killing tensors, the only new constant of motion that is not completely determined by the constants obtained from the Killing vectors is $\dot{r}^2 + \sin^2(r)\,\dot{\phi}^2$, which is valid even for charged particles. However, this constant complements E and Z to give the normalization of the four-velocity, so if we include δ, its value is fixed by the constants we have already been using, $\dot{r}^2 + \sin^2(r)\,\dot{\phi}^2 = 2\Lambda(\delta + E^2 - Z^2)$. After replacing $\dot{\phi}$ with L (2.110), we obtain the effective potential V (2.111).

Shell sources

To use Israel's formalism of connecting spacetimes of Sec. 1.2.2, we first need to compute the extrinsic curvature tensor (1.41) for the cylindrical hypersurface $r = \text{const.}$,

$$\mathbf{K} = \epsilon\sqrt{2\Lambda}\cot r\ \mathrm{d}\Phi^2, \tag{2.123}$$

and the projection of the electromagnetic tensor (1.44),

$$\mathbf{F}_\perp = -\epsilon\sqrt{\Lambda}\ \mathrm{d}\Phi\,. \tag{2.124}$$

As mentioned above, the proper circumference of the hypersurface is

$$\mathcal{C} = \sqrt{\frac{2}{\Lambda}}\,\pi\sin r\,. \tag{2.125}$$

The derivative (1.4) of $\mathcal{C}$ with respect to the proper radius r_p measured from the axis at $r = 0$ is

$$\frac{\mathrm{d}\mathcal{C}}{\mathrm{d}r_p} = 2\pi\cos r\,. \tag{2.126}$$

As expected, we have $|\mathrm{d}\mathcal{C}/\mathrm{d}r_p| \to 2\pi$ at the axes. The sign is negative for the axis at $r = \pi$ because the proper radius is measured from the other axis.

Choosing the opposite direction of the normal, which corresponds to switching the sign of ϵ, is equivalent to moving the hypersurface to $\pi - r$ when dealing with $\mathbf{K}$ and $\mathcal{C}$, which are the quantities relevant for determining whether a specific shell satisfies the conditions specified in Sec. 1.2.2. This simplifies the analysis, as we can focus on only one sign of ϵ as long as we examine the whole interval of r. The (somewhat less interesting) projection of the magnetic field changes its sign.

The trace of $\mathbf{K}$ is obviously

$$K = \epsilon\sqrt{2\Lambda}\cot r\,. \tag{2.127}$$

As expected for the two spacetime's axes, $K \to +\infty$ in the limit of $r \to 0^+$ if the normal field is oriented towards higher values of the radial coordinate ($\epsilon = +1$), and also in the limit of $r \to \pi^-$ for the opposite orientation of the normal.

When talking about shell sources, the original paper Žofka [2019] only considers shells resulting from connecting the spacetime to another instance of itself, taking advantage of the symmetry of $\mathcal{C}$ with respect to $r = \pi/2$. The paper states that for the discussed orientation of the two normals, the pressure along the axis (determined by S_{ZZ}) is positive, while the energy density (i.e., S_{TT}) is equal in magnitude but negative. Indeed, it can be shown that regardless of the

orientation of the normals (represented by ϵ) and even when considering different values of Λ on each side of the hypersurface, we always have

$$S_{TT} = -S_{ZZ} = \frac{\epsilon_- \sqrt{\Lambda_-}\cos(r_-)\sin(r_+) - \epsilon_+ \sqrt{\Lambda_+}\cos(r_+)\sin(r_-)}{4\sqrt{2}\,\pi \sin(r_+)\sin(r_-)}\,, \tag{2.128}$$

where the $\pm$ signs distinguish the spacetimes on either side of the shell as explained in Sec. 1.2.2. This means that this shell cannot simultaneously fulfill both $S_{TT} > 0$ and $S_{ZZ} \geq 0$ as needed for the desired interpretation via four charged particle streams. For the sake of completeness, let us add that $S_{\Phi\Phi} = 0$ and the only non-zero element of the induced three-current on the shell is $s_\Phi = (\epsilon_- \sqrt{\Lambda_-} - \epsilon_+ \sqrt{\Lambda_+})/4\pi$.

Similarly, a hypersurface connecting this spacetime to the Minkowski spacetime or the original Bonnor–Melvin solution also has $S_{TT} = -S_{ZZ}$. However, a reasonable shell connecting this spacetime to the asymptotic region of the Levi–Civita solution of Sec. 1.3.2 can be found, as can be seen in Fig. 2.2. Note that the value of the parameter $\sigma = 0.1$ used here admits the effective gravitational mass interpretation of σ in the Levi–Civita solution.

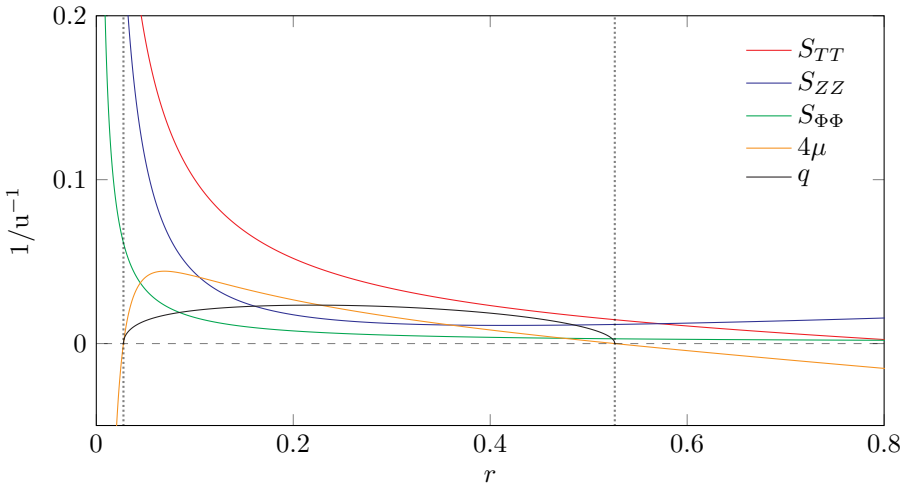

Figure 2.2: The properties of shells on the interface of the Bonnor–Melvin–Λ solution ($\Lambda = 0.4\,\mathrm{u}^{-2}$) and the Levi–Civita solution ($\sigma = 0.1$, $C = 1\,\mathrm{u}$), expressed as functions of the radial coordinate of the shell in the former spacetime. The spacetimes are aligned in such a way that the region with lower r in BMΛ and the asymptotic region of LC are preserved. The induced three-current on the shell has only one non-zero element, $s_\Phi = \sqrt{\Lambda}/4\pi$, which allows us to use (1.60) to compute the magnitude of particle charge q in the region admitting the four-stream interpretation of the shell, located between the two dotted lines.

2.3 Axial inhomogeneous spacetime

The metric of the inhomogeneous solution with an axial magnetic field was presented in Veselý and Žofka [2019b] as

$$\mathrm{d}s^2 = \frac{1}{f}\left(-\mathrm{d}t^2 + \mathrm{d}z^2\right) + \frac{\mathrm{d}f^2}{\gamma f^{\frac{7}{2}} - 4f^4 - \frac{4}{3}\Lambda f^2} + \beta\frac{\gamma f^{\frac{7}{2}} - 4f^4 - \frac{4}{3}\Lambda f^2}{f^3}\,\mathrm{d}\phi^2 \quad (2.129)$$

with

$$\mathbf{F} = \sqrt{\frac{\beta}{f}}\,\mathrm{d}f \wedge \mathrm{d}\phi\,. \quad (2.130)$$

Taking u as an arbitrary unit of length, the dimensions of the coordinates are as follows: t $[\sqrt{\mathrm{u}}]$, f $[u^{-1}]$, z $[\sqrt{\mathrm{u}}]$, and ϕ [u]. Apart from the cosmological constant Λ $[\mathrm{u}^{-2}]$, which can be of either sign, there are two other parameters in the metric, γ $\left[\mathrm{u}^{-1/2}\right]$ and β [u]. The latter needs to be positive for the metric to keep the correct signature. The metric is a product of a warped 2D Minkowski space and a 2D Riemannian metric.

Not before publishing the paper did we realize that perhaps a more convenient form can be obtained after employing the transformation

$$\begin{aligned} \hat{t} &= \frac{1}{\sqrt{\beta}}\,t\,, \qquad & \hat{r} &= \sqrt{\beta}\,f^{-1/2}, \\ \hat{z} &= \frac{1}{\sqrt{\beta}}\,z\,, \qquad & \hat{\phi} &= -\frac{2}{\sigma}\,\phi\,, \end{aligned} \quad (2.131)$$

which leads to (barring the hats)

$$\mathrm{d}s^2 = -r^2\,\mathrm{d}t^2 + \frac{\mathrm{d}r^2}{\mathfrak{M}(r)} + r^2\,\mathrm{d}z^2 + \sigma^2\,\mathfrak{M}(r)\,\mathrm{d}\phi^2, \quad (2.132)$$

where the newly-introduced parameter $\sigma > 0$ and the coordinate r have the dimension of length, while the remaining coordinates are dimensionless. The master function reads

$$\mathfrak{M}(r) = -\frac{\beta^2}{r^2} + \frac{\alpha}{r} - \frac{\Lambda}{3}\,r^2 \quad (2.133)$$

with $\alpha = \gamma\beta^{3/2}/4$ of the dimension of length. The function's roots correspond to the spacetime's axes. The magnetic field is

$$\mathbf{F} = \frac{\beta\sigma}{r^2}\,\mathrm{d}r \wedge \mathrm{d}\phi \quad (2.134)$$

and the corresponding four-potential according to (1.15) is $\mathbf{A} = -\beta\sigma/r\,\mathrm{d}\phi$, while the dual electric field is simply $\star\mathbf{F} = \beta\,\mathrm{d}t \wedge \mathrm{d}z$. The field invariant becomes

$$F_{\mu\nu}F^{\mu\nu} = \frac{2\beta^2}{r^4}\,, \quad (2.135)$$

and the Kretschmann scalar is

$$R_{\alpha\beta\gamma\delta}R^{\alpha\beta\gamma\delta} = \frac{4}{3r^8}\left(2\Lambda^2 r^8 + 9\alpha^2 r^2 - 36\alpha\beta^2 r + 42\beta^4\right). \quad (2.136)$$

We consider only positive values of r, as taking $r < 0$ corresponds to $r > 0$ with the opposite sign of α, and it is obvious from the two scalars that it is not possible to cross $r = 0$ unless both α and β vanish. Unlike in the previous form of the metric, there is nothing stopping us from considering both signs of β now, as the sign only affects the polarity of the magnetic field. While we allow the case $\alpha = 0$, we shall not investigate the case $\beta\Lambda = 0$ in detail here, as we are primarily interested in cosmological solutions with a magnetic field. Note that considering $\alpha = 0$ does not affect the asymptotics of $\mathfrak{M}$.

For the metric to have the correct signature, the master function $\mathfrak{M}$ must be positive. In the following we shall work with

$$\mathfrak{m}(r) = r^2\mathfrak{M}(r) = -\beta^2 + \alpha r - \frac{\Lambda}{3}r^4, \tag{2.137}$$

which has the same non-zero roots as $\mathfrak{M}$, and the value $r = 0$ would correspond to a physical singularity anyway. Assuming that all three parameters are non-zero, $\mathfrak{m}$ is a polynomial of degree four and the general expressions for its roots are too unwieldy to work with. Nonetheless, determining the number of positive roots is possible.

Applying Descartes' rule of signs, for $\Lambda < 0$ there is always one root, as there is only one sign change in the sequence of coefficients of the terms in $\mathfrak{m}$ regardless of the signs of α and β, and the allowed range of r stretches from this axis to positive infinity.

On the other hand, for $\Lambda > 0$ there may be up to two roots. Because $\mathfrak{m}$ is negative both in the neighborhood of $r = 0$ and in the asymptotic region, we just need to determine whether there is any positive maximum. Setting the derivative $\mathfrak{m}'(r) = \alpha - 4\Lambda r^3/3$ equal to zero, we see that the suspected extremum[6] lies at

$$r_0^3 = \frac{3\alpha}{4\Lambda} \tag{2.138}$$

and that α must be positive so that r_0 is also positive. After plugging r_0 into $\mathfrak{m}$, we obtain

$$\mathfrak{m}(r_0) = -\beta^2 + \frac{3\sqrt[3]{6}}{8}\,\frac{\alpha^{4/3}}{\Lambda^{1/3}}\,. \tag{2.139}$$

The threshold value $\mathfrak{m}(r_0) = 0$ corresponds to

$$\alpha_{\mathfrak{M}} = \frac{4}{3}\,|\beta|^{3/2}\,\Lambda^{1/4}, \tag{2.140}$$

for which $\mathfrak{M}$ has one degenerate root and is everywhere non-positive. There are no roots for $\alpha < \alpha_{\mathfrak{M}}$ and $\mathfrak{M}$ is negative. Only for $\alpha > \alpha_{\mathfrak{M}}$ is there an interval of r where $\mathfrak{M}$ is positive as required by the metric. In this case, the spacetime has two separate axes.

Examples of all four variants of the master function $\mathfrak{M}$ with respect to different signs of Λ and values of α are depicted in Fig. 2.3.

Note that, in a way, the degenerate case with $\Lambda > 0$ corresponds to the previous spacetime from Sec. 2.2. Plugging $\alpha_{\mathfrak{M}}$ (2.140) into the double root of the master function r_0 (2.138), we get $r_{0(\mathrm{crit})} = |\beta|^{1/2}\,\Lambda^{-1/4}$. Going backwards

[6]Take note that the extrema of the full master function $\mathfrak{M}$ may lie elsewhere, but this fact is irrelevant in our effort to determine the number of positive roots.

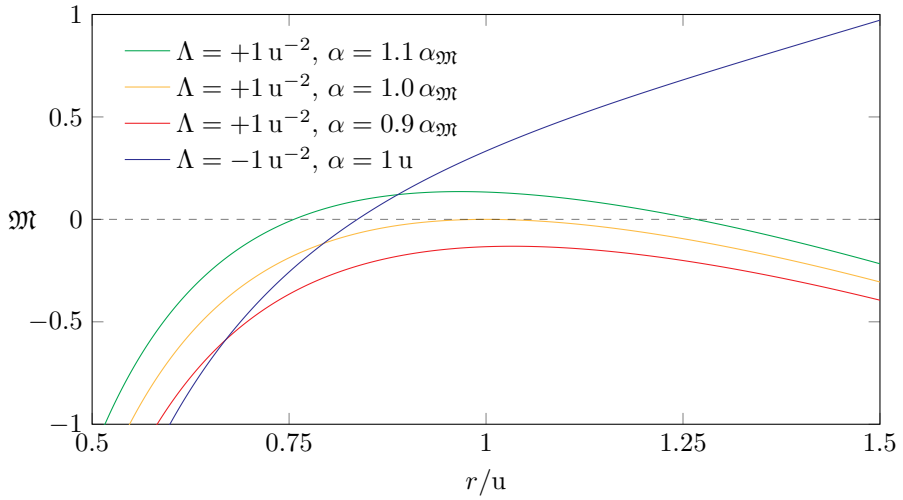

Figure 2.3: The four archetypes of the master function $\mathfrak{M}(r)$ with different parameters Λ and α, but always with $\beta = 1\,\mathrm{u}$. The blue curve represents spacetimes with $\Lambda < 0$ and the green one represents valid spacetimes with $\Lambda > 0$. While the orange curve with $\alpha = \alpha_{\mathfrak{M}} = \frac{4}{3}\,\mathrm{u}$ reaches zero, neither it nor the red curve ever reach positive values, and thus they do not correspond to valid spacetimes.

through the transformation (2.131) (disregarding the case of $\beta < 0$, which we did not allow back then), we obtain $f^2 = \Lambda$, which coincides with (2.17) as seen during the derivation of the homogeneous spacetime. Furthermore, plugging $r_{0(\mathrm{crit})}$ into the electromagnetic field invariant (2.135), we correctly obtain the value $F_{\mu\nu}F^{\mu\nu} = 2\Lambda$ of (2.106). It is not straightforward, however, to consider the previous spacetime as a parametric limit of the presently-investigated one, as a necessary stepping stone during the derivation of the metric (2.129) was considering f as the new radial coordinate, which is, of course, not possible for a constant f.

This solution is almost everywhere of Petrov algebraic type D with the exception of the hypersurface $r = 2\beta^2/\alpha$ and in the limit $r \to \infty$ (if either of them can be found within the particular spacetime), where it is type O. Like in the original Bonnor–Melvin solution, there are four Killing vector fields. Three correspond to the translational symmetries and one to the boost in the t–z plane. The group of isometries is $ISO(1,1) \times E(1)$, the same as for the Bonnor–Melvin solution. Like both the homogeneous and Bonnor–Melvin solutions, this spacetime too belongs to the Kundt class, as the integral curves of the two principal null directions $\sqrt{2}(\partial_t \pm \partial_z)/2r$ are again geodesics with vanishing optical scalars.

While the spacetime does not contain any curvature singularities, there may be conical defects at the axes. The condition (1.2) that ensures elementary flatness at an axis located at $r = r_a$ becomes

$$\lim_{r \to r_a} \sigma^2 \left(\mathfrak{M}'(r)\right)^2 = \sigma^2 \left(\mathfrak{M}'(r_a)\right)^2 = 4 \tag{2.141}$$

due to continuity of $\mathfrak{M}$ and its derivatives at the axes. Therefore, by setting

$$\sigma^2 = \frac{4}{\left(\mathfrak{M}'(r_a)\right)^2} \tag{2.142}$$

we can always eliminate the conical defect for the axis at r_a in the spacetime. There is only one axis for spacetimes with $\Lambda < 0$, so they can always be made

free of the defect. However, there are two axes if $\Lambda > 0$ and $\alpha > \alpha_{\mathfrak{M}}$. Plugging the above value of σ^2 into the condition, elementary flatness for the second axis at r_b is guaranteed if

$$\mathfrak{M}'(r_a) = -\mathfrak{M}'(r_b)\,, \tag{2.143}$$

where we used the fact that the two derivatives must have opposite signs as evident from the analysis of the master function. While one may be tempted to consider this condition to be just as easily satisfiable as the previous one if we fix one of the remaining parameters of the solution, we must keep in mind that unlike σ the other parameters influence the positions of the axes as they all appear in $\mathfrak{M}$. Analysis of the problem reveals that it is actually not possible to fulfill the second condition. To show that, we can compare $\mathfrak{M}$ with its factorization,

$$\begin{aligned} -\frac{3r^2}{\Lambda}\,\mathfrak{M}(r) &= \frac{3\beta^2}{\Lambda} - \frac{3\alpha}{\Lambda}\,r + r^4 \\ &= (r - r_a)(r - r_b)(r - r_c)(r - \overline{r_c})\,, \end{aligned} \tag{2.144}$$

where r_c and $\overline{r_c}$ are the remaining roots of $\mathfrak{M}$, which must be complex conjugate in this case. By expanding the second line and comparing the coefficients at the corresponding powers of r with the first line, we can eliminate the irrelevant complex roots and obtain

$$\begin{aligned} \beta^2 &= \frac{\Lambda}{3} r_a r_b \left(r_a^2 + r_a r_b + r_b^2\right), \\ \alpha &= \frac{\Lambda}{3}\left(r_a + r_b\right)\left(r_a^2 + r_b^2\right). \end{aligned} \tag{2.145}$$

Plugging the values into the derivatives of $\mathfrak{M}$, the condition (2.143) becomes

$$0 = \mathfrak{M}'(r_a) + \mathfrak{M}'(r_b) = \frac{\Lambda}{3}\,\frac{\left(r_a - r_b\right)^2\left(r_a + r_b\right)^3}{r_a^2\, r_b^2}, \tag{2.146}$$

which is clearly not possible to be fulfilled for two distinct positive values of r_a and r_b. See also Fig. 2.4 for the chart of $-\mathfrak{M}'(r_b)/\mathfrak{M}'(r_a)$ demonstrating this issue. Therefore, one of the two axes for the solution with $\Lambda > 0$ must contain a conical defect. This result is consistent with Lim [2018]. Note that

$$\mathfrak{M}'(r) = \frac{4\beta^2}{r^3} - \frac{3\alpha}{r^2} + \frac{2\mathfrak{M}(r)}{r} = \frac{\alpha}{r^2} - \frac{4\Lambda}{3}r - \frac{2\mathfrak{M}(r)}{r} = \frac{\beta^2}{r^3} - \Lambda r - \frac{\mathfrak{M}(r)}{r}\,, \tag{2.147}$$

which means that we can replace the derivatives of $\mathfrak{M}$ in the conditions with the first two terms of any of the expressions as $\mathfrak{M} = 0$ at the axes.

The proper radial distance (corresponding to a definite integral of $\sqrt{g_{rr}}\,\mathrm{d}r$) to an axis from any given point in the spacetime is finite, because the axes are represented by simple roots of $\mathfrak{M}$ and so we are effectively integrating $1/\sqrt{r - r_a}$ in their vicinity, leading to finite results. On the other hand, for $\Lambda < 0$ the proper distance diverges in the limit $r \to \infty$, as the integrand behaves like $1/r$ in the asymptotic region.

Speaking of the asymptotic region, if we consider the leading term of the series $\mathfrak{M}(r) = -\frac{\Lambda}{3}r^2 + \mathcal{O}(1/r)$, perform the transformation $r \to \sqrt{-3/\Lambda}\,/\,x$ and

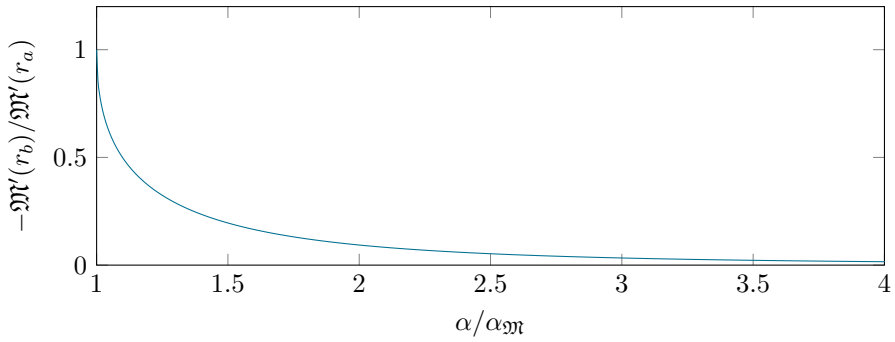

Figure 2.4: The chart of $-\mathfrak{M}'(r_b)/\mathfrak{M}'(r_a)$ as a function of $\alpha/\alpha_{\mathfrak{M}}$ for two axes at $r_a < r_b$ in a spacetime with $\Lambda > 0$. Numerical computations suggest that the value of the function does not depend on the remaining parameters of the metric, even though the coordinates of the axes do. For $\alpha > \alpha_{\mathfrak{M}}$ the function does not reach the required value $-\mathfrak{M}'(r_b)/\mathfrak{M}'(r_a) = 1$ and elementary flatness of both axes can never be achieved. The function approaches 1 in the limit $\alpha \to \alpha_{\mathfrak{M}}$ as the two axes merge.

$\phi \to \sqrt{-3/\Lambda}\,\phi\,/\,\sigma$, we obtain the anti-de Sitter metric as seen in, e.g., Griffiths and Podolský [2009],

$$\mathrm{d}s^2 = \frac{-\frac{3}{\Lambda}}{x^2}\left(-\mathrm{d}t^2 + \mathrm{d}x^2 + \mathrm{d}z^2 + \mathrm{d}\phi^2\right). \tag{2.148}$$

Note, however, that the coordinates in this form of the anti-de Sitter metric are usually considered to be unbounded, but we still consider the ϕ coordinate to be periodic.

After setting $\Lambda = 0$, the simplified master function $\mathfrak{M}_0(r) = -\beta^2/r^2 + \alpha/r$ requires α to be positive, or else $\mathfrak{M}_0$ would be negative for all $r > 0$. It then has a positive root at $r_a = \beta^2/\alpha$ and the allowed region of r stretches to positive infinity. We can use (2.142) to set $\sigma = 2\beta^4/\alpha^3$ to ensure elementary flatness of the axis, which leads to the metric

$$\mathrm{d}s^2 = -r^2\,\mathrm{d}t^2 + \frac{\mathrm{d}r^2}{-\frac{\beta^2}{r^2} + \frac{\alpha}{r}} + r^2\,\mathrm{d}z^2 + \frac{4\beta^8}{\alpha^6}\left(-\frac{\beta^2}{r^2} + \frac{\alpha}{r}\right)\mathrm{d}\phi^2 \tag{2.149}$$

with

$$\mathbf{F} = \frac{2\beta^5}{\alpha^3 r^2}\,\mathrm{d}r \wedge \mathrm{d}\phi\,. \tag{2.150}$$

Now, let us consider the transformation $\rho = \sqrt{\alpha\,(r - r_a)}$ mapping the allowed interval $r \in [r_a, \infty)$ into $\rho \in \mathbb{R}_0^+$ bijectively. After defining new parameters $B = 2/\beta$ and $A = 2^{-3/2}\alpha$, we arrive at the metric

$$\mathrm{d}s^2 = \frac{\left(1 + \frac{1}{4}B^2\rho^2\right)^2}{A^4B^4}\left(2A^2\left(-\mathrm{d}t^2 + \mathrm{d}z^2\right) + \mathrm{d}\rho^2\right) + A^4B^4\left(1 + \frac{1}{4}B^2\rho^2\right)^{-2}\rho^2\,\mathrm{d}\phi^2 \tag{2.151}$$

and the magnetic field

$$\mathbf{F} = \frac{\rho}{A^2B\left(1 + \frac{1}{4}B^2\rho^2\right)^2}\,\mathrm{d}\rho \wedge \mathrm{d}\phi\,. \tag{2.152}$$

The magnetic field invariant is

$$F_{\mu\nu}F^{\mu\nu} = 2A^4B^6\left(1+\frac{1}{4}B^2\rho^2\right)^{-4} \tag{2.153}$$

and the Kretschmann scalar is

$$R_{\alpha\beta\gamma\delta}R^{\alpha\beta\gamma\delta} = \frac{A^8B^{12}\left(3B^4\rho^4-24B^2\rho^2+80\right)}{4\left(1+\frac{1}{4}B^2\rho^2\right)^8}\,. \tag{2.154}$$

The quantities are noticeably similar to those of the Bonnor–Melvin solution of Sec. 1.3.3. It does not appear to be possible to transform the parameter A away without introducing a conical defect, but we recover the Melvin universe if we set $A = 1/B$ and rescale the t and z coordinates.

The solution was obtained using different methods prior to our work. A variant of the metric was perhaps first discovered in Dias and Lemos [2002] by varying the Einstein–Hilbert action. While the paper only deals with the case $\Lambda < 0$, it also presents a rotating generalization of the spacetime and notably examines the solution's mass, charge, and (for the rotating variant) angular momentum per unit length. They also note the spacetime is both timelike and null geodesically complete. Next, a generalization of Ernst's solution generating technique was used to obtain this solution in Astorino [2012]. The transformation $r \to 1+\rho^2/4$ and $\phi \to -2\phi/\sigma$ connects our metric (2.132) to (4.6) of the cited paper with $B = \beta$ and $k = 4\alpha$. The properties of the spacetime are not investigated there, but the paper discusses a rotating variant as well. In Lim [2018] the metric was recovered by applying a limiting procedure to the (anti-)de Sitter–C-metric, generalizing Havrdová and Krtouš [2007] for a non-zero cosmological constant, considering both magnetic and electric components of the electromagnetic field. Some properties of the spacetime are studied in this paper, including electromagnetic fluxes across the plane of constant t and z, and some parametric limits of the metric are provided. The paper also tackles uncharged particle motion, which partly overlaps with our more extensive analysis below, which also includes charged test particles. Properties of the magnetic field and the ADM mass and tensions for spacetimes with $\Lambda < 0$ are studied in Kastor and Traschen [2020]. Moreover, the recent paper Lim [2021] explores a certain type of shell sources, different from those we study in this thesis. Last but not least, a gyraton metric on a variant of this spacetime is studied in Kadlecová and Krtouš [2014].

Particle motion

Let us examine particle motion now. For the metric (2.132), the constants of motion for a charged test particle with the charge-to-mass ratio κ are

$$E = r^2\,\dot{t}\,, \tag{2.155}$$

$$L = \sigma^2\,\mathfrak{M}(r)\,\dot{\phi} - \frac{\beta\sigma\kappa}{r}\,, \tag{2.156}$$

$$Z = r^2\dot{z}\,. \tag{2.157}$$

The effective potential for radial motion satisfying $\dot{r}^2/2 = -V$ then reads

$$V(r) = \frac{\mathfrak{M}(r)}{2}\left(-\delta - \frac{E^2-Z^2}{r^2}\right) + \frac{1}{2\sigma^2}\left(\frac{\beta\sigma\kappa}{r}+L\right)^2 \tag{2.158}$$

and its separated counterpart according to (1.12) is

$$W^2(r) = E^2 + \frac{2r^2}{\mathfrak{M}(r)}V(r) = -r^2\delta + Z^2 + \frac{r^2}{\sigma^2\mathfrak{M}(r)}\left(\frac{\beta\sigma\kappa}{r} + L\right)^2 . \qquad (2.159)$$

First, the interesting limiting cases are motion towards an axis (either the only axis in spacetimes with $\Lambda < 0$ or any of the two axes if $\Lambda > 0$ and $\alpha > \alpha_{\mathfrak{M}}$) and towards the radial infinity for $\Lambda < 0$. When approaching an axis, we perform the limit of $\mathfrak{M} \to 0^+$ (i.e., we approach zero from positive values of $\mathfrak{M}$) while the radial coordinate of the axis r_a is finite. In this case, the first term in V vanishes while the second, positive term survives. This means that a general particle is unable to reach any axis, unless it satisfies two conditions: First, it needs to have $L = -\beta\sigma\kappa/r_a \equiv L_a$ so that $V \to 0$ at the axis, and second, the remaining constants of motion must satisfy the inequality $E^2 \geq -\delta r_a^2 + Z^2$, otherwise the potential is positive in the neighborhood of the axis, prohibiting particle motion there. The second condition follows from the Taylor expansion of the potential at r_a with $L = L_a$ employing the factorization $\mathfrak{M}(r) = f(r)\,(r - r_a)$, which is always possible for valid spacetimes, as an axis is represented by a root of $\mathfrak{M}$ of multiplicity one. We then have

$$\begin{aligned} V(r)\big|_{L=L_a} &= \frac{f(r)\,(r-r_a)}{2}\left(-\delta - \frac{E^2 - Z^2}{r^2}\right) + \frac{\beta^2\kappa^2}{2}\left(\frac{1}{r} - \frac{1}{r_a}\right)^2 \\ &= \frac{-E^2 - \delta r_a^2 + Z^2}{2r_a^2}\, f(r_a)\,(r - r_a) + \mathcal{O}\left((r-r_a)^2\right), \end{aligned} \qquad (2.160)$$

where $f(r_a)\,(r - r_a)$ must be positive near the axis in the area with $\mathfrak{M} > 0$. Therefore, the leading term of the expansion is negative (thus allowing particle motion near the axis) if the strict version of the inequality above holds. In the case of $E^2 = -\delta r_a^2 + Z^2$, the linear term in the expansion of V vanishes and the leading term is the quadratic one with the coefficient $(\beta^2\kappa^2 - 2\delta r_a^3 f(r_a))/2r_a^4$, which again must be negative to allow particle motion near the axis, yielding an additional condition[7]. In this case we additionally have $V' \to 0$, which means the particles would reach the axis in infinite proper time[8]. Note that photons must satisfy $L = 0$ and $E > |Z|$ to reach an axis. These photons then reach the axis in finite affine parameter, as $V'(r_a)$ is non-zero for them, even though for purely-radially moving photons with $Z = L = 0$ the coordinate velocity $|\mathrm{d}r/\mathrm{d}t| = r\sqrt{\mathfrak{M}}$ vanishes as they approach the axis. Considering $E = |Z|$ with $L = 0$ necessarily leads to $\dot{r} = 0$, so no axis is being approached.

The other limit, $r \to \infty$ for $\Lambda < 0$, is easier to analyze. For $\delta = -1$ the potentials diverge to positive infinity, which means that no massive particle whatsoever may ever escape the pull towards the axis. For photons, on the other hand, the limit is finite,

$$\lim_{r\to\infty} V(r)\big|_{\delta=\kappa=0} = \frac{-\Lambda}{6}\left(-E^2 + Z^2\right) + \frac{L^2}{2\sigma^2}\,, \qquad (2.161)$$

[7]Technically we could go on considering that even the quadratic coefficient can be zero, leading to a condition for the cubic coefficient, which could also be zero, and so on. However, the additional constrains would need to be imposed on the spacetime instead of the particle.

[8]Since it is impossible for a massive particle to reach an axis without serious fine-tuning of the initial conditions, the situation is reminiscent of the phenomenon of repulsive gravity, which occurs in naked-singularity spacetimes. We shall briefly discuss it once we observe it properly in Sec. 2.4 and 2.6, as these solutions actually contain singularities.

which means that in the asymptotic region photons with high enough E are not barred from moving arbitrarily far away from the axis[9]. It would take the photons infinite affine parameter to reach $r \to \infty$, however, because $V' \to 0$ for them, although the coordinate velocity of purely radially-moving photons actually diverges in this limit.

Regarding stationary circular orbits in the planes $z = \text{const.}$, let us start with photons. For them, the only non-trivial equation of motion (1.29) is the radial one. Together with the normalization equation (1.6) with $\delta = 0$, we have a set of two equations for the photon coordinate angular velocity $\Omega = \mathrm{d}\phi/\mathrm{d}t$ and the orbiting radius, yielding

$$\Omega^2 = \frac{768\beta^6}{(81\alpha^4 - 256\beta^6\Lambda)\,\sigma^2} \tag{2.162}$$

with the orbit located at

$$r_\gamma = \frac{4}{3}\,\frac{\beta^2}{\alpha}\,, \tag{2.163}$$

provided that $\mathfrak{M}(r_\gamma) > 0$, and $\alpha > 0$ so that r_γ is also positive[10]. The former condition translates to $81\,\alpha^4 > 256\,\beta^6\Lambda$, which also means that we need not worry about Ω being imaginary. For $\Lambda < 0$ the condition is clearly always fulfilled, and the same is, in fact, true for $\Lambda > 0$ as well: By comparing the fourth power of (2.140) to the conditions, we can see that they are equivalent to $\alpha > \alpha_{\mathfrak{M}}(> 0)$, the necessary and sufficient condition for the existence of an interval with $\mathfrak{M} > 0$ for $\Lambda > 0$. This means that there is a photon orbit in every valid spacetime of this family with $\alpha > 0$. The orbits are stable, because $V''(r_\gamma) = 729\,\alpha^6 E^2/\,2048\,\beta^{10} > 0$. After performing the appropriate coordinate transformation, our result (2.163) is equal to (58) in Lim [2018]. Note that purely axial null geodesics can exist anywhere in the spacetime, because for constant r and ϕ the equations of motion yield $\ddot{t} = \ddot{z} = 0$ with $\dot{t} = |\dot{z}|$.

Moving on to orbits of massive particles, to get the constants of motion it might be easier this time to start with the separated potential,

$$W^2\big|_{\text{orbit}} = r^2\left(1 + \frac{1}{\sigma^2\mathfrak{M}(r)}\left(\frac{\beta\sigma\kappa}{r} + L\right)^2\right), \tag{2.164}$$

and its first derivative,

$$\begin{aligned}\left(W^2\big|_{\text{orbit}}\right)' = 2r + \frac{1}{3\,\sigma^2\,r^3\,\mathfrak{M}^2(r)}\Big[&\left(2\Lambda r^4 + 3\alpha r - 6\beta^2\right)\beta^2\sigma^2\kappa^2 \\ &+ 2\left(\Lambda r^4 + 6\alpha r - 9\beta^2\right)\beta\,\sigma\,\kappa\,L\,r + 3\left(3\alpha r - 4\beta^2\right)L^2 r^2\Big].\end{aligned} \tag{2.165}$$

Setting the latter relation to zero, we can express L as

$$L = \frac{\sigma}{3\,(3\alpha r - 4\beta^2)\,r}\left[-(\Lambda r^4 + 6\alpha r - 9\beta^2)\beta\kappa \pm 3r^2\mathfrak{M}(r)\sqrt{\beta^2\kappa^2 - 6\alpha r + 8\beta^2}\right], \tag{2.166}$$

[9]This result is the only discrepancy between our work and Lim [2018], which states that photon motion is unbounded only for radially-moving photons. Numerical integration of the equations of motions seems to support our claims, as we found photons with $L \neq 0$ apparently escaping into radial infinity.

[10]For $\alpha = 0$ the equations of orbital motion for photons do not have any solution if $\beta \neq 0$.

and the corresponding E^2 is equal to W^2 from (2.164) after plugging a particular L in. Since $\mathfrak{M} > 0$, we need not worry about E^2 being negative for any valid r, but the square root in L affects the region of r where circular orbits may be located. First, for $\alpha \leq 0$ (also requiring $\Lambda < 0$), the argument of the square root is positive everywhere and massive particle orbits can be found anywhere in the spacetime (unlike the photon orbit, which is nowhere to be found for $\alpha \leq 0$). On the other hand, for $\alpha > 0$ (and any sign of Λ) the orbits can only be located at

$$r \leq \frac{(8+\kappa^2)\beta^2}{6\alpha} = r_\gamma + \frac{\beta^2\kappa^2}{6\alpha}\,. \tag{2.167}$$

For uncharged particles with $\kappa = 0$, this means that the upper bound for the radii is the photon orbit at r_γ and the inequality in this particular case must be strict, as (2.166) diverges at r_γ for each sign in front of the square root. For charged particles the upper bound shifts above the photon orbit. Regardless of the particle's charge, the allowed region then stretches all the way to the axis located at lower r. Take note that for certain values of κ the numerical value of the shifted upper bound may lie above the r coordinate of the second axis present in spacetimes with $\Lambda > 0$. In these cases, orbits of particles with such κ may lie at any valid r in the spacetime. The denominator of L would suggest a divergence at the photon orbit radius for charged particles as well, but, in fact, this is true for only one of the two sign choices in L. The leading terms in the series expansion of (2.166) at the photon orbit radius r_γ for $\kappa \neq 0$ are

$$\begin{aligned}\frac{L}{\sigma} = {}& \frac{(1 \pm \operatorname{sgn}(\beta\kappa))\,(81\alpha^4 - 256\beta^6\Lambda)\,\beta\kappa}{972\alpha^4}\,(r - r_\gamma)^{-1} \\ & + \frac{-3\,(243\alpha^4 + 256\beta^6\Lambda)\,\kappa^2 \pm \operatorname{sgn}(\beta\kappa)\,(81\alpha^4 - 256\beta^6\Lambda)\,(3\kappa^2 - 4)}{1296\alpha^3\beta\kappa} \\ & + \mathcal{O}(r - r_\gamma)\,.\end{aligned} \tag{2.168}$$

Due to the presence of $1 \pm \operatorname{sgn}(\beta\kappa)$ in the otherwise diverging first term, the divergence vanishes for one of the two signs in L, and the value of the non-diverging L at r_γ is given by the constant second term. The differences between the values of L for charged and uncharged particles in the case of $\alpha > 0$ are illustrated in Fig. 2.5.

Concerning the stability of the orbits, the second derivative of the potential for uncharged particles can be written as

$$\left(W^2\Big|_{\text{orbit}}^{\kappa=0}\right)'' = \frac{4\,(4\beta^2 - 3\alpha r)}{r^2\,\mathfrak{M}(r)} + \frac{6\,(8\beta^2 - 5\alpha r)}{4\beta^2 - 3\alpha r}\,, \tag{2.169}$$

independently of the sign in L (2.166), which was inserted after the derivatives were performed. For $\alpha \leq 0$, the second derivative is clearly positive wherever $\mathfrak{M}(r) > 0$. For $\alpha > 0$, the orbit radii satisfy $4\beta^2 > 3\alpha r$ due to (2.167). Taking into account that $8/5 > 4/3$, (2.169) is again positive in the area where uncharged orbits may be located. Therefore, geodesic stationary circular orbits are always stable in this spacetime. After adding charge, however, some orbits in spacetimes with $\alpha > 0$ may be unstable. Analysis through the `Reduce` function of `Mathematica` reveals that while all orbits located at lower r than the photon orbit radius r_γ are stable, some charged orbits above r_γ may be unstable, which

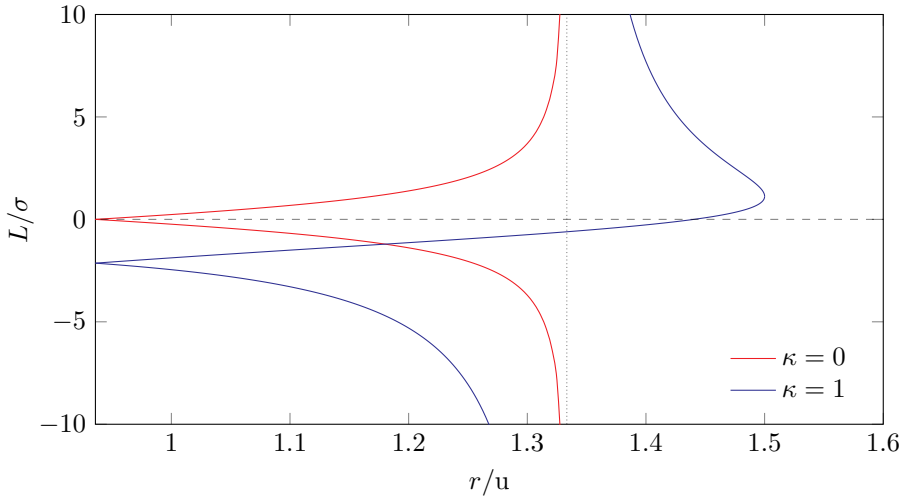

Figure 2.5: Charts of possible values of L for massive particles orbiting at a given r in the axial inhomogeneous spacetime with parameters $\alpha = 4\,\mathrm{u}$, $\beta = 2\,\mathrm{u}$, $\Lambda = -1\,\mathrm{u}^{-2}$, and $\sigma = 1\,\mathrm{u}$. The red curves represent uncharged geodesic orbits, while the blue curves correspond to particles with charge-to-mass ratio $\kappa = 1$. The dotted vertical line denotes photon orbit at $r_\gamma = \frac{4}{3}\,\mathrm{u}$. The left boundary of the chart, where the corresponding pairs of curves converge, is the spacetime's axis located at $r \approx 0.936\,\mathrm{u}$. Valid values of r stretch from the axis to infinity.

has to be checked numerically for each given orbit in a given spacetime. A necessary but not sufficient condition appears to be that the particle's charge-to-mass ratio must fulfill $\kappa^2 > 10$ for spacetimes with $\Lambda < 0$ or $\kappa^2 > 25$ for spacetimes with $\Lambda > 0$. Only orbits corresponding to the L that diverges at r_γ can become unstable. See Fig. 2.6 for an example of unstable charged orbits.

The boost Killing vector field yields another constant of motion, $r^2(z\dot{t} - t\dot{z})$, which can be used to obtain the same expression for $z(t)$ as in the homogeneous case,

$$z(t) = \frac{Z}{E}\,t + z_0\,, \tag{2.170}$$

which is again valid for uncharged and charged test particles alike. There do not appear to be any other second-rank Killing tensors than the metric and the ten symmetrized tensor products of the four Killing vectors, giving us no additional constants.

Shell sources

The extrinsic curvature tensor (1.41) for the shell at $r = \text{const.}$ is more complicated than the one in the homogeneous solution,

$$\mathbf{K} = \epsilon \left(\frac{\sqrt{\mathfrak{M}(r)}}{r}(-\mathrm{d}T^2 + \mathrm{d}Z^2) + \frac{1}{2}\,\frac{\mathfrak{M}'(r)}{\sqrt{\mathfrak{M}(r)}}\,\mathrm{d}\Phi^2 \right). \tag{2.171}$$

The projection of the electromagnetic tensor (1.44) yields

$$\mathbf{F}_\perp = -\frac{\epsilon\beta}{r^2}\,\mathrm{d}\Phi\,. \tag{2.172}$$

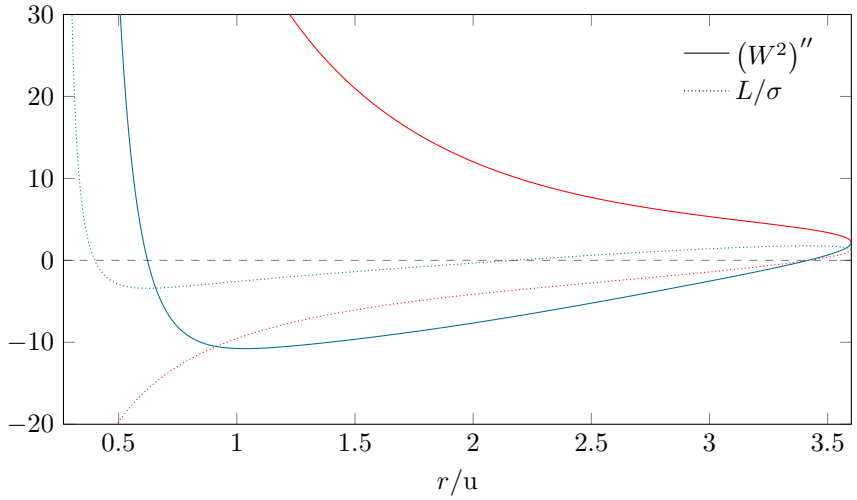

Figure 2.6: Charts of possible values of L (dotted lines) and the corresponding same-colored $(W^2)''$ (solid lines) for charged massive particles with charge-to-mass ratio $\kappa = 10$ in the axial inhomogeneous spacetime with the parameters $\alpha = 5\,\mathrm{u}$, $\beta = 1\,\mathrm{u}$, $\Lambda = -1\,\mathrm{u}^{-2}$, and $\sigma = 1\,\mathrm{u}$, with r stretching from the photon orbit radius $r_\gamma = \frac{4}{15}\,\mathrm{u}$ to the upper orbit bound at $r = \frac{18}{5}\,\mathrm{u}$. The blue lines are the ones that diverge at r_γ, and there is a region in which the blue orbits are unstable with $(W^2)'' < 0$.

The proper circumference (1.3) of the hypersurface is

$$\mathcal{C} = 2\pi\sigma\sqrt{\mathfrak{M}(r)} \tag{2.173}$$

and its derivative with respect to the proper radius r_p (measured from the axis at lower r if $\Lambda > 0$) as given by (1.4) is

$$\frac{\mathrm{d}\mathcal{C}}{\mathrm{d}r_p} = \pi\sigma\mathfrak{M}'(r)\,. \tag{2.174}$$

If the axis is regular and the condition (2.141) holds for it, the derivative's limit becomes the expected 2π. For $\Lambda < 0$, we have $\mathrm{d}\mathcal{C}/\mathrm{d}r_p \to \infty$ in the asymptotic region. Recall that for the original Bonnor–Melvin solution discussed in Sec. 1.3.3 the derivative vanishes in that limit.

Note that the trace of $\mathbf{K}$,

$$K = \epsilon\left(\frac{2\sqrt{\mathfrak{M}(r)}}{r} + \frac{1}{2}\frac{\mathfrak{M}'(r)}{\sqrt{\mathfrak{M}(r)}}\right), \tag{2.175}$$

diverges to positive infinity as we approach the axes, $\lim_{\mathfrak{M}(r)\to 0^+} K = +\infty$, as expected. For the axis at lower r, the normal must must be oriented towards greater values of r (i.e., $\epsilon = +1$) and we have $\mathfrak{M}' > 0$. For spacetimes with $\Lambda > 0$, the second axis has $\mathfrak{M}' < 0$ and the normal field must be oriented in the opposite direction, $\epsilon = -1$, so the two minus signs cancel out.

As in the homogeneous case, a shell between two variants of this spacetime (albeit with different parameters) has $S_{TT} = -S_{ZZ}$ for all possible arrangements of the spacetimes with respect to the hypersurface, which is undesirable for our

purposes. Note that, interestingly, this time $S_{\Phi\Phi} \neq 0$. The same is also true for shells connecting the solution to the corresponding homogeneous solution and the Minkowski and the Bonnor–Melvin spacetimes. On the hand, it is possible to find interpretable shells for both signs of Λ connecting the region containing the axis at lower r to the asymptotic region of the Levi–Civita solution with interpretable values of its parameter σ, see Fig. 2.7 for illustration. Note that for $\sigma < 0$ in the Levi–Civita spacetime, we also found interpretable shells on the interface of the outer region (i.e., greater r) of the axial solution for either sign of Λ and the region containing the singular axis in the Levi–Civita solution.

The above-mentioned paper Lim [2021] examines in great detail shells on the interface of the axial inhomogeneous solution with $\Lambda < 0$ and the anti-de Sitter spacetime in arbitrary dimension $D \geq 4$. Instead of our four-stream interpretation of the shells, the cited paper considers shells containing a charged scalar field. Furthermore, in Veselý and Žofka [2019b] we considered shells leading to the Linet–Tian spacetime, which generalizes the Levi–Civita solution to include the cosmological constant. We found out that it is possible to have a shell made of four particle streams that connects the asymptotic part of the Linet–Tian spacetime to the part of the examined solution with the axis at a lower value of r, while considering the same value of Λ of either sign in both connected spacetimes.

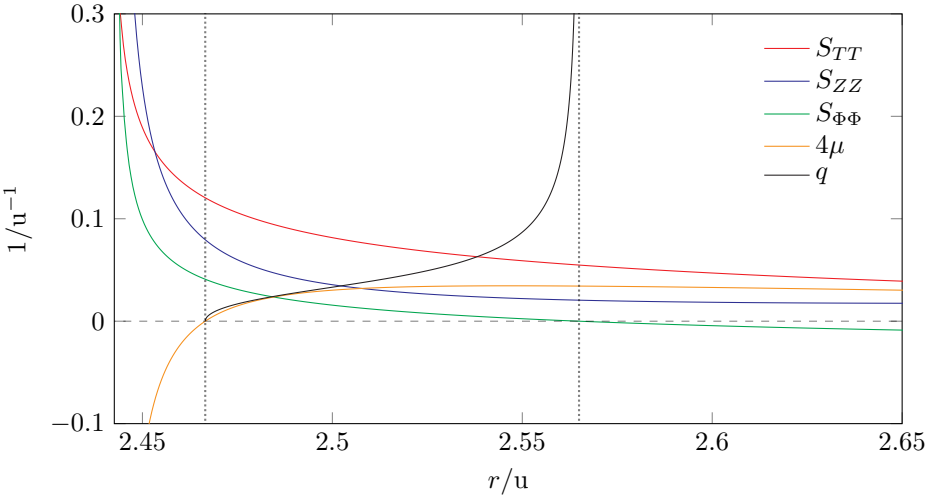

(a) The axial inhomogeneous solution with $\Lambda = 0.2\,\mathrm{u}^{-2}$, $\beta = 7.5\,\mathrm{u}$, $\alpha = 24\,\mathrm{u}$, and $\sigma = 0.7\,\mathrm{u}$. The two axes are located at $r \approx 2.44\,\mathrm{u}$ and $r \approx 6.04\,\mathrm{u}$.

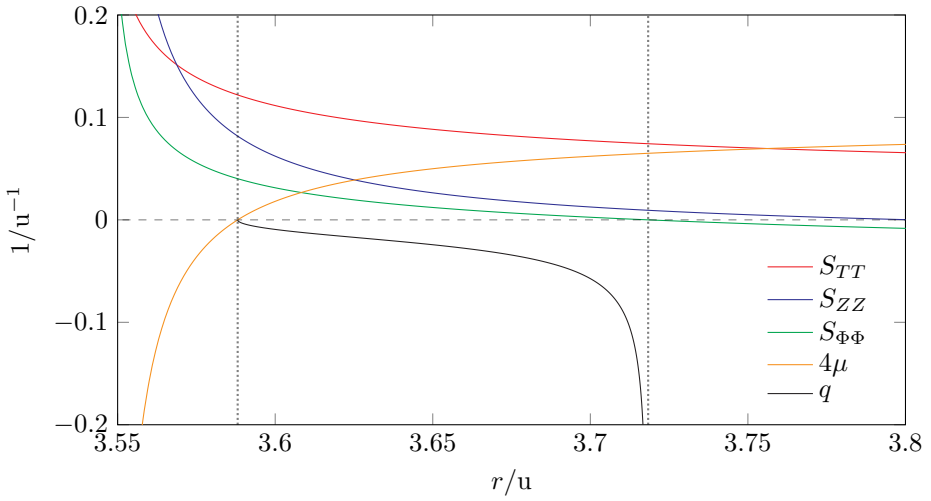

(b) The axial inhomogeneous solution with $\Lambda = -1.2\,\mathrm{u}^{-2}$, $\beta = -8\,\mathrm{u}$, $\alpha = 0.2\,\mathrm{u}$, and $\sigma = 0.4\,\mathrm{u}$. The axis is located at $r \approx 3.55\,\mathrm{u}$.

Figure 2.7: The properties of two shells on the interface of the axial inhomogeneous solution and the Levi–Civita solution (in both cases with $\sigma = 0.2$, $C = 1\,\mathrm{u}$), expressed as functions of the radial coordinate of the shell in the axial spacetime. The spacetimes are aligned in such a way that the region with lower r in the magnetic solution and the asymptotic region of LC are preserved. The expression for the induced three-current on the shell is the same in both cases and has only one non-zero element, $s_\Phi = \beta/4\pi r^2$, which allows us to use (1.60) to compute particle charge q in the region admitting the four-stream interpretation of the shell, which is located between the two dotted lines.

2.4 Radial Bonnor–Melvin

While trying to recover the original Bonnor–Melvin solution from our equations, we stumbled across its variant with a radial magnetic field. Due to its similarity to the forefather spacetime, this is the only solution we decided to examine in this work despite the fact that it is bereft of the cosmological constant. In Veselý and Žofka [2021] we presented two forms of the metric,

$$\mathrm{d}s^2 = -\frac{\mathrm{d}t^2}{1-\alpha^2 r^2} + \mathrm{d}r^2 + \left(1-\alpha^2 r^2\right)\left[\mathrm{e}^{-2\arcsin\alpha r}\,\mathrm{d}z^2 + \sigma^2\mathrm{e}^{2\arcsin\alpha r}\,\mathrm{d}\phi^2\right] \tag{2.176}$$

and

$$\mathrm{d}s^2 = -\frac{\mathrm{d}t^2}{\cos^2\alpha\rho} + \cos^2\alpha\rho\left[\mathrm{d}\rho^2 + \mathrm{e}^{-2\alpha\rho}\,\mathrm{d}z^2 + \sigma^2\mathrm{e}^{2\alpha\rho}\,\mathrm{d}\phi^2\right], \tag{2.177}$$

with the transformation $1-\alpha^2 r^2 = \cos^2\alpha\rho$ connecting the two forms. The expression for the magnetic field is the same in both cases,

$$\mathbf{F} = \alpha\sigma\,\mathrm{d}z\wedge\mathrm{d}\phi\,. \tag{2.178}$$

Unlike in the paper we add the parameter σ [u] here to ensure that ϕ is dimensionless, while the other coordinates have the dimension of length. Apart from σ, the sign of which also determines the orientation of the magnetic field, there is another free parameter α [u^{-1}]. The radial coordinate is bounded, $\alpha r\in(-1,1)$ for (2.176), or $\alpha\rho\in(-\pi/2,\pi/2)$ for (2.177). Not only do the endpoints represent axes, as the proper circumference of circles around them vanishes there, but also the proper length in the z direction vanishes there, so they are pointlike. Using the latter form of the metric from now on, the invariant of the magnetic field is

$$F_{\mu\nu}F^{\mu\nu} = \frac{2\,\alpha^2}{\cos^4\alpha\rho}\,, \tag{2.179}$$

while the Kretschmann scalar is

$$R_{\alpha\beta\gamma\delta}R^{\alpha\beta\gamma\delta} = \frac{8\alpha^4}{\cos^8\alpha\rho}\left(4\cos^4\alpha\rho - 10\cos^2\alpha\rho + 7\right). \tag{2.180}$$

Hence, the axes are singular in this spacetime, as the scalars diverge there, and can be considered two opposite magnetic monopoles giving rise to the magnetic field. The axes are in finite proper radial distance from any point in the spacetime. The electric field dual to (2.178) is $\star\mathbf{F} = \alpha\cos^{-2}(\alpha\rho)\,\mathrm{d}t\wedge\mathrm{d}\rho$.

The spacetime is almost everywhere algebraically general, i.e., type I. At the hypersurface $r=0=\rho$ the solution is type O, and it is type D at $\alpha r=\pm1/\sqrt{10}$ or, equivalently, $\alpha\rho=\pm\arctan(1/3)$. It admits only the three Killing vector fields corresponding to the translational symmetries of the metric, which corresponds to the $E(1)\times E(1)\times E(1)$ group of isometries. The boost symmetry in the z direction, which is present in the original Bonnor–Melvin spacetime, is lost. Furthermore, the metric is invariant under the exchange $z\leftrightarrow\phi$ as long as we rescale ϕ and z so that σ ends up back in the transformed $g_{\phi\phi}$ if we simultaneously also take either $\rho\to-\rho$, or $\alpha\to-\alpha$. The former choice changes the sign of $\mathbf{F}$, as does considering $\alpha\to-\alpha$ & $\rho\to-\rho$, which leaves the metric intact as well.

To determine whether the spacetime belongs to the Kundt class like the previous two, we have to consider the four-velocity of the general null geodesic

$$\mathbf{k} = E\cos^2(\alpha\rho)\,\partial_t \pm \sqrt{E^2 - \cos^{-4}(\alpha\rho)\,(\sigma^{-2}\mathrm{e}^{-2\alpha\rho}L^2 + \mathrm{e}^{2\alpha\rho}Z^2)}\,\partial_\rho \\ + Z\mathrm{e}^{2\alpha\rho}\cos^{-2}(\alpha\rho)\,\partial_z + L\sigma^{-2}\mathrm{e}^{-2\alpha\rho}\cos^{-2}(\alpha\rho)\,\partial_\phi\,, \quad (2.181)$$

which we can obtain from the effective potential V (2.186), which we shall discuss momentarily. The geodesic is parametrized by three constants of motion E, Z, and L. The auxiliary null field $\mathbf{N}$ as required by the algorithm from Poisson [2004] may be derived from $\mathbf{k}$ be choosing the opposite sign of k^ρ and normalizing the field such that $\mathbf{k}\cdot\mathbf{N} = -1$, which generally prevents $\mathbf{N}$ from being geodesic anymore despite its relatedness to $\mathbf{k}$. As it turns out, it is not possible to fix the constants of motion in such a way that expansion and shear vanish, even though twist is zero for any null geodesic. Perhaps the simplest results can be obtained for radial geodesics with $Z = L = 0$, when the expansion scalar yields $\mp 2\alpha E\tan\alpha\rho$ and the shear tensor is $\mp\alpha E\cos^2\alpha\rho\,(\mathrm{e}^{-2\alpha\rho}\mathrm{d}z^2 - \sigma^2\mathrm{e}^{2\alpha\rho}\mathrm{d}\phi^2)$ for the two possible signs in $\mathbf{k}$. Note that it is not possible to consider $E = 0$ as then $\dot{t} = 0$. Therefore, the solution does not belong to the Kundt class.

If we set $\alpha = 0$ and rescale ϕ to dispose of σ, we obtain the flat Minkowski spacetime. Interestingly, its metric is then expressed in the standard Cartesian coordinates instead of the cylindrical ones we used in Sec. 1.3.1.

Note that it is not possible to ensure elementary flatness near the singular axes, as the fraction in (1.2) for $\boldsymbol{\eta} = \partial_\phi$ becomes

$$\frac{g^{\mu\nu}\,(\eta^2)_{,\mu}\,(\eta^2)_{,\nu}}{4\eta^2} = \alpha^2\sigma^2\mathrm{e}^{2\alpha\rho}(1-\tan\alpha\rho)^2, \quad (2.182)$$

which diverges at both axes.

The form of the metric (2.177) is clearly a special case of (3.16) from Bronnikov et al. [2020], but the solution's properties were not studied extensively there. Note that a related metric with similar properties is derived in Richterek et al. [2000], but we have not been able to find a transformation relating our (2.177) and their (27), so we assume that our metric is not a special case of theirs despite the similarities.

Conformal diagram

Although the causal structure of this spacetime is not particularly exciting, in Veselý and Žofka [2021] we presented the Penrose conformal diagram of the solution. The relevant part of the metric (2.177) already has the correct form in compliance with (1.66), with $f(\rho) = 1/\cos^2\alpha\rho$. Omitting the constant of integration, the tortoise coordinate defined by (1.67) is

$$r^* = \frac{\rho}{2} + \frac{\sin 2\alpha\rho}{4\alpha}\,. \quad (2.183)$$

Unfortunately, the relation is not invertible, so we cannot obtain $\rho(r^*)$ to get the transformed metric. That, however, does not hinder our ability to produce the Penrose diagram, as we can still follow the transformations in Sec. 1.2.3 to obtain

ξ and ψ as functions of t and ρ,

$$\psi(t,\rho) = \arctan\left(t + \frac{\rho}{2} + \frac{\sin 2\alpha\rho}{4\alpha}\right) + \arctan\left(t - \frac{\rho}{2} - \frac{\sin 2\alpha\rho}{4\alpha}\right), \tag{2.184}$$

$$\xi(t,\rho) = \arctan\left(t + \frac{\rho}{2} + \frac{\sin 2\alpha\rho}{4\alpha}\right) - \arctan\left(t - \frac{\rho}{2} - \frac{\sin 2\alpha\rho}{4\alpha}\right). \tag{2.185}$$

In the diagram in Fig. 2.8 we plot the lines of constant coordinates t or ρ.

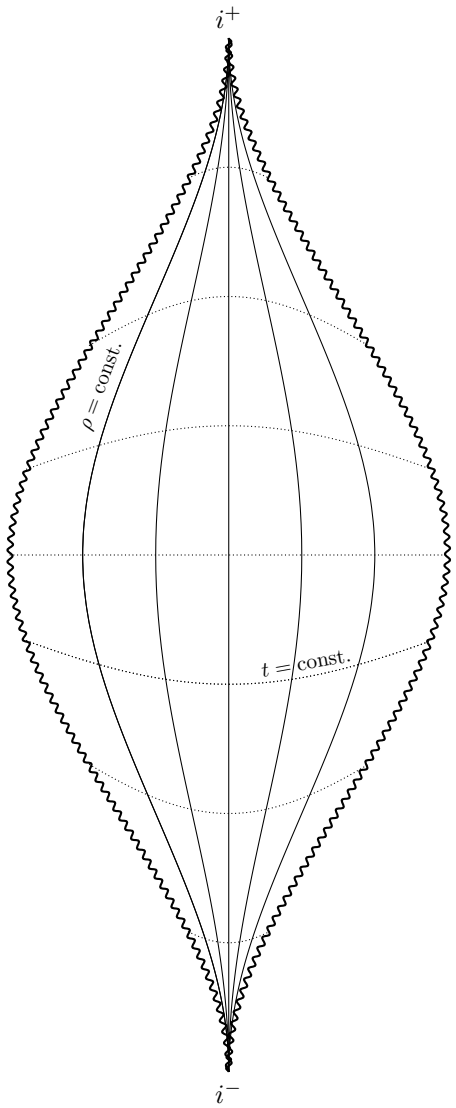

Figure 2.8: The conformal diagram of the non-cosmological spacetime with a radial magnetic field. Apart from the two singularities, which are indicated by wavy lines, each point in the diagram represents a cylindrical surface. Lines of constant coordinate ρ are solid and lines of constant t are dotted.

Particle motion

As explained in Sec. 1.2.1, establishing an electromagnetic four-potential, such as $\mathbf{A} = \alpha\sigma z\,\mathrm{d}\phi$ in accordance with (1.19), necessarily leads to the loss of one constant of motion for spacetimes with a radial magnetic field. This means that the method of the effective potential V (1.10) for radial motion is viable only for uncharged particles in this case, i.e., $\kappa = 0$. Using the radial coordinate ρ, the effective potential satisfying $\dot{\rho}^2/2 = -V$ is

$$V(\rho) = \frac{1}{2}\left(-\frac{\delta}{\cos^2\alpha\rho} - E^2 + \frac{1}{\cos^4\alpha\rho}\left(\sigma^{-2}\mathrm{e}^{-2\alpha\rho}L^2 + \mathrm{e}^{2\alpha\rho}Z^2\right)\right) \tag{2.186}$$

and its separated counterpart is

$$W^2(\rho) = E^2 + 2V = -\frac{\delta}{\cos^2\alpha\rho} + \frac{1}{\cos^4\alpha\rho}\left(\sigma^{-2}\mathrm{e}^{-2\alpha\rho}L^2 + \mathrm{e}^{2\alpha\rho}Z^2\right), \tag{2.187}$$

with the constants of motion

$$E = \dot{t}\,\cos^{-2}\alpha\rho\,, \tag{2.188}$$

$$L = \dot{\phi}\,\sigma^2\mathrm{e}^{2\alpha\rho}\cos^2\alpha\rho\,, \tag{2.189}$$

$$Z = \dot{z}\,\mathrm{e}^{-2\alpha\rho}\cos^2\alpha\rho\,. \tag{2.190}$$

Due to the presence of the cosines in the potentials, the only particles capable of reaching the singularities at $\alpha\rho = \pm\pi/2$ are purely radially moving photons with $\delta = Z = L = 0$, because otherwise the potentials diverge as they approach the singularities. A test particle's inability to reach a naked singularity geodesically appears to be a manifestation of the phenomenon referred to as repulsive gravity, which has been studied in works such as Pugliese et al. [2011, 2013], Luongo and Quevedo [2014], and Boshkayev et al. [2016], as well as having been observed in the Kerr–Newman–(anti-)de Sitter solution in our own Veselý and Žofka [2018] and Veselý and Žofka [2019a]. Timelike radial massive geodesics oscillate around $\rho = 0$ symmetrically.

For $Z = 0$, we can set V and its derivative equal to zero to obtain conditions on stationary circular orbits. For uncharged massive particles with $\delta = -1$, the remaining two constants of motion then read

$$E^2\Big|_{\mathrm{orbit}} = \frac{\cos\alpha\rho - \sin\alpha\rho}{\cos^2\alpha\rho\,(\cos\alpha\rho - 2\sin\alpha\rho)}\,, \tag{2.191}$$

$$L^2\Big|_{\mathrm{orbit}} = \frac{\sigma^2 e^{2\alpha\rho}\cos^2\alpha\rho\ \sin\alpha\rho}{\cos\alpha\rho - 2\sin\alpha\rho}\,. \tag{2.192}$$

Both of these values must be simultaneously positive in order to represent a valid orbiting particle, because negative squares lead to imaginary velocities and vanishing constants of motion mean the particle does not move in the corresponding direction. As Fig. 2.9 shows, the range of admissible radii is $\alpha\rho \in (0, \arctan 1/2)$. From the chart we can also see that the orbits are stable, because the second derivative of the potential

$$V''(\rho)\Big|_{\mathrm{orbit}} = \frac{\alpha^2\,(6\cos^3\alpha\rho - 2\cos^2\alpha\rho\,\sin\alpha\rho - 5\cos\alpha\rho + 4\sin\alpha\rho)}{\cos^4\alpha\rho\,(\cos\alpha\rho - 2\sin\alpha\rho)} \tag{2.193}$$

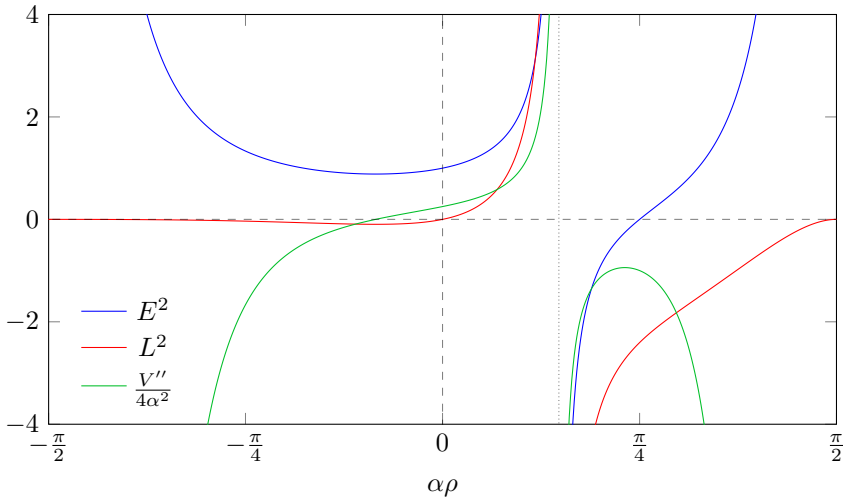

Figure 2.9: The values of E^2, L^2, and rescaled V'' for a hypothetical orbiting massive uncharged test particle at a given radius for the metric (2.177) with $\sigma = 1\,\mathrm{u}$. The admissible range of radii is $\alpha\rho \in (0, \arctan 1/2)$. The right bound is indicated by the dotted line.

is positive in the allowed range.

At $\rho = 0$, an orbiting particle's angular velocity vanishes as $L = 0$, which means that a massive particle can remain static there[11]. Take note that, somewhat counter intuitively, $\rho = 0$ is a cylindrical surface with the proper circumference $2\pi\sigma$. From the inspection of the potential, both uncharged massive particles and photons can move along a spiral instead of a closed orbit at $\rho = 0$ as long as $Z = \pm L/\sigma$, i.e., $\dot{z} = \pm\sigma\dot{\phi}$, because $V'(\rho = 0) = \alpha(Z^2 - \sigma^{-2}L^2)$. From $V(\rho = 0)$ we can see that $E^2 = Z^2 + \sigma^{-2}L^2 - \delta > 0$. As $V''(\rho = 0) = \alpha^2(4Z^2 + 4\sigma^{-2}L^2 - \delta) > 0$, the discussed special cases are stable under perturbations in the radial direction.

There can be no massive geodesic orbits at $\alpha\rho_0 = \arctan 1/2$, because both E and L disappear from the non-zero first derivative of V there, $V'(\rho_0) = -5\alpha\delta/8$ if $Z = 0$. However, it turns out that this is the only allowed radius of photon orbits, which can be seen by expressing Ω^2 from the normalization equation (1.6) and the only non-trivial equation of motion for photons (1.29) and comparing the results. The resulting angular velocity is

$$\Omega = \pm\frac{5}{4\sigma}\exp\left(-\arctan\frac{1}{2}\right). \tag{2.194}$$

The second derivative of the potential shows that photon orbits are stable too,

$$V''|_{\text{photon orbit}} = \frac{125}{32}\alpha^2\sigma^{-2}L^2\exp\left(-2\arctan\frac{1}{2}\right) > 0\,. \tag{2.195}$$

The Hamilton–Jacobi equation (1.20) with the separated ansatz (1.24) unfortunately does not provide an alternative for the effective potential for charged particles, because it is not separable in this case,

$$\Big(R'(\rho)\Big)^2 - \delta\cos^2\alpha\rho - E^2\cos^4\alpha\rho + \mathrm{e}^{2\alpha\rho}\Big(Z'(z)\Big)^2 + \mathrm{e}^{-2\alpha\rho}\left(\alpha\kappa z - \frac{L}{\sigma}\right)^2 = 0\,. \tag{2.196}$$

[11] This even applies for charged particles, as can be seen from the full equations of motion.

As there are no other Killing vectors than the three translational ones, which correspond to the cyclic coordinates in the uncharged Lagrangian, there are no other constants of motion linear in the four-velocity to be found with the procedure exploiting the Killing vectors. Similarly, we have not found any other Killing tensors of rank two but the six symmetrized tensor products of the three Killing vectors and the metric.

While we cannot use the effective potential to describe charged particle motion, we can still work with the full equations of motion (1.29). The first thing to note is that charged particles cannot achieve stationary circular orbits, as for $\rho = \text{const.}$ one of the equations of motion reads

$$\ddot{z} = \kappa\alpha\sigma \cos^{-2}(\alpha\rho)\, \mathrm{e}^{2\alpha\rho}\, \dot{\phi}\,, \tag{2.197}$$

which means that azimuthal motion forces an acceleration in the z direction. Perhaps more interesting, however, is an observation made during numerical experiments with the system: it appears that charged test particles may undergo chaotic motion for certain initial conditions, which can be expected as the charged system does not contain enough constants of motion to be integrable. In Fig. 2.12 at the very end of this section we present Poincaré sections of several charged particle trajectories with similar initial conditions, depicting intersections of the trajectories with a given plane. For a certain range of initial radial positions, the sections fill up a non-zero area, which is symptomatic of deterministic chaos as noted in, e.g., Schuster and Just [2005] and Moon [2008]. While chaotic motion is suspected in these cases, confirming it would require analysis beyond the scope of this work. Note the different scales of the individual sections; the trajectories suspected of deterministic chaos tend to encompass far greater portion of the available radial space.

Shell sources

Using the second form of the metric (2.177), for a cylindrical shell we obtain the extrinsic curvature tensor (1.41)

$$\mathbf{K} = -\frac{\epsilon\alpha}{\cos^2\alpha\rho}\Big(\sin\alpha\rho\ \mathrm{d}T^2 + (\sin\alpha\rho + \cos\alpha\rho)\ \mathrm{d}Z^2 + (\sin\alpha\rho - \cos\alpha\rho)\ \mathrm{d}\Phi^2\Big)\,, \tag{2.198}$$

while the projection of the electromagnetic tensor $\mathbf{F}_\perp$ (1.44) vanishes as in all spacetimes with a radial magnetic field. Therefore, we can consider only $\sigma > 0$ in the following, as the sign of σ only determines the direction of the now-irrelevant magnetic field. The proper circumference (1.3) of the hypersurface is

$$\mathcal{C} = 2\pi\sigma\, \mathrm{e}^{\alpha\rho} \cos\alpha\rho\,. \tag{2.199}$$

Note that the circumference vanishes at both singularities. The maximal circumference $\sqrt{2}\pi\sigma\mathrm{e}^{\pi/4} \approx 9.74\sigma$ is achieved at $\alpha\rho = \pi/4$, and the function is monotonic on either side of the maximum, see Fig. 2.10 for illustration. This means that generally two different radial coordinates correspond to a single value of $\mathcal{C}$. The situation is quite similar to the original Bonnor–Melvin solution, as can be seen by comparing the chart to Fig. 1.1 of Sec. 1.3.3.

Note that the quantities above are symmetric in such a way that reversing the normal by considering $\epsilon \to -\epsilon$ yields the original results if we also consider

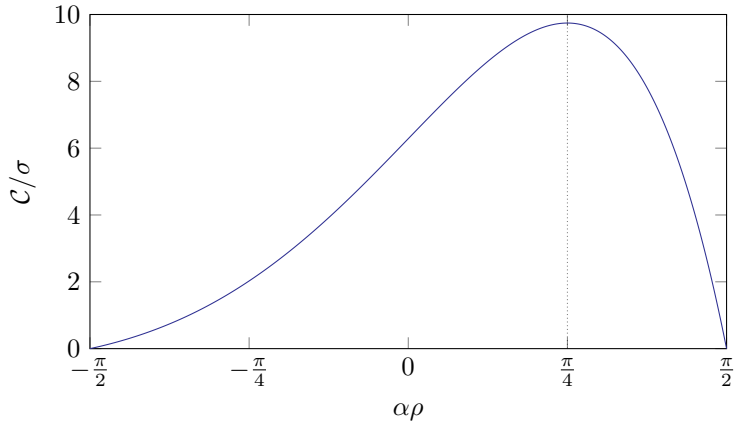

Figure 2.10: The circumference of shells at a given radial coordinate in the radial Bonnor–Melvin spacetime. The maximal value is achieved at $\alpha\rho = \pi/4$.

$\alpha \to -\alpha$ and $\rho \to -\rho$ at the same time. Therefore, in our numerical experiments we can focus on a single direction of the normal if we examine the entire interval of ρ while simultaneously considering both signs of α.

The derivative of $\mathcal{C}$ with respect to the proper radius r_p measured from the axis at lower ρ is given by (1.4),

$$\frac{\mathrm{d}\mathcal{C}}{\mathrm{d}r_p} = 2\pi\alpha\sigma \mathrm{e}^{\alpha\rho}\left(1 - \tan\alpha\rho\right). \tag{2.200}$$

It diverges at the two singular axes.

The trace of $\mathbf{K}$ is

$$K = -\frac{\epsilon\alpha \sin\alpha\rho}{\cos^2\alpha\rho}. \tag{2.201}$$

To see its behavior at the singular axes, for both of them we need to consider $\epsilon = -\mathrm{sgn}(\rho)$ so that the normal field of the hypersurface points towards the other axis. The coordinates of the axes can be written as $\rho = \mathrm{sgn}(\rho)\,\pi/(2\,|\alpha|)$. Plugging both of these into the numerator, we get $-\epsilon\alpha \sin\alpha\rho = |\alpha|$, so K once again diverges to positive infinity as we approach either of the two axes.

Unlike the previous two spacetimes, this one admits an interpretable shell on the interface of two instances of this solution. This particular case is rather unusual, as we have

$$S_{ZZ} = -S_{\Phi\Phi} = \frac{1}{8\pi}\,\frac{\epsilon_+\alpha_+\cos(\alpha_-\rho_-) - \epsilon_-\alpha_-\cos(\alpha_+\rho_+)}{\cos(\alpha_-\rho_-)\cos(\alpha_+\rho_+)}. \tag{2.202}$$

Previously, we had $S_{TT} = -S_{ZZ}$, which defied our preferred interpretation of the shell, as S_{TT} has to be positive and S_{ZZ} simultaneously non-negative. However, it is perfectly acceptable to have $S_{ZZ} = S_{\Phi\Phi} = 0$ (the shell is then made of static particles), so we should view (2.202) equal to zero as another condition binding the shell's radii in the two spacetimes, along with $\mathcal{C}_- = \mathcal{C}_+$,

$$\sigma_-\,\mathrm{e}^{\alpha_-\rho_-}\cos\alpha_-\rho_- = \sigma_+\,\mathrm{e}^{\alpha_+\rho_+}\cos\alpha_+\rho_+\,. \tag{2.203}$$

This means that for a given configuration of the two connected spacetimes both radii are fixed. Even though (2.203) is a transcendental equation, we can express

one of the cosines from (2.202) after setting the relation to zero, insert it into (2.203) and divide the equation by the other cosine (recall that the cosines vanish only in the singularities). We can then effortlessly express one of the radii, e.g.,

$$\alpha_-\rho_- = \alpha_+\rho_+ + \ln\left(\frac{\epsilon_+\sigma_+\alpha_+}{\epsilon_-\sigma_-\alpha_-}\right), \tag{2.204}$$

and use the other equation to obtain the other radius,

$$\alpha_+\rho_+ = \arctan\left(\frac{-\frac{\epsilon_-\alpha_-}{\epsilon_+\alpha_+} + \cos\ln\frac{\epsilon_+\sigma_+\alpha_+}{\epsilon_-\sigma_-\alpha_-}}{\sin\ln\frac{\epsilon_+\sigma_+\alpha_+}{\epsilon_-\sigma_-\alpha_-}}\right). \tag{2.205}$$

Now, we need to check whether

$$S_{TT} = 4\mu = \frac{1}{4\pi}\,\frac{\epsilon_+\alpha_+\sin(\alpha_+\rho_+)\cos^2(\alpha_-\rho_-) - \epsilon_-\alpha_-\sin(\alpha_-\rho_-)\cos^2(\alpha_+\rho_+)}{\cos^2(\alpha_-\rho_-)\cos^2(\alpha_+\rho_+)} \tag{2.206}$$

is positive. Note that due to the aforementioned symmetry of the spacetime, all we have to do is find an interpretable shell for one configuration, and we can get the remaining configurations by switching the appropriate signs if we do not care for the particular values of the parameters. Considering $\epsilon_- = \epsilon_+ = +1$ (i.e., we keep the region with lower ρ in the minus spacetime and the region with higher ρ in the plus spacetime), we can have, e.g.,

$$\left.\begin{array}{ll}\sigma_- = 1\,\mathrm{u}\,, & \alpha_- = 5/\mathrm{u}\\ \sigma_+ = 1\,\mathrm{u}\,, & \alpha_+ = 4/\mathrm{u}\end{array}\right\} S_{TT} \approx 0.228/\mathrm{u}\,, \tag{2.207}$$

while exchanging $\alpha_- \leftrightarrow \alpha_+$ yields the opposite value $S_{TT} \approx -0.228/\mathrm{u}$. This means that there are both interpretable and non-interpretable shells for each variant of the connection of the two spacetimes. The particle streams on the shell are uncharged.

A particularly appealing configuration would be that of the hypersurface connecting two instances of the same spacetime (i.e., with the same parameters α and σ) in such a way that the spacetime could be pictured as existing between two coaxial shells, which would eliminate both singularities. It is possible to conceive such a model due to the fact that there generally are two radial coordinates corresponding to the same circumference as seen in Fig. 2.10. In this case, the orientation of the normals must be the same regardless of the actual sign, $\epsilon_- = \epsilon_+ \equiv \epsilon$. Substituting from (2.203) into (2.202), we get

$$S_{ZZ} = -S_{\Phi\Phi} = \frac{\epsilon\alpha}{8\pi}\,\frac{1 - \mathrm{e}^{\alpha(\rho_- - \rho_+)}}{\cos\alpha\rho_+}\,, \tag{2.208}$$

which vanishes if and only if $\rho_- = \rho_+$, prohibiting two different coordinate radii of the shell and forcing us to abandon this convenient model.

Next, we do not need to look for shell sources in the Levi–Civita spacetime, as the simpler Minkowski spacetime suffices this time. The coordinate radius in the Minkowski solution is $\sigma\,\mathrm{e}^{\alpha\rho}\cos\alpha\rho$ when using the standard cylindrical coordinates. Keeping the region with lower ρ in the magnetic solution, we can see from

$$S_{\Phi\Phi} = \frac{1}{8\pi}\,\frac{\alpha}{\cos\alpha\rho} \tag{2.209}$$

that we need to consider $\alpha > 0$. Denoting ϵ the orientation of the normal in the Minkowski spacetime such that $\epsilon = +1$ means that we preserve the asymptotic region, we have

$$S_{ZZ} = \frac{1}{8\pi} \frac{-\alpha\sigma + \epsilon \mathrm{e}^{-\alpha\rho}}{\sigma \cos \alpha\rho} \,. \tag{2.210}$$

Therefore, S_{ZZ} is clearly negative unless $\epsilon = +1$. Depending on the parameters in the metric, the four functions can be positive near the negative axis in the magnetic solution, as illustrated in Fig. 2.11a. Again, the shell is devoid of electrical charge. If we want to keep the region with higher ρ in our magnetic solution, we can exploit the symmetry of the spacetime. For the sake of completeness, note that we have also found an interpretable shell leading to the asymptotic region of the Levi–Civita solution with interpretable σ.

Finally, the spacetime also admits an interpretable shell connecting it to the original Bonnor–Melvin spacetime of Sec. 1.3.3. Keeping the region with the negative axis from our solution, we found an admissible connection to the asymptotic region of the Bonnor–Melvin solution, see the corresponding Fig. 2.11b. Due to the magnetic field in the forefather solution, this particular configuration leads to the non-zero induced electric three-current on shell

$$\mathbf{s} = -\frac{1}{4\pi} \left(1 + \frac{1}{4} B^2 \rho_{BM}^2\right)^{-2} B \, \mathrm{d}\Phi \,, \tag{2.211}$$

from which we can compute particle charge q using (1.60). ρ_{BM} denotes the radial coordinate in the original solution. In Fig. 2.11b, we use the radius below the maximal circumference, which can be expressed in terms of ρ of the examined radial solution as

$$\rho_{BM}(\rho) = \frac{2}{B^2 \sigma \, \mathrm{e}^{\alpha\rho} \cos \alpha\rho} \left(1 - \sqrt{1 - B^2 \sigma^2 \, \mathrm{e}^{2\alpha\rho} \cos^2 \alpha\rho}\right) . \tag{2.212}$$

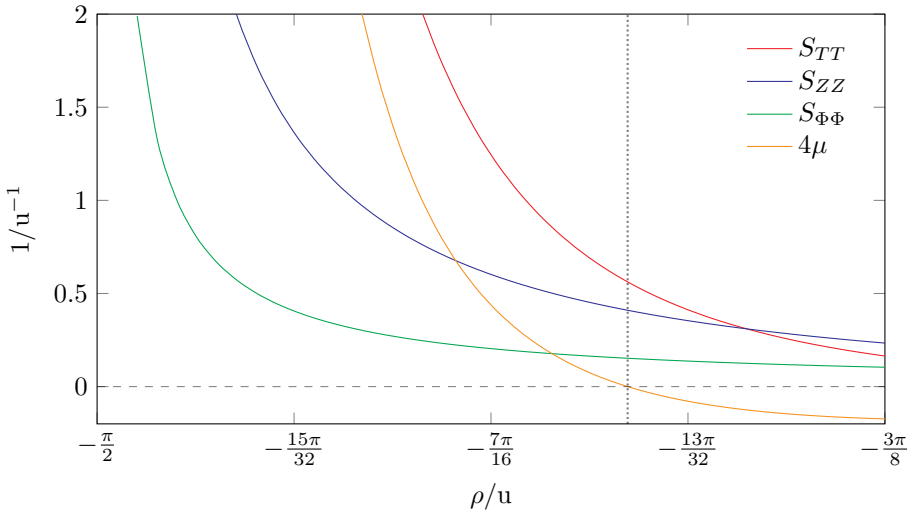

(a) The Minkowski spacetime. The shell is uncharged.

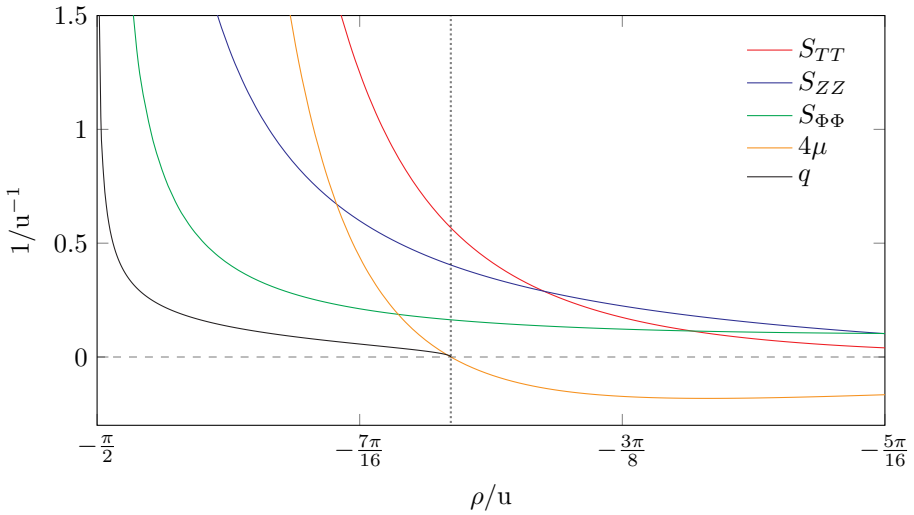

(b) The original Bonnor–Melvin spacetime ($B = -2/\mathrm{u}$).

Figure 2.11: The properties of shells on the interface of the radial Bonnor–Melvin solution (in both cases with $\alpha = 1/\mathrm{u}$, $\sigma = 1\,\mathrm{u}$) and another spacetime, expressed as functions of the radial coordinate of the shell in the former spacetime. The spacetimes are aligned in such a way that the region with lower ρ in the radial Bonnor–Melvin solution and the asymptotic region of the other one are preserved. The region admitting the four-stream interpretation of the shell is located to the left of the dotted line in both cases.

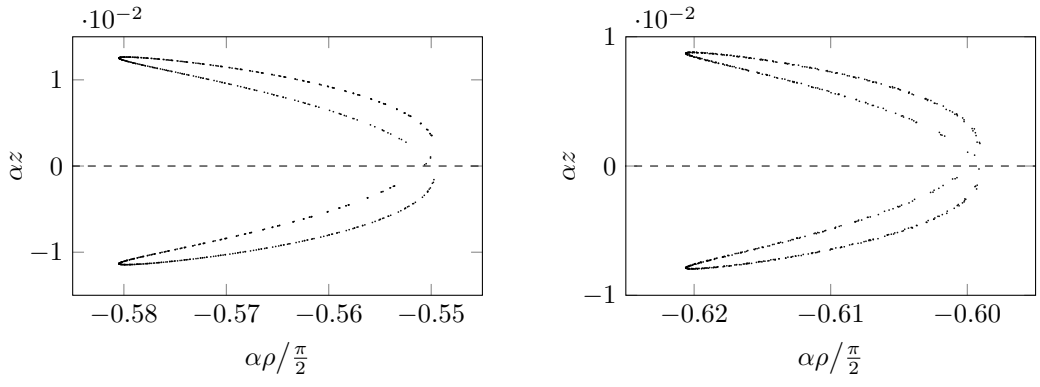

(a) $\xi = -0.55$ (704 points) (b) $\xi = -0.60$ (657 points)

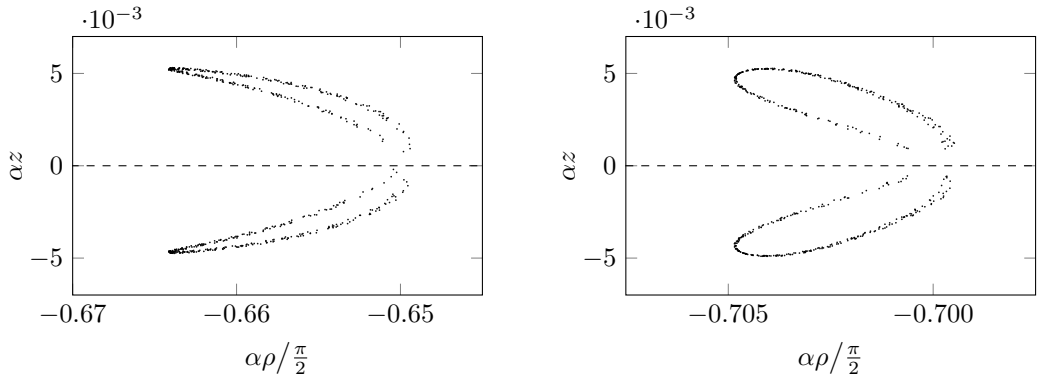

(c) $\xi = -0.65$ (608 points) (d) $\xi = -0.70$ (540 points)

Figure 2.12: Poincaré sections at $\phi = 0$ for charged particle motion in the radial Bonnor–Melvin spacetime with $\alpha = \pi/2\,\mathrm{u}^{-1}$ and $\sigma = 1\,\mathrm{u}$ for various initial radial positions $\alpha\rho = \xi\,\pi/2$ increasingly close to the axis at $\xi = -1$. The initial values of the remaining coordinates are set to zero. The spatial components of the initial four-velocity are fixed at $(\dot{\rho}, \dot{z}, \dot{\phi}) = (0.5, -0.5, 0.04/\mathrm{u})$ and the charge-to-mass ratio of the particles is $\kappa = 5$. The equations of motion have been integrated for the same amount of affine parameter in all cases presented here. For each value of ξ, the number in parenthesis denotes the number of points at which the particle's spatial trajectory intersects the section. The figure is spread over multiple pages.

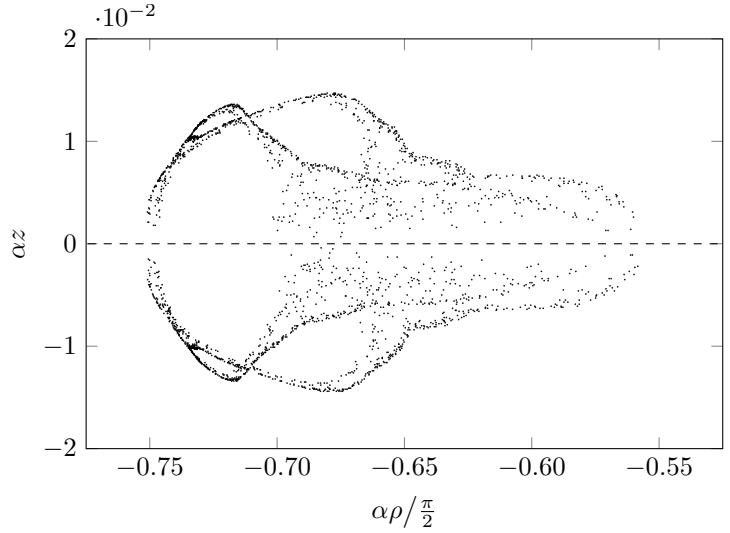

(e) $\xi = -0.75$ (2534 points)

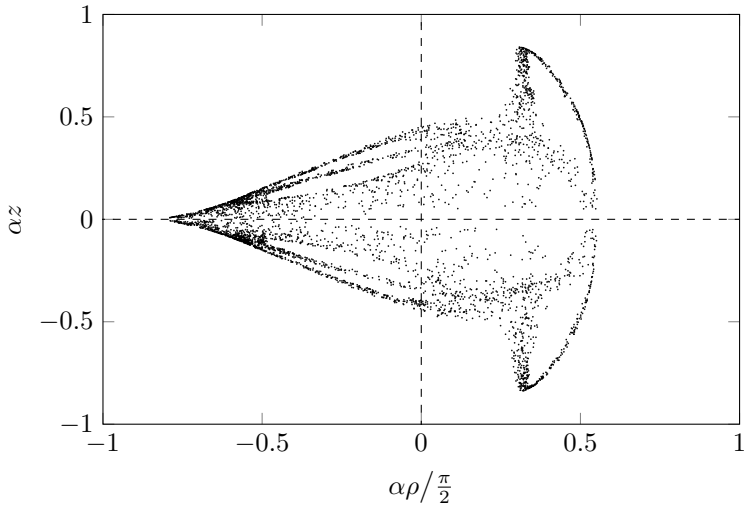

(f) $\xi = -0.80$ (4130 points)

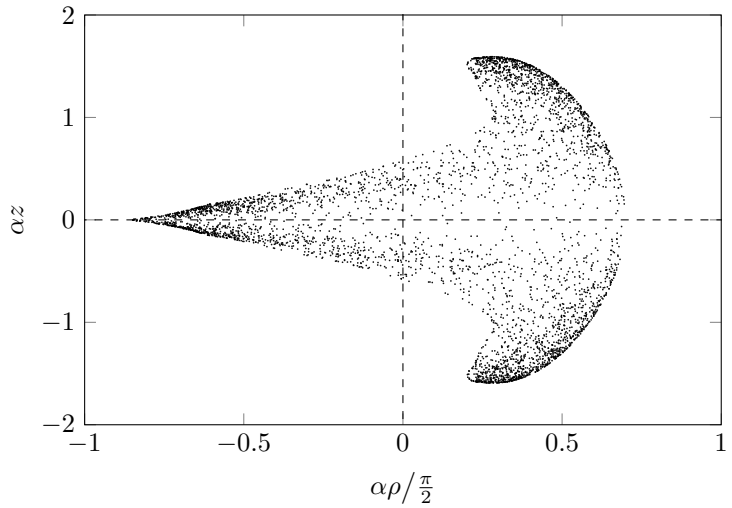

(g) $\xi = -0.85$ (4252 points)

Figure 2.12: Poincaré sections for the radial Bonnor–Melvin spacetime. (cont.)

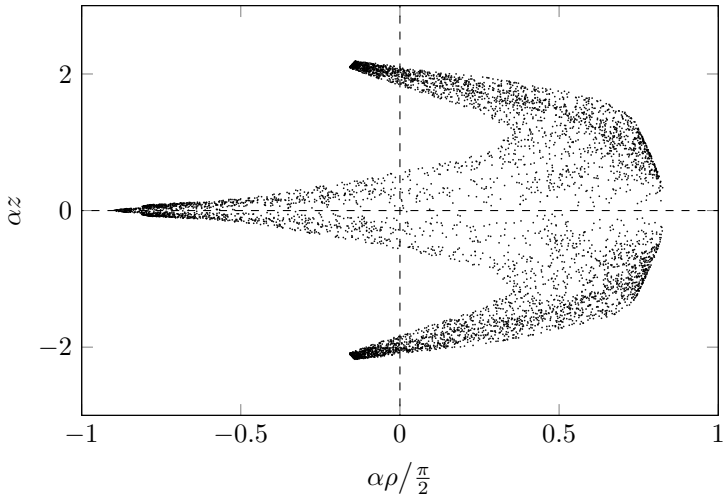

(h) $\xi = -0.90$ (6262 points)

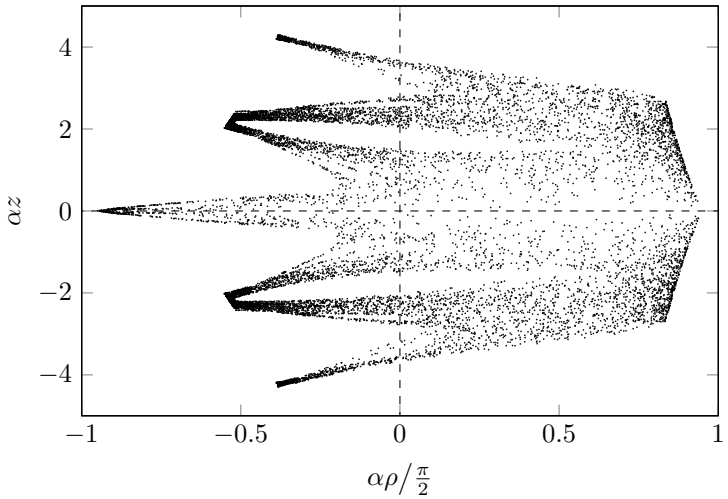

(i) $\xi = -0.95$ (12 602 points)

Figure 2.12: Poincaré sections for the radial Bonnor–Melvin spacetime. (cont.)

2.5 Radial homogeneous spacetime

2.5.1 The hyperbolic-cosine metric

The first of the two cosmological solutions introduced in Veselý and Žofka [2021] was the counterpart to the homogeneous solution of Sec. 2.2 but with a radial magnetic field instead of the axial one. The metric considered in the paper is

$$\mathrm{d}s^2 = -\cosh^2\!\left(\sqrt{-2\Lambda}\,r\right)\mathrm{d}t^2 + \mathrm{d}r^2 + \mathrm{d}z^2 + \sigma^2\mathrm{d}\phi^2, \tag{2.213}$$

where the coordinates t, r and z are of the dimension of length, while ϕ is dimensionless. Apart from the cosmological constant Λ [u^{-2}], which must be negative (unlike in the axial spacetime), there is one additional parameter, σ [u].

The magnetic field is

$$\mathbf{F} = \sigma\sqrt{-\Lambda}\,\mathrm{d}z \wedge \mathrm{d}\phi \tag{2.214}$$

with $\mathbf{A} = \sigma\sqrt{-\Lambda}\,z\,\mathrm{d}\phi$ and the Hodge dual $\star\mathbf{F} = \sqrt{-\Lambda}\cosh\!\left(\sqrt{-2\Lambda}\,r\right)\mathrm{d}t \wedge \mathrm{d}r$. The magnetic field invariant is

$$F_{\mu\nu}F^{\mu\nu} = -2\Lambda\,, \tag{2.215}$$

and the Kretschmann scalar is $16\Lambda^2$. There are no singularities in the spacetime and the coordinates may take any real values except for the cyclic coordinate ϕ. Setting $\Lambda = 0$ yields the Minkowski spacetime. Note that there a reflectional symmetry of the metric functions with respect to $r = 0$, but we cannot consider it an axis proper, because it does not fulfill $g_{\phi\phi} \to 0$ as $g_{\phi\phi}$ is, in fact, constant. This means that the proper circumference of circles at any r is constant as well, including somewhat counter-intuitively also the circumference of the cylinder at $r = 0$ itself.

The solution is everywhere of algebraic type D and it admits six Killing vector fields. There is the usual trinity related to translations, ∂_t, ∂_z, and ∂_ϕ, the field $\sigma^2\phi\,\partial_z - z\,\partial_\phi$ corresponding to rotational symmetry of the spacetime in the z–ϕ plane, and two other fields, $-\sin(\sqrt{-2\Lambda}\,t)\tanh(\sqrt{-2\Lambda}\,r)\,\partial_t + \cos(\sqrt{-2\Lambda}\,t)\,\partial_r$ and $\cos(\sqrt{-2\Lambda}\,t)\tanh(\sqrt{-2\Lambda}\,r)\,\partial_t + \sin(\sqrt{-2\Lambda}\,t)\,\partial_r$, which together with ∂_t correspond to the three Killing vectors of a two-dimensional anti-de Sitter spacetime, as the metric is a direct product of the 2D anti-de Sitter spacetime and a 2D Riemannian metric. As also stated in Griffiths and Podolský [2009], the group of isometries of the family of spacetimes the studied metric belongs to is $SO(2,1) \times E(2)$ and the solution is among the spacetimes studied in Plebański and Hacyan [1979].

The spacetime belongs to the Kundt class, but the two principal null directions we obtained through the algorithm in Griffiths and Podolský [2009], $\cosh^{-1}\left(\sqrt{-2\Lambda}r\right)\partial_t \pm \partial_r$, do not correspond to geodesics. Instead, we have to flash-forward to the effective potential (2.224), which we can use to obtain a general formula for the four-velocity corresponding to a null geodesic. Considering $\dot{r} > 0$, for $E = 1$ and $Z = L = 0$ we obtain $\mathbf{k} = \cosh^{-2}\left(\sqrt{-2\Lambda}r\right)\partial_t + \cosh^{-1}\left(\sqrt{-2\Lambda}r\right)\partial_r$, which actually also yields one of the principal null directions after a non-constant rescaling, which is, however, not obvious to infer beforehand. Next, we select $\mathbf{N} = \left(\partial_t - \cosh\!\left(\sqrt{-2\Lambda}r\right)\partial_r\right)/2$ as the auxiliary null field (not geodesic in this case) with the scalar product $\mathbf{k}\cdot\mathbf{N} = -1$ as required by the algorithm in Poisson

[2004]. We can then see that the null geodesic congruence $\mathbf{k}$ has vanishing optical scalars, proving the solution belongs to the Kundt class.

As noted in Sec. 1.1, with $g_{\phi\phi}$ constant we see that it may not be the best to consider this spacetime to be cylindrically symmetric. The rotational symmetry in the z–ϕ plane, along with the fact that g_{zz} is constant as well, suggest that discarding the periodicity of ϕ and extending it to $\phi \in \mathbb{R}$, thus replacing the considered cylindrical symmetry with a planar one, may be a better way to look at this metric. Furthermore, the subgroup $E(2)$ is also suggestive of the planar interpretation of the coordinates. However, to maintain the theme of the work we shall not do that here and treat ϕ as the angular coordinate as usual.

All things considered, if we discard the periodicity of ϕ, this solution can perhaps be considered to be a generalization of the anti-de Sitter solution for a non-vanishing magnetic field, as the solution is homogeneous and extends into infinity in all spatial directions. The last part is not true about the Bonnor–Melvin–Λ spacetime of Sec. 2.2, as the radial coordinate is bound between the two axes, which is why we refrained from calling that spacetime a generalization of the de Sitter spacetime as the analogy is somewhat weaker. Note, however, that the presence of the homogeneous magnetic field introduces a preferred direction into the spacetime, which means the solution is no longer isotropic.

Conformal diagram

Next, we are going to show the transformations of the radial and time coordinates presented in Sec. 1.2.3, ultimately leading to the construction of the Penrose conformal diagram. None of the transformations affects the expression for $\mathbf{F}$ (2.214). First, the transformation $\cosh^2\!\left(\sqrt{-2\Lambda}r\right) = 1 - 2\Lambda R^2$ brings the metric (2.213) into the form

$$\mathrm{d}s^2 = -\left(1 - 2\Lambda R^2\right)\mathrm{d}t^2 + \frac{\mathrm{d}R^2}{1 - 2\Lambda R^2} + \mathrm{d}z^2 + \sigma^2\mathrm{d}\phi^2, \tag{2.216}$$

as required by (1.66). The tortoise coordinate r^* (1.67) is

$$r^* = \frac{1}{\sqrt{-2\Lambda}}\arctan\!\left(\sqrt{-2\Lambda}\,R\right) = \frac{1}{\sqrt{-2\Lambda}}\arctan\!\left(\sinh\left(\sqrt{-2\Lambda}\,r\right)\right). \tag{2.217}$$

We can invert $r^*(R)$ to obtain the metric

$$\mathrm{d}s^2 = \frac{-\mathrm{d}t^2 + (\mathrm{d}r^*)^2}{\cos^2\!\left(\sqrt{-2\Lambda}\,r^*\right)} + \mathrm{d}z^2 + \sigma^2\mathrm{d}\phi^2. \tag{2.218}$$

The Eddington–Finkelstein coordinates $u = t - r^*$ and $v = t + r^*$ yield

$$\mathrm{d}s^2 = -\frac{\mathrm{d}u\,\mathrm{d}v}{\cos^2\!\left(\sqrt{-\frac{\Lambda}{2}}\,(v-u)\right)} + \mathrm{d}z^2 + \sigma^2\mathrm{d}\phi^2. \tag{2.219}$$

Finally, we perform the transformations (1.72) and (1.73) to get the Penrose coordinates ψ and ξ, leading to the metric

$$\mathrm{d}s^2 = \frac{-\mathrm{d}\psi^2 + \mathrm{d}\xi^2}{(\cos\psi + \cos\xi)^2\cos^2\!\left(\frac{\sqrt{-2\Lambda}\sin\xi}{\cos\psi+\cos\xi}\right)} + \mathrm{d}z^2 + \sigma^2\mathrm{d}\phi^2. \tag{2.220}$$

After inserting $r^*(r)$ from (2.217) into ψ and ξ, we obtain the conformal diagram in Fig. 2.13 by plotting the lines of constant t or r.

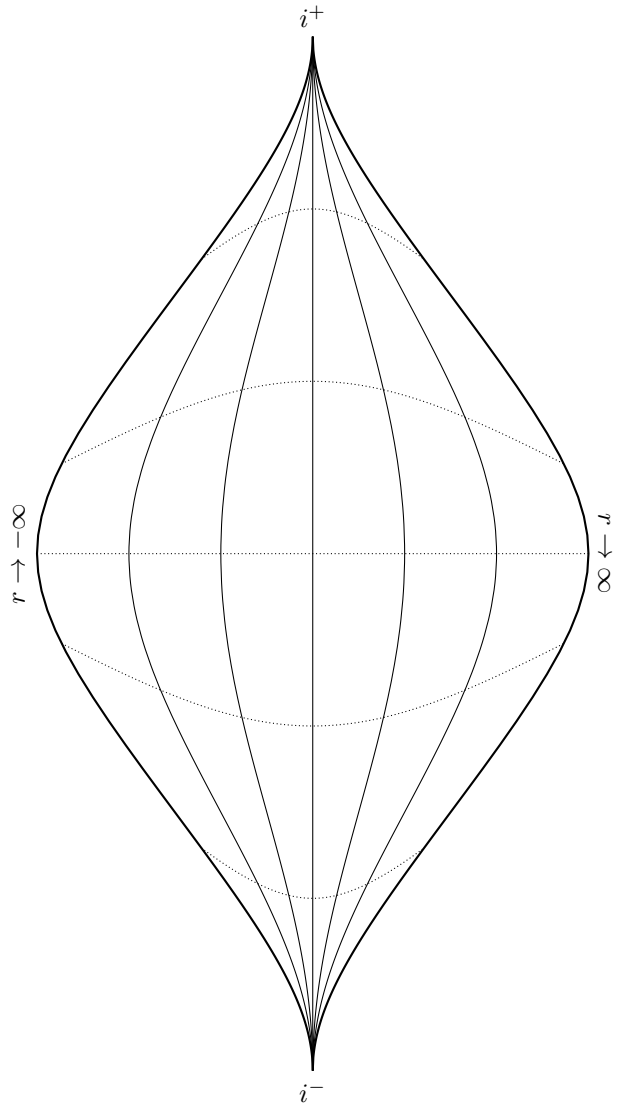

Figure 2.13: The conformal diagram of the hyperbolic-cosine homogeneous cosmological spacetime with a radial magnetic field. Each point in the diagram represents a cylindrical surface. Lines of constant coordinate r are solid and lines of constant t are dotted.

Particle motion

As for the previous spacetime, we have to consider uncharged and charged particle motion separately. The constants of motion for uncharged test particles are

$$E = \dot{t}\,\cosh^2\!\left(\sqrt{-2\Lambda}\,r\right), \tag{2.221}$$

$$L = \dot{\phi}\,\sigma^2, \tag{2.222}$$

$$Z = \dot{z}\,, \tag{2.223}$$

leading to the effective potential

$$V(r) = \frac{1}{2}\left(-\delta - \frac{E^2}{\cosh^2\!\left(\sqrt{-2\Lambda}\,r\right)} + \frac{L^2}{\sigma^2} + Z^2\right), \tag{2.224}$$

which satisfies $\dot{r}^2/2 = -V$, and its separated counterpart

$$W^2(r) = \cosh^2\!\left(\sqrt{-2\Lambda}\,r\right)\left(-\delta + \frac{L^2}{\sigma^2} + Z^2\right), \tag{2.225}$$

which is related to V through (1.12).

The limits of the potentials are straightforward, as the only function appearing in them is the hyperbolic cosine, which satisfies $\cosh(0) = 1$ and it diverges when $r \to \pm\infty$. Because of this, the only negative term in V diminishes when moving away from $r = 0$, and while the limit

$$\lim_{r\to\pm\infty} V(r) = \frac{1}{2}\left(-\delta + \frac{L^2}{\sigma^2} + Z^2\right) \tag{2.226}$$

is finite, it is clearly positive and no particle can ever escape into radial infinity geodesically. Because the potential is monotonic, uncharged test particles oscillate through $r = 0$ in the radial direction.

Regarding circular orbits with $Z = 0$, it is not possible to fix the constants of motion so that the first derivative of (2.224),

$$V'(r) = \frac{\sqrt{-2\Lambda}\,\sinh\left(\sqrt{-2\Lambda}\,r\right)E^2}{\cosh^3\left(\sqrt{-2\Lambda}\,r\right)}\,, \tag{2.227}$$

vanishes for an arbitrary r. However, apart from the limit $r \to \pm\infty$ it does vanish for $r = 0$, and $V(0) = 0$ gives the constraint $E^2 = -\delta + L^2/\sigma^2$ that orbiting particles must satisfy. Specifically for photons, this translates to $\Omega = \pm 1/\sigma$. The second derivative of the potential $V''(0) = -2\Lambda E^2$ is manifestly positive, which means that the orbits are stable.

For charged test particles with $\kappa \neq 0$, the previous method is unusable because z is not a cyclic coordinate anymore, which means that there is no constant of motion corresponding to Z (2.223). However, the Hamilton–Jacobi equation (1.20)

$$\left(R'(r)\right)^2 - \delta - \cosh^{-2}\left(\sqrt{-2\Lambda}r\right)E^2 + \left(Z'(z)\right)^2 + \left(\sqrt{-\Lambda}\kappa z - \frac{L}{\sigma}\right)^2 = 0 \tag{2.228}$$

is separable in this case, with the original E (2.221) and the charged variant of L (2.222),

$$L = \dot{\phi}\,\sigma^2 + \sqrt{-\Lambda}\sigma\kappa z\,. \tag{2.229}$$

Therefore, we can introduce the Carter constant K to obtain the two effective potentials according to (1.25) and (1.26),

$$V_r(r) = -\frac{E^2}{2\cosh^2\left(\sqrt{-2\Lambda}\,r\right)} + K \tag{2.230}$$

and

$$V_z(z) = \frac{1}{2}\left(-\delta + \left(\sqrt{-\Lambda}\kappa z - \frac{L}{\sigma}\right)^2\right) - K\,. \tag{2.231}$$

As $g_{zz} = 1$, the latter potential does not depend on r. The particle's properties must fulfill $-\delta \leq 2K \leq E^2$, otherwise one of the potentials is positive everywhere, which is incompatible with (1.27) or (1.28). Charged test particles oscillate around $r = 0$ in the radial direction and $z_0 = L/(\sigma\sqrt{-\Lambda}\kappa)$ in the z direction. Expressing L from the last relation,

$$L = \sigma\sqrt{-\Lambda}\kappa z_0\,, \tag{2.232}$$

we can replace it in (2.231) to obtain

$$V_z(z) = -\frac{1}{2}\left(\delta + \Lambda\kappa^2\left(z_0 - z\right)^2\right) - K\,, \tag{2.233}$$

and in (2.229) to get

$$\dot{\phi} = \frac{\sqrt{-\Lambda}\kappa}{\sigma}\left(z_0 - z\right). \tag{2.234}$$

Both of these expressions more openly reflect the spacetime's translational symmetry in z by employing the replacement constant of motion z_0 in lieu of L. As z_0 can be arbitrary, charged test particles (with suitable constants of motion) can be found at any z. Setting $V_z = 0$, we can see that the maximum distance along the z axis (both coordinate and proper, as $g_{zz} = 1$) a given particle can move away from z_0 is

$$\Delta z_{\max} = \sqrt{\frac{\delta + 2K}{-\Lambda\kappa^2}}\,. \tag{2.235}$$

To sum up the equations for charged test particle motion, the evolution of the system can be decomposed into two independent subsets of equations, one for $t(\tau)$ and $r(\tau)$ using the equations (2.221) and $\dot{r}^2 = -2V_r$ with (2.230), and the other for $\phi(\tau)$ and $z(\tau)$ using (2.234) and $\dot{z}^2 = -2V_z$ with (2.233). The constants of motion E, K, and z_0 are fixed by the initial conditions.

Regarding circular orbits, the derivatives of V_r (2.230) are the same as the respective derivatives of V (2.224), which means that charged orbits can be located only at $r = 0$ and they are stable in the radial direction as well. From $V_r(0) = 0$ we have $E = 2K$, replacing the previous constraint on the constants of motion. To make sure that the orbits are located in a plane perpendicular to the axis, we also require $V_z = 0 = \mathrm{d}V_z/\mathrm{d}z$. The derivative yields $z = z_0$, which, however, means that the particles do not actually orbit at all, as from (2.234) we have $\dot{\phi} = 0$, so the spacetime does not admit circular orbits of charged test particles

in the planes of constant z. Nevertheless, if we were interested in these static particles, from $V_z = 0$ we would see that $(E =)\, 2K = -\delta$. The static particles are stable in the z direction too, because $\mathrm{d}^2 V_z/\mathrm{d}z^2 = -\Lambda\kappa^2 > 0$.

The rotational Killing vector fields yields the additional constant[12] $\phi\dot{z} - z\dot{\phi}$, which is valid only for uncharged particles with $\kappa = 0$. We can then express one of the coordinates as the function of the other, such as

$$\phi(z) = \frac{L}{\sigma^2 Z}\, z + \phi_0 \mod 2\pi\,. \tag{2.236}$$

The last two Killing vectors, however, yield more interesting results. These vectors represent the symmetries of the electromagnetic field, so their constants

$$\begin{aligned} A &= \sinh\!\left(\sqrt{-2\Lambda}\, r\right) \cosh\!\left(\sqrt{-2\Lambda}\, r\right) \sin\!\left(\sqrt{-2\Lambda}\, t\right)\, \dot{t} + \cos\!\left(\sqrt{-2\Lambda}\, t\right)\, \dot{r}\,, \\ B &= \sinh\!\left(\sqrt{-2\Lambda}\, r\right) \cosh\!\left(\sqrt{-2\Lambda}\, r\right) \cos\!\left(\sqrt{-2\Lambda}\, t\right)\, \dot{t} - \sin\!\left(\sqrt{-2\Lambda}\, t\right)\, \dot{r} \end{aligned} \tag{2.237}$$

are valid even for charged particles unlike (2.120) for the axial homogeneous solution of Sec. 2.2. After replacing $\dot{t} = E \cosh^{-2}\!\left(\sqrt{-2\Lambda}\, r\right)$, we can express r and $\dot{r}$ from the constants as functions of coordinate time t,

$$r(t) = \frac{1}{2\sqrt{-2\Lambda}} \ln\!\left(\frac{E + A\sin\!\left(\sqrt{-2\Lambda}\, t\right) + B\cos\!\left(\sqrt{-2\Lambda}\, t\right)}{E - A\sin\!\left(\sqrt{-2\Lambda}\, t\right) - B\cos\!\left(\sqrt{-2\Lambda}\, t\right)}\right), \tag{2.238}$$

$$\dot{r}(t) = A\cos\!\left(\sqrt{-2\Lambda}\, t\right) - B\sin\!\left(\sqrt{-2\Lambda}\, t\right). \tag{2.239}$$

These functions are compared to a numerical computation in Fig. 2.14. The argument of the logarithm in (2.238) is always positive, as inserting the three relevant constants of motion into the fraction enables us to rewrite it as $\exp\!\left(2\sqrt{-2\Lambda}\, r\right)$, which is manifestly positive. Note that this substitution leads to the loss of the dependence on t and (2.238) becomes simply $r = r$.

Considering Killing tensors of rank two does not yield any new independent constants of motion.

Shell sources

The extrinsic curvature tensor (1.41) for a shell at $r = \text{const.}$ is

$$\mathbf{K} = -\epsilon\sqrt{-2\Lambda}\, \tanh\!\left(\sqrt{-2\Lambda}\, r\right)\, \mathrm{d}T^2 \tag{2.240}$$

and the projection of the electromagnetic tensor $\mathbf{F}_\perp$ (1.44) vanishes. The proper circumference (1.3) of the hypersurface

$$\mathcal{C} = 2\pi\sigma \tag{2.241}$$

[12] This is the first instance of many constants of motion with a 'naked' ϕ coordinate not inside the argument of a trigonometric function we encounter throughout this work. It seems appropriate to stress here that such constants must be understood locally, ignoring the discontinuity of ϕ at the endpoints of its interval of periodicity by, e.g., shifting the coordinate if necessary. While the issue is not as glaring there, note that we actually implicitly assume the same wherever $\dot{\phi}$ is involved, as this quantity is ill-defined on the endpoints of the interval.

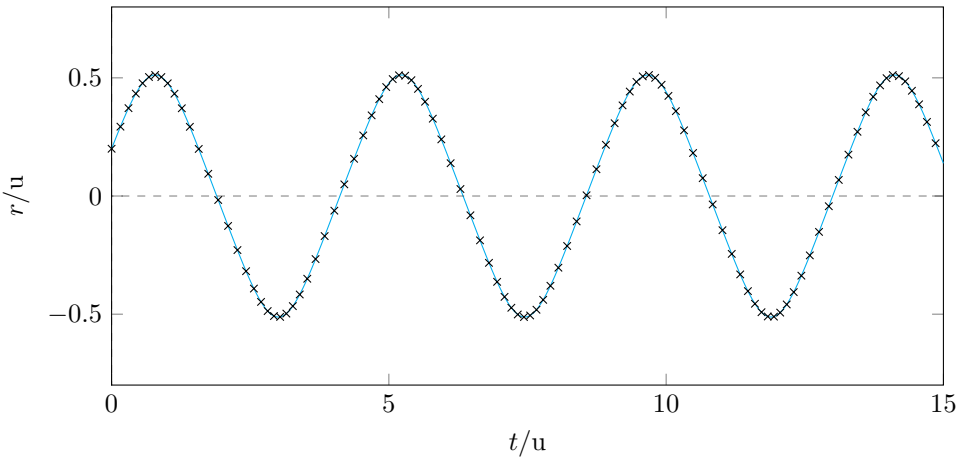

(a) The chart of $r(t)$ (2.238).

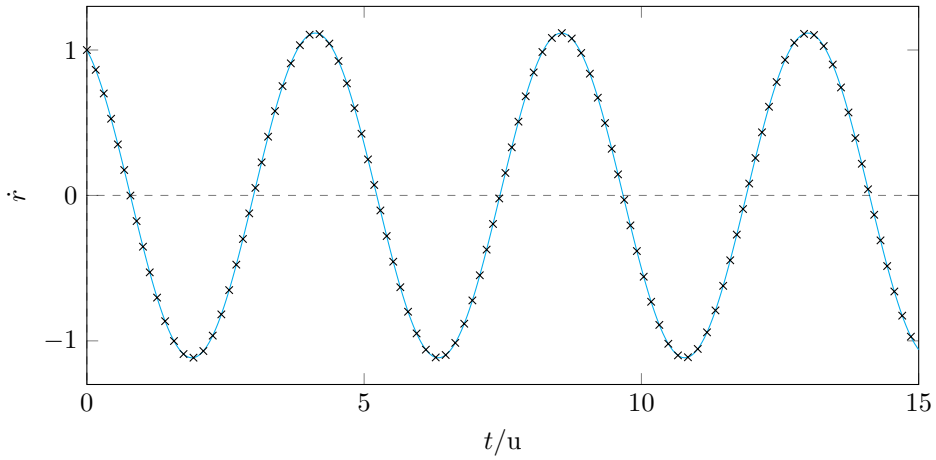

(b) The chart of $\dot{r}(t)$ (2.239).

Figure 2.14: The comparison of the cyan theoretical curves to the data points obtained by numerical integration of the equations of motion for a massive charged particle with $\kappa = 1$ in the spacetime with $\Lambda = -1\,\mathrm{u}^{-2}$ and $\sigma = 1\,\mathrm{u}$. The relevant initial conditions are $t = 0$, $r = 0.2\,\mathrm{u}$, $\dot{t} \approx 1.66$, and $\dot{r} = 1$. The important constants of motion are $E \approx 1.80$, $A = 1$, and $B \approx 0.496$. The shown range of t corresponds to the total proper time of approximately $10.7\,\mathrm{u}$. Neighboring marks in the charts are $0.1\,\mathrm{u}$ of proper time apart. The particle's movement in the two remaining spatial dimensions is irrelevant.

does not depend on the radial coordinate r, which can therefore be chosen arbitrarily. Due to the symmetries of the spacetime, choosing the opposite sign of ϵ corresponds to repositioning the hypersurface $r \to -r$.

The trace of $\mathbf{K}$,

$$K = \epsilon \sqrt{-2\Lambda}\, \tanh\left(\sqrt{-2\Lambda}\, r\right), \tag{2.242}$$

does not diverge anywhere in the spacetime, which is consistent with the fact that there is no axis where $g_{\phi\phi} \to 0$. It is interesting to note, however, that at $r = 0$, which remains a prominent hypersurface for the metric, we have $K = -2\Lambda\epsilon r + \mathcal{O}(r^3)$. Therefore, as we leave $r = 0$ and venture into either part of the spacetime, the normal field pointing towards the corresponding region always has a positive divergence.

First, a shell connecting two variants of this spacetime cannot be made of particle streams as it necessarily has $S_{TT} = 0$. However, note that if the shell is located at $r = 0$ in both instances of the spacetime, the induced stress-energy tensor vanishes, $\mathbf{S} = 0$, regardless of the orientation of the two normals and the value of Λ on either side of the shell. This means we can change the value of Λ at $r = 0$ or consider only the region with $r > 0$, 'bouncing back' when approaching $r = 0$, without the need to cater to the junction conditions.

An interpretable shell is also not possible to be used to connect this spacetime to the Minkowski spacetime, as then $S_{ZZ} = -2\mu$, so we cannot have both $S_{ZZ} \geq 0$ and $\mu > 0$ at the same time (and it is not possible to have $\mathbf{S} = 0$ for this connection). We were unable to find numerically any admissible connection to the Levi–Civita spacetime.

On a more positive note, we can find an interpretable shell connecting the spacetime to the region containing the axis of the original Bonnor–Melvin solution. It is not possible to connect the asymptotic region, as then S_{TT} would inevitably be negative. Depending on the parameters of the two spacetimes, the interval of the allowed shell's coordinate radii in the radial homogeneous solution can be either empty, bounded, or only half-bounded. The last two possibilities are illustrated in Fig. 2.15, where we keep the region with negative radial infinity in the examined solution. However, we can exploit the symmetry of the spacetime to retain the other region instead. Like for the analogous shell in the radial Bonnor–Melvin solution, the induced three-current is due to the original Bonnor–Melvin solution, so the expression is almost the same as (2.211),

$$\mathbf{s} = \frac{1}{4\pi}\left(1 + \frac{1}{4}B^2\rho_{BM}^2\right)^{-2} B\, \mathrm{d}\Phi\,, \tag{2.243}$$

except for the opposite sign, which arises from the fact that this time we keep the region containing the axis instead of the asymptotic region. We again use the lower possible value of the coordinate in the Bonnor–Melvin solution,

$$\rho_{BM} = \frac{2}{B^2\sigma}\left(1 - \sqrt{1 - B^2\sigma^2}\right), \tag{2.244}$$

which does not depend on r, because neither does the circumference $\mathcal{C}$ (2.241).

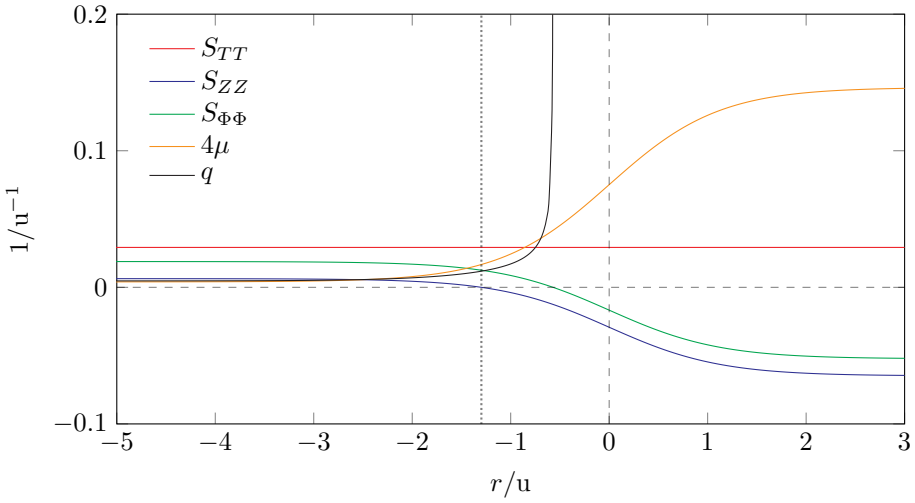

(a) The homogeneous solution with $\Lambda = -0.4\,\mathrm{u}^{-2}$ and $\sigma = 1\,\mathrm{u}$. The region admitting the four-stream interpretation of the shell extends from negative infinity to the dotted line.

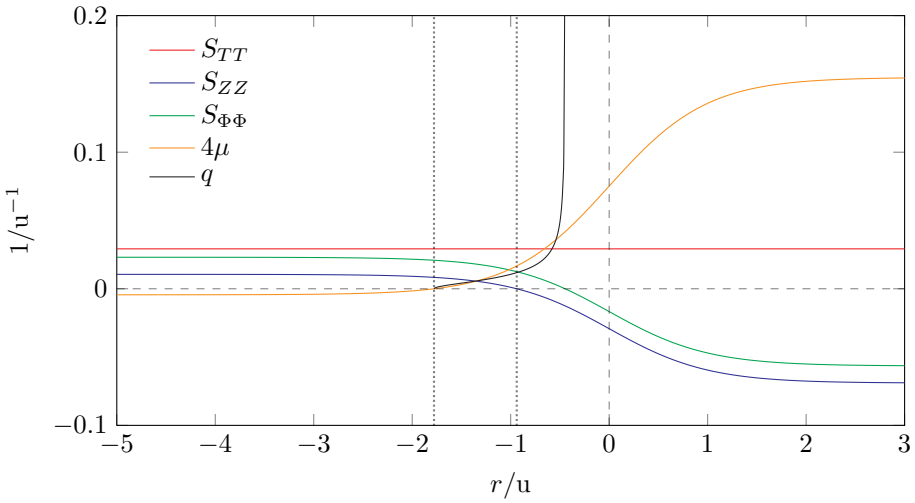

(b) The homogeneous solution with $\Lambda = -0.5\,\mathrm{u}^{-2}$ and $\sigma = 1\,\mathrm{u}$. The region admitting the four-stream interpretation of the shell is located between the two dotted lines.

Figure 2.15: The properties of two shells on the interface of the radial homogeneous solution and the Bonnor–Melvin solution (in both cases with $B = 0.7/\mathrm{u}$), expressed as functions of the radial coordinate of the shell in the homogeneous spacetime. The spacetimes are aligned in such a way that the region with negative radial infinity in the homogeneous solution and the region containing the axis in the Bonnor–Melvin spacetime are preserved. Note that the value of S_{TT} is the same in both charts, as it does not depend on Λ.

2.5.2 The general metric

A more general variant of the solution (2.213) is

$$\mathrm{d}s^2 = -\left(\mathrm{e}^{\sqrt{-2\Lambda}\,r} + a\,\mathrm{e}^{-\sqrt{-2\Lambda}\,r}\right)^2 \mathrm{d}t^2 + \mathrm{d}r^2 + \mathrm{d}z^2 + \sigma^2\mathrm{d}\phi^2 \tag{2.245}$$

with still

$$\mathbf{F} = \sigma\sqrt{-\Lambda}\,\mathrm{d}z \wedge \mathrm{d}\phi \tag{2.246}$$

and the same constant electromagnetic field invariant -2Λ and Kretschmann scalar $16\Lambda^2$ as the hyperbolic-cosine metric. The spacetime has six independent Killing vector fields corresponding to the same symmetries and is again of type D everywhere.

The dimensionless real parameter a can be chosen arbitrarily. Taking $a = 1$ and rescaling the temporal coordinate, we recover the previous metric (2.213) by simply using the definition $\cosh x = \left(\mathrm{e}^{x} + \mathrm{e}^{-x}\right)/2$. Another interesting option is to set $a = 0$, which yields a metric with a single exponential function

$$\mathrm{d}s^2 = -\mathrm{e}^{2\sqrt{-2\Lambda}\,r}\mathrm{d}t^2 + \mathrm{d}r^2 + \mathrm{d}z^2 + \sigma^2\mathrm{d}\phi^2. \tag{2.247}$$

Note that we can consider the transformation $r \to -r$ to keep the other exponential of (2.245), but this does not affect the underlying physics. Finally, $a = -1$ leads to

$$\mathrm{d}s^2 = -\sinh^2\!\left(\sqrt{-2\Lambda}\,r\right)\mathrm{d}t^2 + \mathrm{d}r^2 + \mathrm{d}z^2 + \sigma^2\mathrm{d}\phi^2. \tag{2.248}$$

We originally discounted this metric in our paper as we thought of the cosine metric as the more convenient one since hyperbolic cosine is positive everywhere, while sine has one root. However, as it turns out, the root at $r = 0$ corresponds to something much more profound than a simple coordinate singularity:

We can apply the transformation

$$R = \frac{1}{2\sqrt{-2\Lambda}}\left(\mathrm{e}^{\sqrt{-2\Lambda}\,r} - a\,\mathrm{e}^{-\sqrt{-2\Lambda}\,r}\right) \tag{2.249}$$

to (2.245) and rescale $t \to t/2$, which yields the metric

$$\mathrm{d}s^2 = -\left(a - 2\Lambda R^2\right)\mathrm{d}t^2 + \frac{\mathrm{d}R^2}{a - 2\Lambda R^2} + \mathrm{d}z^2 + \sigma^2\mathrm{d}\phi^2 \tag{2.250}$$

with $\mathbf{F}$ (2.246) unchanged. For $a = 1$ we obtain (2.216) of the cosine solution. Seeing this form of the metric, it is now clear that the hyperbolic-sine spacetime is qualitatively different from the cosine one: negative values of a lead to horizons appearing at $R = \pm\sqrt{a/2\Lambda}$ and there is a dynamical region with $g_{tt} > 0$ and $g_{RR} < 0$ between them, where the usually timelike Killing vector field ∂_t becomes spacelike. What is more, the solution with a single exponential (i.e., $a = 0$) features a double horizon at $R = 0$ corresponding to $r \to -\infty$ in the original coordinates, which leaves the double horizon in infinite proper distance from any other point in the spacetime. This makes it the extremal version of the spacetime. Recall that the investigated scalars are constant (and finite) everywhere, which suggests that there are no curvature singularities in the spacetime despite the presence of the horizons, and the two static regions at either side of the extremal horizon or the two non-degenerate horizons are exact copies of each other. The

situation is, therefore, different than for the well-known black-hole solutions or even for the black-string solution examined in the following section, as their horizons separate a region with a singularity and an asymptotic region. The horizons are Killing horizons, as the norm of the Killing vector field ∂_t vanishes there. Using the form of metric (2.250) is, therefore, preferable to the previous ones, as it covers the horizons and the dynamical region of the spacetime if applicable.

While we can consider an arbitrary a, only its sign is important and we can hence limit ourselves to, e.g., $a \in \{-1, 0, 1\}$, corresponding to the sinh, single-exp, and cosh metric tensors, respectively. To see that, we can use the identities

$$2b\cosh(x - x_0) = b\,\mathrm{e}^{-x_0}\mathrm{e}^{x} + b\,\mathrm{e}^{x_0}\mathrm{e}^{-x} \tag{2.251}$$

and

$$2b\sinh(x - x_0) = b\,\mathrm{e}^{-x_0}\mathrm{e}^{x} - b\,\mathrm{e}^{x_0}\mathrm{e}^{-x}. \tag{2.252}$$

Therefore, any linear combination of two exponential functions appearing in g_{tt} of (2.245) with $a \neq 0$ can be expressed as a rescaled hyperbolic function with a shifted argument. More specifically, in our case ($x = \sqrt{-2\Lambda}\,r$) the coefficient by the first exponential in the metric (2.245) is fixed, so we have $b = \mathrm{e}^{x_0}$. Plugging this into the second term of the above identities and comparing it with the metric, we obtain $x_0 = \ln\sqrt{|a|}$. Having replaced a with b and x_0, we can now certainly rescale the t coordinate to remove b from the metric and shift the radial coordinate to remove x_0, yielding either the sinh metric (for $a < 0$), or the cosh metric (for $a > 0$). As **F** (2.246) is invariant under these transformations, we can always recover the corresponding hyperbolic spacetime in its simplest form for any non-zero a. Perhaps an easier argument can be made for the transformed metric (2.250), where the transformation $t \to kt$ and $R \to R/l$ is equivalent to $a \to l^2 a$ in the metric as long as $|k| = |l|$.

The conformal diagrams of the solutions with $a = 0$ and $a = -1$, constructed using the procedure outlined in Sec. 1.2.3 from the metric (2.250), illustrate the causal structure of the spacetimes in Fig. 2.16. Recall that the conformal diagram of the metric with $a = 1$ can be found in Fig. 2.13.

We leave further investigation of this set of solutions for an upcoming paper. In the paper, we intend to forgo the cylindrical symmetry considered in this thesis and drop the periodicity of the ϕ coordinate, as it does not appear suitable for this spacetime.

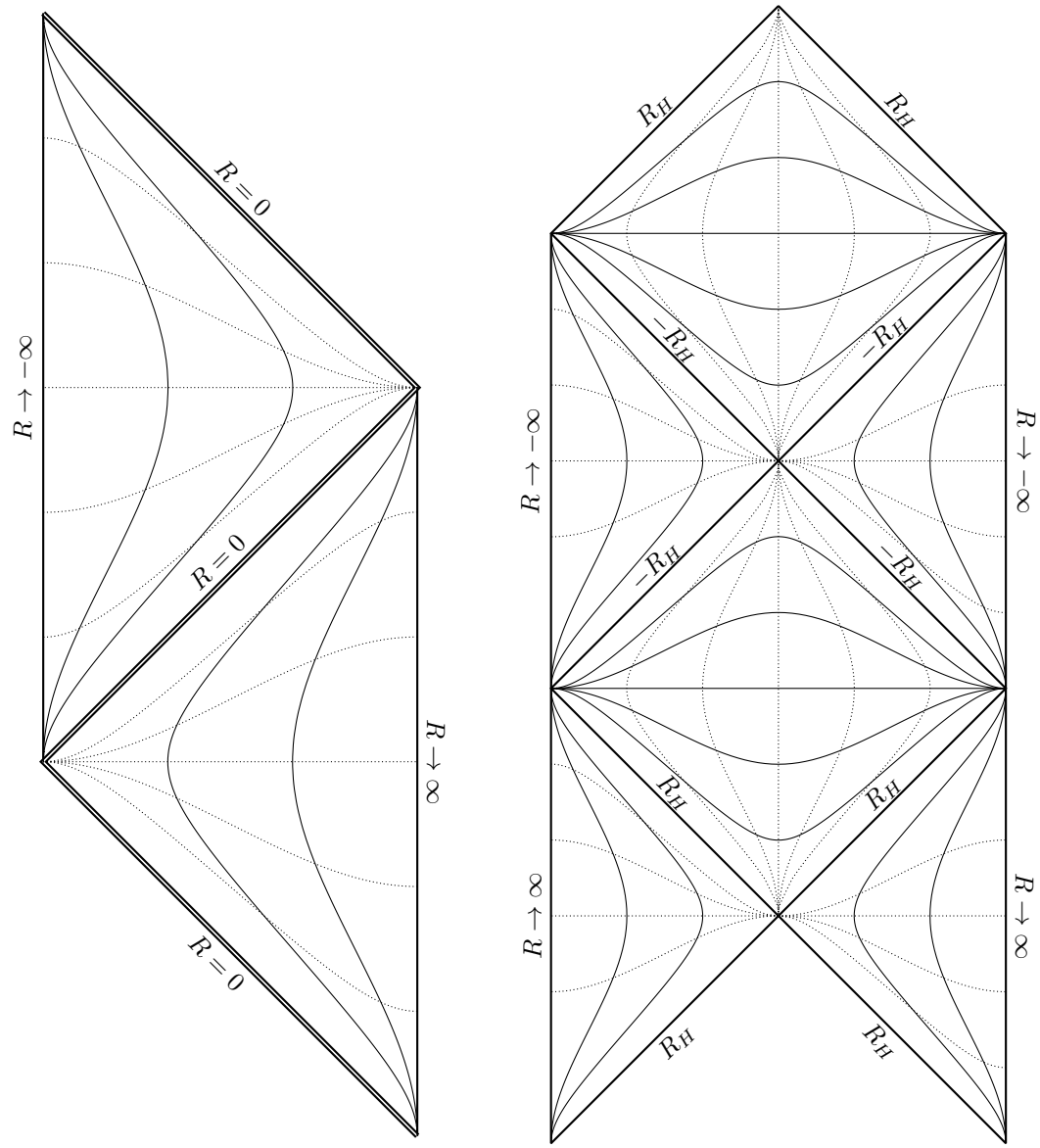

(a) The extremal, single-exponential variant of the metric with $a = 0$. There is a double horizon at $R = 0$.

(b) The hyperbolic-sine variant of the metric with $a = -1$. There are two horizons of multiplicity one at $R = \pm R_H$ with $R_H = \sqrt{a/2\Lambda}$.

Figure 2.16: The conformal diagrams of two variants of the homogeneous cosmological solution with a radial magnetic field. Each point in the diagram represents a cylindrical surface. Lines of constant coordinate r are solid and lines of constant t are dotted. The hyperbolic-cosine variant of the metric with $a = 1$ is depicted in Fig. 2.13.

2.6 Radial inhomogeneous spacetime

The last of the solutions examined in Veselý and Žofka [2021] is the radial variant of the inhomogeneous spacetime of Sec. 2.3. The original form of the metric presented in the paper is

$$\mathrm{d}s^2 = -\frac{\gamma f^{\frac{7}{2}} + 4f^4 - \frac{4}{3}\Lambda f^2}{f^3}\mathrm{d}t^2 + \frac{\mathrm{d}f^2}{\gamma f^{\frac{7}{2}} + 4f^4 - \frac{4}{3}\Lambda f^2} + \frac{1}{f}\left(\mathrm{d}z^2 + \beta^2\mathrm{d}\phi^2\right) \quad (2.253)$$

with

$$\mathbf{F} = \beta\,\mathrm{d}z \wedge \mathrm{d}\phi\,. \quad (2.254)$$

Using the arbitrary unit of length u, we have t $\left[\mathrm{u}^{3/2}\right]$, f $[u^{-1}]$, z $[\sqrt{\mathrm{u}}]$, and ϕ $[\sqrt{\mathrm{u}}]$, and the parameters are Λ $[\mathrm{u}^{-2}]$, γ $\left[\mathrm{u}^{-1/2}\right]$, and β [1]. The signs of all parameters can be chosen arbitrarily.

To obtain a more convenient form of the metric, we can use a transformation not unlike (2.131) in Sec. 2.3,

$$\begin{aligned} \hat{t} &= \frac{2}{\sqrt{|\beta|\,\mathrm{u}}}\,t\,, \qquad \hat{r} = \sqrt{|\beta|\,\mathrm{u}}\,f^{-1/2}, \\ \hat{z} &= \frac{1}{\sqrt{|\beta|\,\mathrm{u}}}\,z\,, \qquad \hat{\phi} = \sqrt{\frac{|\beta|}{\mathrm{u}}}\,\phi\,, \end{aligned} \quad (2.255)$$

while simultaneously rescaling $\hat{\beta} = \beta\,\mathrm{u}$. We include the unit of length u in the transformations so that the new coordinates (omitting the hats in the following) t and r (as well as the parameter β) have the dimension of length, while z and ϕ are dimensionless. The transformed metric reads

$$\mathrm{d}s^2 = -\mathfrak{N}(r)\,\mathrm{d}t^2 + \frac{\mathrm{d}r^2}{\mathfrak{N}(r)} + r^2\left(\mathrm{d}z^2 + \mathrm{d}\phi^2\right) \quad (2.256)$$

with the master function

$$\mathfrak{N}(r) = \frac{\beta^2}{r^2} - \frac{\alpha}{r} - \frac{\Lambda}{3}\,r^2, \quad (2.257)$$

which differs from $\mathfrak{M}$ (2.133) in Sec. 2.3 by the signs of the first two terms. The dimension of $\alpha = -\gamma\,|\beta|^{3/2}/4$ is u. The expression for the magnetic field $\mathbf{F}$ remains (2.254). The potential is $\mathbf{A} = \beta z\,\mathrm{d}\phi$ and the invariant has the same form as (2.135) in Sec. 2.3,

$$F_{\mu\nu}F^{\mu\nu} = \frac{2\beta^2}{r^4}\,. \quad (2.258)$$

The Hodge dual of the field is $\star\mathbf{F} = \beta r^{-2}\,\mathrm{d}t\wedge\mathrm{d}r$. The expressions for the magnetic field and its dual are reminiscent of those for the field (2.134) of Sec. 2.3, except that the coefficients for the magnetic and electric fields are exchanged. Take note that this form of the metric, more in line with (2.132), is slightly different from (38) in Veselý and Žofka [2021], because we have moved β so that the limit of vanishing magnetic field can be performed far more easily, and changed the sign of the $1/r$ term in $\mathfrak{N}$ to avoid unnecessary minus signs further down the road.

The solution is a warped product of a 2D black-hole spacetime (compare, e.g., Lemos [1995]) and $\mathbb{R}_2$. Again, in the following we shall focus primarily on the case $\beta\Lambda \neq 0$, as we are interested in cosmological magnetic solutions, but the value of α can be arbitrary.

The radial coordinate r can take any positive value. Like in Sec. 2.3, considering negative values of r corresponds to considering the opposite sign of α for $r > 0$. Unless both α and β vanish, there is a physical singularity located at $r = 0$, because the Kretschmann scalar

$$R_{\alpha\beta\gamma\delta}R^{\alpha\beta\gamma\delta} = \frac{4}{3r^8}\left(2\Lambda^2 r^8 + 9\alpha^2 r^2 - 36\alpha\beta^2 r + 42\beta^4\right), \tag{2.259}$$

which has the same form as (2.136), diverges there, along with the electromagnetic field invariant (2.258) for $\beta \neq 0$. The singular axis cannot be regularized with respect to Sec. 1.1.1, as the fraction in (1.2) becomes simply $\mathfrak{N}(r)$, which diverges as $r \to 0^+$. Note that the axis is located in finite proper radial distance from points in its coordinate vicinity, as $\sqrt{g_{rr}} = r/|\beta| + \mathcal{O}(r^2)$, so the integral is finite.

Unlike the axial spacetime discussed in Sec. 2.3, negative values of $\mathfrak{N}$ do not disrupt the signature of the metric. Instead, the physical interpretation of the radial and temporal coordinate exchanges there, and the radii where $\mathfrak{N} = 0$ form the horizons, like in the well-known black-hole spacetimes due to the similarity of the metric (2.256) with those of the Reissner–Nordström–(anti-)de Sitter family (see, e.g., Stuchlík and Hledík [2002]). The norm of the timelike Killing vector field ∂_t vanishes at the horizons, which means that these null surfaces are Killing horizons. However, unlike the mentioned spherically-symmetric spacetimes, the studied solution is cylindrically symmetric, which means that it is more appropriate to call it a black-string spacetime instead of a black hole.

To determine the horizon structure, we need to analyze the master function $\mathfrak{N}$. We shall do so in a manner analogous to our analysis of $\mathfrak{M}$ in Sec. 2.3, as expressing the roots directly again proves to be infeasible. Working with

$$\mathfrak{n}(r) = r^2\,\mathfrak{N}(r) = \beta^2 - \alpha r - \frac{\Lambda}{3}r^4, \tag{2.260}$$

we can see that this time for $\Lambda > 0$ there is exactly one positive root, separating the static region with the singularity and the dynamical asymptotic region as $r \to \infty$. For $\Lambda < 0$, there can be up to two distinct roots. Because $\mathfrak{n}$ is positive both near the singularity and in the asymptotic region, we need the determine whether it has a negative minimum in the relevant interval of $r > 0$. Setting the derivative equal to zero yields the analogue of (2.138) for the extremum,

$$r_0^3 = -\frac{3\alpha}{4\Lambda}, \tag{2.261}$$

which means that α, unlike Λ, must be positive for r_0 to also be positive. Inserting r_0 into $\mathfrak{n}$, we get

$$\mathfrak{n}(r_0) = \beta^2 - \frac{3\sqrt[3]{6}}{8}\,\frac{\alpha^{4/3}}{(-\Lambda)^{1/3}}. \tag{2.262}$$

The threshold value $\mathfrak{n}(r_0) = 0$ corresponds to

$$\alpha_{\mathfrak{N}} = \frac{4}{3}\,|\beta|^{3/2}\,(-\Lambda)^{1/4}, \tag{2.263}$$

in which case the master function $\mathfrak{N}$ has one degenerate root and is everywhere non-negative, unlike its counterpart $\mathfrak{M}$ from Sec. 2.3, which is non-positive in the threshold case. For $\alpha > \alpha_{\mathfrak{N}}$, there are two roots of $\mathfrak{N}$ corresponding to two horizons and there is a dynamical region of the spacetime between them, where $g_{tt} > 0$ and $g_{rr} < 0$ in the used coordinates and the Killing vector field ∂_t becomes spacelike. For $\alpha < \alpha_{\mathfrak{N}}$ there are no horizons and the spacetime is everywhere static and contains a naked singularity.

For $\alpha = \alpha_{\mathfrak{N}}$, the root of the master function $\mathfrak{N}$ corresponds to a degenerate horizon at $r = |\beta|^{1/2}\,(-\Lambda)^{-1/4}$ separating the two static regions. Again, the inverse of the transformation (2.255) yields the value $f^2 = -\Lambda$ corresponding to (2.72) of the homogeneous solution discussed in Sec. 2.5, but it cannot be seen as a straightforward limit of the present spacetime, as our derivation of the inhomogeneous spacetime relied on using the invariant f as a radial coordinate, which would be impossible if it was constant. Note that the proper radial distance to the degenerate horizon from any other point in the spacetime is infinite, which is not true for the two single horizons in the case of $\alpha > \alpha_{\mathfrak{N}}$.

Examples of $\mathfrak{N}$ corresponding to all four possible horizon configurations are depicted in Fig. 2.17.

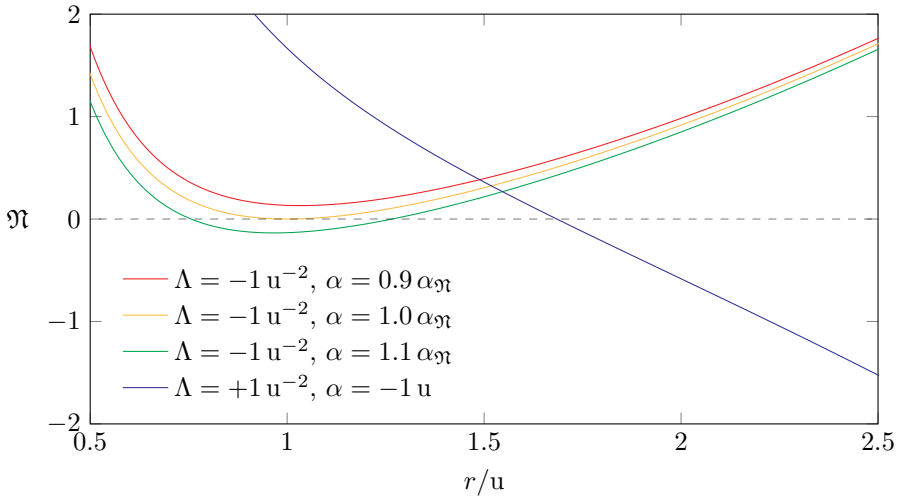

Figure 2.17: The four archetypes of the master function $\mathfrak{N}(r)$ with different parameters Λ and α, but always with $\beta = 1\,\mathrm{u}$. All four of them correspond to valid spacetimes. The blue curve represents spacetimes with $\Lambda > 0$, which always contain a single cosmological horizon, while the remaining three curves represent spacetimes with $\Lambda < 0$ and $\alpha_{\mathfrak{N}} = \frac{4}{3}\,\mathrm{u}$. The spacetime with the green curve of $\mathfrak{N}(r)$ contains two horizons, the spacetime with the orange curve has one double horizon, and the red curve corresponds to a naked singularity.

Taking into account that it is possible to perform a duality transformation of the electromagnetic field without breaking the Einstein–Maxwell equations (and thereby transition from a purely magnetic field to an electric one in our case), this solution can be viewed as a cylindrically-symmetric analogue of the above-mentioned Reissner–Nordström–(anti-)de Sitter spacetime, as both solutions are static, electrovacuum, and contain the cosmological constant. However, for $\Lambda > 0$ the possible horizon structure is different: While both families of solutions always contain the cosmological horizon, RN(a)dS may also contain up to two black-hole

horizons closer to the singularity, unlike the presently-studied solution. For $\Lambda < 0$, both spacetimes can have up to two black-hole (or black-string) horizons.

Like both the well-known black-hole solutions and the Bonnor–Melvin spacetime, this solution is also of Petrov algebraic type D, except for the hypersurface $r = 2\beta^2/\alpha$ (if $\alpha > 0$) and in the limit $r \to \infty$, where it is type O. There are four Killing vector fields, three for the translational symmetries and one for the rotational symmetry in the z–ϕ plane, corresponding to the $E(1) \times E(2)$ group of isometries. This suggests that it may be of interest here to either make the z coordinate periodic to replace the cylindrical symmetry with a toroidal one, or to extend the angular coordinate to $\phi \in \mathbb{R}$ to obtain planar symmetry. While Lemos and Zanchin [1996] considers both cylindrical and toroidal symmetry and the similar spacetime of Lemos [1995] is described there mainly in terms of planar symmetry, the toroidal interpretation seems to be preferred in the literature. Having said that, we shall consider cylindrical symmetry to remain consistent with the the rest of this work.

Note that unlike the other cosmological spacetimes examined in the work, this one does not belong to the Kundt class. Considering the general four-velocity corresponding to a null geodesic obtained through the effective potential (2.287) discussed later, we have

$$\mathbf{k} = \frac{E}{\mathfrak{N}(r)}\,\partial_t \pm \sqrt{E^2 - \frac{\mathfrak{N}(r)}{r^2}(Z^2 + L^2)}\,\partial_r + \frac{Z}{r^2}\,\partial_z + \frac{L}{r^2}\,\partial_\phi\,. \tag{2.264}$$

Like in the homogeneous case, the vectors we obtain for $Z = L = 0$, namely $(\partial_t/\mathfrak{N}(r) \pm \partial_r)E$, correspond to the two principal null directions, but this time only their shear and twist vanish, while their expansion scalar is $\theta = \pm 2E/r$. It turns out that it is not possible to fix the constants E, Z, and L in such a way that all three scalars vanish. Therefore, there is not a single null geodesic congruence with all three optical scalars equal to zero and the spacetime indeed does not belong to the Kundt class. However, having an expanding null geodesic congruence with vanishing shear and twist, this solution belongs to the Robinson–Trautman family instead.

Like in the axial solution of Sec. 2.3, the asymptotic form of the spacetime for $\Lambda < 0$ is the anti-de Sitter solution, because if we take the leading term of the series $\mathfrak{N}(r) = -\frac{\Lambda}{3}r^2 + \mathcal{O}(1/r)$, perform the transformation $r \to \sqrt{-3/\Lambda}\,/\,x$ and rescale t, we again obtain the metric

$$\mathrm{d}s^2 = \frac{-\frac{3}{\Lambda}}{x^2}\left(-\mathrm{d}t^2 + \mathrm{d}x^2 + \mathrm{d}z^2 + \mathrm{d}\phi^2\right). \tag{2.265}$$

Unlike the axial solution the spacetimes with $\Lambda > 0$ here also have an asymptotic region, even tough it is dynamical. For the metric with the leading term of the series of $\mathfrak{N}(r)$, the transformation $r \to \sqrt{3/\Lambda}\,/\,\eta$ and $t \to \sqrt{3/\Lambda}\,x$ yields the metric

$$\mathrm{d}s^2 = \frac{\frac{3}{\Lambda}}{\eta^2}\left(-\mathrm{d}\eta^2 + \mathrm{d}x^2 + \mathrm{d}z^2 + \mathrm{d}\phi^2\right), \tag{2.266}$$

so the solution with $\Lambda > 0$ is asymptotically de Sitter.

Note that this solution shares some noteworthy similarities with the Linet–Tian spacetime, i.e., the Levi–Civita solution with a non-zero cosmological constant. The Linet–Tian solution normally has only three Killing vector fields,

which correspond to the usual 'cylindrical' translations, but for certain values of the parameters in the metric, da Silva et al. [2000] observed that the solution obtains an additional Killing vector corresponding to rotations in the z–ϕ plane and that the solution also contains horizons.

The form of the metric (2.256) coincides with (2) of Huang and Liang [1995], (2.3) of Lemos and Zanchin [1996], and the metric discussed in Brill et al. [1997] with $k = 0$. Mass and charge in the ADM or Brown and York formalism is examined in each of the three papers. In the last two papers, the authors consider a negative cosmological constant only, even though the metric admits either sign of Λ. In Lemos and Zanchin [1996] the authors also notably introduce a rotating variant of the spacetime with $\Lambda < 0$, which has since been generalized to higher dimensions in Awad [2003] and to non-linear electromagnetic fields in Hendi [2010], and its analogues within various frameworks of modified gravity have been considered in papers such as Dehghani [2003] and Hendi [2008]. Hawking radiation from the black-string variant of the spacetime is studied in Sharif and Javed [2012]. Interestingly, the solution has experienced a surge in interest in the recent years. Han et al. [2019] and Hong et al. [2020] study thermodynamic properties of the metric, following a similarly-themed paper Gwak [2017] dealing with a variant of the spacetime with $\Lambda < 0$ and spherical symmetry generalized to higher dimensions. Furthermore, in Feng et al. [2021] the authors consider the spacetime as a heat engine.

Conformal diagrams

The relevant part of the metric (2.256) is in the form (1.66) with $f(r) = \mathfrak{N}(r)$ as required during our process of obtaining the Penrose conformal diagrams. Because the presence of the horizons leads to a more complicated causal structure, there are going to be four diagrams as there are four possible horizon configurations, and the diagrams are generally going to be composed of several blocks connected at the horizons.

For non-extremal spacetimes, we can express the tortoise coordinate (1.67) as

$$r^* = -\sum_{r_i} \frac{r_i^2 \ln\left(\frac{r}{r_i} - 1\right)}{\alpha + \frac{4}{3}\Lambda r_i^3} + c\,, \tag{2.267}$$

where r_i are the roots of $\mathfrak{N}(r)$ and c is the constant of integration. Take note that in the extremal case the master function has a double root and the integral of $1/\mathfrak{N}$ has to change accordingly. As explained in Sec. 1.2.3, in each spacetime block we fix the value of c to eliminate the imaginary part of r^*, which can arise due to the logarithms and complex roots of $\mathfrak{N}$, but the imaginary part is always constant in each block. The relation $r^*(r)$ is not invertible in elementary functions, which prohibits us from writing down the metric tensors of the blocks explicitly. Nonetheless, the transformations in Sec. 1.2.3 allow us to construct the conformal diagrams by plotting the lines of constant t or r in the Penrose coordinates

$$\psi(t,r) = \arctan\left(t - \Re\sum_{r_i} \frac{r_i^2 \ln\left(\frac{r}{r_i}-1\right)}{\alpha+\frac{4}{3}\Lambda r_i^3}\right) + \operatorname{sgn}(\mathfrak{N})\,\arctan\left(t + \Re\sum_{r_i} \frac{r_i^2 \ln\left(\frac{r}{r_i}-1\right)}{\alpha+\frac{4}{3}\Lambda r_i^3}\right) \tag{2.268}$$

and

$$\xi(t,r) = \arctan\left(t - \Re\sum_{r_i} \frac{r_i^2 \ln\left(\frac{r}{r_i}-1\right)}{\alpha+\frac{4}{3}\Lambda r_i^3}\right) - \operatorname{sgn}(\mathfrak{N})\,\arctan\left(t + \Re\sum_{r_i} \frac{r_i^2 \ln\left(\frac{r}{r_i}-1\right)}{\alpha+\frac{4}{3}\Lambda r_i^3}\right), \tag{2.269}$$

which have to be shifted in such a way as to complete the block structure of the given diagram.

Starting with the case $\Lambda > 0$, there is only one horizon configuration, with a cosmological horizon separating the static area containing the singularity and the dynamical asymptotic region. For each of the two regions there is a different type of block, which need to be connected at the horizon. The diagram in Fig. 2.18a represents the maximal analytical extension of the spacetime.

For $\Lambda < 0$, there are three different possible horizon configurations, similar to the black hole solutions of the Reissner–Nordström family. The simplest causal structure is that of the naked-singularity solution, which consists of only one static region extending from the singularity to radial infinity. Its diagram is presented in Fig. 2.18b. Next, the extremal configuration of Fig. 2.18c has one double horizon separating two static regions, which means there are two different types of blocks connected at the double horizon. To achieve maximal analytical extension, copies of the diagram need to be connected vertically at the double horizon. Finally, the black string solution has two horizons with a dynamical region between them. There are, therefore, three types of blocks that must be connected at the proper horizon after possibly being appropriately rotated. This configuration is represented by the diagram in Fig. 2.18d. Maximal analytical extension is performed by vertically connecting copies of diagram along the outer horizon at $r = r_2$.

The case of $\Lambda = 0$

Note that even when considering $\Lambda = 0$, this solution is still almost everywhere of algebraic type D and contains the four independent Killing vector fields. This sets it apart from the non-cosmological radial Bonnor–Melvin solution of Sec. 2.4, which means that it is not such a parametric limit for the cosmological spacetime. Of course, the original Bonnor–Melvin solution of Sec. 1.3.3 also cannot be a parametric limit, not only because of the different alignment of the magnetic field, but mainly because our solution contains a singularity at $r = 0$ even for $\Lambda = 0$ while the Melvin universe is singularity free.

The simplified master function $\mathfrak{N}_0(r) = \beta^2/r^2 - \alpha/r$ has a single root at $r_H = \beta^2/\alpha$ corresponding to a horizon as long as α is positive. The horizon separates the static region, which contains the singular axis, and the dynamical asymptotic region, which is reminiscent of spacetimes with a positive cosmological constant. On the other hand, if $\alpha \leq 0$, the master function $\mathfrak{N}_0$ is positive for all $r > 0$, the spacetime does not contain any horizons and is static everywhere. The Penrose conformal diagrams of the two alternatives, which like in the full spacetime had to be computed numerically as $r^*(r)$ is still not invertible, are presented in Fig. 2.19. Note that the metric for $\Lambda = 0$ becomes a special case of (27)[13] in Richterek et al. [2000] and (3.14) in Bronnikov et al. [2020].

[13]There is typo in relation (31).

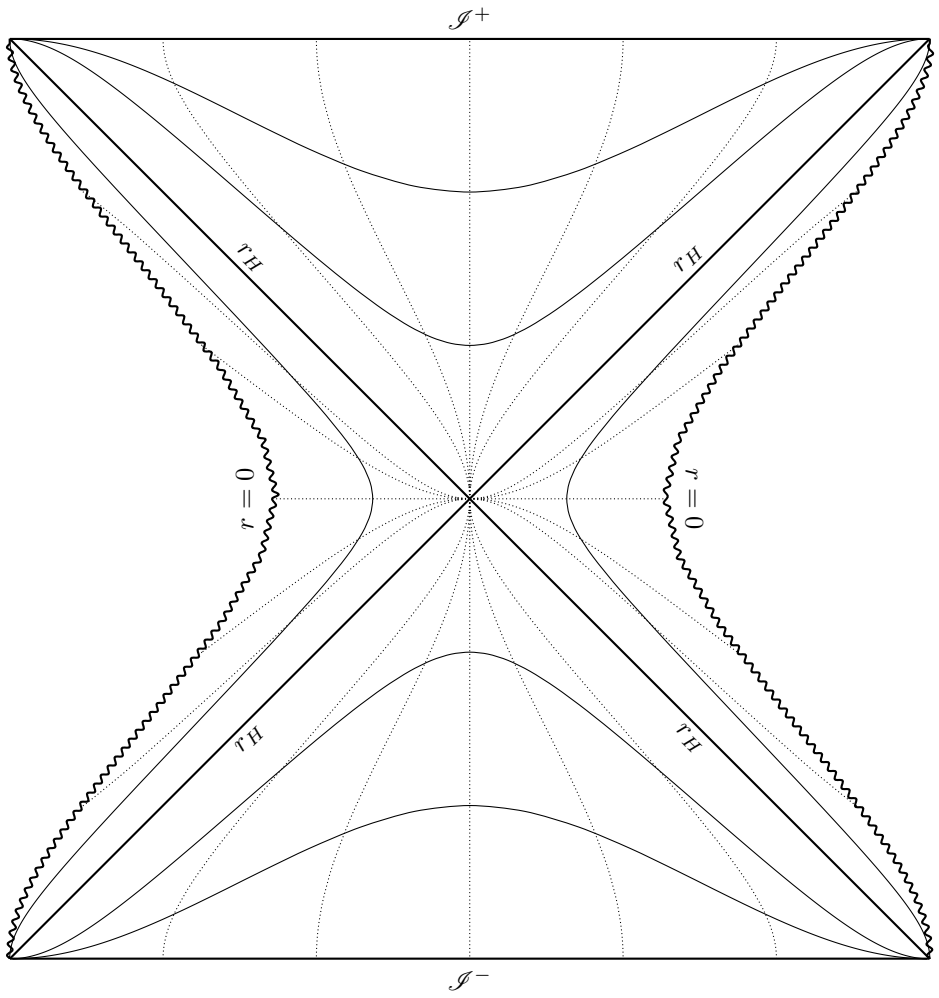

(a) The only possible horizon configuration for $\Lambda > 0$. The spacetime contains a horizon at $r = r_H$.

Figure 2.18: The conformal diagrams of the inhomogeneous cosmological spacetime with a radial magnetic field. Each point in the diagram represents a cylindrical surface. Lines of constant coordinate r are solid, lines of constant t are dotted and the wavy lines represent the singularity at $r = 0$. The figure is spread over multiple pages.

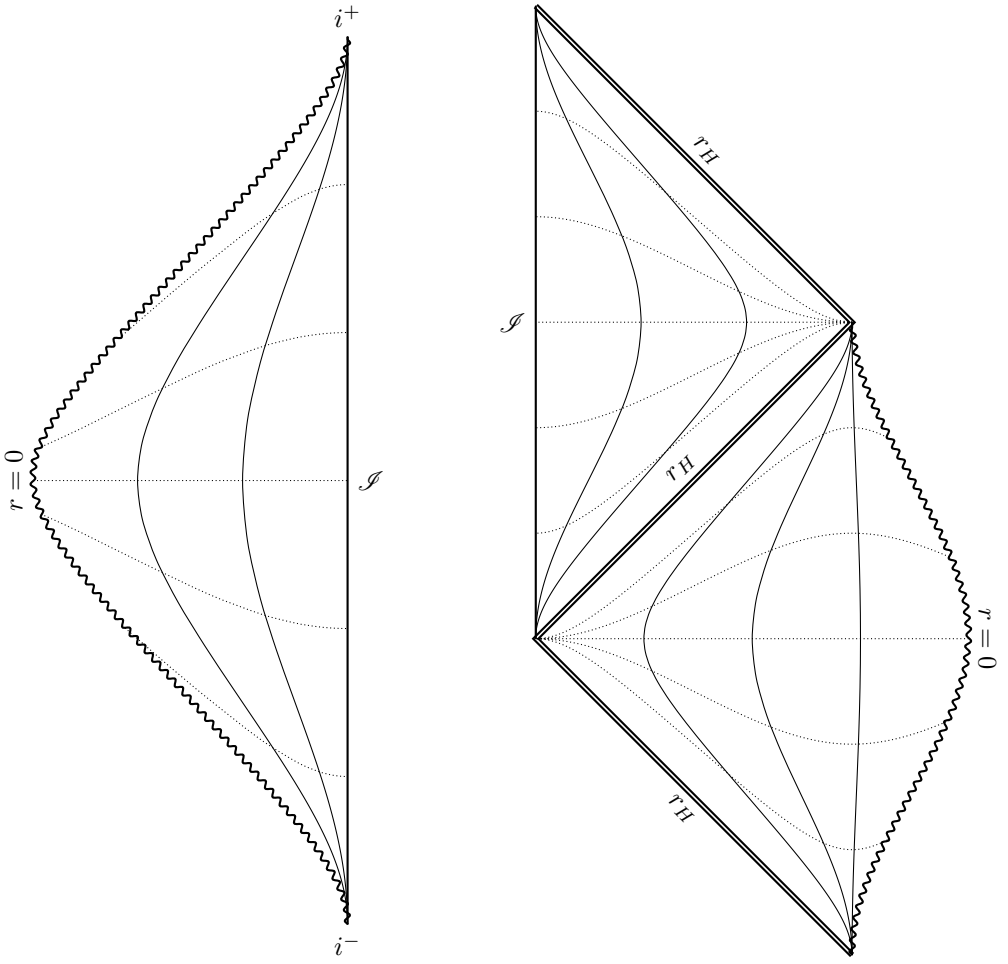

(b) The naked singularity for $\Lambda < 0$ with $\alpha < \alpha_{\mathfrak{N}}$.

(c) The extremal spacetime for $\Lambda < 0$ with $\alpha = \alpha_{\mathfrak{N}}$. There is a degenerate horizon at $r = r_H$.

Figure 2.18: The conformal diagrams of the inhomogeneous cosmological spacetime with a radial magnetic field. (cont.)

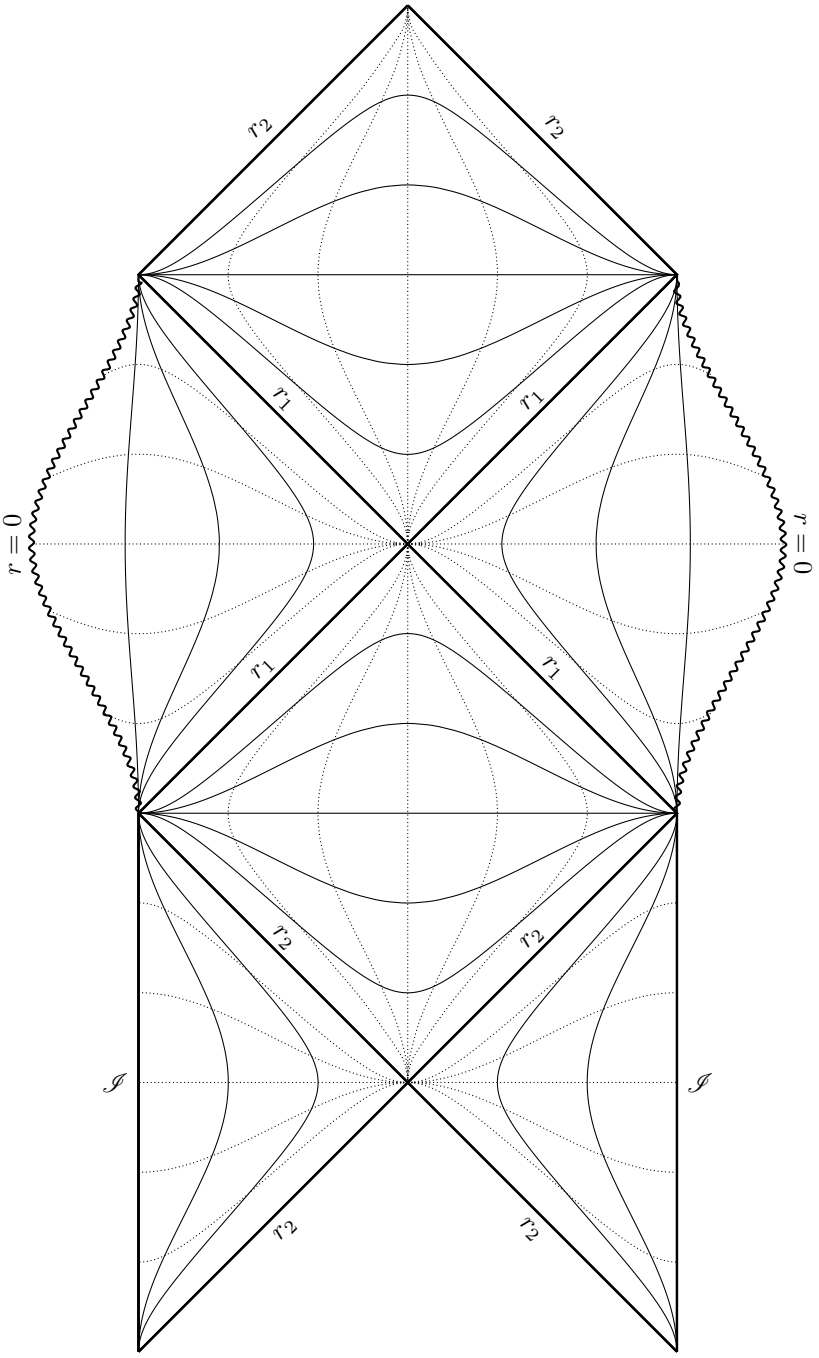

(d) The black-string spacetime for $\Lambda < 0$ with $\alpha > \alpha_{\mathfrak{N}}$. There are two horizons, an inner horizon at $r = r_1$ and an outer one at $r = r_2$.

Figure 2.18: The conformal diagrams of the inhomogeneous cosmological spacetime with a radial magnetic field. (cont.)

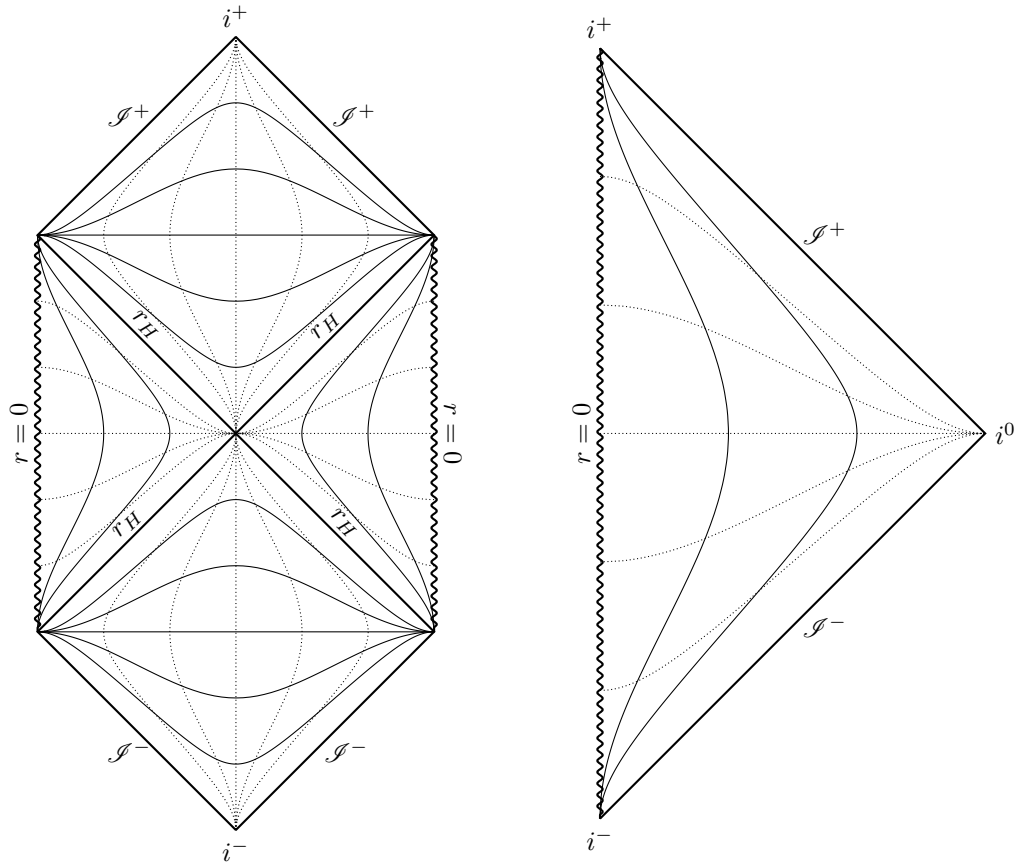

(a) The case with $\alpha > 0$. There is a single horizon at $r = r_H$.

(b) The naked-singularity spacetime for $\alpha \leq 0$.

Figure 2.19: The conformal diagrams of the inhomogeneous spacetime with a radial magnetic field for $\Lambda = 0$. Each point in the diagram represents a cylindrical surface. Lines of constant coordinate r are solid, lines of constant t are dotted and the wavy lines represent the singularity at $r = 0$.

To obtain metric tensors more resembling (1.86) of the original Bonnor–Melvin solution, we can perform similar transformations that led us to (2.151) for the axial inhomogeneous spacetime of Sec. 2.3.

Disregarding the case of $\alpha = 0$, which will be discussed separately, for the horizonless spacetimes with $\alpha < 0$, we consider $\rho = \sqrt{-\alpha r}$ and $\beta = 2/B$ (we do not need to redefine α this time to eliminate numerical factors in $g_{\rho\rho}$) to get

$$\mathrm{d}s^2 = -\frac{4\alpha^2\left(1+\frac{1}{4}B^2\rho^2\right)}{B^2\rho^4}\,\mathrm{d}t^2 + \frac{B^2\rho^6}{\alpha^4\left(1+\frac{1}{4}B^2\rho^2\right)}\,\mathrm{d}\rho^2 + \frac{\rho^4}{\alpha^2}\left(\mathrm{d}z^2+\mathrm{d}\phi^2\right) \quad (2.270)$$

with the magnetic field

$$\mathbf{F} = \frac{2}{B}\,\mathrm{d}z \wedge \mathrm{d}\phi\,. \quad (2.271)$$

The invariants are

$$F_{\mu\nu}F^{\mu\nu} = \frac{8\alpha^4}{B^2\rho^8} \quad (2.272)$$

and

$$R_{\alpha\beta\gamma\delta}R^{\alpha\beta\gamma\delta} = \frac{4\alpha^8\left(3B^4\rho^4+48B^2\rho^2+224\right)}{B^4\rho^{16}}\,. \quad (2.273)$$

Note that, interestingly, unlike the original Bonnor–Melvin spacetime, this metric does not contain second powers of the term $1+\frac{1}{4}B^2\rho^2$. Also note that apart from the singularity at $\rho=0$, there is not any degeneracy in the metric.

For $\alpha>0$, the situation is more complicated. To convert the metric into a Bonnor–Melvin-like form, we need to use two separate transformations on either side of the horizon. First, for the static region with $0<r<r_H$ we consider $\rho=-\sqrt{\alpha\left(r_H-r\right)}\in\left(-\left|\beta\right|,0\right)$. We choose the negative sign for this ρ in order to be able to use $\rho>0$ for the asymptotic region so that $r\to\infty\Leftrightarrow\rho\to\infty$. Redefining $B=2/\beta$ and $A=2^{-3/2}\alpha$, we get

$$\mathrm{d}s^2=-\frac{A^2B^4\rho^2}{2\left(1-\frac{1}{4}B^2\rho^2\right)^2}\,\mathrm{d}t^2+\frac{\left(1-\frac{1}{4}B^2\rho^2\right)^2}{A^4B^4}\,\mathrm{d}\rho^2+\frac{2\left(1-\frac{1}{4}B^2\rho^2\right)^2}{A^2B^4}\left(\mathrm{d}z^2+\mathrm{d}\phi^2\right), \tag{2.274}$$

and the singularity is located at $\rho=-2/\left|B\right|$. On the other hand, the dynamic asymptotic region with $r>r_H$ requires us to consider $\rho=\sqrt{\alpha\left(r-r_H\right)}\in(0,\infty)$. Using the same A and B, we get

$$\mathrm{d}s^2=\frac{A^2B^4\rho^2}{2\left(1+\frac{1}{4}B^2\rho^2\right)^2}\,\mathrm{d}t^2-\frac{\left(1+\frac{1}{4}B^2\rho^2\right)^2}{A^4B^4}\,\mathrm{d}\rho^2+\frac{2\left(1+\frac{1}{4}B^2\rho^2\right)^2}{A^2B^4}\left(\mathrm{d}z^2+\mathrm{d}\phi^2\right). \tag{2.275}$$

In both cases, the magnetic field is

$$\mathbf{F}=\frac{2}{B}\,\mathrm{d}z\wedge\mathrm{d}\phi\,, \tag{2.276}$$

but the expressions for its invariant

$$F_{\mu\nu}F^{\mu\nu}=\frac{2A^4B^6}{\left(1+\frac{1}{4}\operatorname{sgn}(\rho)B^2\rho^2\right)^4} \tag{2.277}$$

and the Kretschmann scalar

$$R_{\alpha\beta\gamma\delta}R^{\alpha\beta\gamma\delta}=\frac{A^8B^{12}\left(3B^4\rho^4-24\operatorname{sgn}(\rho)B^2\rho^2+80\right)}{4\left(1+\frac{1}{4}\operatorname{sgn}(\rho)B^2\rho^2\right)^8} \tag{2.278}$$

differ for either transformation. Both metric tensors contain a degeneracy (corresponding to the horizon) at $\rho=0$, which is by our definition an endpoint of the allowed values of ρ in both cases. The two metric tensors can be again brought together by considering the transformation $r=\operatorname{sgn}(\rho)\,\rho^2$. We also redefine $\alpha=A/\sqrt{2}$ to eliminate numerical factors in g_{rr}, which leads to

$$\mathrm{d}s^2=\frac{\alpha^2B^4r}{4\left(1+\frac{1}{4}B^2r\right)^2}\,\mathrm{d}t^2-\frac{\left(1+\frac{1}{4}B^2r\right)^2}{\alpha^4B^4r}\,\mathrm{d}r^2+\frac{4\left(1+\frac{1}{4}B^2r\right)^2}{\alpha^2B^4}\left(\mathrm{d}z^2+\mathrm{d}\phi^2\right) \tag{2.279}$$

with the unchanged expression for the magnetic field $\mathbf{F}=2/B\,\mathrm{d}z\wedge\mathrm{d}\phi$. The singularity is located at $r=-4/B^2$ and the horizon at $r=0$. Negative values of

r correspond to the static region and positive values to the dynamical asymptotic region. In these coordinates, the magnetic field invariant is

$$F_{\mu\nu}F^{\mu\nu} = \frac{\alpha^4 B^6}{2\left(1+\frac{1}{4}B^2 r\right)^4} \tag{2.280}$$

and the Kretschmann scalar is

$$R_{\alpha\beta\gamma\delta}R^{\alpha\beta\gamma\delta} = \frac{\alpha^8 B^{12}\left(3B^4r^2 - 24B^2 r + 80\right)}{64\left(1+\frac{1}{4}B^2 r\right)^8}\,. \tag{2.281}$$

Note that in the final forms of the metric tensors (2.270) and (2.279) the sign of the parameter α is irrelevant as it appears only in even powers in spite of the fact that we split the original metric in these two branches with respect to the sign of the original α. The new solutions can also be considered contenders for the title of the radial Bonnor–Melvin solution, which we had already bestowed upon the spacetime from Sec. 2.4.

Briefly returning to the case of $\alpha = 0$, a simple rescaling of the z and ϕ coordinates yields the conformastatic metric

$$\mathrm{d}s^2 = -\frac{\beta^2}{r^2}\,\mathrm{d}t^2 + \frac{r^2}{\beta^2}\left(\mathrm{d}r^2 + \mathrm{d}z^2 + \mathrm{d}\phi^2\right) \tag{2.282}$$

with the magnetic field

$$\mathbf{F} = \frac{1}{\beta}\,\mathrm{d}z \wedge \mathrm{d}\phi\,. \tag{2.283}$$

The magnetic field invariant, $F_{\mu\nu}F^{\mu\nu} = 2\beta^2/r^4$, is still the same as in the full spacetime and the Kretschmann scalar has the value of $56\beta^4/r^8$. This metric is a special case of (3.15) in Bronnikov et al. [2020] with $q = 1/\beta$ and $b = 0$.

Particle motion

Moving on to particle motion, recall that this spacetime can contain a dynamical area hidden beyond a horizon, where $\mathfrak{N} < 0$ and r becomes the new time coordinate. In our examination of particle motion, we focus solely on the static areas with $\mathfrak{N} > 0$. We are more interested in the static regions as they are thought to better correspond to the real universe than the dynamical regions and an observer in a static region would never be able to observe the insides of a dynamical region through a horizon.

Starting with uncharged particles with $\kappa = 0$, the three constants of motion are

$$E = \dot{t}\,\mathfrak{N}(r)\,, \tag{2.284}$$

$$L = \dot{\phi}\,r^2, \tag{2.285}$$

$$Z = \dot{z}\,r^2. \tag{2.286}$$

Using them, we can write the effective potential satisfying $\dot{r}^2/2 = -V$ as

$$V(r) = \frac{\mathfrak{N}(r)}{2}\left(-\delta + \frac{L^2+Z^2}{r^2}\right) - \frac{E^2}{2}\,, \tag{2.287}$$

and the separated potential according to (1.12) is

$$W^2(r) = \mathfrak{N}(r)\left(-\delta + \frac{L^2+Z^2}{r^2}\right). \tag{2.288}$$

There are three interesting coordinate limits to examine. First, when approaching the singularity the potentials diverge to positive infinity, which means that incoming particles always turn back. The only exception are purely radially moving photons with $Z = L = \delta = 0$, which are the only particles capable of falling into the singularity geodesically, as we then have $V(r) = -E^2/2$. Like in the non-cosmological spacetime of Sec. 2.4, we consider this to be another example of repulsive gravity, which is usually studied in the context of naked-singularity spacetimes. However, the singularity is geodesically inaccessible for massive test particles (regardless of their charge, as will be shown later) even if the static area containing the singularity is covered by a horizon from the viewpoint of an observer in the asymptotic region. Next, for the horizons we consider the limit of $\mathfrak{N} \to 0^+$, which again leads to $V \to -E^2/2$ but this time for all uncharged particles regardless of their other parameters, so they act attractively. Finally, for $\Lambda < 0$ we can also consider the limit $r \to \infty$, in which case the potential diverges for all massive particles, preventing them from escaping into radial infinity. However, some photons may escape if the limit

$$\lim_{r\to\infty} V(r)\Big|_{\delta=0} = \frac{-\Lambda}{6}\left(L^2+Z^2\right) - \frac{E^2}{2} \tag{2.289}$$

is negative for them.

For stationary photon orbits in the planes $z = \text{const.}$, the only non-trivial equation of motion is the radial one, which together with the normalization equation yields

$$\Omega^2 = -\frac{81\alpha^4 + 256\beta^6\Lambda}{768\beta^6} \tag{2.290}$$

for the photon coordinate angular velocity $\Omega = \mathrm{d}\phi/\mathrm{d}t$. Because Ω^2 must be positive, we need to have $\Lambda < 0$ and $|\alpha| < \alpha_{\mathfrak{N}}$. The orbit can be found at

$$r_\gamma = \frac{4}{3}\frac{\beta^2}{\alpha}, \tag{2.291}$$

which means that α must be positive. Both conditions combined, we get that photon orbits can only be found in spacetimes with a negative Λ and $\alpha \in (0, \alpha_{\mathfrak{N}})$. These parameters lead to a naked singularity, so $\mathfrak{N}$ is always positive at the photon orbit (as well as everywhere else). Note that for $\alpha = \alpha_{\mathfrak{N}}$, r_γ coincides with the degenerate horizon radius. The orbits are stable, as the second derivative of V is $729\,\alpha^6 L^2/\,2048\,\beta^{10} > 0$ for them.

For massive particle orbits, we can get the particle's constants of motion using the usual equations $V(r) = 0$ and $V'(r) = 0$, leading to

$$E^2 = -\frac{2\,\mathfrak{N}^2(r)\,r^2}{3\alpha r - 4\beta^2} \tag{2.292}$$

and

$$L^2 = \frac{\left(2\beta^2 - \alpha r + \frac{2}{3}\Lambda r^4\right) r^2}{3\alpha r - 4\beta^2}. \tag{2.293}$$

Both of the squares must be positive to represent real constants. From E^2 we see that we need to have $3\alpha r < 4\beta^2$, and L^2 further requires $2\beta^2 - \alpha r + \frac{2}{3}\Lambda r^4 < 0$, while it must simultaneously hold that $\mathfrak{N}(r) > 0$ so that the orbits are in the static part of the spacetime. The `Reduce` function of `Mathematica` reveals that for $\Lambda > 0$ the conditions cannot be fulfilled, so these spacetimes do not allow any geodesic orbits at all, including photon ones. For $\Lambda < 0$, the sign of α matters. For $\alpha > 0$, there are massive geodesical orbits only in naked-singularity spacetimes, specifically in a region bounded from above by the photon orbit radius r_γ, while the lower bound is given by the corresponding root of the numerator in L^2. For $\alpha \leq 0$, the orbits can be found at any r greater than the root.

For charged particles with $\kappa \neq 0$, we need to transition from the Lagrangian formalism to the Hamilton–Jacobi equation (1.20). For the separated action (1.24), the equation becomes

$$-r^2\,\mathfrak{N}(r)\Big(R'(r)\Big)^2 + \delta r^2 + \frac{E^2 r^2}{\mathfrak{N}(r)} - \Big(Z'(z)\Big)^2 - (\beta\kappa z - L)^2 = 0\,, \tag{2.294}$$

which is clearly separable. The constant of motion E remains

$$E = \dot{t}\,\mathfrak{N}(r)\,, \tag{2.295}$$

but L is now

$$L = r^2\,\dot{\phi} + \beta\kappa z\,. \tag{2.296}$$

Introducing the Carter constant K, we can establish the two effective potentials (1.25) and (1.26),

$$V_r(r) = \frac{\mathfrak{N}(r)}{2}\left(-\delta + \frac{K}{r^2}\right) - \frac{E^2}{2} \tag{2.297}$$

and

$$V_z(r,z) = \frac{1}{2r^4}\Big((\beta\kappa z - L)^2 - K\Big)\,. \tag{2.298}$$

The Carter constant must be non-negative so that V_z is not positive everywhere. As (2.297) has the same form as (2.287), what has been said about the limits of the radial effective potential remains true after replacing $L^2 + Z^2$ in (2.287) with K. Like in the homogeneous case, we denote

$$L = \beta\kappa z_0 \tag{2.299}$$

to better see the translational symmetry along the z axis. We can then rewrite V_z as

$$V_z(r,z) = \frac{1}{2r^4}\Big(\beta^2\kappa^2\,(z_0 - z)^2 - K\Big)\,, \tag{2.300}$$

and (2.296) as

$$\dot{\phi} = \frac{\beta\kappa}{r^2}\,(z_0 - z)\,, \tag{2.301}$$

using z_0 instead of L alongside the other constants of motion E and K. Determined by the turning points at $V_z = 0$, the maximal coordinate distance from z_0 along the z axis that a particle may reach does not depend on r,

$$\Delta z_{\max} = \sqrt{\frac{K}{\beta^2\kappa^2}}\,, \tag{2.302}$$

but the corresponding proper distance $r\,\Delta z_{\max}$ does.

Contrary to the homogeneous spacetime, the full set of equations governing charged test particle motion cannot be separated into two independent subsets, as all components of the four-velocity are functions of $r(\tau)$, which is given by $\dot{r}^2 = -2V_r$ with V_r being (2.297). The relation (2.284) gives $t(\tau)$. The evolution of the last two coordinates, $z(\tau)$ and $\phi(\tau)$, is determined by $\dot{z}^2 = -2V_z$ with (2.300), and (2.301), respectively. Both of these two differential equations also explicitly depend on z. The initial conditions determine the constants of motion E, K, and z_0.

Like in the homogeneous case, there cannot be any electrogeodesic circular orbits, because considering $\partial V_z/\partial z = 0$ leads to $z = z_0$, which in turn means that $\dot{\phi} = 0$ from (2.301). However, it is possible to fulfill the other conditions arising from the two potentials required to keep the particle static in this set of coordinates. From $V_z = 0$ (2.300), we see that this particle must have $K = 0$ and that the particle's charge is irrelevant in this analysis. After plugging this value into (2.297), $V_r = 0$ leads to $E^2 = -\delta\mathfrak{N}(r_0)$ for a particle static at $r = r_0$. Finally, $V_r' = -\delta\mathfrak{N}'(r_0)/2 = 0$ means that the static particle must be located in an extremum of $\mathfrak{N}$ (note that photons with $\delta = 0$ cannot be static in any coordinate system, as that would violate the normalization of their four-velocity). Expressing α from $\mathfrak{N}'(r_0) = 0$, we obtain $\alpha = 2(3\beta^2 + \Lambda r_0^4)/3r_0$, which leads to $\mathfrak{N}(r_0) = -(\beta^2 + \Lambda r_0^4)/r_0^2$. This means that for $\Lambda > 0$, the extremum has to lie in the dynamic region beyond the horizon, which means no static particles can be found there. For $\Lambda < 0$, static particles at r_0 satisfying $\mathfrak{N}(r_0) > 0$ can be found if the spacetime is that of a naked singularity, with no horizons and $\alpha < \alpha_{\mathfrak{N}}$. This is yet another manifestation of repulsive gravity, akin to the cases investigated in, e.g., Pugliese et al. [2011, 2013] and in our previous work Veselý and Žofka [2018, 2019a].

Like in the homogeneous case, for uncharged particles we can obtain the additional constant $r^2\left(\phi\dot{z} - z\dot{\phi}\right)$ from the rotational Killing vector. We can then obtain the analogue of (2.236),

$$\phi(z) = \frac{L}{Z}\,z + \phi_0 \mod 2\pi\,. \tag{2.303}$$

No additional constants of motion are to be gained from second-rank Killing tensors.

Shell sources

The extrinsic curvature tensor (1.41) is

$$\mathbf{K} = \epsilon\left(-\frac{1}{2}\,\frac{\mathfrak{N}'(r)}{\sqrt{\mathfrak{N}(r)}}\,\mathrm{d}T^2 + \frac{\sqrt{\mathfrak{N}(r)}}{r}\left(\mathrm{d}Z^2 + \mathrm{d}\Phi^2\right)\right) \tag{2.304}$$

and the projection of the electromagnetic tensor $\mathbf{F}_\perp$ (1.44) vanishes for the last time in this work. The proper circumference (1.3) of the hypersurface takes the same form as in flat geometry,

$$\mathcal{C} = 2\pi r, \tag{2.305}$$

but its derivative with respect to the proper radius of the shell r_p, as given by (1.4), is not constant,

$$\frac{\mathrm{d}\mathcal{C}}{\mathrm{d}r_p} = 2\pi\sqrt{\mathfrak{N}(r)}\,. \tag{2.306}$$

The derivative vanishes at the horizons and the formula does not work in the dynamical regions, because r does not represent the radial coordinate. In the static regions, however, the formula correctly expresses the change of $\mathcal{C}$ when the proper radius changes, even though the value of the proper radius itself is debatable if the shell is above the black-string horizons. The derivative diverges at the singular axis and for $\Lambda < 0$ also in the limit of $r \to \infty$.

The trace of $\mathbf{K}$ mirrors (2.175) of the axial inhomogenenous solution, only with the two master functions swapped,

$$K = \epsilon\left(\frac{2\sqrt{\mathfrak{N}(r)}}{r} + \frac{1}{2}\,\frac{\mathfrak{N}'(r)}{\sqrt{\mathfrak{N}(r)}}\right). \tag{2.307}$$

When approaching the axis at $r = 0$, we need to orient the normal field so that it points towards the asymptotic region to obtain the correct limit, thus setting $\epsilon = +1$. After inserting $\mathfrak{N}$ (2.257), we get the expected result $\lim_{r\to 0^+} K = +\infty$.

Regarding shell sources, this spacetime appears to be quite readily connectible through an interpretable shell to other solutions talked about in this thesis, but we have not been able to find such a configuration that would eliminate all singularities in the resulting spacetime. For $\Lambda < 0$, interpretable shells can be found both for naked-singularity spacetimes and for spacetimes with horizons. In the latter case they seem to be much easier to find in the inner region containing the singularity, but we also found examples of admissible shells above the black-string horizons.

First, it is possible to connect two instances of the spacetime through an interpretable shell. The shell must be located at the same radial coordinate in both spacetimes, there is no induced three-current and the energy-stress tensor satisfies $S_{ZZ} = S_{\Phi\Phi}$. Unfortunately, noting that

$$S_{TT} = \frac{1}{4\pi r}\left(\epsilon_-\sqrt{\mathfrak{N}_-(r)} - \epsilon_+\sqrt{\mathfrak{N}_+(r)}\right), \tag{2.308}$$

it is not possible to connect two asymptotic regions together ($-\epsilon_- = \epsilon_+ = 1$), which would be the most interesting configuration as it would be singularity-free. On the other hand, interpretable shells can connect the region with the singularity to another region with the singularity or the asymptotic region, in both cases with different metric parameters (including opposite signs of Λ). For illustration, see Fig. 2.20, where we consider opposite signs of Λ on each side of the shell. However, it is possible to switch any of the two signs and still find an interpretable shell, because in our examples they are found near the singularity at $r = 0$, where the term with Λ in $\mathfrak{N}$ (2.257) gets suppressed by the other two terms with negative powers of r. This is also true for the connections to the Minkowski spacetime presented later in Fig. 2.22. Note that for one configuration we found admissible shells not only near the singularity, but also above the black-string horizons of one of the solutions. These extra shells in our example do not admit the opposite sign of Λ in the other spacetime.

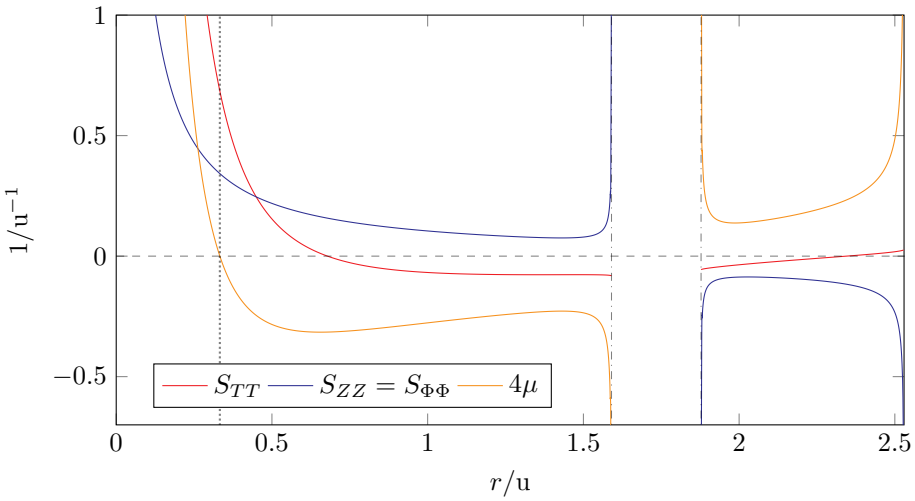

(a) Connection to the asymptotic region. Interpretable shells can be found to the left of the dotted line.

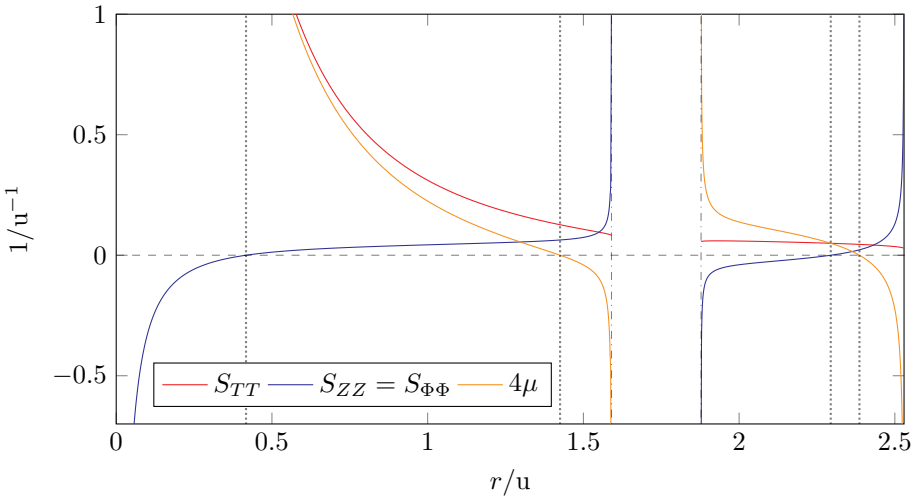

(b) Connection to the region with the axis. Interpretable shells can be found on either side of the black-string horizons of one of the two solutions in the two regions between the dotted line pairs.

Figure 2.20: The properties of shells on the interface of two instances of the radial inhomogeneous solution. The radial coordinate of the shell is the same in both spacetimes. The instance with the parameters $\Lambda = -1\,\mathrm{u}^{-2}$, $\beta = 3\,\mathrm{u}$, and $\alpha = 7\,\mathrm{u}$ always keeps the region with the axis. It has two black-string horizons marked by the two dash-dotted lines. The two figures represent connections to either part of the spacetime with the parameters $\Lambda = 1\,\mathrm{u}^{-2}$, $\beta = 1\,\mathrm{u}$ and $\alpha = -5\,\mathrm{u}$. This spacetime has a cosmological horizon at $r \approx 2.53\,\mathrm{u}$. There is no induced three-current on the shells.

Connecting the part of the spacetime containing the singularity to the homogeneous counterpart of Sec. 2.5.1 through interpretable shells is also possible for both signs of Λ in the inhomogeneous spacetime, as shown in Fig. 2.21. We found admissible connections both above and below the black-string horizons.

For the Minkowski, Levi–Civita, and Bonnor–Melvin spacetimes, it is generally possible to find interpretable shells connecting the part of the radial spacetime with the singularity to a part of each of the three spacetimes. In Fig. 2.22, we present connections to both the outer and the inner parts of the Minkowski spacetime, with both signs of Λ in the examined solution. Connections preserving the singular axis of the studied spacetime are possible for the remaining two solutions as well.

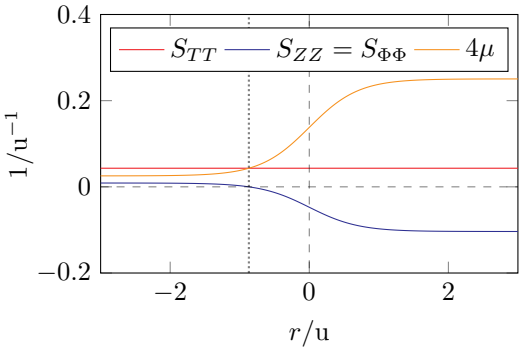

(a) $\Lambda = -1\,\mathrm{u}^{-2}$, $\beta = 1\,\mathrm{u}$, $\alpha = 5\,\mathrm{u}$; $\sigma = 5\,\mathrm{u}$. The shell is above the outer black-string horizon in the inhomogeneous solution. The admissible region is to the left of the dotted line.

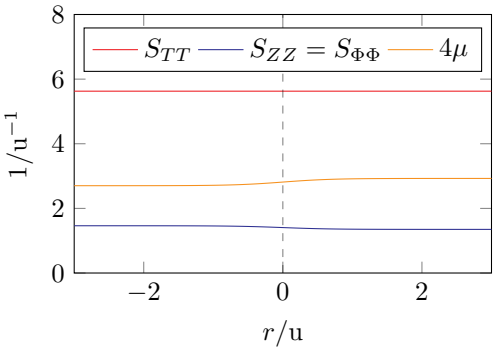

(b) $\Lambda = -1\,\mathrm{u}^{-2}$, $\beta = 1\,\mathrm{u}$, $\alpha = 5\,\mathrm{u}$; $\sigma = 0.1\,\mathrm{u}$. The shell is below the inner black-string horizon in the inhomogeneous solution. Any radial coordinate r in the homogeneous solution is admissible.

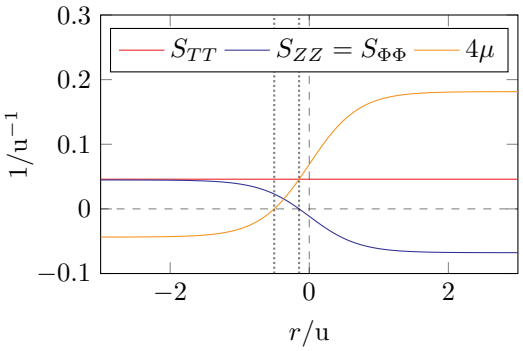

(c) $\Lambda = -1\,\mathrm{u}^{-2}$, $\beta = 1\,\mathrm{u}$, $\alpha = 1\,\mathrm{u}$; $\sigma = 1\,\mathrm{u}$. There are no horizons in the inhomogeneous solution and it contains a naked singularity. The admissible region is located between the two dotted lines.

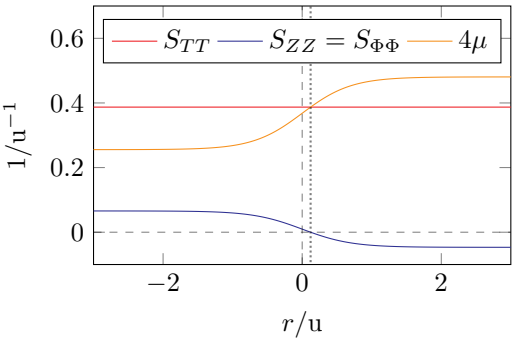

(d) $\Lambda = 1\,\mathrm{u}^{-2}$, $\beta = 5\,\mathrm{u}$, $\alpha = 1\,\mathrm{u}$; $\sigma = 1\,\mathrm{u}$. There is a cosmological horizon in the inhomogeneous solution above the shell. The admissible region is to the left of the dotted line.

Figure 2.21: The properties of shells on the interface of the radial inhomogeneous and homogeneous solutions expressed as functions of the radial coordinate in the homogeneous spacetime. The value of the radial coordinate in the inhomogeneous solution is equal to the value of the parameter σ of the homogeneous solution, which always has $\Lambda = -1\,\mathrm{u}^{-2}$. The spacetimes are aligned in such a way that the region with the singular axis in the inhomogeneous solution and the region with negative radial infinity in the homogeneous solution are preserved. There is no induced three-current on the shells and the value of S_{TT} is constant in each chart.

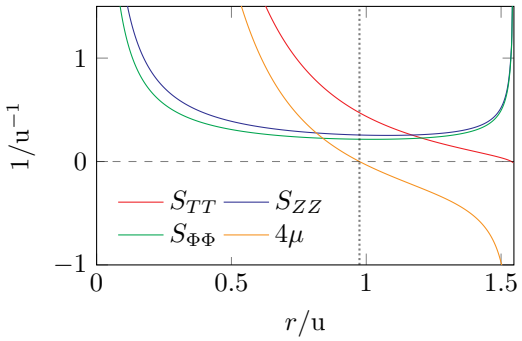

(a) $\Lambda = 0.5\,\mathrm{u}^{-2}$, $\beta = 10\,\mathrm{u}$, $\alpha = -8\,\mathrm{u}$. The cosmological horizon is at $r \approx 1.55\,\mathrm{u}$. We connect the asymptotic part of the Minkowski spacetime.

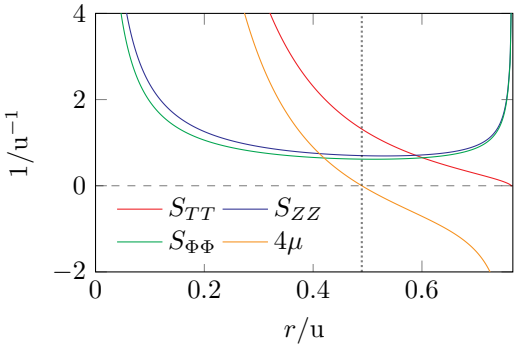

(b) $\Lambda = -0.8\,\mathrm{u}^{-2}$, $\beta = 7\,\mathrm{u}$, $\alpha = 8\,\mathrm{u}$. The inner black-string horizon is at $r \approx 0.77\,\mathrm{u}$. We connect the asymptotic part of the Minkowski spacetime.

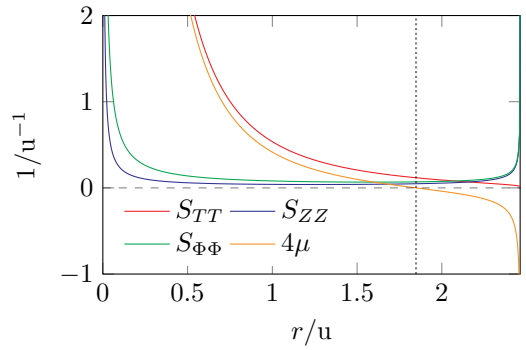

(c) $\Lambda = 0.2\,\mathrm{u}^{-2}$, $\beta = 8\,\mathrm{u}$, $\alpha = -5\,\mathrm{u}$. The cosmological horizon is at $r \approx 2.46\,\mathrm{u}$. We connect the part of the Minkowski spacetime with the axis.

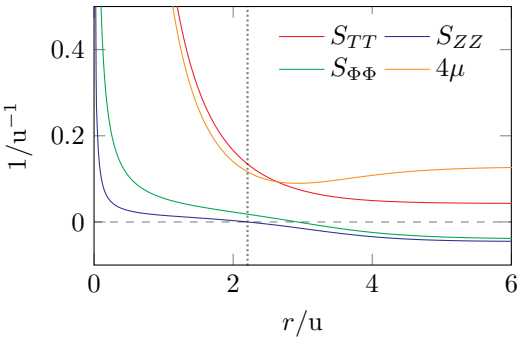

(d) $\Lambda = -0.75\,\mathrm{u}^{-2}$, $\beta = 10\,\mathrm{u}$, $\alpha = -5\,\mathrm{u}$. The examined spacetime does not contain any horizons. We connect the part of the Minkowski spacetime with the axis.

Figure 2.22: The properties of shells on the interface of the radial inhomogeneous solution (for both signs of Λ) and the Minkowski spacetime (for both the asymptotic region and the part with the axis). The value of the radial coordinate of the shell is the same in both spacetimes. We preserve the region with the singular axis in the examined magnetic solution. There is no induced three-current on the shell. In each chart, the four-stream interpretation of the shell is possible in the region to the left of the dotted line.

2.7 Azimuthal homogeneous spacetime

Taking the axial metric (2.104) and the corresponding magnetic field (2.105), we can perform the coordinate change explained in Sec. 2.1.3 to obtain the metric

$$\mathrm{d}s^2 = -\mathrm{d}t^2 + \frac{1}{2\Lambda}\left(\mathrm{d}r^2 + \sin^2 r\,\mathrm{d}z^2\right) + \sigma^2\mathrm{d}\phi^2 \tag{2.309}$$

and the magnetic field

$$\mathbf{F} = \frac{1}{2\sqrt{\Lambda}}\sin r\,\mathrm{d}r \wedge \mathrm{d}z \tag{2.310}$$

with the dual electric field $\star\mathbf{F} = \sigma\sqrt{\Lambda}\,\mathrm{d}t \wedge \mathrm{d}\phi$. Coordinates r, z and ϕ are dimensionless, while t and the newly-introduced parameter σ have the dimension of length. Note that $r \in [0, \pi]$ and the proper radial distance between the two endpoints of the interval is finite. The z coordinate is degenerate at the endpoints of the interval of r, so for $t = \text{const.}$ the spacetime can be thought of being reduced to a flat ring at the extreme values of r. The cosmological constant Λ has to be positive. The values of the invariants remain the same, $F_{\mu\nu}F^{\mu\nu} = 2\Lambda$ and the Kretschmann scalar is equal to $16\Lambda^2$. The local properties of the metric are the same as in the axial homogeneous solution of Sec. 2.2.

The spacetime is of Petrov algebraic type D. There are six Killing vectors: ∂_t, ∂_z, and ∂_ϕ for the translational symmetries, $\sigma^2\phi\,\partial_t + t\,\partial_\phi$ for boost in the ϕ direction, and $\sin z\,\partial_r + \cot r\cos z\,\partial_z$ with $\cos z\,\partial_r - \cot r\sin z\,\partial_z$ (together with ∂_z) correspond to rotations on the two-sphere with constant t and ϕ. Due to the solution's relatedness to the axial homogeneous spacetime of Sec. 2.2, this solution clearly admits the $ISO(1,1) \times SO(3)$ group of isometries and belongs to the Kundt class too.

While the corresponding axial homogeneous spacetime discussed in Sec. 2.2 had properties that were agreeable with our preferred cylindrical symmetry, after swapping g_{zz} and $g_{\phi\phi}$ the metric (2.309) appears less suitable to be interpreted in that way. For instance, there is no axis in the spacetime as $g_{\phi\phi}$ is constant. Instead, perhaps a better way of interpreting this metric is through toroidal symmetry, with z replaced with another 2π-periodic angular coordinate ζ. We can imagine the torus as arising from a cylinder of radius $(\sin r)/\sqrt{2\Lambda}$ with the ζ coordinate going around the circumference of the cylinder. The ϕ coordinate is measured along the axis of the cylinder. By identifying $\phi = 0$ and $\phi = 2\pi$, we transform the cylinder into a topological torus. Note that such a construction also suits the extrinsic curvature scalar of the shells we use in our applications of the Israel formalism, which we shall briefly elaborate on in the corresponding section. Interestingly, recall that in classical electrodynamics an azimuthal magnetic field may be found along a straight wire with an electric current, which is manifestly a cylindrically-symmetric configuration.

Particle motion

Regarding electrogeodesics, it should come as no surprise that the effective potential for radial motion fulfilling $\dot{r}^2/2 = -V$ is similar to (2.111),

$$V(r) = \Lambda\left(-\delta - E^2 + \frac{2}{\sin^2 r}\left(\frac{\kappa}{2}\cos r + \sqrt{\Lambda}\,Z\right)^2 + \frac{L^2}{\sigma^2}\right), \tag{2.311}$$

while the separated potential satisfying (1.12) is

$$W^2(r) = E^2 + \frac{V(r)}{\Lambda} = -\delta + \frac{2}{\sin^2 r}\left(\frac{\kappa}{2}\cos r + \sqrt{\Lambda}\, Z\right)^2 + \frac{L^2}{\sigma^2}\,. \tag{2.312}$$

The constants of motion are

$$E = \dot{t}\,, \tag{2.313}$$

$$L = \sigma^2\dot{\phi}\,, \tag{2.314}$$

$$Z = \frac{1}{2\Lambda}\left(\dot{z}\sin^2 r - \kappa\sqrt{\Lambda}\cos r\right). \tag{2.315}$$

When approaching the endpoints of the interval of r, the term with Z in the potentials generally diverges, turning away particles. For two special values of Z, namely

$$Z_\pm = \pm\frac{\kappa}{2\sqrt{\Lambda}}\,, \tag{2.316}$$

the potentials are monotonic, and the particle can reach $r = 0$ for Z_- or $r = \pi$ for Z_+ (or both of them if $\kappa = 0 = Z$).

For stationary circular orbits in the planes $z = \text{const.}$, the constant of motion Z must be set to

$$Z|_{\dot{z}=0} = -\frac{\kappa}{2\sqrt{\Lambda}}\cos r_0 \tag{2.317}$$

in order to eliminate motion along the z axis for a particle at a particular r_0. The potential then becomes constant,

$$V|_{\dot{z}=0} = \Lambda\left(-\delta - E^2 + \frac{L^2}{\sigma^2}\right), \tag{2.318}$$

and setting it equal to zero gives us a constraint on the particle's constants of motion. As $V'(r)|_{\dot{z}=0} = 0$, the second condition on the constants of motion is missing in this case. Therefore, particle orbits, including those of photons, can be located at any r in the spacetime. Concerning the stability, we have $V''(r)|_{\dot{z}=0} = \Lambda\kappa^2$, which means that orbits of charged particles are stable. For geodesic orbits, all derivatives vanish, so the orbits are in the state of indifference. From (2.318) follows that photons must fulfill $L/\sigma = \pm E$. Therefore, for the coordinate angular velocity of photons $\Omega = \mathrm{d}\phi/\mathrm{d}t$ we now have $\Omega = \pm 1/\sigma$.

For the toroidal interpretation of the metric, stationary circular orbits in the ζ direction with $\phi = \text{const.}$ correspond to orbits in planes $z = \text{const.}$ of the axial homogeneous solution as discussed in Sec. 2.2 due to the relatedness of the two spacetimes.

The boost Killing vector yields the constant $\phi\dot{t} - t\dot{\phi}$, which is applicable for both uncharged and charged particles. We can then write

$$\phi(t) = \frac{L}{\sigma^2 E}\, t + \phi_0 \mod 2\pi\,. \tag{2.319}$$

The two rotational Killing vectors produce constants valid only for uncharged particles,

$$\begin{aligned} A &= \sin(z)\,\dot{r} + \sin(r)\cos(r)\cos(z)\,\dot{z}\,,\\ B &= \cos(z)\,\dot{r} - \sin(r)\cos(r)\sin(z)\,\dot{z}\,. \end{aligned} \tag{2.320}$$

We can use these constants to obtain the analogues of (2.121) and (2.122) from the axial spacetime of Sec. 2.2,

$$r(z) = \arctan\left(\frac{2\Lambda Z}{A\cos z - B\sin z}\right) \mod \pi\,, \tag{2.321}$$

$$\dot{r}(z) = A\sin z + B\cos z\,. \tag{2.322}$$

The theoretical results are compared to numerical integration of the equations of motion in Fig. 2.23.

As usual, the second-rank Killing tensors do not provide us with constants of motion independent from those gained from the Killing vectors and the normalization of the four-velocity.

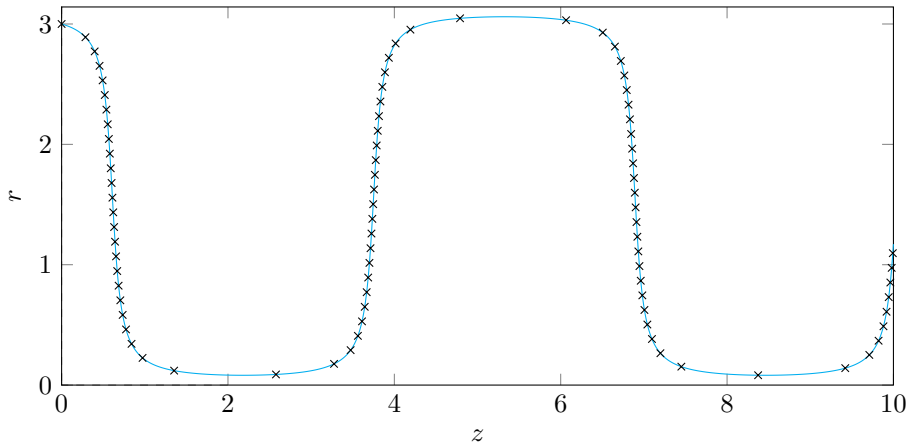

(a) The chart of $r(z)$ (2.321).

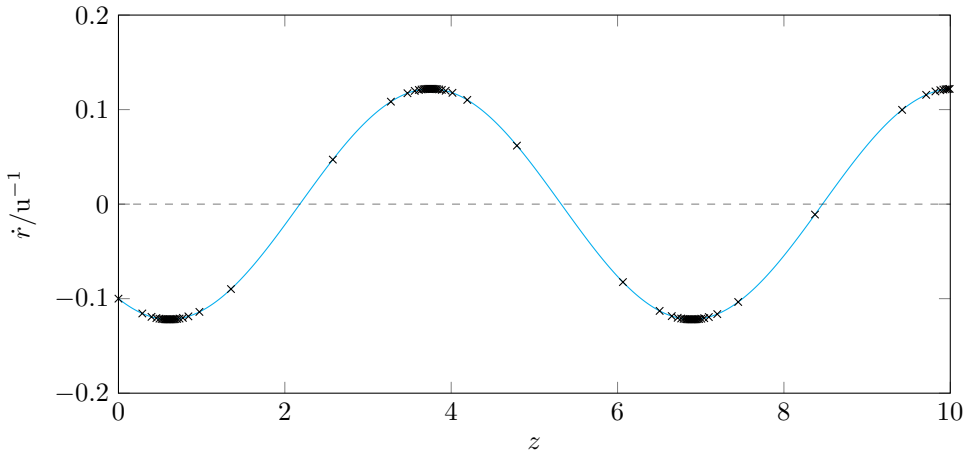

(b) The chart of $\dot{r}(z)$ (2.322).

Figure 2.23: The comparison of the cyan theoretical curves to the data points obtained by numerical integration of the equations of motion for a massive uncharged particle in the spacetime with $\Lambda = 1\,\mathrm{u}^{-2}$ and $\sigma = 1\,\mathrm{u}$. The relevant initial conditions are $r = 3$, $z = 0$, $\dot{r} = -0.1/\mathrm{u}$, and $\dot{z} = 0.5/\mathrm{u}$. The important constants of motion are $Z \approx 0.00498\,\mathrm{u}$, $A \approx -0.0699/\mathrm{u}$, and $B = -0.1/\mathrm{u}$. The shown range of z corresponds to the total proper time of approximately 85.6 u. Neighboring marks in the charts are 1 u of proper time apart.

Shell sources

The extrinsic curvature tensor (1.41) is

$$\mathbf{K} = \epsilon \sqrt{2\Lambda} \cot r \, \mathrm{d}Z^2 \tag{2.323}$$

and the projection of the electromagnetic tensor (1.44) is

$$\mathbf{F}_\perp = -\epsilon \sqrt{\Lambda} \, \mathrm{d}Z \,. \tag{2.324}$$

While the two above quantities are similar to those for the axial homogeneous spacetime, the proper circumference (1.3) of the hypersurface is the same as in the radial homogeneous solution and independent of r,

$$\mathcal{C} = 2\pi\sigma \,. \tag{2.325}$$

As in the axial solution, changing the direction of the normal corresponds to moving the hypersurface to $\pi - r$ as far as $\mathbf{K}$ is concerned, only the sign of $\mathbf{F}_\perp$ changes. The trace K is the same as in the axial case, $K = \epsilon \sqrt{2\Lambda} \cot r$, which notably means that it diverges at the endpoints of the interval of r even though $g_{\phi\phi}$ is constant (and non-zero) here. Instead, g_{zz} vanishes there. This suggests that the toroidal interpretation of the coordinates may be preferable to the cylindrical one. We then have a toroidal shell, and a diverging extrinsic curvature is to be expected when the minor radius of a torus approaches zero. However, for the sake of compatibility with the previous shells examined in this work, let us keep considering the shell to be cylindrical.

As with the other homogeneous spacetimes, not even this one admits a shell made of four particle streams on the interface of two instances of this solution. This time, the culprit is the relation $S_{TT} = -S_{\Phi\Phi}$ valid for these shells. It can be shown analytically that it is also not possible to find an interpretable shell leading to the Minkowski spacetime.

However, we found an interpretable shell connecting a part of this spacetime to a region of the Levi–Civita solution that does not contain the curvature singularity, as demonstrated in Fig. 2.24a. Levi–Civita's parameter σ lies at the very end of the extended physically-reasonable interval as discussed in Sec. 1.3.2. Note that as $\sigma > 1/2$, the connected region contains a non-regularizable axis at infinite radial coordinate, so it is not the asymptotic region. The induced three-current on the shell reads $\mathbf{s} = \sqrt{\Lambda}/4\pi \, \mathrm{d}Z$, which means we can use (1.58) to obtain the charge of the streams q.

Moreover, interpretable shells can also be found on the interface of the examined spacetime and the asymptotic region of the original Bonnor–Melvin spacetime. For the configuration in Fig. 2.24b, we select the higher possible value of the radial coordinate in the Bonnor–Melvin spacetime,

$$\rho_{BM} = \frac{2}{B^2\sigma} \left(1 + \sqrt{1 - B^2\sigma^2}\right), \tag{2.326}$$

and the induced three-current reads

$$\mathbf{s} = \frac{1}{4\pi} \left(\sqrt{\Lambda} \, \mathrm{d}Z - \left(1 + \frac{1}{4} B^2 \rho_{BM}^2\right)^{-2} B \, \mathrm{d}\Phi \right). \tag{2.327}$$

As neither of the spatial components vanishes, the four particle currents are grouped into two pairs with respect to the magnitude of electric charge they carry according to (1.63).

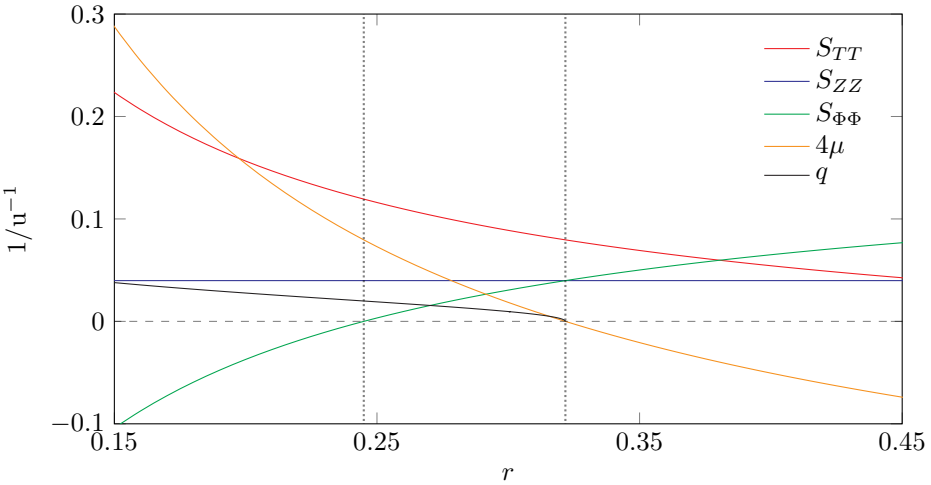

(a) The azimuthal homogeneous solution ($\Lambda = 0.5\,\mathrm{u}^{-2}$, $\sigma = 1\,\mathrm{u}$) and the Levi–Civita solution ($\sigma = 1$, $C = 1\,\mathrm{u}$). The singularity in the Levi–Civita spacetime is avoided.

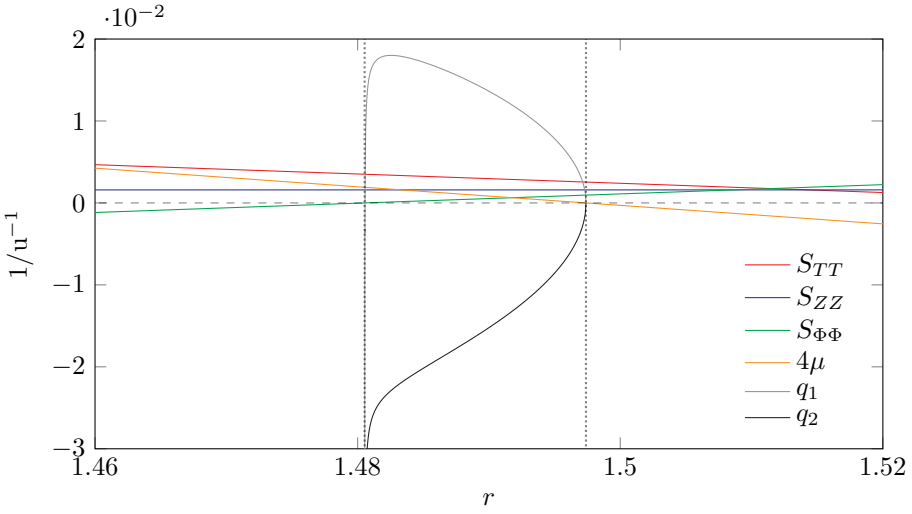

(b) The azimuthal homogeneous solution ($\Lambda = 1\,\mathrm{u}^{-2}$, $\sigma = 1\,\mathrm{u}$) and the Bonnor–Melvin solution ($B = 0.8/\mathrm{u}$).

Figure 2.24: The properties of shells on the interface of the azimuthal homogeneous solution and another spacetime, expressed as functions of the radial coordinate of the shell in the homogeneous solution. The spacetimes are aligned in such a way that the region with lower r in the homogeneous solution and the region with higher radial coordinate in the other spacetime are preserved. In both cases, the region admitting the four-stream interpretation of the shell is located between the two dotted lines and the value of S_{ZZ} does not depend on r.

2.8 Azimuthal inhomogeneous spacetime

Using the method described in Sec. 2.1.3, we can convert the axial inhomogeneous spacetime from Sec. 2.3 into a spacetime with an azimuthal magnetic field with the metric

$$\mathrm{d}s^2 = -r^2\mathrm{d}t^2 + \frac{\mathrm{d}r^2}{\mathfrak{M}(r)} + \mathfrak{M}(r)\,\mathrm{d}z^2 + r^2\mathrm{d}\phi^2. \tag{2.328}$$

The master function $\mathfrak{M}$ is the same as in the axial case,

$$\mathfrak{M}(r) = -\frac{\beta^2}{r^2} + \frac{\alpha}{r} - \frac{\Lambda}{3}r^2. \tag{2.329}$$

The magnetic field reads

$$\mathbf{F} = \frac{\beta}{r^2}\,\mathrm{d}r \wedge \mathrm{d}z \tag{2.330}$$

with the four-potential $\mathbf{A} = -\beta/r\,\mathrm{d}z$. The dual electric field is $\star\mathbf{F} = \beta\,\mathrm{d}t \wedge \mathrm{d}\phi$. The coordinates t and ϕ are dimensionless, while r and z, as well as the parameters α and β, have the dimension of length. The magnetic field's invariant is

$$F_{\mu\nu}F^{\mu\nu} = \frac{2\beta^2}{r^4} \tag{2.331}$$

and the Kretschmann scalar is

$$R_{\alpha\beta\gamma\delta}R^{\alpha\beta\gamma\delta} = \frac{4}{3r^8}\left(2\Lambda^2 r^8 + 9\alpha^2 r^2 - 36\alpha\beta^2 r + 42\beta^4\right). \tag{2.332}$$

Both expressions are the same as those in Sec. 2.3 and 2.6. It is again reasonable to consider only positive values of r, as negative values correspond to the opposite sign of α. The local properties of the spacetime are the same as in the axial inhomogeneous solution of Sec. 2.3.

Since the sign of $\mathfrak{M}$ affects the signature of the metric like in the axial case, the analysis performed in Sec. 2.3 is valid here as well. For $\Lambda < 0$ the coordinate r can always take on values from a left-bounded interval. For $\Lambda > 0$ the threshold value of

$$\alpha_{\mathfrak{M}} = \frac{4}{3}\,|\beta|^{3/2}\,\Lambda^{1/4} \tag{2.333}$$

gives the lower bound on the value of the parameter α that valid spacetimes must respect, $\alpha > \alpha_{\mathfrak{M}}$. Then, the range of r is given by the interval bounded by the positive roots of $\mathfrak{M}$. For illustration we refer the reader to Fig. 2.3 in Sec. 2.3.

The spacetime is almost everywhere type D. At the hypersurface $r = 2\beta^2/\alpha$ and in the limit $r \to \infty$ (if these radial coordinates are valid in the particular spacetime), the solution is of type O. There are four Killing vector fields corresponding to the three translational symmetries and boost in the ϕ direction, yielding the $ISO(1,1) \times E(1)$ group of isometries, and the solution belongs to the Kundt class like its axial counterpart.

Unlike the axial solution of Sec. 2.3, the endpoints of the interval of r do not correspond to the spacetime's axes. The axis would be located at $r = 0$, which lies outside the allowed range of r. Therefore, the axis is not located within the spacetime and we do not need to apply the procedure from Sec. 1.1.1 to regularize it. Instead, at the endpoints of the interval the metric element g_{zz} vanishes and

for $t = \text{const.}$ the spacetime resembles a flat ring there. Note that if we did not opt to limit the interval of r, the metric would change its signature as the radial coordinate would cross the points where $\mathfrak{M} = 0$. While we do not admit such a possibility in this thesis, we intend to study the signature change in our future work.

Analogously to the homogeneous case, a toroidal interpretation of the metric with a periodic coordinate ζ replacing z may be in order here. Again, ζ represents rotation around the tube, with the minor radius being $\sqrt{\mathfrak{M}(r)}$ this time. However, as $g_{\phi\phi}$ and, therefore, also the proper circumference along the ϕ direction depend on r too, the geometry is harder to visualize now.

Like in the axial spacetime, for $\Lambda < 0$ the asymptotic region extends to infinite proper radial distance. Considering the leading term of $\mathfrak{M}$ in the asymptotic region, we may recover the anti-de Sitter metric (2.148) using an analogous transformation as in Sec. 2.3.

Note that alongside the axial inhomogeneous solution, the azimuthal variant (with $\Lambda < 0$) too is briefly discussed in Dias and Lemos [2002]. The paper also presents a generalization of the spacetime with added linear momentum in the z direction.

Particle motion

Moving on to electrogeodesics, the three constants of motion are

$$E = r^2 \dot{t}\,, \tag{2.334}$$

$$L = r^2 \dot{\phi}\,, \tag{2.335}$$

$$Z = \mathfrak{M}(r)\,\dot{z} - \frac{\beta\kappa}{r}\,. \tag{2.336}$$

We can then establish the effective potential for radial motion

$$V(r) = \frac{\mathfrak{M}(r)}{2}\left(-\delta - \frac{E^2 - L^2}{r^2}\right) + \frac{1}{2}\left(\frac{\beta\kappa}{r} + Z\right)^2, \tag{2.337}$$

which satisfies $\dot{r}^2/2 = -V$. The separated potential (1.12) reads

$$W^2(r) = E^2 + \frac{2r^2}{\mathfrak{M}(r)}V(r) = -r^2\delta + L^2 + \frac{r^2}{\mathfrak{M}(r)}\left(\frac{\beta\kappa}{r} + Z\right)^2. \tag{2.338}$$

These potentials differ from (2.158) and (2.159) only by the change $Z \leftrightarrow L$.

Regarding the limits of the potentials, the conclusions from Sec. 2.3 are valid here as well, as long as we remember to exchange $Z \leftrightarrow L$. The limits $\mathfrak{M} \to 0^+$ generally diverge to positive infinity, so most particles are turned back when approaching r_a such that $\mathfrak{M}(r_a) = 0$. However, particles with $Z = -\beta\kappa/r_a \equiv Z_a$ are not turned back, and for them we have $V \to 0$. Further, it must hold that $E^2 \geq -\delta r_a^2 + L^2$ so that the potential is negative in the vicinity of r_a, thus allowing particle motion. If the equality is valid, further conditions from the series expansion of V at r_a follow. For $\Lambda < 0$, in the limit $r \to \infty$ the potential diverges for massive particles with $\delta = -1$. On the other hand, some photons may escape into radial infinity if the limit

$$\lim_{r\to\infty} V(r)\Big|_{\delta=0} = \frac{-\Lambda}{6}\left(-E^2 + L^2\right) + \frac{Z^2}{2} \tag{2.339}$$

is negative for them.

Stationary circular orbits, however, differ considerably from those examined in Sec. 2.3. First, to prevent motion along the z axis at a particular r_0, we need to have

$$Z|_{\dot{z}=0} = -\frac{\beta\kappa}{r_0}\,. \tag{2.340}$$

We then have

$$V(r_0)\Big|_{\dot{z}=0} = \frac{\mathfrak{M}(r_0)}{2}\left(-\delta - \frac{E^2-L^2}{r_0^2}\right) \tag{2.341}$$

and

$$V'(r_0)\Big|_{\dot{z}=0} = \frac{1}{6r_0^3}\left(12\beta^2 - 9\alpha r_0\right)\left(-\delta - \frac{E^2-L^2}{r_0^2}\right) - \frac{\mathfrak{M}(r_0)\,\delta}{r_0}\,. \tag{2.342}$$

Discounting first the case of $\mathfrak{M}(r_0) = 0$, we set the potential equal to zero to see that orbiting particles must fulfill $L^2 = E^2 + \delta r_0^2$. Inserting that into the derivative, the first term vanishes, so the second term must be zero at a particular r_0 to allow an orbit there. This is never possible to achieve for massive particles, but for photons with $\delta = 0$ the second term is identically zero. This means that while there cannot be any massive orbiting particles in the spacetime, photons can orbit at any valid r. Their coordinate angular velocity $\Omega = \mathrm{d}\phi/\mathrm{d}t$ is ± 1, just like in the previous section. Noting that photons have $\kappa = 0$, the second (and any other higher) derivative of the potential vanishes for them, which means the orbits are in a state of indifference. On the other hand, if $\mathfrak{M}(r_0) = 0$ and so r_0 corresponds to a finite endpoint of the allowed interval of the radial coordinate, even massive particles with appropriate constants of motion are apparently able to orbit there, because the troublesome second term in (2.342) vanishes. However, full analysis is difficult in the used coordinate system because the metric changes its signature there. We leave this question for our follow-up work mentioned earlier.

Like in the homogeneous case, if we want to consider the toroidal interpretation of the coordinates, the ζ coordinate corresponds to ϕ of the axial inhomogeneous solution if we omit the parameter σ that is specific to the axial spacetime. Therefore, orbits in the ζ direction correspond fully to the orbits studied in Sec. 2.3 with $\sigma = 1\,\mathrm{u}$.

This solution, too, has its analogy of the boost Killing vector field from the homogeneous spacetime, which yields the constant $r^2\big(\phi\dot{t} - t\dot{\phi}\big)$, also valid for charged particles. We can then obtain the counterpart to (2.319),

$$\phi(t) = \frac{L}{E}\,t + \phi_0 \mod 2\pi\,. \tag{2.343}$$

Unfortunately, not even this last solution apparently admits second-rank Killing tensors that produce independent constants of motion.

Shell sources

As in the homogeneous counterpart, the extrinsic curvature tensor (1.41)

$$\mathbf{K} = \epsilon\left(\frac{\sqrt{\mathfrak{M}(r)}}{r}\left(-\mathrm{d}T^2 + \mathrm{d}\Phi^2\right) + \frac{1}{2}\,\frac{\mathfrak{M}'(r)}{\sqrt{\mathfrak{M}(r)}}\,\mathrm{d}Z^2\right) \tag{2.344}$$

and the projection of the electromagnetic tensor (1.44)

$$\mathbf{F}_\perp = -\frac{\epsilon\beta}{r^2}\,\mathrm{d}Z \tag{2.345}$$

are similar to those for the corresponding axial solution, while the proper circumference (1.3) of the hypersurface is the same as in the radial inhomogeneous solution,

$$\mathcal{C} = 2\pi r\,. \tag{2.346}$$

Also like in the radial solution the circumference's derivative with respect to the proper radius r_p is not constant, but instead

$$\frac{\mathrm{d}\mathcal{C}}{\mathrm{d}r_p} = 2\pi\sqrt{\mathfrak{M}(r)}\,, \tag{2.347}$$

which vanishes at the endpoints of the interval of r. Note that the notion of the shell's proper radius is not well defined here, as the axis that would be located at $r = 0$ lies well outside the allowed range of r, so we cannot measure distance to it. Instead, we may replace the proper radius with the proper radial distance to the lower endpoint of the interval of r in the derivative and it becomes well defined again as the rate of change of the shell's proper circumference when an invariant normal characteristic size changes. The trace K is again the same as in the corresponding axial solution, (2.175), so it diverges as we approach the points where $\mathfrak{M}(r) = 0$. Like in the case of the homogeneous spacetime, this is an argument in favor of the toroidal interpretation of the coordinates, as this divergence corresponds to a vanishing minor radius of the now-toroidal shell. Another argument in favor of the toroidal interpretation is that even though the spacetime does not admit the value $r = 0$, it would correspond to a vanishing circumference of circles along the tube of the torus and the scalar would diverge there as well. Nonetheless, in the following we shall retain the cylindrical interpretation so that we can consider shells leading to the other spacetimes discussed in this work.

As for the previous solution, all shells between two instances of this spacetime have $S_{TT} = -S_{\Phi\Phi}$ regardless of their particular configuration, which means these shells cannot be interpreted using four particle streams. The same is also true for all shells connecting the inhomogeneous spacetime to the previous homogeneous one.

For $\Lambda > 0$, we found an interpretable shell connecting a part of this solution with the axis at higher r to a part of the Minkowski spacetime (Fig. 2.25a) and the Bonnor–Melvin spacetime (Fig. 2.25b), both also containing the axis. For the latter connection, we have to select the lower value of the radial coordinate in the Bonnor–Melvin solution,

$$\rho_{BM} = \frac{2}{B^2 r}\left(1 - \sqrt{1 - B^2 r^2}\right), \tag{2.348}$$

and the induced three-current

$$\mathbf{s} = \frac{1}{4\pi}\left(-\frac{\beta}{r^2}\,\mathrm{d}Z + \left(1 + \frac{1}{4}B^2\rho_{BM}^2\right)^{-2} B\,\mathrm{d}\Phi\right) \tag{2.349}$$

requires two pairs of streams to carry different charge determined by (1.63). In the other two subfigures of Fig. 2.25, the induced three current has only one non-zero element, $s_Z = -\beta/4\pi r^2$, which allows us to use (1.58) to compute particle charge q.

For $\Lambda < 0$, the only spacetime we managed to find a connection to through an interpretable shell was the part of the Levi–Civita solution that contains the (singular) axis. Properties of a shell connecting it to the asymptotic region of the examined solution can be found in Fig. 2.25c. Note that the negative value of σ in the Levi–Civita solution does not admit a physically-realistic source as mentioned in the corresponding Sec. 1.3.2.

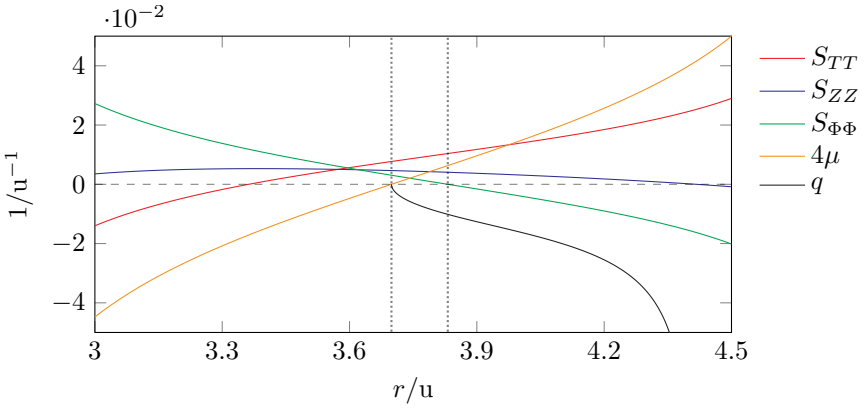

(a) The azimuthal inhomogeneous solution ($\Lambda = 0.2\,\mathrm{u}^{-2}$, $\beta = 6\,\mathrm{u}$, $\alpha = 15\,\mathrm{u}$) and the Minkowski spacetime.

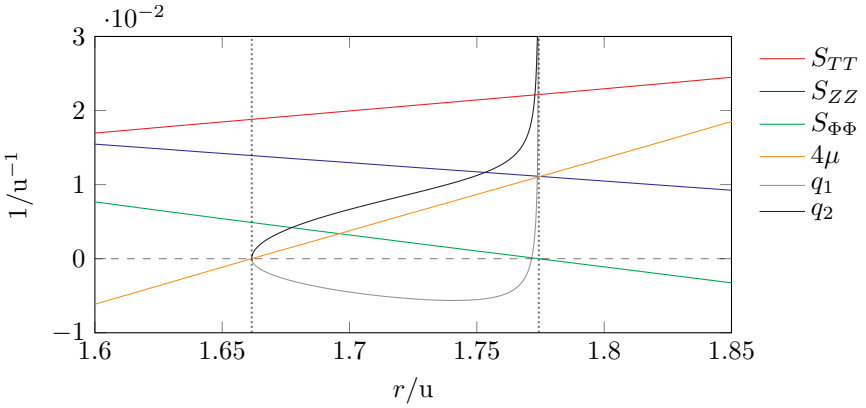

(b) The azimuthal inhomogeneous solution ($\Lambda = 0.4\,\mathrm{u}^{-2}$, $\beta = 1.5\,\mathrm{u}$, $\alpha = 3\,\mathrm{u}$) and the Bonnor–Melvin spacetime ($B = 0.05/\mathrm{u}$).

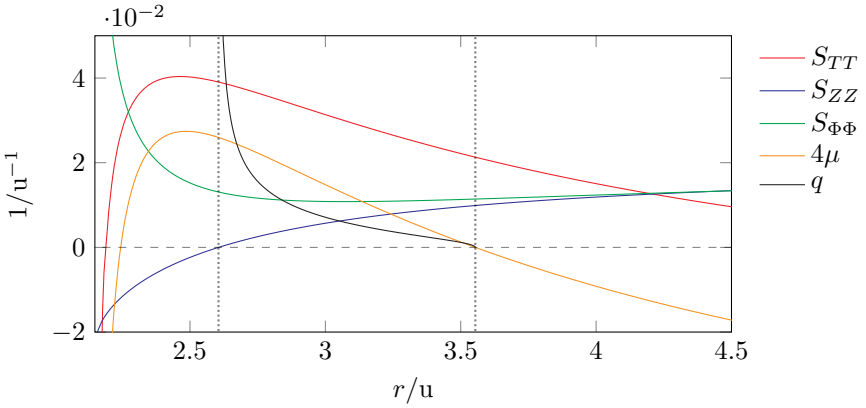

(c) The azimuthal inhomogeneous solution ($\Lambda = -0.2\,\mathrm{u}^{-2}$, $\beta = -2\,\mathrm{u}$, $\alpha = 1.2\,\mathrm{u}$) and the Levi–Civita spacetime ($\sigma = -0.5$, $C = 1.5\,\mathrm{u}$). The preserved axis of the Levi–Civita spacetime is singular.

Figure 2.25: The properties of shells connecting the azimuthal inhomogeneous solution to all of the spacetimes of Sec. 1.3, expressed as functions of the radial coordinate of the shell in the azimuthal solution. The spacetimes are always aligned in such a way that the region with higher r of the azimuthal spacetime and the region with the axis of the other solution are preserved. In all cases, the region admitting the four-stream interpretation of the shell is located between the dotted lines.

3. Miscellanea

3.1 Additional remarks on shell sources

When examining individual solutions, we tried to find shell sources with reasonable properties using Israel's formalism explained in Sec. 1.2.2. On the other side of the hypersurface, we considered another instance of the same solution and the well-known 'historical' spacetimes of Sec. 1.3. For the inhomogeneous solutions we also examined shells leading to their corresponding homogeneous counterparts. Now that all cylindrical solutions of interest to us have been properly introduced, we can consider shells that connect different examined solutions together regardless of the alignment of their respective magnetic fields.

It turns out that the only connections mixing our spacetimes together that never admit interpretable shells are those between the three homogeneous spacetimes. All shells on the interface of the axial and radial homogeneous spacetimes fulfill $S_{ZZ} = -2\mu = S_{\Phi\Phi} - S_{TT}$; on the interface of the axial and azimuthal solutions $S_{TT} = 2\mu = -S_{ZZ} - S_{\Phi\Phi}$; and on the interface of the radial and azimuthal spacetimes $S_{\Phi\Phi} = -2\mu = S_{ZZ} - S_{TT}$. None of these hypersurfaces is able to satisfy the conditions imposed on a shell made of four particle currents, namely $S_{TT} > 0$, $\mu > 0$, $S_{ZZ} \geq 0$, and $S_{\Phi\Phi} \geq 0$, as explained in Sec. 1.2.2.

Every other spacetime pair that has not been yet discussed admits an interpretable shell for one or more particular configurations of the two solutions. Up until this point we usually supported our claims with appropriate charts, but we have to draw a line here in order not to overwhelm the reader with figures that, frankly, appear quite similar to each other for the most part. Instead, we shall provide charts for and discuss only the most interesting cases. All of our results are then summarized in Table 3.1 at the very end of this section.

Most of the charts we shall provide here may not seem unusual by themselves, but they will be of interest once we start discussing their mass per unit length later in this section. First, there is Fig. 3.1, which depicts shells that involve the radial homogeneous solution. The shell of Fig. 3.1a connects it to the radial Bonnor–Melvin solution and has atypically low mass despite belonging to a singular spacetime. On the other hand, the shell of Fig. 3.1b, which connects the radial homogeneous spacetime to the azimuthal inhomogeneous solution, along with the four connections of the axial inhomogeneous spacetime presented in Fig. 3.2, has higher mass than expected, even though there are no singularities in the composite spacetimes. Finally, Fig. 3.3 depicts a shell on the interface of the Bonnor–Melvin–Λ and radial Bonnor–Melvin solutions, the unit mass of which can cross the threshold value. These figures serve to show us that there is nothing manifestly peculiar about the other properties of the shells that would set them apart at first glance from the shells we examined previously.

The chart in Fig. 3.4, however, is more remarkable. It concerns a shell on the interface of the radial inhomogeneous solution and the radial Bonnor–Melvin spacetime. While neither the region admitting interpretable shells nor the shells' mass per unit length are particularly exciting, it is interesting to observe the behavior of shells outside of the interpretable region. We use the radial coordinate of the radial Bonnor–Melvin solution ρ as the independent variable in the chart.

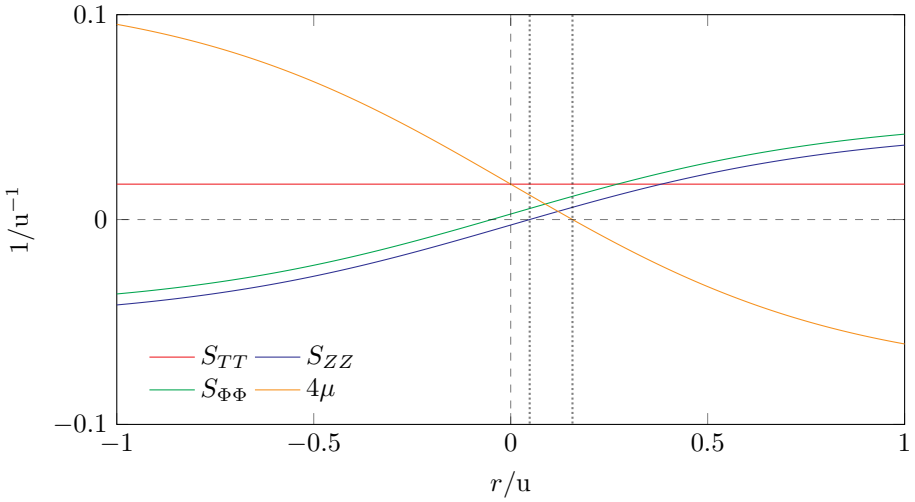

(a) The radial homogeneous solution ($\Lambda = -0.7\,\mathrm{u}^{-2}$, $\sigma = 0.5\,\mathrm{u}$) and the radial Bonnor–Melvin spacetime ($\alpha = 0.02/\mathrm{u}$, $\sigma = 6\,\mathrm{u}$). The region admitting the four-stream interpretation of the shell is located between the dotted lines. The streams are uncharged.

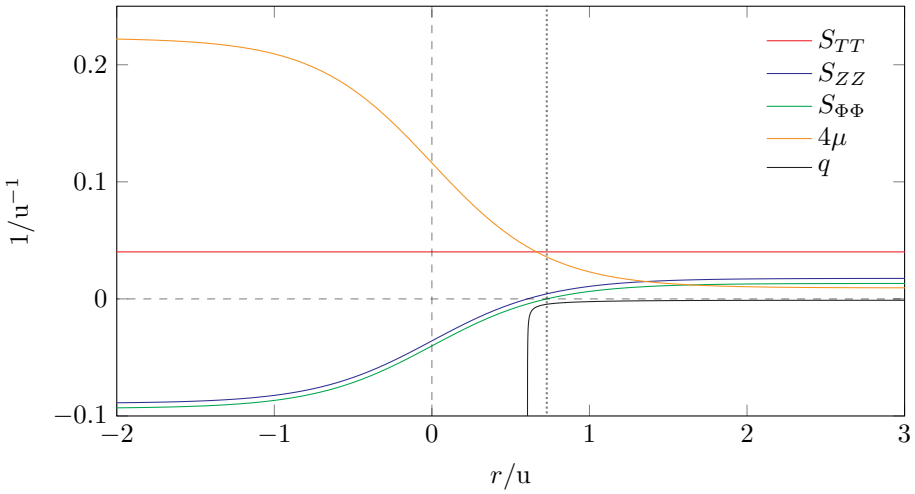

(b) The radial homogeneous spacetime ($\Lambda = -0.9\,\mathrm{u}^{-2}$, $\sigma = 5\,\mathrm{u}$) and the azimuthal inhomogeneous solution ($\Lambda = -0.7\,\mathrm{u}^{-2}$, $\beta = -2\,\mathrm{u}$, $\alpha = -3\,\mathrm{u}$). The region admitting the four-stream interpretation of the shell is located to the right of the dotted line. The induced three-current on the shell has one non-zero element, $s_Z = \beta/4\pi\sigma^2$, which allows us to use (1.58) to compute particle charge q.

Figure 3.1: The properties of shells on the interface of the radial homogeneous solution and another spacetime, expressed as functions of the radial coordinate of the shell in the homogeneous solution. In both cases, the value of S_{TT} does not depend on r and the spacetimes are aligned in such a way that the region with positive radial infinity in the homogeneous solution and the region with the axis at lower radial coordinate in the other spacetime are preserved.

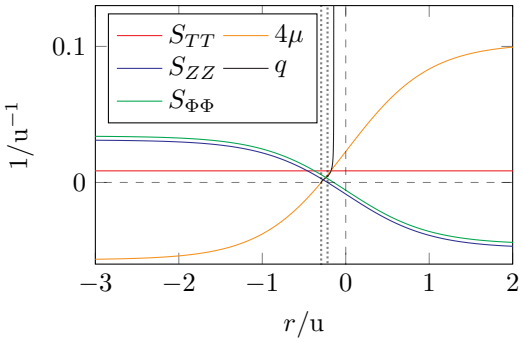

(a) The region with the axis at lower radial coordinate of the axial inhomogeneous solution ($\Lambda = 10^{-3}\,\mathrm{u}^{-2}$, $\beta = 8\,\mathrm{u}$, $\alpha = 11\,\mathrm{u}$, $\sigma = 10\,\mathrm{u}$) connected to the radial homogeneous spacetime ($\Lambda = -0.5\,\mathrm{u}^{-2}$, $\sigma = 5\,\mathrm{u}$).

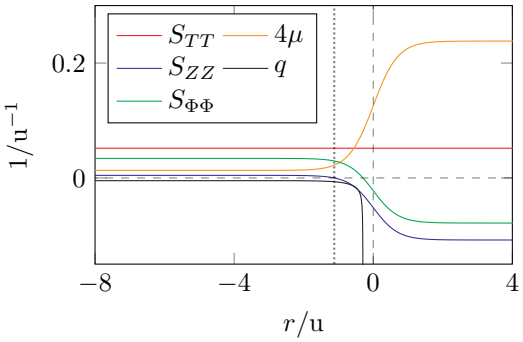

(b) The region with the axis at lower radial coordinate of the axial inhomogeneous solution ($\Lambda = -0.5\,\mathrm{u}^{-2}$, $\beta = -4\,\mathrm{u}$, $\alpha = 2\,\mathrm{u}$, $\sigma = 10\,\mathrm{u}$) connected to the radial homogeneous spacetime ($\Lambda = -1\,\mathrm{u}^{-2}$, $\sigma = 9\,\mathrm{u}$). The four-stream interpretation of the shell is possible in the region to the left of the dotted line.

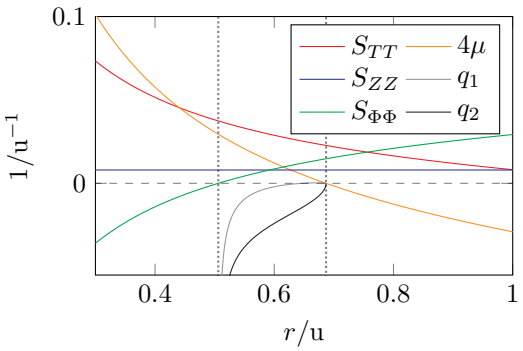

(c) The region with the axis at higher radial coordinate of the axial inhomogeneous solution ($\Lambda = 0.4\,\mathrm{u}^{-2}$, $\beta = 4.7\,\mathrm{u}$, $\alpha = 19\,\mathrm{u}$, $\sigma = 3\,\mathrm{u}$) connected to the azimuthal homogeneous spacetime ($\Lambda = 0.2\,\mathrm{u}^{-2}$, $\sigma = 5\,\mathrm{u}$).

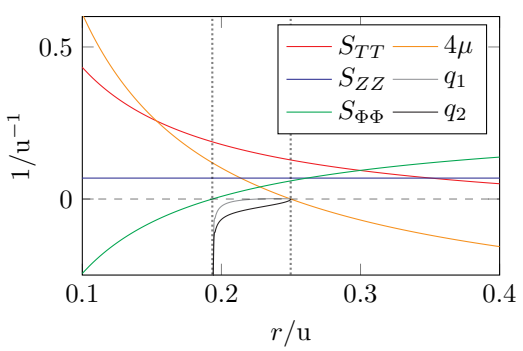

(d) The asymptotic region of the axial inhomogeneous solution ($\Lambda = -0.3\,\mathrm{u}^{-2}$, $\beta = 0.4\,\mathrm{u}$, $\alpha = 5\,\mathrm{u}$, $\sigma = 2\,\mathrm{u}$) connected to the azimuthal homogeneous spacetime ($\Lambda = 0.8\,\mathrm{u}^{-2}$, $\sigma = 5\,\mathrm{u}$). This is the only solution without a conical defect in the axial spacetime.

Figure 3.2: The properties of shells on the interface of the axial inhomogeneous solution and the radial or azimuthal homogeneous solution, expressed as functions of the radial coordinate of the shell in the given homogeneous spacetime, which always keeps the region with lower values of r. Unless stated otherwise, the four-stream interpretation of the shell is possible in the region between the dotted lines.

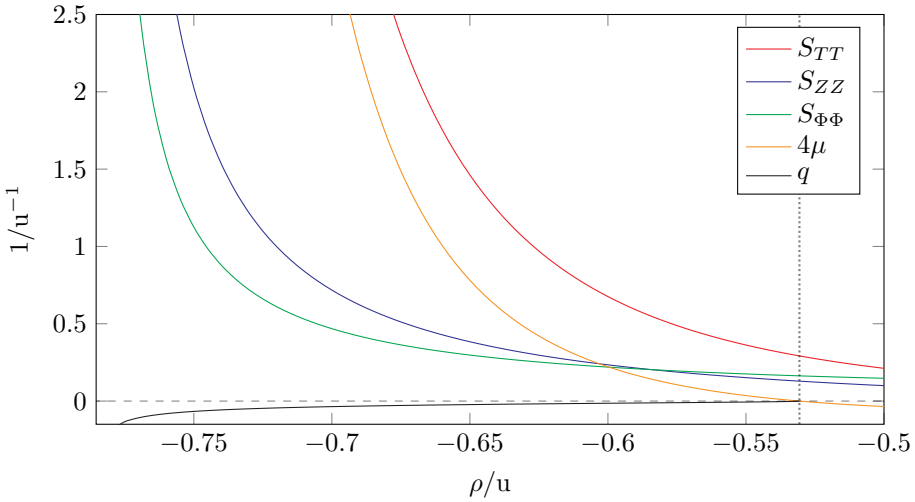

Figure 3.3: The properties of shells on the interface of the Bonnor–Melvin–Λ solution ($\Lambda = 0.5\,\mathrm{u}^{-2}$) and the radial Bonnor–Melvin spacetime ($\alpha = 2/\mathrm{u}$, $\sigma = 0.8\,\mathrm{u}$), expressed as functions of the radial coordinate of the shell in the latter spacetime. The spacetimes are aligned in such a way that the region with higher r in BMΛ and the region containing the singular axis at $\rho \approx -0.785\,\mathrm{u}$ in the radial Bonnor–Melvin solution are preserved. The induced three-current on the shell has only one non-zero element, $s_\Phi = -\sqrt{\Lambda}/4\pi$, which allows us to use (1.60) to compute particle charge q in the region admitting the four-stream interpretation of the shell, located to the left of the dotted line.

We can see that some of the quantities related to the induced stress-energy tensor $\mathbf{S}$ reach their quite prominent extrema for a certain value of ρ that does not look significant in any way. Computing the radial coordinate in the radial inhomogeneous spacetime r, however, we see that this ρ corresponds to the maximum accessible value of r and that the shell is nearing the cosmological horizon in the inhomogeneous spacetime. Indeed, by examining the circumference $\mathcal{C}$ (2.199) of cylinders in the radial Bonnor–Melvin spacetime, we find that this particular value of ρ corresponds to the maximum of $\mathcal{C}$. This figure can be viewed as a reminder that we observe the properties of the shells from the point of view of one of the two connected spacetimes, but something interesting can be going on in the other one. While we should in general be able to choose the radial coordinate of either of the two spacetimes as the independent variable, expressing one radius often tends to be much easier than expressing the other in practice. Note that similar charts can also be produced for shells that connect the radial inhomogeneous solution to, e.g., the Bonnor–Melvin–Λ spacetime, probably because the circumference of the shell in the Bonnor–Melvin–Λ solution (2.125) is given by a formula similar to (2.199). Both functions have a global maximum and are monotonic on either side of it.

Speaking of the radial inhomogeneous solution, it should be pointed out that we were sadly not able to construct a single shell connecting the spacetime to any other solution considered in this work that would eliminate the singular axis. On the other hand, every valid shell for the radial Bonnor–Melvin spacetime eliminates one of its two singular axes. It may be possible to eliminate both of them through the use of multiple shells. Interestingly, out of all the investigated

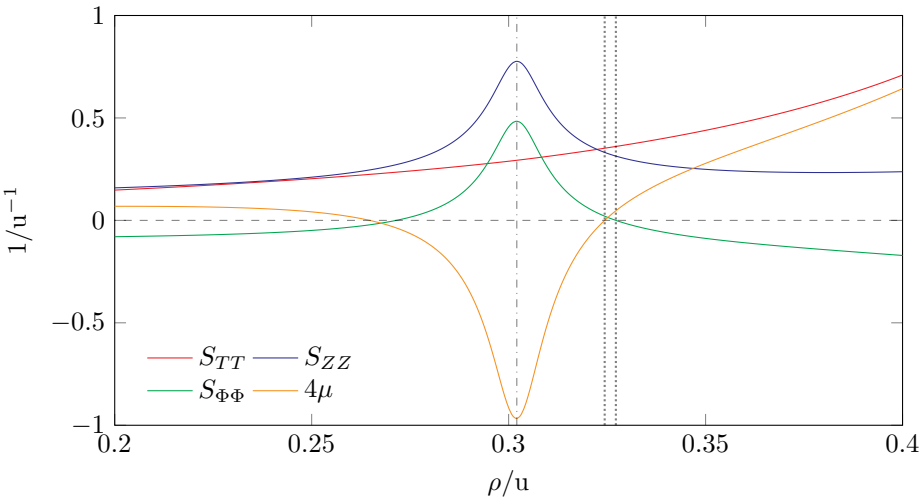

(a) The induced quantities on the shell.

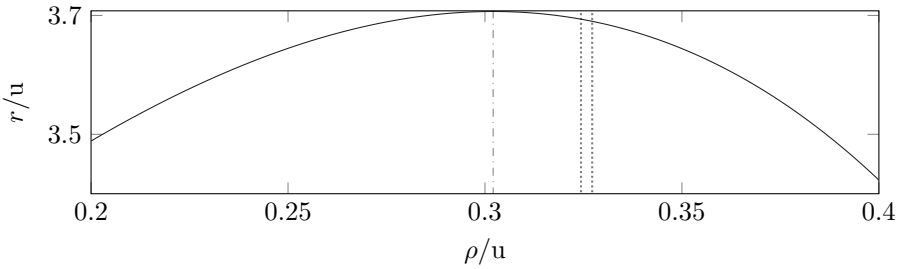

(b) The value of the radial coordinate r in the radial inhomogeneous solution needed to match the circumference of cylinders at a given ρ in the radial Bonnor–Melvin spacetime. Note that the maximal value at the vertical axis $r \approx 3.708\,\mathrm{u}$ corresponds to the cosmological horizon of the radial inhomogeneous solution.

Figure 3.4: The properties of shells on the interface of the radial Bonnor–Melvin solution ($\alpha = 2.6/\mathrm{u}$, $\sigma = 2.39\,\mathrm{u}$) and the radial inhomogeneous solution ($\Lambda = 0.3\,\mathrm{u}^{-2}$, $\beta = -0.6\,\mathrm{u}$, $\alpha = -5\,\mathrm{u}$), expressed as functions of the radial coordinate of the shell in the former spacetime. The spacetimes are aligned in such a way that the region with higher ρ in the radial Bonnor–Melvin solution and the region with the singular axis of the inhomogeneous spacetime are preserved. The region admitting the four-stream interpretation of the shell is located between the dotted lines. The shell is uncharged. Disregarding now the allowed region, note that some of the induced quantities on the shell tend to their (locally) extreme values when the shell approaches the cosmological horizon in the inhomogeneous solution, with the closest value of the radial coordinate marked by the dashdotted line. This value corresponds to the maximal circumference of cylinders in the considered radial Bonnor–Melvin spacetime.

solutions these two singular spacetimes appear to be the most congenial to be used in Israel's cut-and-paste formalism, as they are the only two examined spacetimes that admit shells compliant with our demands and sewn onto every other solution considered in this thesis.

Finally, note that, curiously, neither axial nor azimuthal magnetic field allow the homogeneous and its corresponding inhomogeneous solutions to be brought together through an interpretable shell, but it is possible to connect any pair of a homogeneous spacetime and an inhomogeneous one if their magnetic fields have different directions. Only radial magnetic field also admits an interpretable shell on the interface of the homogeneous and inhomogeneous solutions.

Our numerical computations suggest that at least one configuration for all the other pairs of spacetimes that were not explicitly discussed admits an interpretable shell. However, we did not find anything noteworthy about these configurations, so we shall settle for their brief summary in Table 3.1 only. Note that the table does not contain information about which regions of the solutions are preserved.

3.1.1 Mass per unit proper length

Now that all discovered interpretable shells related to the studied spacetimes have been introduced, it is time to turn our attention towards the shells' mass per unit proper length M_1 (1.65). We omitted that information when we discussed individual shells, because we believe that it is better to gather the data in one place. That place is the perhaps slightly confusing Fig. 3.5. In it, all curves of M_1 corresponding to every presented interpretable shell are plotted. We understand that having so many curves in one chart makes it difficult to find one's footing in it. However, we can more plainly see the prominence of the critical value of $M_1 = 1/4$ as talked about in Sec. 1.2.2 now. Žofka and Bičák [2007] claim that further conditions must be met if $M_1 = 1/4$ is to remain the upper bound of mass per unit length of cylinders in regular spacetimes when the cosmological constant is involved, but it is not clear what the conditions should be for our examined solutions, so we did not cater for them specifically. Nonetheless, we see that only a single shell has its unit mass cross (very slightly) the value of $M_1 = 1/4$ and not many more approach it at an extreme value of the shell's radial coordinate. Note that Žofka and Bičák [2007] discovered curves crossing the line when examining the cosmological variant of the Levi–Civita spacetime, which makes the rarity of that occurrence for our plethora of cosmological solutions rather surprising.

First, the shell of Fig. 3.3, which is the one crossing $M_1 = 1/4$, connects the Bonnor–Melvin–Λ and radial Bonnor–Melvin solutions, the latter of which does not include the cosmological constant but one of its two singularities prevails. While its unit mass is usually above the critical value, for an extreme value of coordinate radii it approaches $M_1 \to 0.248$, which itself is quite close to the threshold value. The two shells for which the `Maple` software determines the limit to be exactly $M_1 = 1/4$ are the connections of again the radial Bonnor–Melvin solution of Fig. 2.11a and the azimuthal inhomogeneous solution of Fig. 2.25a, in both cases to the Minkowski spacetime. Interestingly, the two composite solutions approach that value from the opposite sides of the chart, as the former spacetime is singular while the latter is regular. The two spacetimes also admit shells leading

to the original Bonnor–Melvin spacetime, which happen to have a limit close to $M_1 = 1/4$, but not quite, as $M_1 \to 0.252$ for Fig. 2.11b and $M_1 \to 0.247$ for Fig. 2.25b.

In the vast majority of cases, the shells in the considered composite spacetimes without any curvature singularities have $M_1 < 1/4$ and those with at least one of them have M_1 greater than the critical value[1] despite the fact that virtually all of them contain a non-zero cosmological constant on at least one side of the shell. The only non-cosmological connections are those of the radial Bonnor–Melvin solution of Sec. 2.4 either to another instance of itself of (2.207) or to the better-known spacetimes of Sec. 1.3 illustrated in Fig. 2.11. Note that in these cases, we have $M_1 > 1/4$ as expected, because there is always a curvature singularity present in the part (or parts) of the radial Bonnor–Melvin solution we keep.

The shells that do not conform to the divide mostly arise from connections of a pair of the cosmological solutions we study. The only deviant connection that involves an elder spacetime from Sec. 1.3 is that of Fig. 2.24a, where we connect a part of the singularity-free azimuthal homogeneous solution to a part of the Levi–Civita solution with a conical defect but not a curvature singularity. Note that the parameter σ of the Levi–Civita solution in this case lies at the upper boundary of the interval that admits realistic sources. We consider a value of σ lying outside that interval in Fig. 2.25c, but the preserved part of the Levi–Civita solution contains the singular axis anyway, so the obtained $M_1 > 1/4$ is not a cause for concern.

The other regular spacetimes with $M_1 > 1/4$ are the connection of the radial homogeneous and azimuthal inhomogeneous solutions of Fig. 3.1b, and the connections involving the axial inhomogeneous solution illustrated in Fig. 3.2, both to the radial or azimuthal homogeneous spacetimes. All of the individual spacetimes demonstrated the ability to admit an interpretable shell to another regular spacetime with $M_1 < 1/4$. Note that in Fig. 3.2, in three of the four considered connections the axial solution keeps a region with an axis, which in all cases involves a conical defect. However, the last shell does not contain the defect and still has $M_1 > 1/4$, and the connections of Fig. 2.7 have $M_1 < 1/4$ despite involving the defect. Therefore, the conical defect does not appear to play a key role with respect to M_1. This is corroborated by Bičák and Žofka [2002], which states that introducing a conical defect to the Minkowski spacetimes connected to the asymptotic part of the Levi–Civita solution does not have any major repercussions for the shells.

There is only one only singular connection with $M_1 < 1/4$, namely that of Fig. 3.1a, where we connect a part of the radial Bonnor–Melvin solution (which must always contain a singularity) and a part of the radial homogeneous solution. As noted in Sec. 1.2.2, the papers cited there do not say that singular connections must fulfill $M_1 > 1/4$. However, since it is the only discovered singular case with a below-critical M_1, it merits a dashed curve in Fig. 3.5 nevertheless. Note that this configuration can also yield a shell with $M_1 > 1/4$ for different parameters of the two involved spacetimes.

In Table 3.1 summarizing all shells corresponding to all pairs of the examined spacetimes, we also list whether their mass per unit length is lower or greater than $M_1 = 1/4$.

[1] Recall, however, that only regular spacetimes are expected to respect the threshold value.

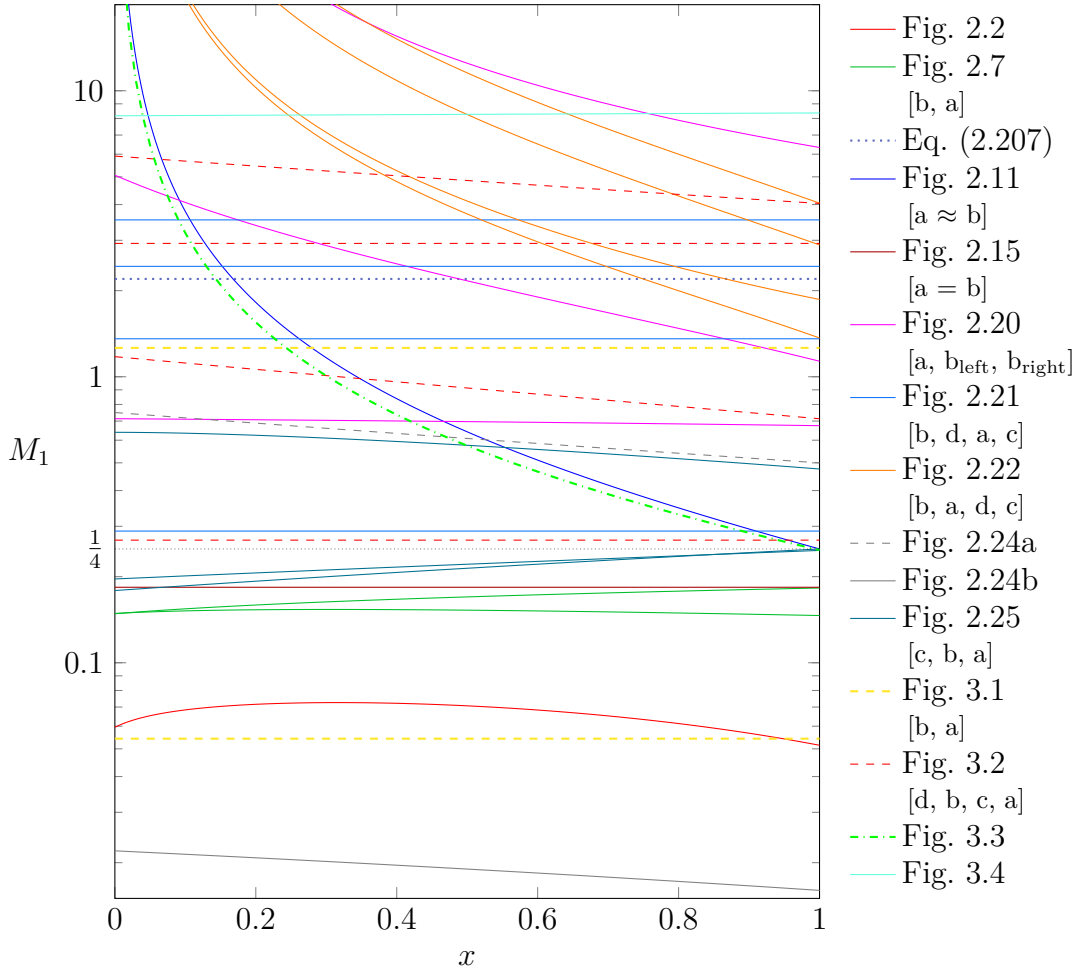

Figure 3.5: The chart of mass per unit length M_1 for every interpretable shell considered in this work. The independent variable x is the rescaled coordinate radius of the shell, $r = r_{\min} + (r_{\max} - r_{\min})\, x$, so that the value $x = 0$ corresponds to the minimal admissible radius $r_{\min}$ and $x = 1$ to the maximal radius $r_{\max}$. Note that the charts where the interval of the permitted coordinate radii is not bounded all have a constant value of M_1. For the sake of completeness, we also plot the value of M_1 for the shell connecting two instances of the radial Bonnor–Melvin solution (2.207) even though its radii are fixed. Except for this case, the legend entries refer to the figure showing the other properties of the corresponding shell. If there are multiple configurations presented in the same figure, the color of the curves remains the same and the legend entry lists the subfigures that share the style of their curves in the order of descending M_1. Note that the curves for Fig. 2.11a and 2.11b overlap almost perfectly, so we plot only the former one. Also note that while the legend entry implies that Fig. 2.25b has higher M_1 than Fig. 2.25a, the latter has the slightly higher limit of $M_1 \to 1/4$ for $x \to 1$. When approaching $x \to 1$, the dash-dotted curve for Fig. 3.3 crosses the critical value of $M_1 = 1/4$. The dashed curves are located in their entirety on the opposite side of the critical value than expected.

	BMΛ	Ax. in.	Rad. BM	Rad. h.	Rad. in.	Az. h.	Az. in.	Mink.	LC	BM
BMΛ (Sec. 2.2)	✗	✗	Fig. 3.3 S (±)	✗	✓ S (+)	✗	✓ R (−)	✗	Fig. 2.2 R (−)	✗
Ax. in. (Sec. 2.3)		✗	✓ S (+)	Fig. 3.2a, b CD (+)	✓ S (+)	Fig. 3.2c, d CD/R (+)	✓ CD (−)	✗	Fig. 2.7 CD (−)	✗
Rad. BM (Sec. 2.4)			Eq. (2.207) S (+)	Fig. 3.1a S (±)	Fig. 3.4 S (+)	✓ S (+)	✓ S (+)	Fig. 2.11a S (+)	✓ S (+)	Fig. 2.11b S (+)
Rad. h. (Sec. 2.5.1)				✗	Fig. 2.21 S (+)	✗	Fig. 3.1b R (+)	✗	✗	Fig. 2.15 R (−)
Rad. in. (Sec. 2.6)					Fig. 2.20 S (+)	✓ S (+)	✓ S (+)	Fig. 2.22 S (+)	✓ S (+)	✓ S (+)
Az. h. (Sec. 2.7)						✗	✗	✗	Fig. 2.24a CD (+)	Fig. 2.24b R (−)
Az. in. (Sec. 2.8)							✗	Fig. 2.25a R (−)	Fig. 2.25c S (+)	Fig. 2.25b R (−)

Table 3.1: Information about shells on the interface of every pair of spacetimes considered in this work. In every cell that corresponds to a shell that admits the desired four-particle-stream interpretation, there is either a check mark (✓) or a reference to the corresponding figure if we provided one. If a particular pair of solutions does not admit an interpretable shell, the corresponding cell contains a cross mark (✗). Furthermore, we also note whether the syncretic spacetimes are completely regular (R) or if they contain a conical defect but no curvature singularities (CD) or if there is at least one curvature singularity (S). The (±) signs denote whether the shell's mass per unit length is greater (+) or lower (−) than the prominent value of $M_1 = 1/4$. The unit mass of the shell of Fig. 3.3 connecting the Bonnor–Melvin–Λ and radial Bonnor–Melvin spacetimes crosses the value of $M_1 = 1/4$. For the connections of the radial homogeneous and the radial Bonnor–Melvin spacetimes, the shell in Fig. 3.1a has $M_1 < 1/4$, but we also found shells with $M_1 > 1/4$. Note that their unit mass does not depend on the shell's radius. The connection of the axial inhomogeneous and azimuthal homogeneous solutions of Fig. 3.2c contains an axis with a conical defect in the former spacetime, while the shell in Fig. 3.2d leads to the regular asymptotic region.

3.2 General numerical solutions

The cosmological solutions examined in this work contain additional symmetries, which prevents them from being the most general static, cosmological, cylindrical spacetimes with a magnetic field. While we were not able to solve the relevant equations analytically (provided they have a closed-form solution in the first place), it is possible to examine the equations numerically to assess some of the properties that the general metric should have. To that end, we shall take advantage of the `Mathematica` software to find numerical solutions to the system (2.7)–(2.10) for the axial (or azimuthal) magnetic field and (2.65)–(2.68) for the radial case to determine the metric functions in our original ansatz (1.1).

More precisely, in each set we use the last equation to substitute f^2 into the previous ones, which yields a set of three equations for A', B', and C' as functions of the radial coordinate[2]. The equations are of second order, so as initial conditions we have to choose the values of the three functions and their first derivatives at a particular r. Since the radial coordinate does not explicitly appear in the system, we can shift it arbitrarily, which allows us to set the initial conditions always at $r = 0$. Moreover, as the system contains only derivatives of the metric functions, we can set $A(0)$, $B(0)$, and $C(0)$ arbitrarily without affecting their derivatives. We choose $A(0) = B(0) = C(0) = 0$ for simplicity, but these values are simply gauge and can be transformed away through a simple rescaling of a given coordinate by a constant factor[3]. Therefore, the interesting physical properties of the solution are determined by the initial derivatives $A'(0)$, $B'(0)$, and $C'(0)$, and the cosmological constant Λ, which is the only parameter appearing in the differential equations. We shall generate these four values randomly (discarding solutions with negative f^2) and catalog the resulting spacetimes by their properties, focusing on the number of axes and singularities. These families of solutions are then listed in two subsections pertaining to a particular orientation of the magnetic field.

In the charts demonstrating our results, we plot both the metric elements $g_{tt} = -\mathrm{e}^A$, $g_{zz} = \mathrm{e}^B$, and $g_{\phi\phi} = \mathrm{e}^C$ (recall that $g_{rr} = 1$), and the corresponding derivatives A', B', and C'. Moreover, to pinpoint curvature singularities we also plot $F_{\mu\nu}F^{\mu\nu} = 2f^2$ with f^2 computed from (2.10) or (2.68), as well as the Kretschmann scalar

$$R_{\alpha\beta\gamma\delta}R^{\alpha\beta\gamma\delta} = \frac{1}{4}\left((A')^4 + (B')^4 + (C')^4\right) + \left(A''(A')^2 + B''(B')^2 + C''(C')^2\right) + \left((A'')^2 + (B'')^2 + (C'')^2\right) + \frac{1}{4}\left((A')^2(B')^2 + (A')^2(C')^2 + (B')^2(C')^2\right). \quad (3.1)$$

Noting that the Ricci scalar

$$-R = \frac{1}{2}\left(A'B' + A'C' + B'C'\right) + \left((A')^2 + (B')^2 + (C')^2\right) + \left(A'' + B'' + C''\right) \quad (3.2)$$

[2]Note that the metric (1.1) has $g_{rr} = 1$, which means that the difference of the radial coordinate between two points corresponds to their proper radial distance.

[3]Forcing $C(r = 0) = 0 \leftrightarrow g_{\phi\phi}(r = 0) = 1$ may lead to a conical defect at an axis, which could have been avoided by choosing a different value of $C(0)$. A simple rescaling of the angular coordinate ϕ cannot affect the defect, but we can eliminate it if we simultaneously also redefine the bounds of the coordinate. Even though such a redefinition alters the spacetime, the metric and local physics stay the same. Therefore, we are not going to pay attention to conical defects in this section.

becomes $R = 4\Lambda$ for electrovacuum spacetimes, we use it to replace C'' for axial magnetic fields or A'' for radial magnetic fields in (3.1), which helps mitigate numerical fluctuations of the Kretschmann scalar in some cases.

3.2.1 Axial magnetic field

Boost-symmetric solutions

Before dealing with general initial conditions, let us see whether we are able to reproduce the two axial solutions of Sec. 2.2 and 2.3. What these spacetimes have in common is their boost symmetry in the t–z plane. To recover these solutions numerically, we set $A'(0) = B'(0)$. Because the system (2.7)–(2.10) is invariant under the transposition $A' \leftrightarrow B'$, considering the same initial conditions for these two functions ensures that we have $A(r) = B(r)$ in the whole domain.

First, considering non-zero values of the initial derivatives, we obtain solutions corresponding to the axial inhomogeneous spacetime of Sec. 2.3. The numerical spacetimes do not appear to contain any curvature singularities as the two monitored scalars do not seem to diverge anywhere. The case of $\Lambda > 0$ is depicted in Fig. 3.6a. The solution contains two axes as expected. For $\Lambda < 0$, there is an axis and an asymptotic region, in which the electromagnetic field invariant tends to zero and A', B', and C' all tend to the same constant, as illustrated in Fig. 3.6b. This means that a suitable rescaling of the coordinates by a constant factor could lead to $-g_{tt} = g_{zz} = g_{\phi\phi}$ as $r \to \infty$. Therefore, in the asymptotic region we have

$$\mathrm{d}s^2 = e^{2\alpha r}\left(-\mathrm{d}t^2 + \mathrm{d}z^2 + \mathrm{d}\phi^2\right) + \mathrm{d}r^2 \tag{3.3}$$

with a real constant α satisfying $2\alpha = A' = B' = C'$. Defining a new radial coordinate $x = \mathrm{e}^{-\alpha r}/\alpha$, the metric becomes the anti-de Sitter

$$\mathrm{d}s^2 = \frac{\alpha^{-2}}{x^2}\left(-\mathrm{d}t^2 + \mathrm{d}x^2 + \mathrm{d}z^2 + \mathrm{d}\phi^2\right). \tag{3.4}$$

By comparing this metric to (2.148), we see that $\alpha = \sqrt{-\Lambda/3}$. Indeed, in Fig. 3.6b the derivatives tend to 2α. Therefore, our numerical results are consistent with the analytic spacetime.

If we consider the even more special case of vanishing $A'(0)$ and $B'(0)$, we recover the homogeneous Bonnor–Melvin–Λ solution discussed in Sec. 2.2 if we also consider $\Lambda > 0$. The functions $A(r) = B(r)$ then remain constant in the whole domain. From (2.10) we can see that $A'(0) = B'(0) = 0$ implies $f^2(0) = \Lambda$. Inserting these into the previous three equations, we get that $A''(0) = B''(0) = 0$ too, which is also propagated for other values of the radial coordinate. Therefore, g_{tt} and g_{zz} remain constant (as well as g_{rr} by definition), as do the two tracked scalars, which become $F_{\mu\nu}F^{\mu\nu} = 2\Lambda$ and $R_{\alpha\beta\gamma\delta}R^{\alpha\beta\gamma\delta} = 16\Lambda^2$. The curve of $g_{\phi\phi}$ clearly corresponds to $g_{\phi\phi}$ of (2.102) for a particular choice of σ and with a shifted radial coordinate. The results are fully consistent with the analytic solution and are illustrated in Fig. 3.6c. Note that changing the initial $C'(0)$ only shifts the entire chart along the horizontal axis.

For $A'(0) = B'(0) = 0$, considering $\Lambda < 0$ yields $f^2 < 0$. Therefore, there are no new solutions in this class.

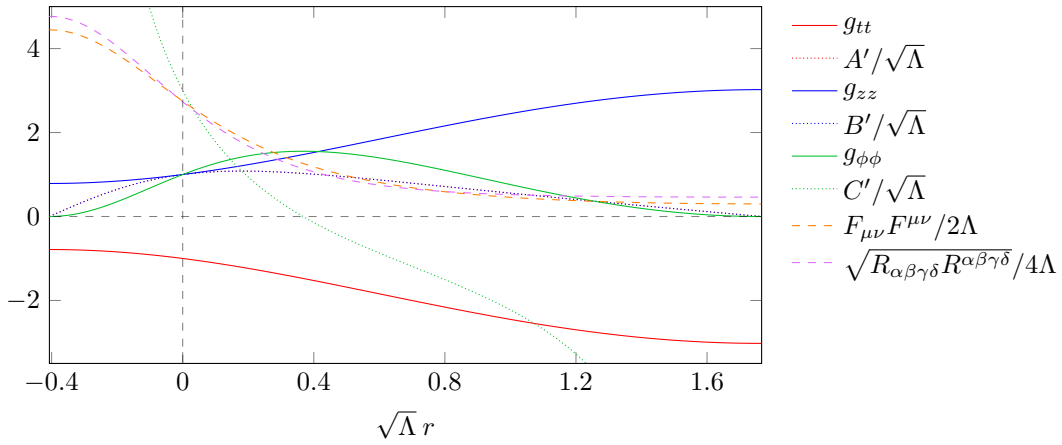

(a) Initial conditions $A'(0) = B'(0) = \sqrt{\Lambda}$ and $C'(0) = 3\sqrt{\Lambda}$ with $\Lambda = 1\,\mathrm{u}^{-2}$. The endpoints of the interval of r correspond to two regular axes.

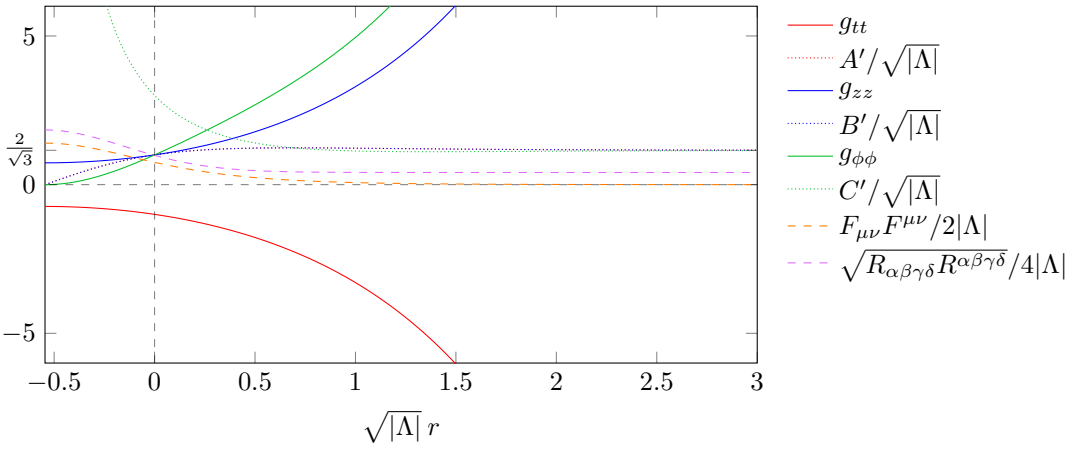

(b) Initial conditions $A'(0) = B'(0) = \sqrt{|\Lambda|}$ and $C'(0) = 3\sqrt{|\Lambda|}$ with $\Lambda = -1\,\mathrm{u}^{-2}$. There is one axis in the spacetime and the solution appears to extend to $r \to \infty$.

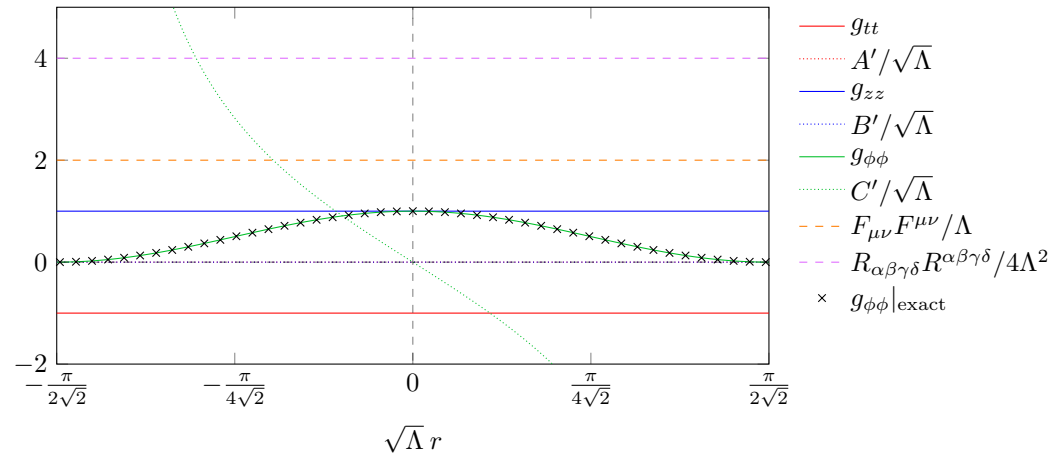

(c) Initial conditions $A'(0) = B'(0) = C'(0) = 0$ with $\Lambda = 1\,\mathrm{u}^{-2}$. The endpoints of the interval of r correspond to two axes. The curve of $g_{\phi\phi}$ overlaps well with the shifted exact solution (2.102), $g_{\phi\phi}|_{\mathrm{exact}} = \sin^2\left(\sqrt{2\Lambda}\,r - \pi/2\right)$, marked by crosses in the plot.

Figure 3.6: Numerical spacetimes with an axial magnetic field and boost symmetry; the curves of A' and B' overlap in each chart. The first two solutions correspond to the axial inhomogeneous spacetime of Sec. 2.3, the last one to the homogeneous Bonnor–Melvin–Λ solution of Sec. 2.2.

General solutions

We shall now leave boost symmetry behind and examine solutions satisfying $A'(0) \neq B'(0)$, which do not have any counterpart in the exact solutions examined previously in this work.

As it turns out, the general solutions seem to have a similar structure to the inhomogeneous spacetimes of Sec. 2.3 with the notable difference that there are curvature singularities on the axes, as especially the Kretschmann scalar (3.1) diverges there very markedly. For $\Lambda > 0$, the solutions contain two singular axes. Interestingly, on one of the axes g_{tt} diverges and g_{zz} vanishes, while on the other axis the opposite limits hold, as illustrated in Fig. 3.7a. For $\Lambda < 0$, there is one singular axis and a regular asymptotic region, in which $F_{\mu\nu}F^{\mu\nu} \to 0$ and the derivatives of the metric functions all tend to $2\sqrt{-\Lambda/3}$, so the asymptotic behavior of the solution appears to be the same as in the boost-symmetric case (i.e., the solution tends to the anti-de Sitter spacetime). We have discovered two different patterns for the axis. In the solution of Fig. 3.7b we have $g_{tt} \to -\infty$ and $g_{zz} \to 0$ as we approach the axis. On the other hand, the solution depicted in Fig. 3.7c has the opposite limits, $g_{tt} \to 0$ and $g_{zz} \to \infty$.

It does not appear that $C'(0)$ coinciding with either $A'(0)$ or $B'(0)$ leads to any solutions different from those already discussed.

Note that the habilitation thesis Žofka [2021], which features some overlap with this work, also contains a chapter on general numerical spacetimes with an axial magnetic field. However, the results there differ from ours. Seeing that we were also able to recover the exact solutions numerically, which the older work did not attempt, we suspect that a mistake invalidating the results must have been made in the habilitation thesis.

3.2.2 Radial magnetic field

Solutions with rotational symmetry

Apart from the three translational symmetries, the cosmological solutions with a radial magnetic field of Sec. 2.5 and 2.6 also contain a rotational symmetry in the z–ϕ plane, corresponding to $B' = C'$. Similarly to the axial case, the radial system (2.65)–(2.68) is invariant under $B' \leftrightarrow C'$, so setting $B'(0) = C'(0)$ ensures that the derivatives stay the same throughout the whole domain.

The situation here is quite more complicated than for the spacetimes with axial magnetic fields, as the solutions of Sec. 2.5 and 2.6 may contain horizons and admit multiple causal configurations. Unfortunately, our ansatz for the metric (1.1) is ill-suited to deal with dynamical regions, as the signs of the metric elements are fixed. A complex $A(r)$ could be considered to change the sign of g_{tt}, but $g_{rr} = 1$ is fixed regardless, so it can never become negative as needed in the dynamical regions of our solutions. Even though we are not able to explore the dynamical regions numerically, we are able to identify the horizons in our numerical solutions, as they can be found at those values of r where the integration of the system fails with g_{tt} approaching zero (as it also must change its sign there), while the other metric elements and especially the two examined scalars are finite.

Starting again with the inhomogeneous case and focusing first on solutions

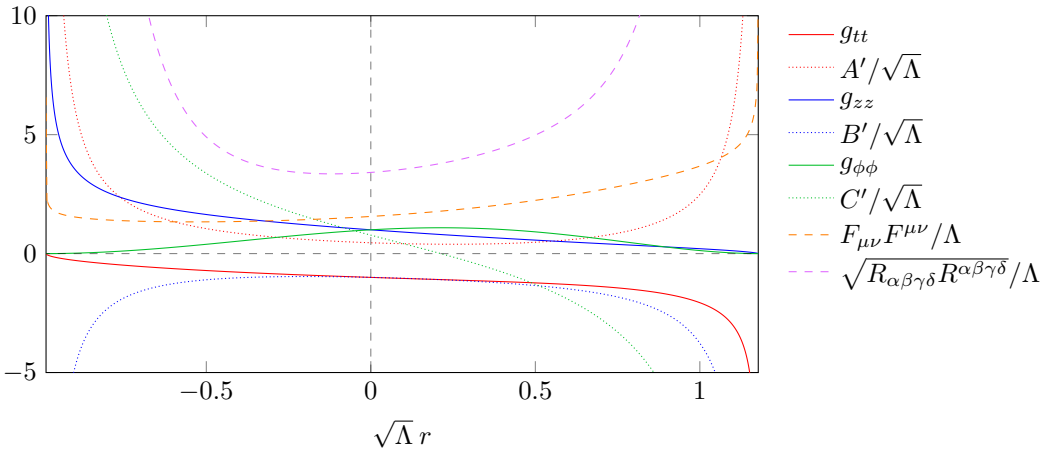

(a) Initial conditions $A'(0) \approx 0.455\sqrt{\Lambda}$, $B'(0) \approx -0.999\sqrt{\Lambda}$, and $C'(0) \approx 0.776\sqrt{\Lambda}$ with $\Lambda = 7\,\mathrm{u}^{-2}$. The endpoints of the interval of r correspond to two singular axes.

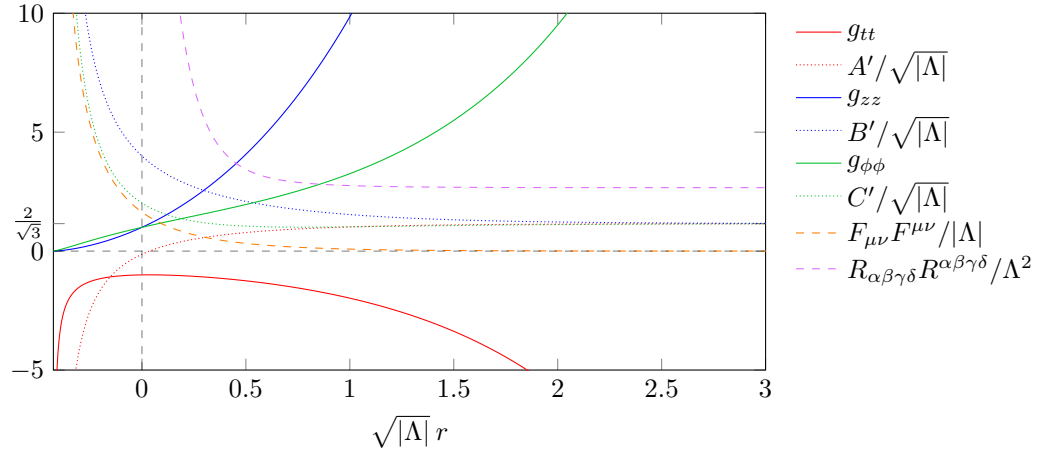

(b) Initial conditions $A'(0) \approx -0.133\sqrt{|\Lambda|}$, $B'(0) \approx 4.00\sqrt{|\Lambda|}$, and $C'(0) \approx 2.02\sqrt{|\Lambda|}$ with $\Lambda = -5.6\,\mathrm{u}^{-2}$. There is one singular axis in the spacetime and the solution appears to extend to $r \to \infty$.

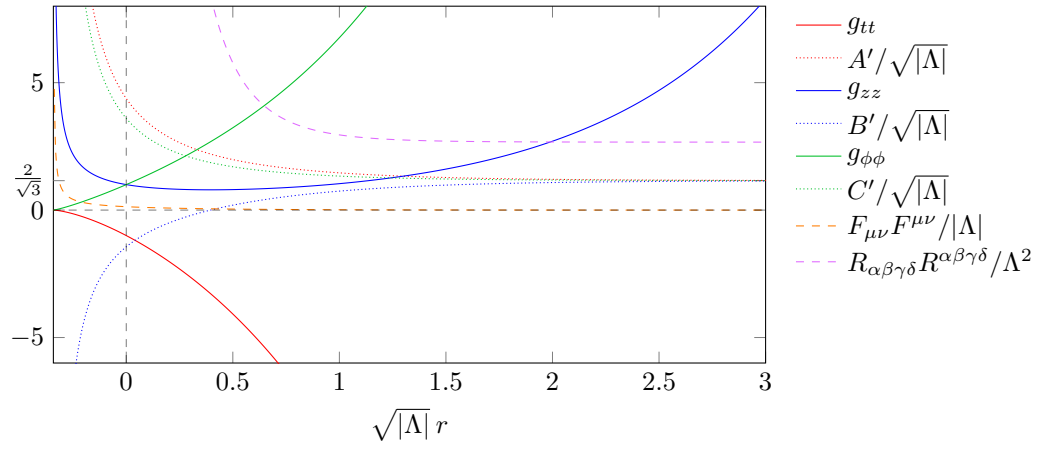

(c) Initial conditions $A'(0) \approx 4.38\sqrt{|\Lambda|}$, $B'(0) \approx -1.44\sqrt{|\Lambda|}$, and $C'(0) \approx 3.60\sqrt{|\Lambda|}$ with $\Lambda = -5\,\mathrm{u}^{-2}$. There is one singular axis in the spacetime and the solution appears to extend to $r \to \infty$.

Figure 3.7: Numerical spacetimes with an axial magnetic field that do not have boost symmetry.

with $\Lambda > 0$, the exact spacetime suggests that there is only one possible configuration, which contains a singular axis and a horizon separating the static region with the axis and the dynamical asymptotic region. Indeed, our numerical experiments seem to support this structure, as we were not able to find any other distinct spacetimes. Our results for the static region are illustrated in Fig. 3.8a.

For $\Lambda < 0$, the exact solution admits three different causal configurations. First, the black-string solution contains a dynamical region sandwiched between two static regions delimited by the horizons. As mentioned above, we cannot explore the dynamical region numerically, but we were able to find solutions clearly corresponding both to the inner static region with the axis (Fig. 3.8b), which is notably quite similar to the solution with $\Lambda > 0$ of Fig. 3.8a, and also to the asymptotic region (Fig. 3.8c). Next, there is the naked-singularity variant of the spacetime, which does not contain any horizons and it can be fully explored using our numerical computations. It contains a singular axis and an asymptotic region, as illustrated in Fig. 3.8d. The last configuration is the extremal one with a single horizon of multiplicity two, which separates two static regions. So far, we were able to draw the figures using randomly-generated initial conditions, as both the naked spacetimes and the black-string solutions require the initial conditions to fulfill a certain inequality, which gives us enough leeway to satisfy the requirements without any further effort on our part. The extremal case, however, imposes a condition in the form of an equality, which is virtually impossible to be satisfied using randomly-generated numbers. Fortunately, knowing the exact solution beforehand, we can use it to our advantage to fine-tune the initial conditions to obtain an extremal solution numerically. For us to be able to match the exact metric (2.256) to the ansatz (1.1), we need to replace the radial coordinate in (2.256), which shall be denoted $\hat{r}$ in the following, with the proper radial distance r used in the ansatz. More precisely, we only need to do so in the derivatives of the metric functions, which are the only relevant initial data we need for our numerical computations. Considering $g_{tt}(x) = -\exp A(x)$, where x stands for either r or $\hat{r}$ (there is no transformation of the timelike coordinate), we have

$$\frac{\mathrm{d}A(x)}{\mathrm{d}x} = \frac{\mathrm{d}}{\mathrm{d}x}\ln(-g_{tt}(x)) = \frac{1}{g_{tt}(x)}\frac{\mathrm{d}g_{tt}(x)}{\mathrm{d}x}\,. \tag{3.5}$$

Since r is the proper radial distance, i.e., $\mathrm{d}r = \sqrt{g_{\hat{r}\hat{r}}(\hat{r})}\,\mathrm{d}\hat{r}$, the desired derivative can be expressed as

$$A'(r) \equiv \frac{\mathrm{d}A(r)}{\mathrm{d}r} = \frac{\mathrm{d}A(\hat{r})}{\mathrm{d}\hat{r}}\frac{\mathrm{d}\hat{r}}{\mathrm{d}r} = \frac{1}{g_{tt}(\hat{r})\sqrt{g_{\hat{r}\hat{r}}(\hat{r})}}\frac{\mathrm{d}g_{tt}(\hat{r})}{\mathrm{d}\hat{r}}\,, \tag{3.6}$$

and analogously for $B'(r) = C'(r)$. We can insert any admissible $\hat{r}_0$ and use the obtained A' and $B' = C'$ as the initial conditions for our problem, setting $r(\hat{r}_0) = 0$ as the initial r can be chosen arbitrarily. In order to draw our charts, we computed the initial values for the spacetime with $\Lambda = -1\,\mathrm{u}^{-2}$, $\beta = 1\,\mathrm{u}$, and α fixed by (2.263). With the degenerate horizon at $\hat{r} = 1\,\mathrm{u}$, we examine the region containing the axis in Fig. 3.8e starting from $\hat{r}_0 = 3/5\,\mathrm{u}$, and we use $\hat{r}_0 = 2\,\mathrm{u}$ for the asymptotic region in Fig. 3.8f. It is not possible to see the horizon in the two charts, as the proper radial distance from any point in the spacetime to the degenerate horizon is infinite, but note that the two examined scalars have the

same values as $r \to \infty$ in the region under the horizon, and as $r \to -\infty$ in the region above the horizon. The extremal solutions are very vulnerable to rounding errors in numerical computations, as they can push the solution towards a black-string spacetime or a naked-singularity one. Increasing the `WorkingPrecision` parameter of `NDSolve` in `Mathematica` can delay these effects considerably.

In all cases with $\Lambda < 0$, the derivatives of the metric functions A' and $B' = C'$ tend to $2\sqrt{-\Lambda/3}$ in the asymptotic region. In a completely analogous manner to the axial spacetimes, this is consistent with the anti-de Sitter limit (2.265) of the exact spacetime.

Regarding numerical analogues of the homogenous solutions investigated in Sec. 2.5, a similar argument like the one for the spacetimes with an axial magnetic field explains that the exact spacetimes are recovered for $B'(0) = C'(0) = 0$. Relation (2.68) then implies that $f^2(0) = -\Lambda$, which means that this time Λ must be negative so that we obtain a magnetic field. Inserting these initial values into the three differential equations we aim to solve numerically, we see that the second derivatives vanish, $B''(0) = C''(0) = 0$, which again remains valid for the entire interval of r. Unlike the axial case, we cannot change the initial A' arbitrarily without affecting the physics of the spacetime, as the spacetime admits three different causal configurations as we already know from Sec. 2.5.2. Limiting ourselves first to $A'(0) \geq 0$, the threshold $A'(0)$ is easy to find from the exact solution: The metric with a single exponential function (2.247) is the extremal boundary between (2.213) and (2.248) containing the hyperbolic functions. The derivative of $A(r)$ for (2.247) is constant in the entire region, $A'(r) = 2\sqrt{-2\Lambda}$, and it indeed gives the threshold $A'(0)$ setting the other configurations apart. Fig. 3.9 containing illustrations of numerical solutions corresponding to all three possible causal configurations seems to confirm this notion. Performing the transformation $r \to -r$, which inverts the charts along the vertical axis, corresponds to setting $A'(0) \to -A'(0)$. Charts for negative $A'(0)$ are, therefore, only mirror images of charts with positive $A'(0)$. Note that like in the inhomogeneous case, it is not possible to work with the dynamical region of the sinh metric in the used coordinates, as the numerical integration of the equations cannot go beyond $g_{tt} = 0$ because of the fixed radial component of the metric, so Fig. 3.9c only depicts the static regions of the spacetime. Compare that to the horizon of the extremal solution of Fig. 3.9b, which lies in infinite proper radial distance (used as our independent variable) from any other point in the spacetime, meaning the numerical integration could be extended infinitely in both directions, provided there are no problems with machine precision of the integration.

General solutions

There seems to be a broader palette of spacetimes with $B'(0) \neq C'(0)$. Starting with the case of $\Lambda > 0$, we found four different types of spacetimes, which are illustrated in Fig. 3.10. In all four cases, the interval of r is finite and both endpoints apparently always correspond to curvature singularities, as the two monitored scalars diverge. The solutions can be split into two pairs based on the behavior of $g_{\phi\phi}$. One pair of spacetimes contains two singular axes, while the other pair contains a singular axis and a singular asymptotic region with $g_{\phi\phi} \to \infty$, so the circumference of circles around the axis diverges. Interestingly,

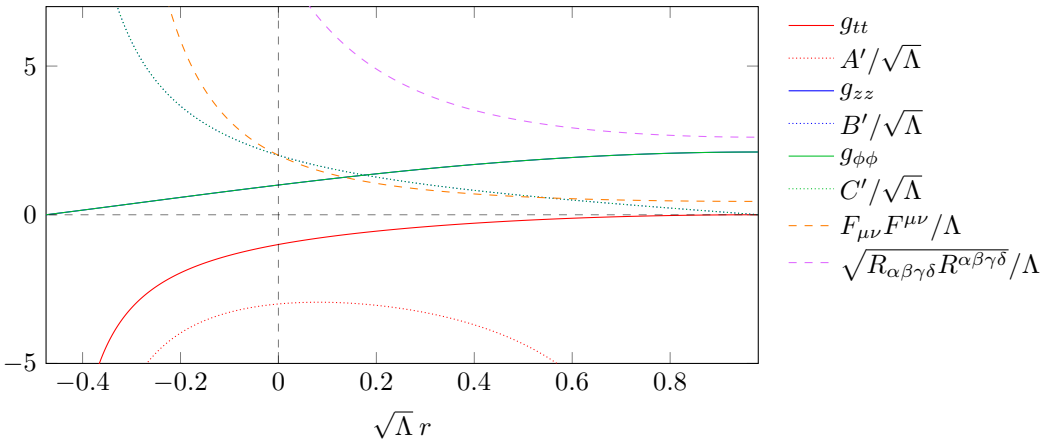

(a) Initial conditions $A'(0) = -3\sqrt{\Lambda}$, $B'(0) = C'(0) = 2\sqrt{\Lambda}$ with $\Lambda = 1\,\mathrm{u}^{-2}$. The lower endpoint of the interval of r corresponds to a singular axis, the upper to a horizon.

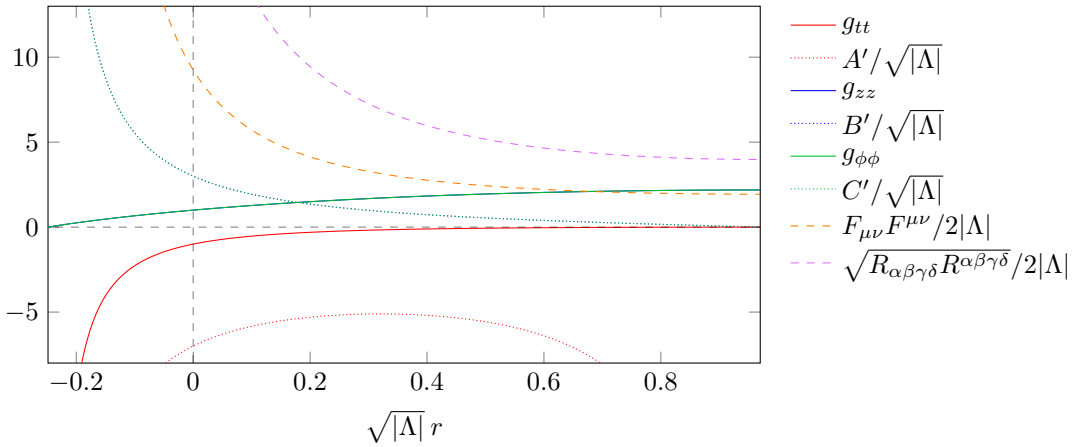

(b) Initial conditions $A'(0) = -7\sqrt{|\Lambda|}$, $B'(0) = C'(0) = 3\sqrt{|\Lambda|}$ with $\Lambda = -1\,\mathrm{u}^{-2}$. The lower endpoint of the interval of r corresponds to a singular axis, the upper to a horizon.

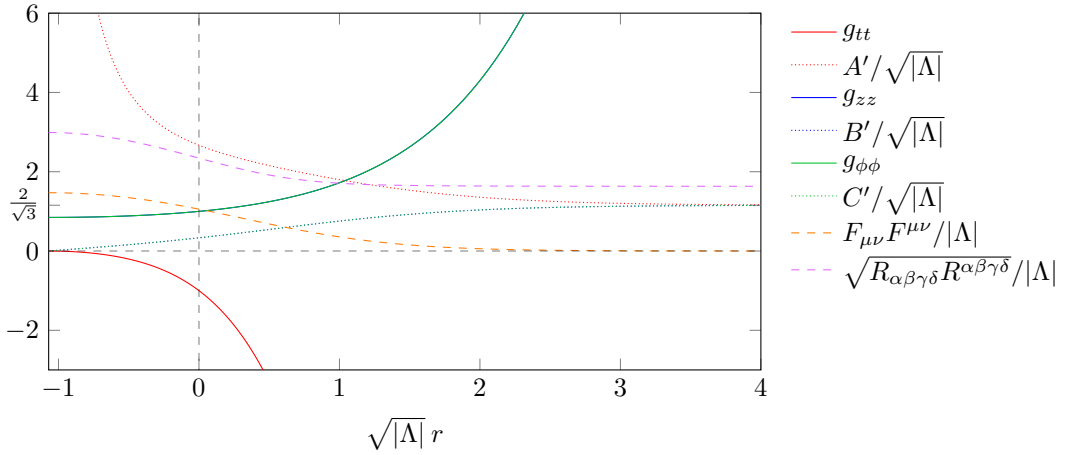

(c) Initial conditions $A'(0) = 8/3\,\sqrt{|\Lambda|}$, $B'(0) = C'(0) = 1/3\,\sqrt{|\Lambda|}$ with $\Lambda = -9\,\mathrm{u}^{-2}$. The lower endpoint of the interval of r corresponds to a horizon and the solution appears to extend to $r \to \infty$.

Figure 3.8: Numerical spacetimes with a radial magnetic field and rotational symmetry corresponding to the inhomogeneous spacetime of Sec. 2.6. The curves of B' and C' overlap in each chart, as well as the curves of g_{zz} and $g_{\phi\phi}$. The figure is spread over multiple pages.

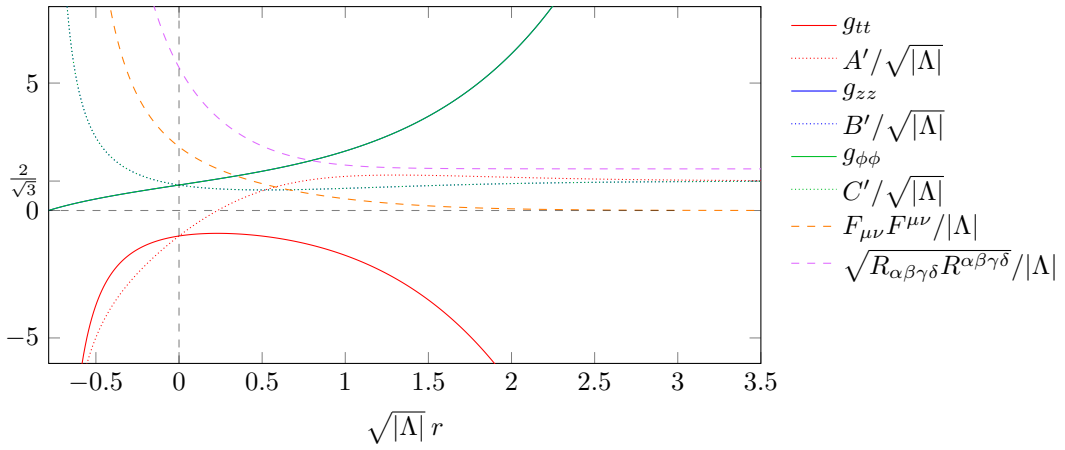

(d) Initial conditions $A'(0) = -\sqrt{|\Lambda|}$, $B'(0) = C'(0) = \sqrt{|\Lambda|}$ with $\Lambda = -1\,\mathrm{u}^{-2}$. The lower endpoint of the interval of r corresponds to a singular axis and the solution appears to extend to $r \to \infty$.

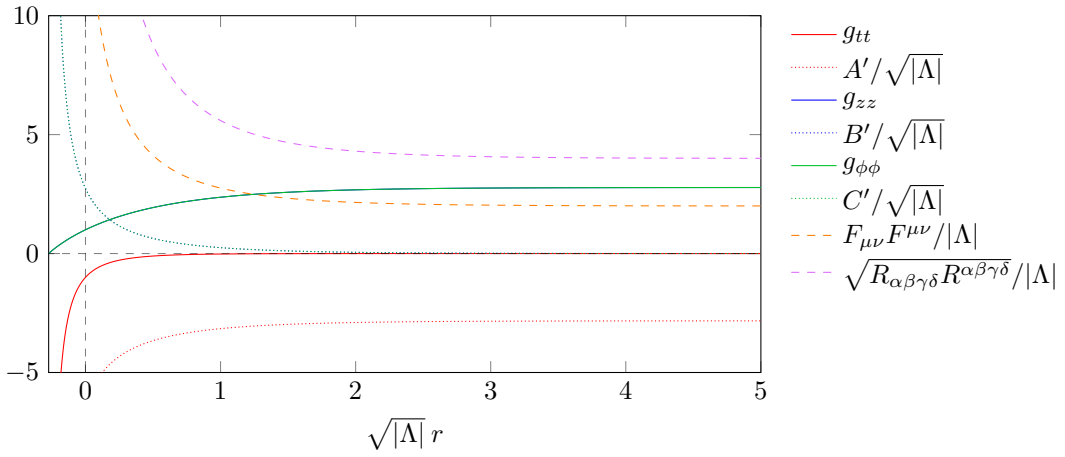

(e) Initial conditions $A'(0) = -\frac{58}{3}\sqrt{\frac{2|\Lambda|}{19}}$, $B'(0) = C'(0) = \frac{4}{9}\sqrt{38\,|\Lambda|}$ with $\Lambda = -1\,\mathrm{u}^{-2}$. There is one singular axis in the spacetime and the solution appears to extend to $r \to \infty$.

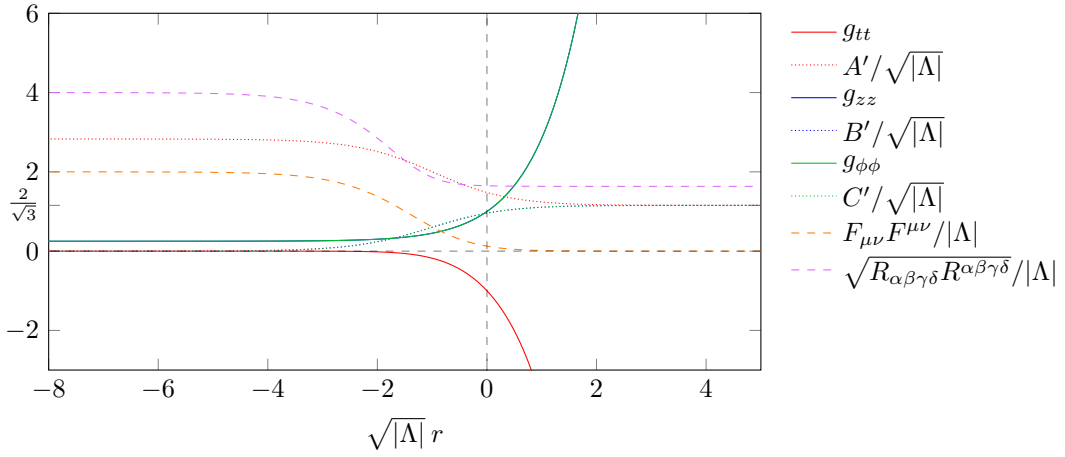

(f) Initial conditions $A'(0) = \frac{17}{2}\sqrt{\frac{|\Lambda|}{33}}$, $B'(0) = C'(0) = \frac{1}{2}\sqrt{\frac{11|\Lambda|}{3}}$ with $\Lambda = -1\,\mathrm{u}^{-2}$. The solution appears to extend from $r \to -\infty$ to the asymptotic region with $r \to \infty$.

Figure 3.8: Numerical spacetimes corresponding to the radial inhomogeneous spacetime of Sec. 2.6. (cont.)

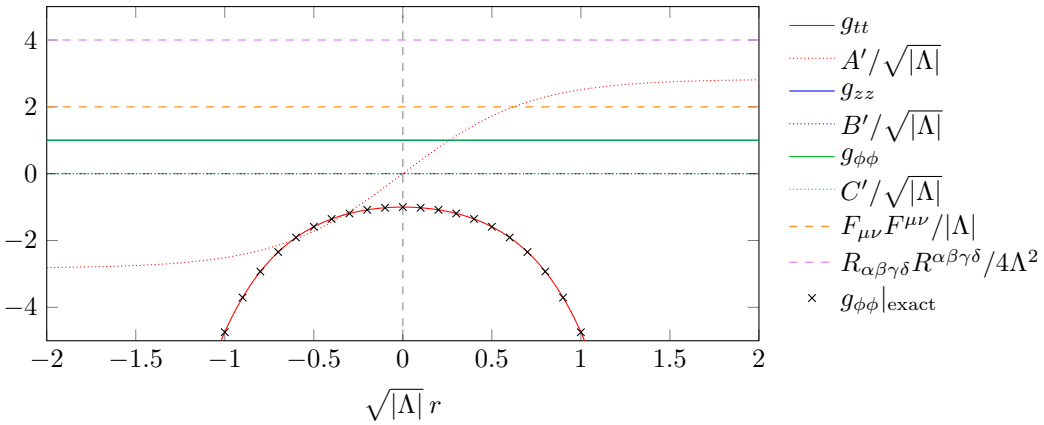

(a) Initial conditions $A'(0) = B'(0) = C'(0) = 0$ with $\Lambda = -1\,\mathrm{u}^{-2}$. The radial coordinate r appears to be unbounded. The curve of g_{tt} overlaps well with the exact solution (2.213), $g_{tt}|_{\text{exact}} = -\cosh^2\left(\sqrt{-2\Lambda}r\right)$, marked by crosses in the plot.

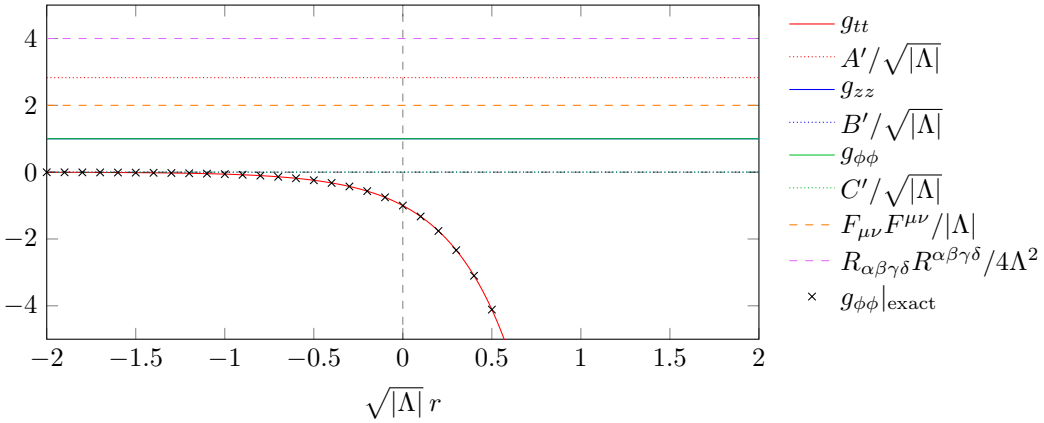

(b) Initial conditions $A'(0) = 2\sqrt{2\,|\Lambda|}$, $B'(0) = C'(0) = 0$ with $\Lambda = -1\,\mathrm{u}^{-2}$. The radial coordinate r appears to be unbounded. The curve of g_{tt} overlaps well with the exact solution (2.247), $g_{tt}|_{\text{exact}} = -\mathrm{e}^{2\sqrt{-2\Lambda}\,r}$, marked by crosses in the plot.

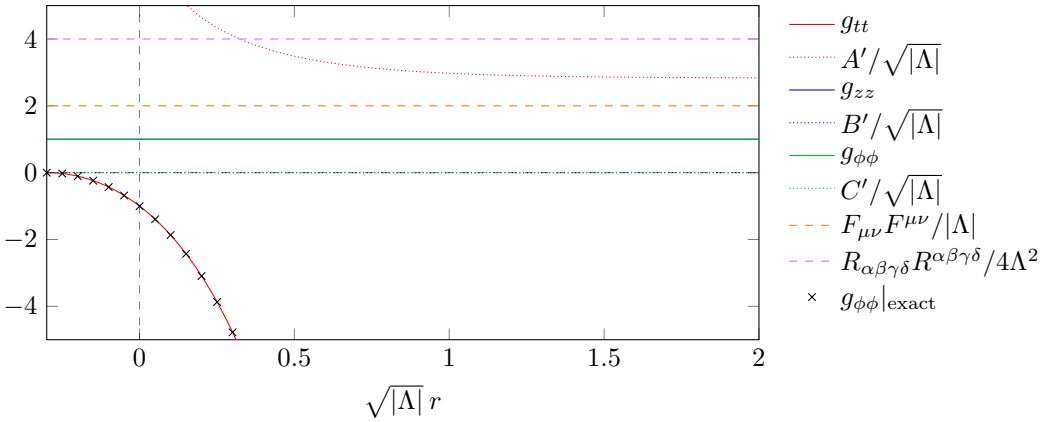

(c) Initial conditions $A'(0) = 5\sqrt{2\,|\Lambda|}$, $B'(0) = C'(0) = 0$ with $\Lambda = -1\,\mathrm{u}^{-2}$. The interval of r is left-bounded and the endpoint corresponds to a horizon. The curve of g_{tt} overlaps well with the marked exact solution (2.248), $g_{tt}|_{\text{exact}} \approx -5.25\sinh^2\left(\sqrt{-2\Lambda}(r + 0.300)\right)$, which had to be shifted and rescaled to match the considered initial conditions.

Figure 3.9: Numerical spacetimes with a radial magnetic field and rotational symmetry corresponding to the homogeneous spacetimes of Sec. 2.5. The curves of B' and C' overlap in each chart, as well as the curves of g_{zz} and $g_{\phi\phi}$.

the singular asymptotic region is located in finite proper radial distance from any other point in the spacetime, as the (bounded) radial coordinate corresponds to proper distance. The solutions within each pair then differ in the limits of the remaining two metric functions. Note that the solution of Fig. 3.10c bears striking similarities to the non-cosmological radial Bonnor–Melvin spacetime of Sec. 2.4, because the plotted functions look like those in the metric (2.176), as they have a single extremum and the same limits, and the interval of r is also bounded by two singular axes. Unlike the exact spacetime, however, the numerical spacetime contains the cosmological constant, but it can be argued that due to the properties of the cosmological term its effects are much less prominent in spacetimes without an asymptotic region, such as this one.

Turning our attention to spacetimes with $\Lambda < 0$ now, we found six qualitatively different solutions, which are illustrated in Fig. 3.11. Three of them contain a regular asymptotic region as $r \to \infty$. For them, the limits of the derivatives tend to the familiar value of $2\sqrt{-\Lambda/3}$ while $F_{\mu\nu}F^{\mu\nu} \to 0$, suggesting that the spacetimes are once more asymptotically anti-de Sitter. The interval of r is left-bounded and the endpoint corresponds to a curvature singularity. As we approach the singularity, two metric functions always vanish while the last one diverges. All three combinations are possible, which notably includes the case of $g_{\phi\phi} \to \infty$ of Fig. 3.11a. In this case, the singularity does not represent an axis, but instead we are dealing with a singular asymptotic region in finite proper distance as discussed above. The solution then does not contain any axes. Next, we found three solutions with a finite interval of r. These solutions invariantly contain a singular axis at which $g_{\phi\phi}$ and g_{zz} vanish and g_{tt} diverges. The other endpoint of r is singular too. Like for the spacetimes with the anti-de Sitter asymptotics, this endpoint admits any combination of two vanishing and one diverging metric functions, which again notably includes $g_{\phi\phi}$ determining whether the endpoint represents a second singular axis or a singular asymptotic region.

Interestingly, finite endpoints of the interval of r in the present figures always seem to correspond to a singularity, as the two examined scalars diverge there. Therefore, we were not able to find a single configuration supporting (non-degenerate) horizons. This leads us to think that spacetimes containing at least one horizon may be a subset of measure zero within the larger set of all cylindrically-symmetric and static spacetimes with a radial magnetic field. We already know that spacetimes with a further rotational symmetry may contain horizons, but if there is another similar subset, it is extremely unlikely to be discovered by numerical experiments. Barring this subset, like in the axial case the general spacetimes thus always contain a naked singularity, which is less desirable from the physical point of view. The spacetimes with an extra symmetry tend to have more favorable properties.

While it is merely a conjecture for spacetimes with horizons, extremal spacetimes by their very nature form a subset of measure zero within the given family of solutions. Having said that, we happened by accident upon a solution that appears to near some sort of an extremal state, as illustrated in Fig. 3.12. A small change in $C'(0)$ while keeping the other initial conditions fixed results in a dramatic change in the properties of the spacetime, as a regular asymptotic region with $r \to \infty$ is replaced by a singular axis at a finite r, while the left part of the spacetime appears virtually unaffected by this change. Fine-tuning $C'(0)$

further, it is possible to extend the plateau seen in both charts. It is, therefore, not inconceivable that a spacetime with constant g_{zz} and $g_{\phi\phi}$ as $r \to \infty$ can be found, extending the plateau infinitely. The suggested infinite plateau would not lead to a degenerate horizon in infinite proper distance, however, as in place of $g_{tt} \to 0$ we have $g_{tt} \to -\infty$ there. Instead, this asymptotic behavior would be the same as for any of the homogeneous spacetimes seen in Fig. 3.9. Unfortunately, we were not able to achieve sufficient numerical precision to actually obtain such a spacetime numerically, provided the equations even admit it in the first place.

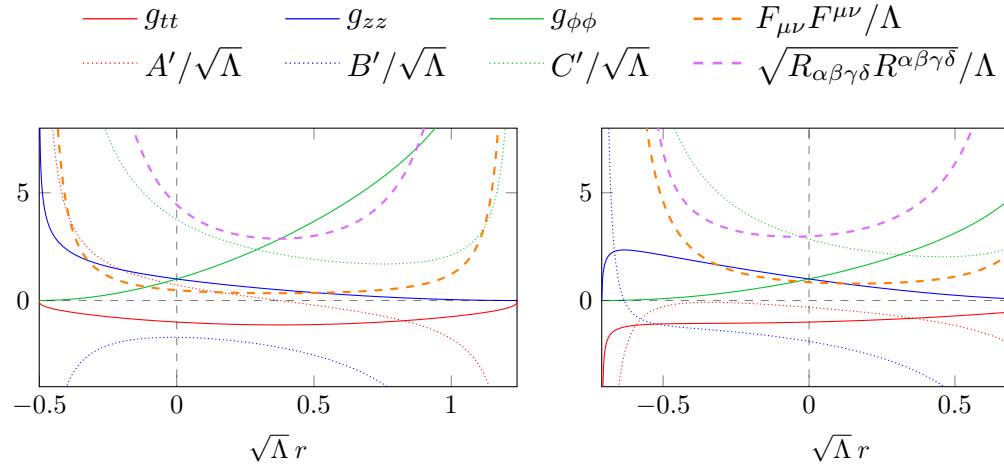

(a) Initial conditions $A'(0) \approx 0.714\sqrt{\Lambda}$, $B'(0) \approx -1.71\sqrt{\Lambda}$, and $C'(0) \approx 3.76\sqrt{\Lambda}$ with $\Lambda = 7\,\mathrm{u}^{-2}$. The solution has a singular axis and a singular asymptotic region.

(b) Initial conditions $A'(0) \approx -0.316\sqrt{\Lambda}$, $B'(0) \approx -1.90\sqrt{\Lambda}$, and $C'(0) \approx 2.85\sqrt{\Lambda}$ with $\Lambda = 10\,\mathrm{u}^{-2}$. The solution has a singular axis and a singular asymptotic region.

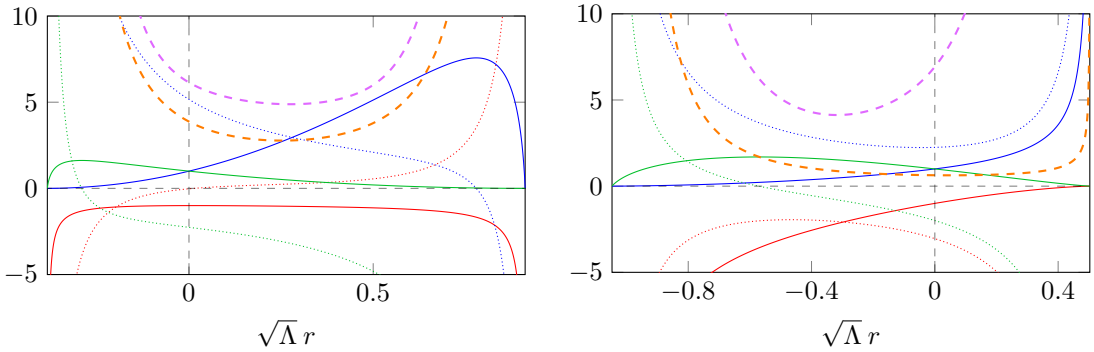

(c) Initial conditions $A'(0) \approx -0.0248\sqrt{\Lambda}$, $B'(0) \approx 5.16\sqrt{\Lambda}$, and $C'(0) \approx -2.26\sqrt{\Lambda}$ with $\Lambda = 2\,\mathrm{u}^{-2}$. The solution has two singular axes.

(d) Initial conditions $A'(0) \approx -3.05\sqrt{\Lambda}$, $B'(0) \approx 2.25\sqrt{\Lambda}$, and $C'(0) \approx -2.00\sqrt{\Lambda}$ with $\Lambda = 6\,\mathrm{u}^{-2}$. The solution has two singular axes.

Figure 3.10: Numerical spacetimes with a radial magnetic field and $\Lambda > 0$ that do not have rotational symmetry. The legend is above the figures and it is valid for each of the four charts.

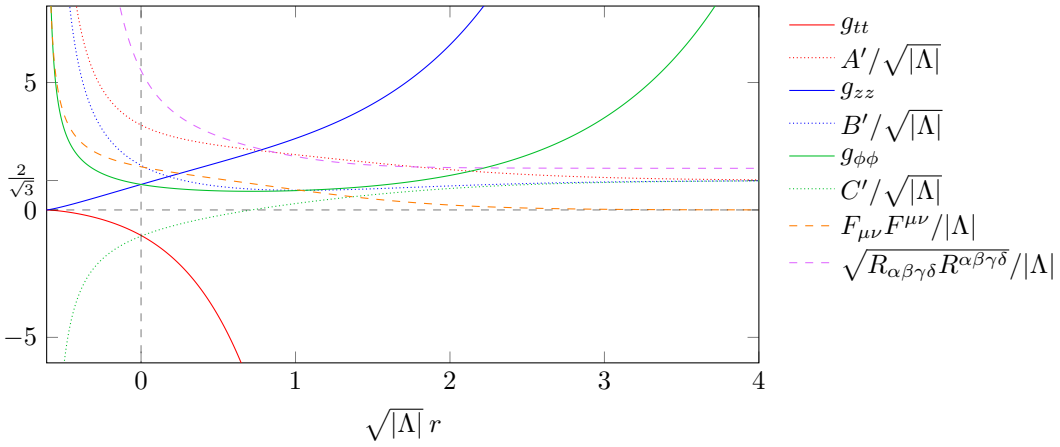

(a) Initial conditions $A'(0) \approx 3.33\sqrt{|\Lambda|}$, $B'(0) \approx 1.75\sqrt{|\Lambda|}$, and $C'(0) \approx -1.03\sqrt{|\Lambda|}$ with $\Lambda = -6\,\mathrm{u}^{-2}$. The lower endpoint of the interval of r corresponds to a singular asymptotic region and there is a regular asymptotic region as $r \to \infty$.

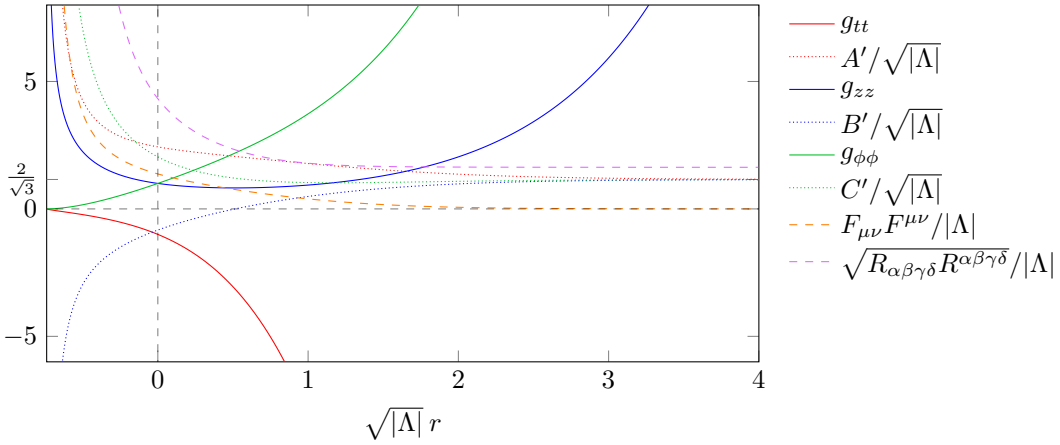

(b) Initial conditions $A'(0) \approx 2.43\sqrt{|\Lambda|}$, $B'(0) \approx -0.830\sqrt{|\Lambda|}$, and $C'(0) \approx 2.04\sqrt{|\Lambda|}$ with $\Lambda = -4\,\mathrm{u}^{-2}$. The lower endpoint of the interval of r corresponds to a singular axis and there is a regular asymptotic region as $r \to \infty$.

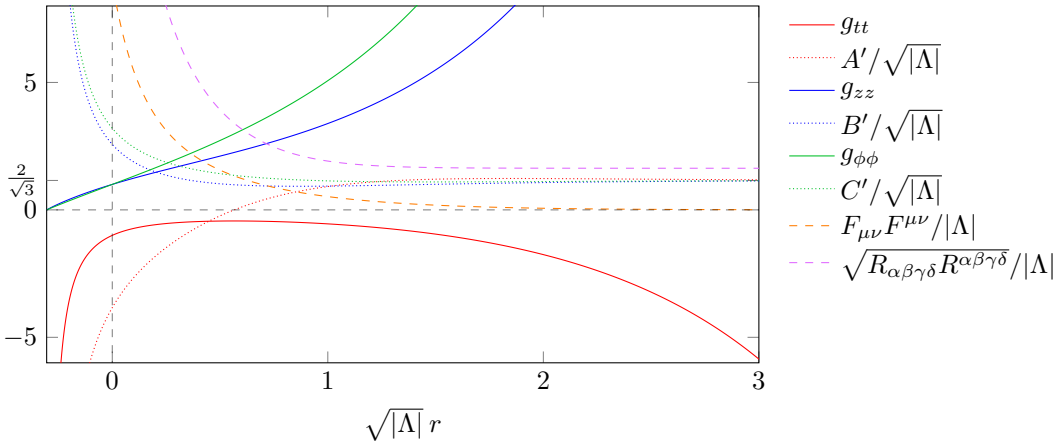

(c) Initial conditions $A'(0) \approx -3.84\sqrt{|\Lambda|}$, $B'(0) \approx 2.57\sqrt{|\Lambda|}$, and $C'(0) \approx 3.20\sqrt{|\Lambda|}$ with $\Lambda = -4\,\mathrm{u}^{-2}$. The lower endpoint of the interval of r corresponds to a singular axis and there is a regular asymptotic region as $r \to \infty$.

Figure 3.11: Numerical spacetimes with a radial magnetic field and $\Lambda < 0$ that do not have rotational symmetry. The figure is spread over multiple pages.

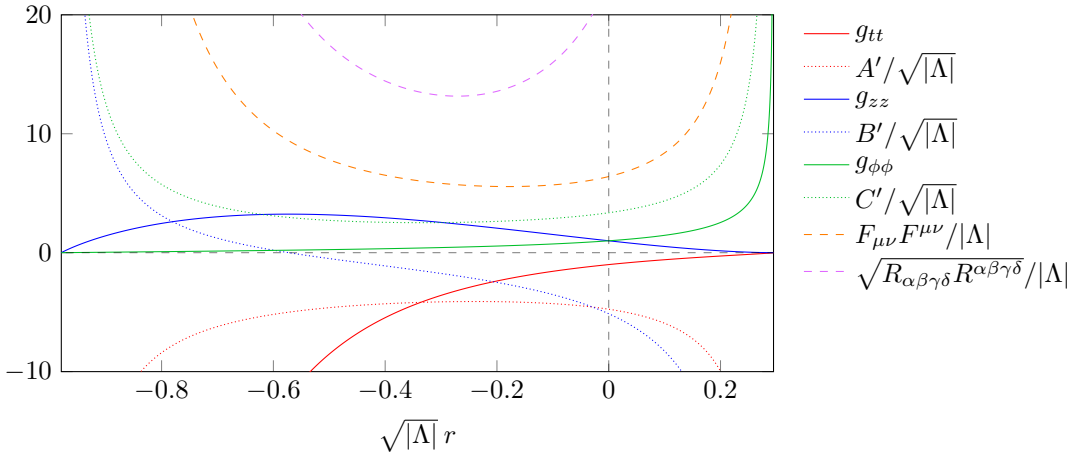

(d) Initial conditions $A'(0) \approx -4.75\sqrt{|\Lambda|}$, $B'(0) \approx -5.13\sqrt{|\Lambda|}$, and $C'(0) \approx 3.36\sqrt{|\Lambda|}$ with $\Lambda = -3\,\mathrm{u}^{-2}$. The lower endpoint of the interval of r corresponds to a singular axis and the greater endpoint to a singular asymptotic region.

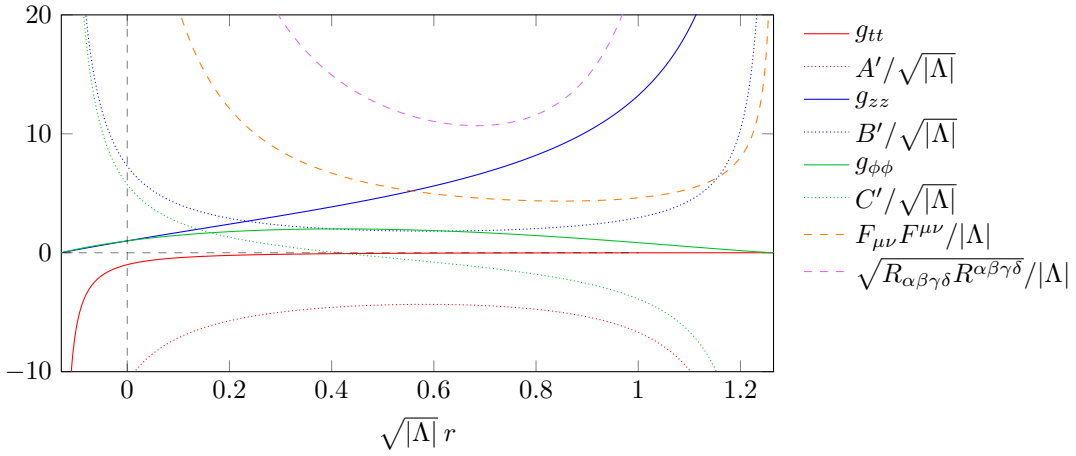

(e) Initial conditions $A'(0) \approx -10.9\sqrt{|\Lambda|}$, $B'(0) \approx 7.28\sqrt{|\Lambda|}$, and $C'(0) \approx 5.74\sqrt{|\Lambda|}$ with $\Lambda = -0.4\,\mathrm{u}^{-2}$. There are two singular axes in the spacetime.

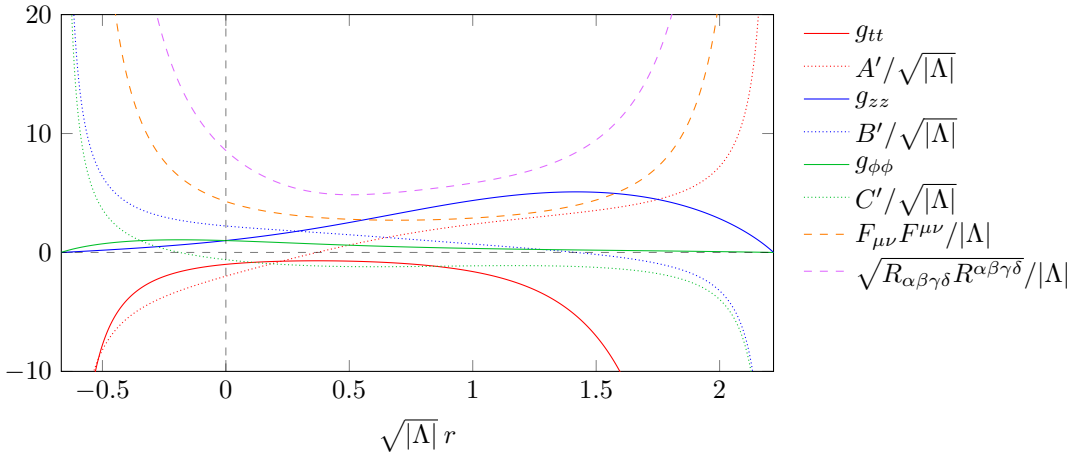

(f) Initial conditions $A'(0) \approx -1.99\sqrt{|\Lambda|}$, $B'(0) \approx 2.23\sqrt{|\Lambda|}$, and $C'(0) \approx -0.607\sqrt{|\Lambda|}$ with $\Lambda = -6\,\mathrm{u}^{-2}$. There are two singular axes in the spacetime.

Figure 3.11: Numerical spacetimes with a radial magnetic field and $\Lambda < 0$. (cont.)

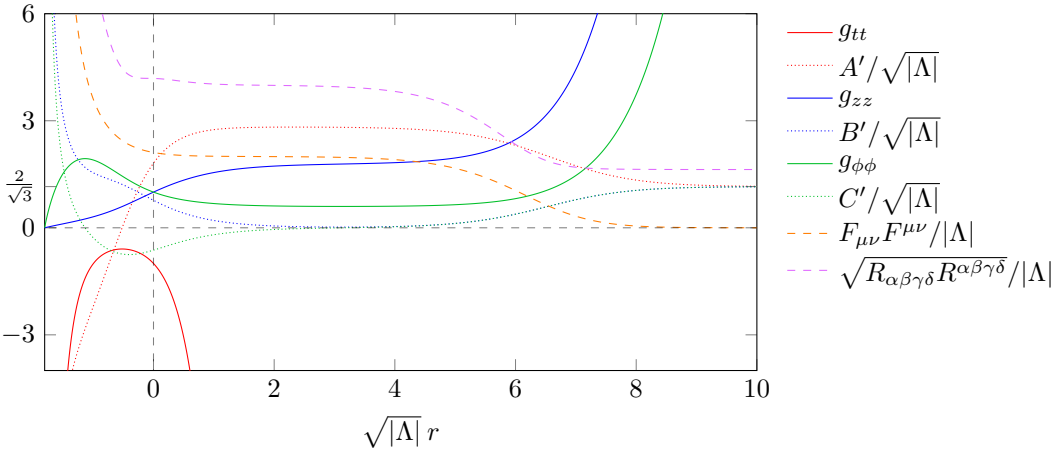

(a) $C'(0) = -0.6265\sqrt{|\Lambda|}$. The solution has a singular axis and a regular asymptotic region as $r \to \infty$. This spacetime is qualitatively the same as the one in Fig. 3.11c.

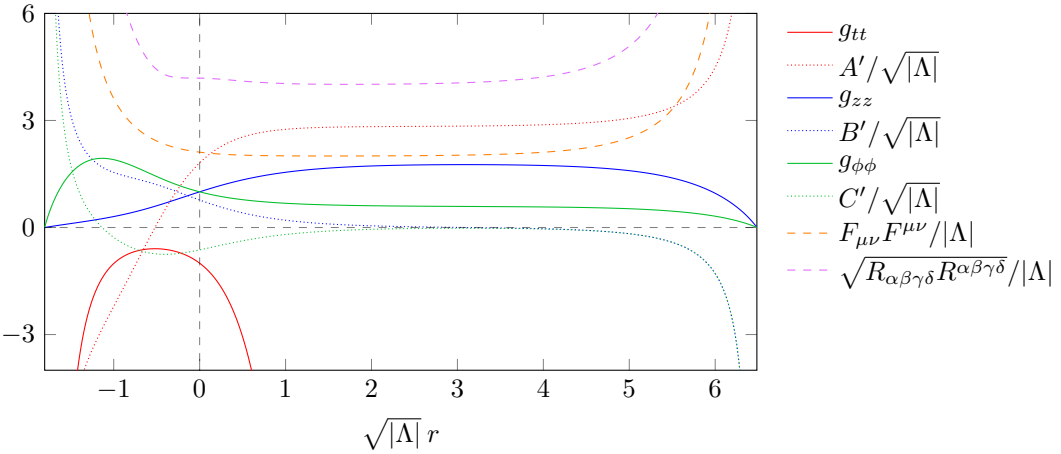

(b) $C'(0) = -0.627\sqrt{|\Lambda|}$. The solution has two singular axes. The spacetime is qualitatively the same as the one in Fig. 3.11f.

Figure 3.12: Numerical spacetimes with a radial magnetic field without rotational symmetry that seem to near an extremal state. Both spacetimes have the same $\Lambda = -4\,\mathrm{u}^{-2}$ and $A'(0) \approx 1.81\sqrt{|\Lambda|}$ with $B'(0) \approx 0.771\sqrt{|\Lambda|}$, while their $C'(0)$ slightly differs, $C'_{(\mathrm{a})}(0)/C'_{(\mathrm{b})}(0) \approx 0.9992$.

3.3 The Painlevé property

The full equations for $w(f) = f'(r)^2$ we want to solve are second-order ODEs (2.53) for the axial and azimuthal cases and (2.94) for the radial case. Both equations can be written together as

$$w\ddot{w} - \dot{w}^2 + \left[\frac{w}{f} \mp 6f\left(f^2 \mp \Lambda\right)\right]\dot{w} - 8\left(f^2 \mp \Lambda\right)^2 f^2 \pm 2w\left(11f^2 \mp 9\Lambda\right) = 0\,, \tag{3.7}$$

where the upper sign applies in the axial/azimuthal case and the lower sign in the radial case. The dots denote derivatives of $w(f)$ with respect to f.

According to Slavyanov and Lay [2000], considerable research was done at the beginning of the 20$^{\text{th}}$ century on second-order ODEs that have the so-called Painlevé property, which means that their solutions do not contain any movable critical points, i.e., essential singularities that depend on the initial data, so their position cannot be determined from the forms of the functions appearing in the equation itself. Considered in the complex domain, these equations can either be solved using known functions (albeit not necessarily elementary ones), or belong to one of the six Painlevé equations, the solutions of which are Painlevé transcendents. Ince [1956] provides a full catalog of all fifty admissible classes of second-order ODEs without movable singularities, and a set of necessary (not sufficient) conditions that the equation must fulfill to have the Painlevé property. It would be very convenient if (3.7) were among them, as it could point us to their solutions.

Denoting $p = \mathrm{d}w/\mathrm{d}f$, we rewrite the equations as $\ddot{w} = R(f, w, p)$ with

$$R(f,w,p) = \frac{1}{w}p^2 - \left[\frac{1}{f} \mp \frac{6f}{w}\left(f^2 \mp \Lambda\right)\right]p + \left[\frac{8f^2}{w}\left(f^2 \mp \Lambda\right)^2 \mp 2\left(11f^2 \mp 9\Lambda\right)\right]. \tag{3.8}$$

First, we require R to be a rational function of w and p with coefficients analytic in f, which is fulfilled for $f \in \mathbb{R} \setminus \{0\}$. Let us inspect the other conditions in the two subregions of f where the coefficients are analytic. R needs to be a polynomial in p of degree at most two, which is also true in our case. We can write

$$\frac{\mathrm{d}^2 w}{\mathrm{d}f^2} = L(f,w)p^2 + M(f,w)p + N(f,w) \tag{3.9}$$

with functions L, M, and N evident from (3.8).

Ince gives two constraints on the form of these functions. $L(f_0, w)$ must only have at most simple poles and belong to one of the five types listed in his work, or be identically zero. The second condition states that if $D(f, w)$ is the least common denominator of the partial fractions in L, then we must be able to express $M = \mu(f, w)/D(f, w)$ and $N = \nu(f, w)/D(f, w)$, with degrees of μ and ν as polynomials in w not exceeding the degree of D by more than one and three, respectively.

For us $D = w$ and both $\mu = wM$ and $\nu = wN$ are also of degree one in w, so the second condition is fulfilled. However, while $L(f_0, w) = 1/w$ indeed only has

one simple pole in $w = 0$, it does not belong to any of the five listed types[4]. Since these conditions were necessary, we conclude that our equations unfortunately do not have the Painlevé property.

Take note that at first glance, it may seem that the equations (3.7) belong to one of the canonical equations listed under type II in Ince [1956], as the 'master' equation for these classes is

$$\frac{\mathrm{d}^2 w}{\mathrm{d}f^2} = \frac{1}{w}\left(\frac{\mathrm{d}w}{\mathrm{d}f}\right)^2 + \left[A(f)w + B(f) + \frac{C(f)}{w}\right]\frac{\mathrm{d}w}{\mathrm{d}f} + D(f)w^3 + E(f)w^2 + F(f)w + G(f) + \frac{H(f)}{w}\,. \quad (3.10)$$

(3.7) is of the above form with B, C, G, and H being the only non-zero functions. However, to avoid movable critical points, two further conditions must be met: $A(f)D(f) = 0$ and $C(f)H(f) = 0$, the latter of which does not hold in our case.

As the equations are not endowed with the Painlevé property, we cannot take advantage of the previous research on this topic and have to look for a solution elsewhere. It is also possible, however, that the equations do not have a closed-form solution at all...

[4]As $L(f_0, w) = 1/w$ has the principal part $1/w$ at the pole, it cannot belong to any other type than type I. However, L would then need to be $2/w$ to be included in that type. A numerical factor such as this one may seem rather insignificant, but note that the classification was performed using the simpler equation $\ddot{w} = L\dot{w}^2$, where (not counting integration constants) $L = 1/w$ means $w = \exp(f)$, while $L = 2/w$ yields $w = 1/f$, a completely different result.

Conclusion

This thesis is a review of a particular class of exact solutions to the Einstein–Maxwell equations of the classical 4D general theory of relativity. The solutions are inspired by the Bonnor–Melvin solution, a cylindrically-symmetric electrovacuum spacetime containing a magnetic field aligned along the axis of symmetry. Barring one exception, the spacetimes we examined further admit a non-zero cosmological constant, and they all contain a magnetic field aligned along one of the three spatial coordinates of the usual cylindrical coordinate system. Any other alignment is incompatible with cylindrical symmetry.

By direct manipulation of the Einstein–Maxwell equations we derived seven solutions in total. Their basic properties are summarized in Table C.1. The six cosmological solutions are of algebraic type D like the original Bonnor–Melvin solution and mostly belong among the Kundt spacetimes with the exception of the inhomogeneous solution with a radial magnetic field, which belongs to the Robinson–Trautman family and notably is the only examined cosmological solution containing a curvature singularity. The corresponding pairs of the axial and azimuthal solutions have the same local properties, only their global topological properties (i.e., which coordinates are periodic) differ. We also obtained one solution without the cosmological constant, which has a radial magnetic field. This solution differs considerably not only from the cosmological solutions, but also from the original Bonnor–Melvin solution. The non-cosmological solution contains two curvature singularities, belongs to neither the Kundt nor the Robinson–Trautman family, is of the most general type I and admits only the three translational Killing vector fields corresponding to static cylindrical symmetry, while the Bonnor–Melvin solution with the axial magnetic field also admits boost symmetry in the direction of the axis.

During our investigation, we examined test particle motion of both uncharged and charged massive particles as well as photons using the method of the effective potential, focusing mainly on stationary circular orbits. Remarkably, we discovered that charged particles may undergo chaotic motion for the non-cosmological solution with the radial magnetic field. Moreover, we investigated shell sources for the spacetimes, requiring them to be composed of particle streams to have reasonable physical properties. Resulting mainly from numerical experiments, the pairs of spacetimes admitting these shells on their interface are listed in Table 3.1. We also noted that regular composite spacetimes mostly but not always admit only shells with mass per unit proper length lower than 1/4, which is a value observed in similar contexts in the literature for non-cosmological spacetimes.

It should be noted that while we assumed cylindrical symmetry for each spacetime, some of them appear more suited for either toroidal or planar symmetry. In this respect, the worst offenders are the homogeneous spacetimes with a radial or an azimuthal magnetic field. Recall that also the inhomogeneous solution with a radial magnetic field is often examined in the context of toroidal symmetry in the literature.

Needless to say, a treatise of similar length as this entire thesis could probably be written about any single one of the examined spacetimes separately, and a lot of research can still be done beyond the select topics that we decided to focus on.

First and foremost, in our future work we intend to investigate more closely the radial homogeneous solution of Sec. 2.5 and its twin, the spacetime of the Appendix, which is locally the same but has a different global structure as per our choice. In the follow-up work, we notably intend to shed the shackles of cylindrical symmetry, because it is ill-suited for the radial homogeneous solution, and unwind the ϕ coordinate. The two azimuthal solutions also deserve further investigation, especially with regards to the endpoints of the admissible interval of the radial coordinate.

Of course, the most natural continuation of this work is to solve the equations for the general solutions with no additional symmetry as we have already tried in Sec. 3.3 but to no avail. While numerical experiments performed in Sec. 3.2 suggest that the equations admit various families of solutions, we must keep in mind that neither of them necessarily has to correspond to an exact spacetime with a metric that can be expressed using analytical functions. Indeed, even the original Bonnor–Melvin solution also contains additional boost symmetry.

An alternative path would be to dispose of the requirement of staticity and look for dynamical solutions. That would enable us to investigate phenomena such as gravitational collapse or cosmic censorship. However, even the present static equations are notoriously difficult to solve so one would apprehend an uphill battle here. As yet unpublished results suggest, there are, for instance, solutions combining a dynamic cylindrical spacetime generated by an electromagnetic field together with perfect fluid but some of the standard energy conditions are broken.

Another possible way that this work can be extended is to examine parametric limits of the spacetimes in a covariant manner. A coordinate-free approach based on the Cartan–Karlhede algorithm was developed in Paiva et al. [1993] and is also discussed in Stephani et al. [2009]. The parametric limits we considered in this work were always viewed from the perspective of a certain system of coordinates, which may result in certain limiting spacetimes remaining hidden from us, as explained in Paiva et al. [1993]. The application of the Cartan–Karlhede algorithm, however, may require us to work with up to tenth covariant derivatives of the Riemann tensor, which is why we settled with the less rigorous approach in this work.

Among other things that may merit further investigation are, e.g., thermodynamic properties of the spacetimes and the stability of the solutions under perturbations, which have already been studied for some of the solutions but not for all. The chaotic motion that was discovered in the radial Bonnor–Melvin solution of Sec. 2.4 can be investigated using the proper apparatus of chaos theory. It is also possible to consider the dual electric counterparts to the spacetimes and investigate particle motion there. Even though it is magnetic fields that are observed on cosmological scales, the electrostatic counterparts of our spacetimes may have a better interpretation of the sources, as, for example, electric monopoles are preferable to magnetic monopoles. And the list could go on...

	Λ	Type	Family	Isometry	Main features
Bonnor–Melvin (Sec. 1.3.3)	0	D	Kundt	$ISO(1,1) \times E(1)$	Axis $\to \infty$
Bonnor–Melvin–Λ (Sec. 2.2)	$+$	D	Kundt	$ISO(1,1) \times SO(3)$	Axis $\to$ axis
Axial inhomogeneous (Sec. 2.3)	$\pm$	D	Kundt	$ISO(1,1) \times E(1)$	$\Lambda > 0$: axis $\to$ axis $\Lambda < 0$: axis $\to \infty$
Radial Bonnor–Melvin (Sec. 2.4)	0	I	✗	$E(1) \times E(1) \times E(1)$	Singularity $\to$ singularity
Radial homogeneous (Sec. 2.5)	$-$	D	Kundt	$SO(2,1) \times E(2)$	$-\infty \to (0-2$ horizons$) \to \infty$
Radial inhomogeneous (Sec. 2.6)	$\pm$	D	Robinson–Trautman	$E(1) \times E(2)$	$\Lambda > 0$: singularity $\to$ horizon $\to \infty$ $\Lambda < 0$: singularity $\to (0-2$ horizons$) \to \infty$
Azimuthal homogeneous (Sec. 2.7)	$+$	D	Kundt	$ISO(1,1) \times SO(3)$	r bounded
Azimuthal inhomogeneous (Sec. 2.8)	$\pm$	D	Kundt	$ISO(1,1) \times E(1)$	$\Lambda > 0$: r bounded $\Lambda < 0$: r left-bounded

Table C.1: A summary of the properties of the spacetimes examined in this thesis compared to the original Bonnor–Melvin solution. Column 'Λ' contains the admissible signs of the cosmological constant and column 'Type' the Petrov algebraic classification of the Weyl tensor. Column 'Family' classifies the spacetimes with respect to null geodesic congruences; the radial Bonnor–Melvin solution does not belong to any such family. The structure of the Killing vector fields of the spacetimes is given in column 'Isometry'. Finally, in column 'Main features' we summarize the structure of the spacetimes as the radial coordinate in the preferred form of the metric increases. Note that wherever any examined spacetime contains a curvature singularity, it is a singular axis. For the two azimuthal spacetimes, the endpoints of the interval of the radial coordinate r are neither axes nor curvature singularities and they warrant further investigation. As not to omit anything, recall that both the Bonnor–Melvin and Bonnor–Melvin–Λ spacetimes have an axial magnetic field.

Appendix: Spatially-cylindrical spacetimes

In this appendix, we examine static spacetimes with the cylindrical symmetry limited to the spatial part of the metric. Specifically, we borrow the spatial part from the Minkowski spacetime of Sec. 1.3.1, but g_{tt} is allowed to depend on all three spatial coordinates. To preserve staticity, g_{tt} cannot depend on t and we keep the metric diagonal, i.e.,

$$\mathrm{d}s^2 = -\exp A(\rho, z, \phi)\,\mathrm{d}t^2 + \mathrm{d}\rho^2 + \mathrm{d}z^2 + \rho^2\,\mathrm{d}\phi^2\,. \tag{A.1}$$

Vacuum solution

First, let us discuss a vacuum solution without the cosmological constant. In order to find vacuum solutions, the Einstein equations (2.1) are equivalent to $\mathbf{R} = 0$, where $\mathbf{R}$ is the Ricci tensor. Nevertheless, we shall focus on the Einstein tensor, solving $\mathbf{G} = 0$, as we will eventually proceed to add Λ and a magnetic field anyway. The non-zero, independent elements of $\mathbf{G}$ are

$$G_{\rho\rho} = \frac{1}{4}\left(\left(A_{,z}^2 + 2A_{,zz}\right) + \frac{2}{\rho}A_{,\rho} + \frac{1}{\rho^2}\left(A_{,\phi}^2 + 2A_{,\phi\phi}\right)\right), \tag{A.2}$$

$$G_{\rho z} = -\frac{1}{4}\left(A_{,\rho}A_{,z} + 2A_{,\rho z}\right), \tag{A.3}$$

$$G_{\rho\phi} = -\frac{1}{4}\left(A_{,\rho}A_{,\phi} + 2A_{,\rho\phi} - \frac{2}{\rho}A_{,\phi}\right), \tag{A.4}$$

$$G_{zz} = \frac{1}{4}\left(\left(A_{,\rho}^2 + 2A_{,\rho\rho}\right) + \frac{2}{\rho}A_{,\rho} + \frac{1}{\rho^2}\left(A_{,\phi}^2 + 2A_{,\phi\phi}\right)\right), \tag{A.5}$$

$$G_{z\phi} = -\frac{1}{4}\left(A_{,z}A_{,\phi} + 2A_{,z\phi}\right), \tag{A.6}$$

$$G_{\phi\phi} = \frac{\rho^2}{4}\left(\left(A_{,\rho}^2 + A_{,z}^2\right) + 2\left(A_{,\rho\rho} + A_{,zz}\right)\right). \tag{A.7}$$

Solving these equations leads us to the metric

$$\mathrm{d}s^2 = -\left(a\,\rho\cos\phi + b\,\rho\sin\phi + c\,z + d\right)^2\mathrm{d}t^2 + \mathrm{d}\rho^2 + \mathrm{d}z^2 + \rho^2\,\mathrm{d}\phi^2\,. \tag{A.8}$$

It contains parameters a, b, and c of the dimension of 1/u, and dimensionless d. If we set $a = b = c = 0$ and $d = 1$, we obtain the Minkowski solution in cylindrical coordinates. However, it can be shown that even when the first three parameters are non-zero, this metric in fact also represents the Minkowski spacetime. Both the Ricci and the Kretschmann scalars vanish, and the metric allows the full set of ten Killing vectors, which means we are dealing with a maximally-symmetric spacetime. Then, the uniqueness theorem for maximally-symmetric spaces of Weinberg [1972] says that there must exist a coordinate transformation between our metric and the usual Minkowski one, as both metrics are maximally symmetric, have the same Ricci scalar and the same signature. In fact, an easier way of seeing this is by examining the Riemann tensor itself, as it vanishes.

We can transform this metric to the Cartesian coordinates by considering $x = \rho\cos\phi$ and $y = \rho\sin\phi$ to obtain

$$\mathrm{d}s^2 = -\left(a\,x + b\,y + c\,z + d\right)^2 \mathrm{d}t^2 + \mathrm{d}x^2 + \mathrm{d}y^2 + \mathrm{d}z^2\,. \tag{A.9}$$

Note that these forms of the metric contain a degeneracy on the hypersurface where $g_{tt} = 0$.

It is not possible to solve the Einstein equations for a cosmological variant of this spacetime, as then $G_{tt} + \Lambda g_{tt} = -\Lambda \exp A(\rho, z, \phi)$, which requires us to consider $\Lambda = 0$. Note that the ansatz (A.1) yields $G_{tt} = 0$.

Magnetic solution

Let us now add an axial magnetic field to the mix. With

$$\mathbf{F} = B(\rho, z, \phi)\,\mathrm{d}\rho \wedge \mathrm{d}\phi\,, \tag{A.10}$$

we shall first make sure that the four-current $\mathbf{J}$ obtained from the Maxwell equations (2.3) vanishes,

$$8\pi\rho^2\mathbf{J} = \left(A_{,\phi}B + 2B_{,\phi}\right)\partial_\rho - \left(A_{,\rho}B + 2B_{,\rho} - \frac{2B}{\rho}\right)\partial_\phi = 0\,, \tag{A.11}$$

and that the Maxwell equation (2.4),

$$\mathrm{d}\mathbf{F} = -B_{,z}\,\mathrm{d}\rho \wedge \mathrm{d}z \wedge \mathrm{d}\phi = 0\,, \tag{A.12}$$

is fulfilled. We use these relations to determine B. The equations can be satisfied for $A(\rho, z, \phi) = A_1(\rho, \phi) + A_2(z)$, leading to $B = \beta\rho\exp(-A_1(\rho, \phi)/2)$. However, one of the Einstein equations (2.1),

$$G_{tt} + \Lambda g_{tt} - 8\pi T_{tt} = -\left(\beta^2 + \Lambda \mathrm{e}^{A_1(\rho,\phi)}\right)\mathrm{e}^{A_2(z)} = 0\,, \tag{A.13}$$

clearly requires a constant A_1 to be solvable, and we can always rescale the t coordinate to have $A_1 \equiv 0$. The cosmological constant must be negative, as we then have $\Lambda = -\beta^2$. Omitting A_1, the remaining non-trivial Einstein equations require

$$2A_2''(z) + \left(A_2'(z)\right)^2 + 4\Lambda - 4\beta^2 = 0\,, \tag{A.14}$$

which is somewhat reminiscent of some of the relations encountered in Sec. 2.1.

We can solve these equations to obtain the metric

$$\mathrm{d}s^2 = -\left(\mathrm{e}^{\sqrt{-2\Lambda}\,z} + a\,\mathrm{e}^{-\sqrt{-2\Lambda}\,z}\right)^2 \mathrm{d}t^2 + \mathrm{d}\rho^2 + \mathrm{d}z^2 + \rho^2\,\mathrm{d}\phi^2 \tag{A.15}$$

with the magnetic field

$$\mathbf{F} = \sqrt{-\Lambda}\,\rho\,\mathrm{d}\rho \wedge \mathrm{d}\phi\,. \tag{A.16}$$

As it stands, this spacetime appears to be something of a cross between the axial and radial homogeneous solutions of Sec. 2.2 and Sec. 2.5.2, respectively. We have an axial magnetic field like in Sec. 2.2, but unlike that solution the cosmological constant must be negative here, $\Lambda < 0$. A negative Λ is consistent with the radial solution of Sec. 2.5.2, and the metric (A.15) certainly resembles (2.245) more than

the axial counterparts, but we should keep in mind that g_{tt} in the present metric is a function of z instead of the radial coordinate, which makes this solution only axially symmetric instead of cylindrically.

Like in the radial homogeneous solution, the magnetic field invariant is

$$F_{\mu\nu}F^{\mu\nu} = -2\Lambda\,, \tag{A.17}$$

and the Kretschmann scalar has the usual value for our homogeneous spacetimes $16\Lambda^2$. Like in all the other homogeneous solutions, there are six independent Killing vector fields and the spacetime is of Petrov algebraic type D.

The properties of the metric allow the axis to be located at an arbitrary value of the radial coordinate, so it is reasonable to dispose of the axis altogether by applying a transformation from the polar to Cartesian coordinates in the planes of constant t and z. Considering $x = \rho\cos\phi$ and $y = \rho\sin\phi$, we obtain

$$\mathrm{d}s^2 = -\left(\mathrm{e}^{\sqrt{-2\Lambda}\,z} + a\,\mathrm{e}^{-\sqrt{-2\Lambda}\,z}\right)^2 \mathrm{d}t^2 + \mathrm{d}x^2 + \mathrm{d}y^2 + \mathrm{d}z^2 \tag{A.18}$$

with

$$\mathbf{F} = \sqrt{-\Lambda}\,\mathrm{d}x \wedge \mathrm{d}y\,. \tag{A.19}$$

This metric and the magnetic field are manifestly locally identical to (2.245) and (2.246) of Sec. 2.5.2, respectively, barring a linear rescaling of one of the coordinates, which explains the striking similarities between the two spacetimes. Only our chosen interpretation of the coordinates is different.

Therefore, a lot of what was said about the radial homogeneous spacetime is also valid here. Again, it is possible to consider $a \in \{-1, 0, 1\}$ only, as we can apply specific coordinate transformations to normalize an arbitrary a to the one from the set with the same sign. Effectively, we can then consider three separate cases of the metric (A.15) with different g_{tt},

$$-g_{tt} = \begin{cases} \cosh^2\left(\sqrt{-2\Lambda}\,z\right) & \text{if } a = +1\,, \\ \exp\left(2\sqrt{-2\Lambda}\,z\right) & \text{if } a = 0\,, \\ \sinh^2\left(\sqrt{-2\Lambda}\,z\right) & \text{if } a = -1\,. \end{cases} \tag{A.20}$$

Like in Sec. 2.5.2 the three options have different causal structures given by the number of horizons. Note that if we decide to keep the originally-proposed interpretation of the coordinates, the horizons are topologically planes instead of cylinders. A better form of the metric similar to (2.250),

$$\mathrm{d}s^2 = -\left(a - 2\Lambda Z^2\right)\mathrm{d}t^2 + \mathrm{d}x^2 + \mathrm{d}y^2 + \frac{\mathrm{d}Z^2}{a - 2\Lambda Z^2}\,, \tag{A.21}$$

can be obtained using a transformation analogous to (2.249), which does not affect $\mathbf{F}$.

Finally, note that our ansatz (A.1) does not allow magnetic fields that would be understood as radial and azimuthal in the original coordinates, as one is unable to find any solutions compliant with the Einstein–Maxwell equations in these cases.

Bibliography

N. Aghanim, Y. Akrami, M. Ashdown, J. Aumont, C. Baccigalupi, M. Ballardini, A. J. Banday, R. B. Barreiro, N. Bartolo, S. Basak, et al. Planck 2018 results VI. Cosmological parameters. *Astronomy & Astrophysics*, 641:A6, 2020.

G. L. Alberghi, D. A. Lowe, and M. Trodden. Charged false vacuum bubbles and the AdS/CFT correspondence. *Journal of High Energy Physics*, 1999(07): 020–020, 1999.

M. Astorino. Charging axisymmetric space-times with cosmological constant. *Journal of High Energy Physics*, 2012(6):1–15, 2012.

M. Astorino, G. Compère, R. Oliveri, and N. Vandevoorde. Mass of Kerr-Newman black holes in an external magnetic field. *Physical Review D*, 94:024019, 2016.

A. M. Awad. Higher-dimensional charged rotating solutions in (A)dS spacetimes. *Classical and Quantum Gravity*, 20(13):2827, 2003.

C. Bambi, G. J. Olmo, and D. Rubiera-Garcia. Melvin universe in Born-Infeld gravity. *Physical Review D*, 91:104010, 2015.

A. Barnes. A comment on a paper by Carot et al. *Classical and Quantum Gravity*, 17(13):2605, 2000.

J. Bičák and M. Žofka. Notes on static cylindrical shells. *Classical and Quantum Gravity*, 19(14):3653, 2002.

W. B. Bonnor. Static magnetic fields in general relativity. *Proceedings of the Physical Society. Section A*, 67(3):225–232, 1954.

I. Booth, M. Hunt, A. Palomo-Lozano, and H. Kunduri. Insights from Melvin–Kerr–Newman spacetimes. *Classical and Quantum Gravity*, 32(23):235025, 2015.

K. Boshkayev, E. Gasperin, A. C. Gutierrez-Pineres, H. Quevedo, and S. Toktarbay. Motion of test particles in the field of a naked singularity. *Physical Review D*, 93(2):024024, 2016.

D. R. Brill, J. Louko, and P. Peldán. Thermodynamics of $(3 + 1)$-dimensional black holes with toroidal or higher genus horizons. *Physical Review D*, 56: 3600–3610, 1997.

R. Brito, V. Cardoso, and P. Pani. Superradiant instability of black holes immersed in a magnetic field. *Physical Review D*, 89:104045, 2014.

K. A. Bronnikov, N. O. Santos, and A. Wang. Cylindrical systems in general relativity. *Classical and Quantum Gravity*, 37(11):113002, 2020.

J. Carot. Some developments on axial symmetry. *Classical and Quantum Gravity*, 17(14):2675, 2000.

J. Carot, J. M. M. Senovilla, and R. Vera. On the definition of cylindrical symmetry. *Classical and Quantum Gravity*, 16(9):3025, 1999.

F. Carrasco, C. Palenzuela, and O. Reula. Pulsar magnetospheres in general relativity. *Physical Review D*, 98:023010, 2018.

S. M. Carroll. The cosmological constant. *Living reviews in relativity*, 4(1):1–56, 2001.

S. Coleman and F. De Luccia. Gravitational effects on and of vacuum decay. *Physical Review D*, 21:3305–3315, 1980.

E. J. Copeland and T. W. B. Kibble. Cosmic strings and superstrings. *Proceedings of the Royal Society A: Mathematical, Physical and Engineering Sciences*, 466 (2115):623–657, 2010.

M. F. A. da Silva, A. Wang, F. M. Paiva, and N. O. Santos. Levi-Cività solutions with a cosmological constant. *Physical Review D*, 61(4):044003, 2000.

S. P. de Alwis, F. Muia, V. Pasquarella, and F. Quevedo. Quantum transitions between Minkowski and de Sitter spacetimes. *Fortschritte der Physik*, 68(9): 2000069, 2020.

M. H. Dehghani. Charged rotating black branes in anti–de Sitter Einstein-Gauss-Bonnet gravity. *Physical Review D*, 67(6):064017, 2003.

Ó. J. C. Dias and J. P. S. Lemos. Magnetic strings in anti-de Sitter general relativity. *Classical and Quantum Gravity*, 19(8):2265–2276, 2002.

R. Durrer and A. Neronov. Cosmological magnetic fields: their generation, evolution and observation. *The Astronomy and Astrophysics Review*, 21(1), 2013.

W. E. East. Cosmic censorship upheld in spheroidal collapse of collisionless matter. *Physical Review Letters*, 122(23):231103, 2019.

H. Feng, Y. Huang, W. Hong, and J. Tao. Charged torus-like black holes as heat engines. *Communications in Theoretical Physics*, 73(4):045403, 2021.

W. Fischler, D. Morgan, and J. Polchinski. Quantum nucleation of false-vacuum bubbles. *Physical Review D*, 41:2638–2641, 1990.

B. Freivogel, V. E. Hubeny, A. Maloney, R. C. Myers, M. Rangamani, and S. Shenker. Inflation in AdS/CFT. *Journal of High Energy Physics*, 2006 (03):007–007, 2006a.

B. Freivogel, Y. Sekino, L. Susskind, and C.-P. Yeh. Holographic framework for eternal inflation. *Physical Review D*, 74:086003, 2006b.

V. P. Frolov and P. Krtouš. Charged particle in higher dimensional weakly charged rotating black hole spacetime. *Physical Review D*, 83(2), 2011.

Z. Fu and D. Marolf. Bag-of-gold spacetimes, Euclidean wormholes, and inflation from domain walls in AdS/CFT. *Journal of High Energy Physics*, 2019(11): 1–46, 2019.

G. W. Gibbons and C. A. R. Herdeiro. The Melvin universe in Born-Infeld theory and other theories of nonlinear electrodynamics. *Classical and Quantum Gravity*, 18(9):1677–1690, 2001.

G. W. Gibbons and C. M. Warnick. Aspherical photon and anti-photon surfaces. *Physics Letters B*, 763:169–173, 2016.

J. B. Griffiths and J. Podolský. *Exact Space-Times in Einstein's General Relativity*. Cambridge Monographs on Mathematical Physics. Cambridge University Press, 2009. ISBN 978-0-511-63386-7.

J. B. Griffiths and J. Podolský. The Linet-Tian solution with a positive cosmological constant in four and higher dimensions. *Physical Review D*, 81:064015, 2010.

M. C. Gutzwiller. *Chaos in Classical and Quantum Mechanics*. Interdisciplinary Applied Mathematics. Springer-Verlag, 1990. ISBN 978-1-4612-6970-0.

B. Gwak. Thermodynamics with pressure and volume under charged particle absorption. *Journal of High Energy Physics*, 2017(11):1–16, 2017.

E. Hackmann and H. Xu. Charged particle motion in Kerr-Newmann space-times. *Physical Review D*, 87(12):124030, 2013.

E. Hackmann, B. Hartmann, C. Lämmerzahl, and P. Sirimachan. Test particle motion in the space-time of a Kerr black hole pierced by a cosmic string. *Physical Review D*, 82:044024, 2010a.

E. Hackmann, C. Lämmerzahl, V. Kagramanova, and J. Kunz. Analytical solution of the geodesic equation in Kerr-(anti-) de Sitter space-times. *Physical Review D*, 81(4):044020, 2010b.

Y.-W. Han, X.-X. Zeng, and Y. Hong. Thermodynamics and weak cosmic censorship conjecture of the torus-like black hole. *The European Physical Journal C*, 79(3):1–6, 2019.

L. Havrdová and P. Krtouš. Melvin universe as a limit of the C-metric. *General Relativity and Gravitation*, 39(3):291–296, 2007.

S. H. Hendi. Rotating black branes in Brans–Dicke–Born–Infeld theory. *Journal of Mathematical Physics*, 49(8):082501, 2008.

S. H. Hendi. Rotating black string with nonlinear source. *Physical Review D*, 82 (6):064040, 2010.

W. Hong, B. Mu, and J. Tao. Testing the weak cosmic censorship conjecture in torus-like black hole under charged scalar field. *International Journal of Modern Physics D*, 29(12):2050078, 2020.

C.-G. Huang and C.-B. Liang. A torus-like black hole. *Physics Letters A*, 201(1): 27–32, 1995.

E. L. Ince. *Ordinary Differential Equations*. Dover Books on Mathematics. Dover Publications, 1956. ISBN 9780486603490.

W. Israel. Singular hypersurfaces and thin shells in general relativity. *Il Nuovo Cimento B*, 44(1):1–14, 1966.

K. Jedamzik and L. Pogosian. Relieving the Hubble tension with primordial magnetic fields. *Physical Review Letters*, 125(18):181302, 2020.

H. Kadlecová and P. Krtouš. Gyratons on Melvin spacetime. *Physical Review D*, 82(4):044041, 2010.

H. Kadlecová and P. Krtouš. The gyraton solutions on generalized Melvin universe with cosmological constant. In *Proceedings of RAGtime 10–13: Workshops on black holes and neutron stars*, 2014.

D. Kastor and J. Traschen. Melvin magnetic fluxtube/cosmology correspondence. *Classical and Quantum Gravity*, 32(23):235027, 2015.

D. Kastor and J. Traschen. Geometry of AdS-Melvin spacetimes. *Classical and Quantum Gravity*, 38(4):045016, 2020.

K. Kuchař. Charged shells in general relativity and their gravitational collapse. *Czechoslovak Journal of Physics B*, 18(4):435–463, 1968.

K. E. Kunze. Cosmological magnetic fields. *Plasma Physics and Controlled Fusion*, 55(12):124026, 2013.

J. Langer. Thin cylindrical shells in general relativity. *Czechoslovak Journal of Physics B*, 19(7):807–820, 1969.

J. P. S. Lemos. Two-dimensional black holes and planar general relativity. *Classical and Quantum Gravity*, 12(4):1081, 1995.

J. P. S. Lemos and V. T. Zanchin. Rotating charged black strings and three-dimensional black holes. *Physical Review D*, 54:3840–3853, 1996.

T. Levi-Civita. $\mathrm{d}s^2$ einsteiniana in campi newtoniani. IX: L'analogo del potenziale logaritmico. *Rendiconti della Reale Accademia dei Lincei*, 28:101–109, 1919.

T. Levi-Civita. Republication of: Einsteinian $\mathrm{d}s^2$ in Newtonian fields. IX: The analog of the logarithmic potential. *General Relativity and Gravitation*, 43(8): 2321–2330, 2011.

A. J. Lichtenberg and M. A. Lieberman. *Regular and chaotic dynamics*. Applied Mathematical Sciences. Springer-Verlag, 1992. ISBN 0-387-97745-7.

Y.-K. Lim. Electric or magnetic universe with a cosmological constant. *Physical Review D*, 98(8):084022, 2018.

Y.-K. Lim. Solenoid configurations and gravitational free energy of the AdS–Melvin spacetime. *Entropy*, 23(11):1477, 2021.

B. Linet. The static, cylindrically symmetric strings in general relativity with cosmological constant. *Journal of Mathematical Physics*, 27(7):1817–1818, 1986.

O. Luongo and H. Quevedo. Characterizing repulsive gravity with curvature eigenvalues. *Physical Review D*, 90(8):084032, 2014.

H. Maeda and C. Martínez. Energy conditions in arbitrary dimensions. *Progress of Theoretical and Experimental Physics*, 2020(4), 2020. 043E02.

M. Mars and J. M. M. Senovilla. Axial symmetry and conformal Killing vectors. *Classical and Quantum Gravity*, 10(8):1633, 1993.

M. A. Melvin. Pure magnetic and electric geons. *Physics Letters*, 8(1):65–68, 1964.

M. A. Melvin. Dynamics of cylindrical electromagnetic universes. *Physical Review*, 139:B225–B243, 1965.

C. W. Misner, K. S. Thorne, and J. A. Wheeler. *Gravitation*. Freeman San Francisco, 1973. ISBN 0-7167-0344-0.

F. C. Moon. *Chaotic and fractal dynamics: An introduction for applied scientists and engineers*. John Wiley & Sons, 2008. ISBN 978-3-527-61751-7.

A. Neronov and I. Vovk. Evidence for strong extragalactic magnetic fields from Fermi observations of TeV blazars. *Science*, 328(5974):73–75, 2010.

I. Olasagasti and A. Vilenkin. Gravity of higher-dimensional global defects. *Physical Review D*, 62(4):044014, 2000.

F. M. Paiva, M. J. Rebouças, and M. A. H. McCallum. On limits of spacetimes–a coordinate-free approach. *Classical and Quantum Gravity*, 10(6):1165, 1993.

S. Perlmutter, G. Aldering, G. Goldhaber, R. A. Knop, P. Nugent, P. G. Castro, S. Deustua, S. Fabbro, A. Goobar, D. E. Groom, et al. Measurements of Ω and Λ from 42 high-redshift supernovae. *The Astrophysical Journal*, 517(2): 565, 1999.

J. F. Plebański and S. Hacyan. Some exceptional electrovac type D metrics with cosmological constant. *Journal of Mathematical Physics*, 20(6):1004–1010, 1979.

E. Poisson. *A Relativist's Toolkit: The Mathematics of Black-Hole Mechanics*. Cambridge University Press, 2004. ISBN 9781139451994.

I. Prasetyo and H. S. Ramadhan. Gravity of a noncanonical global monopole: conical topology and compactification. *General Relativity and Gravitation*, 48 (1):1–19, 2016.

J. Pétri. Multipolar electromagnetic fields around neutron stars: general-relativistic vacuum solutions. *Monthly Notices of the Royal Astronomical Society*, 472(3):3304–3336, 2017.

D. Pugliese, H. Quevedo, and R. Ruffini. Circular motion of neutral test particles in Reissner-Nordström spacetime. *Physical Review D*, 83(2):024021, 2011.

D. Pugliese, H. Quevedo, and R. Ruffini. Equatorial circular orbits of neutral test particles in the Kerr-Newman spacetime. *Physical Review D*, 88(2):024042, 2013.

E. Radu. A note on Schwarzschild black hole thermodynamics in a magnetic universe. *Modern Physics Letters A*, 17(34):2277–2281, 2002.

A. K. Raychaudhuri and M. M. Som. Stationary cylindrically symmetric clusters of particles in general relativity. In *Mathematical Proceedings of the Cambridge Philosophical Society*, volume 58, pages 338–345. Cambridge University Press, 1962.

L. Richterek, J. Novotný, and J. Horský. New Einstein-Maxwell fields of Levi-Civita's type. *Czechoslovak Journal of Physics*, 50(8):925–948, 2000.

A. G. Riess, A. V. Filippenko, P. Challis, A. Clocchiatti, A. Diercks, P. M. Garnavich, R. L. Gilliland, C. J. Hogan, S. Jha, R. P. Kirshner, et al. Observational evidence from supernovae for an accelerating universe and a cosmological constant. *The Astronomical Journal*, 116(3):1009, 1998.

H. G. Schuster and W. Just. *Deterministic Chaos: An Introduction*. John Wiley & Sons, 2005. ISBN 9783527604807.

M. Sharif and W. Javed. Fermions tunneling from charged anti-de Sitter black holes. *Canadian Journal of Physics*, 90(9):903–909, 2012.

S. Y. Slavyanov and W Lay. *Special Functions: A Unified Theory Based on Singularities*. Oxford University Press, 2000. ISBN 978-0198505730.

P. Sommers. On Killing tensors and constants of motion. *Journal of Mathematical Physics*, 14(6):787–790, 1973.

H. Stephani, D. Kramer, M. MacCallum, C. Hoenselaers, and E. Herlt. *Exact solutions of Einstein's field equations*. Cambridge University Press, 2009. ISBN 978-0521467025.

Z. Stuchlík and S. Hledík. Properties of the Reissner-Nordström spacetimes with a nonzero cosmological constant. *Acta Physica Slovaca*, 52(5):363–407, 2002.

K. Subramanian. The origin, evolution and signatures of primordial magnetic fields. *Reports on Progress in Physics*, 79(7):076901, 2016.

T. Tahamtan and M. Halilsoy. Stable magnetic universes revisited. *Astrophysics and Space Science*, 343(1):435–443, 2013.

F. Tavecchio, G. Ghisellini, L. Foschini, G. Bonnoli, G. Ghirlanda, and P. Coppi. The intergalactic magnetic field constrained by Fermi/Large Area Telescope observations of the TeV blazar 1ES 0229+200. *Monthly Notices of the Royal Astronomical Society: Letters*, 406(1):L70–L74, 2010.

K. S. Thorne. Energy of infinitely long, cylindrically symmetric systems in general relativity. *Physical Review*, 138:B251–B266, 1965.

K. S. Thorne. Nonspherical Gravitational Collapse–A Short Review. In J. R. Klauder, editor, *Magic Without Magic: John Archibald Wheeler*, pages 231–258. Freeman San Francisco, 1972.

Q. Tian. Cosmic strings with cosmological constant. *Physical Review D*, 33: 3549–3555, 1986.

A. A. Tseytlin. Melvin solution in string theory. *Physics Letters B*, 346(1):55–62, 1995.

J. Veselý and M. Žofka. Electrogeodesics and Extremal Horizons in Kerr–Newman–(anti-)de Sitter. In *Domoschool-International Alpine School of Mathematics and Physics*, pages 313–332. Springer, 2018.

J. Veselý and M. Žofka. The Kerr–Newman–(anti-)de Sitter spacetime: Extremal configurations and electrogeodesics. *General Relativity and Gravitation*, 51(11): 156, 2019a.

J. Veselý and M. Žofka. Cosmological magnetic field: The boost-symmetric case. *Physical Review D*, 100:044059, 2019b.

J. Veselý and M. Žofka. Cylindrical spacetimes due to radial magnetic fields. *Physical Review D*, 103(2):024048, 2021.

M. Visser. The Kerr spacetime - a brief introduction. In *The Kerr Spacetime: Rotating Black Holes in General Relativity*, pages 3–37. Cambridge University Press, 2009.

A. Z. Wang, M. F. A. da Silva, and N. O. Santos. On parameters of the Levi-Civita solution. *Classical and Quantum Gravity*, 14(8):2417, 1997.

S. Weinberg. *Gravitation and cosmology: principles and applications of the general theory of relativity*. John Wiley & Sons, 1972. ISBN 978-0471925675.

J. P. Wilson and C. J. S. Clarke. 'Elementary flatness' on a symmetry axis. *Classical and Quantum Gravity*, 13(7):2007, 1996.

C.-M. Yoo, T. Harada, and H. Okawa. 3D simulation of spindle gravitational collapse of a collisionless particle system. *Classical and Quantum Gravity*, 34 (10):105010, 2017.

M. Žofka. Bonnor-Melvin universe with a cosmological constant. *Physical Review D*, 99(4), 2019.

M. Žofka. *Selected exact solutions of Einstein equations and their properties*. Habilitation thesis, Charles University, Prague, 2021.

M. Žofka and J. Bičák. Cylindrical spacetimes with $\Lambda \neq 0$ and their sources. *Classical and Quantum Gravity*, 25(1):015011, 2007.

M. Žofka and J. Langer. Relativistic solenoids. *Czechoslovak Journal of Physics*, 55(2):157–165, 2005.

List of publications

J. Veselý and M. Žofka.
Electrogeodesics and Extremal Horizons in Kerr–Newman–(anti-)de Sitter.
In *Domoschool-International Alpine School of Mathematics and Physics*, pages 313-332. Springer, 2018.
DOI: 10.1007/978-3-030-18061-4_11

J. Veselý and M. Žofka.
The Kerr–Newman–(anti-)de Sitter spacetime: Extremal configurations and electrogeodesics.
General Relativity and Gravitation, 51(11):156, 2019.
DOI: 10.1007/s10714-019-2639-6

J. Veselý and M. Žofka.
Cosmological magnetic field: The boost-symmetric case.
Physical Review D, 100:044059, 2019.
DOI: 10.1103/PhysRevD.100.044059

J. Veselý and M. Žofka.
Cylindrical spacetimes due to radial magnetic fields.
Physical Review D, 103(2):024048, 2021.
DOI: 10.1103/PhysRevD.103.024048